Electronic Structure of Impurities and Vortices in Short Coherence Length Superconductors

Final Report

Submitted to the Office of Naval Research

November 1, 1998

Principal Investigator: Michael E. Flatté, Assistant Professor
Department of Physics and Astronomy
Phone: (319) 335-0201
Fax: (319) 353-1115
e-mail: flatte@rashi.physics.uiowa.edu

Grant No. N00014-96-1-1012

PROGRAM GOALS

This grant is for a twenty-seven month investigation of the influence of impurities and vortices on the nearby electronic structure in a short coherence length superconductor. The primary goal is to develop self-consistent calculations of the electronic structure near various defects, focusing on the local density of states (LDOS) measurable by an STM. These calculations are to be compared with analytic results in various limits. Pairing functions of d-wave and s-wave symmetry are to be considered. Results for the local electronic structure are expected to be of great utility in understanding macroscopic measurements such as planar tunneling spectra, critical currents and the magnetic penetration depth.

PROGRESS

In the first year of support we developed a new Green's function technique, which we call the Koster-Slater technique, for calculating the local electronic structure in superconductors. This technique allows us to calculate the changes in the order parameter self consistently and is applicable to weak or strong-coupling superconductors with arbitrary order parameters. In a practical numerical calculation the Koster-Slater technique allows for essentially arbitrarily fine energy resolution in the calculated tunneling spectra, and requires approximately one hour to run for a high-temperature superconductor on a high-end desktop workstation. In contrast, the Bogoliubov-de Gennes equations have lousy energy resolution for realistic superconducting energy gaps, and we estimate would require six months to run for a single spectrum (if there were a computer with one million MB of memory).

The initial application of this technique was to an isotropically gapped low-temperature superconductor because of recent STM results on the local

density of states near magnetic impurities on niobium (Don Eigler's group, IBM Almaden). We explained the qualitative features of the data with a calculation based on a free-electron model (first attached reprint). We have also explored many general features of the STM spectra around impurities on isotropically gapped superconductors using the remarkable energy resolution of the Koster-Slater technique (second attached reprint). These include the spectra around non-magnetic and magnetic impurities in isotropically gapped superconductors with long and short coherence lengths.

A major theoretical conclusion of this work was that use of the correct detailed band structure of a material is critical for an accurate calculation of the STM spectra near an impurity. This is the case because the energy scale of impurities is atomic (eV), even though the energy of states created within the gap is of order the gap (meV). Hence the impurity potential mixes in states of the superconducting host which are very far away from the Fermi surface, and so a correct band-structure for those far away states is necessary. We are currently setting up a realistic band-structure model for niobium, based on thirty-four tight-binding parameters going out to the third nearest neighbors, which will allow us to compare quantitatively with the experimental data.

We have also produced an analytic model for the impurity within the s-wave superconductor based on a delta-function potential. Previous models assumed particle-hole symmetry, and thus produced pathological results for the local STM spectra. Our new analytic model has a single parameter which accounts for the actual case of no particle-hole symmetry. Thus the qualitative behavior of the local STM spectra can be understood without a detailed numerical calculation. This model is detailed in the attached preprint.

Once the utility of the new technique was demonstrated on isotropically gapped superconductors we applied it to anisotropically gapped superconduc-

tors with a tight-binding band structure. The order parameters chosen were anisotropic s-wave and d-wave. STM spectra for magnetic and non-magnetic impurities in these superconductors have been calculated (third attached reprint). For magnetic impurities we find that the sharp localized states within the gap which are present for isotropically gapped superconductors broaden into resonant states in the anisotropically gapped superconductors. These resonant states have highly asymmetric lineshapes and are present for both d-wave and anisotropic s-wave order parameters. Resonant states also are present for non-magnetic impurities for both types of order parameter. Hence it is not sufficient merely to observe resonances to determine the order parameter symmetry — the energies of those resonances must be determined as well.

The most striking result from these investigations was a fit to experimental *planar* tunneling spectra from three different groups on YBCO. None of these spectra look like a clean d-wave superconductor's density of states. Nevertheless all four tunneling curves examined were fit by adding nonmagnetic impurities of essentially the *same scattering strength* to a d-wave superconductor in different concentrations and assuming slightly different voltage resolutions (third attached reprint). We believe that these impurities, which are present in concentrations on the order of 1% even in nominally clean samples, are oxygen vacancies near the surface of YBCO. These results are also supported by scanning tunneling spectroscopy (STS) on the YBCO surface.

LIST OF ATTACHED PAPERS

1. Michael E. Flatté and Jeff M. Byers, "Local Electronic Structure of a Single Magnetic Impurity in a Superconductor", *Physical Review Letters* **78**, 3761-3764 (1997). Development of the Koster-Slater technique and first application (magnetic impurities on niobium).

2. Michael E. Flatté and Jeff M. Byers, "Local Electronic Structure of Defects in Superconductors", *Physical Review B*, **56**, 11213 (1997). Further development of the Koster-Slater technique and application to magnetic and non-magnetic impurities in isotropically gapped superconductors with long and short coherence lengths. Outline of technique for anisotropically gapped superconductors.

3. Michael E. Flatté and Jeff M. Byers, "Impurity effects on quasiparticle c-axis tunneling and STM spectra in high-T_c cuprates", *Physical Review Letters* **80**, 4546-4549 (1998). Application of the Koster-Slater technique to anisotropic-gap superconductors, including d-wave and extended s-wave gaps in $YBa_2Cu_3O_7$. Explanation of planar tunneling spectra from several groups as due to oxygen vacancies at the surface.

4. Michael E. Flatté and Jeff M. Byers, "Local Electronic Structure of Defects in Superconductors", a chapter in *Solid State Physics, Volume 52,* Academic Press, New York, 1998. (Invited). Extended summary of work performed under this grant and prior to it on local properties of impurities in superconductors.

INVITED TALKS

1. "Local Properties of Impurities in Superconductors", Solid State Seminar at Iowa State University, October 3, 1996.

2. "Local Properties of Impurities in Superconductors", Solid State Seminar at Harvard University, April 24, 1997.

3. Michael E. Flatté, "Local electronic properties of defects in superconductors", 1998 March Meeting of the American Physical Society, Los Angeles, March 16-20, 1998.

4. Michael E. Flatté, "Local electronic properties of defects in superconductors", Solid State Seminar, U. Pittsburgh, April 23, 1998.

5. Michael E. Flatté, "Local electronic properties of defects in superconductors", Departmental Colloquium, U. Georgia, September 3, 1998.

CONTRIBUTED CONFERENCE PRESENTATIONS

1. M. E. Flatté and J. M. Byers, "Local electronic structure of a single magnetic impurity in a superconductor", Gordon Research Conference on Superconductivity, Ventura, CA, January 12-17, 1997.

2. "Local electronic properties of a single magnetic impurity in a superconductor", Michael E. Flatté and Jeff M. Byers, American Physical Society March Meeting, Kansas City, March 21, 1997.

3. "Local electronic properties of defects in superconductors", Gordon Research Conference on Strongly Correlated Electron Systems, Plymouth NH, July 19-24, 1998.

Local Electronic Structure of a Single Magnetic Impurity in a Superconductor

Michael E. Flatté[1] and Jeff M. Byers[2]
[1]*Department of Physics and Astronomy, University of Iowa, Iowa City, Iowa 52242*
[2]*Materials Physics, Naval Research Laboratory, Washington, D.C. 20375*
(Received 11 July 1996)

We present the first three-dimensional, self-consistent calculation of the electronic structure near a strong classical magnetic impurity in a superconductor. Localized excited states are found within the energy gap which are half electron and half hole. The spatial structure of the positive-frequency (electronlike) spectral weight (or local density of states) can differ strongly from that of the negative frequency (holelike) spectral weight. The effect of the impurity on the continuum states above the energy gap is calculated with good spectral resolution for the first time. For sufficiently strong impurity potentials, the order parameter may change sign at the impurity site. [S0031-9007(97)03084-6]

PACS numbers: 74.80.–g, 74.25.Ha, 61.16.Ch

Magnetic impurities have a dramatic effect on superconductivity. Most works on the experimental and theoretical effects of magnetic impurities have focused on bulk thermodynamic quantities, such as the reduction of the superconducting transition temperature T_c with increasing magnetic impurity concentration [1]. Theoretical approaches to treat the thermodynamic effects of impurities include Born scattering (Abrikosov-Gor'kov theory) [2] and approximate solutions to all orders in the impurity potential for classical [3–5] and quantum [6,7] spins. A key issue addressed in Ref. [3] was the evolution of localized excited states (not obtainable in Born theory) around impurities into an impurity band, eventually leading to gapless superconductivity at high enough impurity concentrations. The effects of impurities on bulk properties have also been treated within a strong-coupling formalism (e.g., Ref. [8]), but only very recently self-consistently and beyond the Born approximation [7]. Concern about bulk properties in the above and related work did not extend to properties very near the impurity.

Among the first properties calculated in the vicinity of an impurity were the structures of screening clouds around a charged impurity [9,10] and a magnetic impurity [10,11] in a superconductor (characterized by exponentially decaying Friedel-like oscillations). The oscillation of the order parameter around a magnetic impurity was first evaluated without self-consistency [12,13]. A self-consistent calculation of the order parameter at the impurity and very far away for *weak* impurity potentials was done by Schlottmann [14]. Interest in local properties near impurities has been revived by advances in scanning tunneling microscopy (STM) near impurities embedded in a metallic medium [15].

The differential conductivity measured by a STM at a point $\mathbf{x}$, voltage V, and temperature T can be related to the local density of states (LDOS) at the tip location as follows:

$$\frac{dI(\mathbf{x},V,T)}{dV} = \sum_\sigma \int_{-\infty}^{\infty} \frac{d\omega}{2\pi N_o} \frac{\partial n(\omega)}{\partial \omega} \operatorname{Im} G_\sigma(\mathbf{x},\mathbf{x};\omega). \quad (1)$$

Here σ is the spin direction of the electron ($\pm 1/2$), N_o is the normal-state density of states for each spin direction at the Fermi level, and dI/dV is in units of the normal-metal's differential conductivity. $n(\omega) = [1 + \exp\beta(\omega - eV)]^{-1}$ where e is the electron's charge and $\beta = 1/T$. The LDOS is proportional to the imaginary part of the retarded Green's function fully dressed by the interaction of the electronic system with the impurity. The LDOS was calculated near impurities for superconductors with isotropic and anisotropic gaps within the Born approximation [16]. A self-consistent calculation of the LDOS of a vortex core in a superconductor was performed using the Schrödinger-like Bogoliubov–de Gennes (BdG) equations [17,18] and compared with measurements by an STM on superconducting $NbSe_2$ [19].

Recent STM results near a magnetic impurity [20] indicate that (1) discrete states are evident within the energy gap and the LDOS associated with them is asymmetric with voltage around $V = 0$, and (2) the LDOS becomes indistinguishable from the bulk density of states within a distance greater than the Fermi wavelength, but much less than the coherence length.

We will present a fully self-consistent calculation of the local electronic structure near a magnetic impurity, which is based on a Koster-Slater-like Green's function technique rather than the BdG equations [21]. Since the original application of the Green's function algorithm to localized vibrational modes [22], it has been applied to numerous problems, including conduction electrons in metals [23] and impurity states in magnets [24], but not to superconductors. The Green's function method works within a sphere whose radius is determined by the range of the inhomogeneous potential. In contrast, the BdG equations need to be solved in a large sphere whose radius is determined by the required spectral resolution. In essence we shall invert in real space the Dyson equation [25],

$$\int d\mathbf{x}''[\delta(\mathbf{x} - \mathbf{x}'') - \mathbf{g}_\sigma(\mathbf{x},\mathbf{x}'',\omega)\mathbf{V}(\mathbf{x}'')]\mathbf{G}_\sigma(\mathbf{x}'',\mathbf{x}';\omega) = \mathbf{g}_\sigma(\mathbf{x},\mathbf{x}';\omega), \quad (2)$$

0031-9007/97/78(19)/3761(4)$10.00

where

$$\mathbf{g}_\sigma(\mathbf{x},\mathbf{x}';\omega) = \begin{pmatrix} g_\sigma(\mathbf{x},\mathbf{x}';\omega) & f_\sigma(\mathbf{x},\mathbf{x}';\omega) \\ f^*_\sigma(\mathbf{x},\mathbf{x}';-\omega) & -g^*_{-\sigma}(\mathbf{x},\mathbf{x}';-\omega) \end{pmatrix}; \tag{3}$$

the same relationship exists among $\mathbf{G}_\sigma$, G_σ, and F_σ, and

$$\mathbf{V}(\mathbf{x}) = \begin{pmatrix} \sigma V_S(\mathbf{x}) + V_0(\mathbf{x}) & \delta\Delta(\mathbf{x}) \\ \delta\Delta(\mathbf{x}) & \sigma V_S(\mathbf{x}) - V_0(\mathbf{x}) \end{pmatrix}. \tag{4}$$

$\delta\Delta(\mathbf{x}) = \Delta(\mathbf{x}) - \Delta_o$, where $\Delta(\mathbf{x})$ is the position-dependent order parameter and Δ_o is the order parameter of the homogeneous superconductor. $V_S(\mathbf{x})$ is a localized, spin-dependent potential, such as one originating from a classical spin. $V_0(\mathbf{x})$ is a localized nonmagnetic potential. The quantization direction of the superconductor's spins is chosen parallel to the direction of the classical spin and so that spin-up electrons are attracted to the impurity. $G_\sigma \neq G_{-\sigma}$ due to the differences in the potential in Eq. (4). For a BCS superconductor with an isotropic order parameter in a parabolic band, for ω much smaller than the Fermi energy, the homogeneous retarded Green's functions are

$$\begin{aligned} g_\sigma(\mathbf{x},\mathbf{x}';\omega) &= -\frac{\pi N_o}{k_F r}\, e^{-\sqrt{\Delta_o^2-\omega^2}\, r/\pi\xi\Delta_o} \\ &\quad \times \left(\cos k_F r + \frac{\omega}{\sqrt{\Delta_o^2-\omega^2}} \sin k_F r\right), \\ f_\sigma(\mathbf{x},\mathbf{x}';\omega) &= -\frac{\pi N_o \Delta_o}{k_F r\sqrt{\Delta_o^2-\omega^2}}\, e^{-\sqrt{\Delta_o^2-\omega^2}\, r/\pi\xi\Delta_o} \\ &\quad \times \sin k_F r, \end{aligned} \tag{5}$$

where $r = |\mathbf{x} - \mathbf{x}'|$, Δ_o is the order parameter, and $\xi = \hbar v_F/\pi\Delta_o$ is the coherence length. These expressions are valid for ω above and below Δ_o so long as the imaginary parts of both f_σ and g_σ are multiplied by $\operatorname{sgn}\omega$. For a pairing strength γ, the self-consistency equation is

$$\delta\Delta(\mathbf{x}) = \gamma \sum_\sigma \int_{-\infty}^{\infty} d\omega n(\omega)\, \mathrm{Im} F_\sigma(\mathbf{x},\mathbf{x};\omega) - \Delta_o\,. \tag{6}$$

One strength of this formalism is its reliance on the short-range nature of the inhomogeneous potential. The solution of Eq. (2) requires inverting the frequency-dependent real-space matrices $\mathbf{M}_\sigma(\omega) = \boldsymbol{\delta}(\mathbf{x} - \mathbf{x}') - \mathbf{g}_\sigma(\mathbf{x},\mathbf{x}';\omega)\mathbf{V}(\mathbf{x}')$. For $\mathbf{x}'$'s where $\mathbf{V}(\mathbf{x}')$ is negligible, that portion of $\mathbf{M}_\sigma(\omega)$ is triangular and trivially invertible. Hence the numerical complexity of inverting $\mathbf{M}_\sigma(\omega)$ is determined by the range of $\mathbf{V}(\mathbf{x})$, which is governed by the range of the longest-range potential, which in this Letter will be $\delta\Delta(\mathbf{x})$.

As a special case of Eq. (2), the energies of the localized states within the gap correspond to those $\omega > 0$ where $\det \mathbf{M}_\sigma(\omega) = 0$. We model the impurity with a Gaussian $V_S(\mathbf{x})$ of range k_F^{-1}. Figure 1 shows the dependence of the localized state energies for the first two angular momentum channels on the strength of the magnetic potential, $v_s = \pi N_o |\sigma \int d\mathbf{x} V_S(\mathbf{x})|$. We note that a localized state implies local pair-breaking excitations of energy less than $2\Delta_o$. If

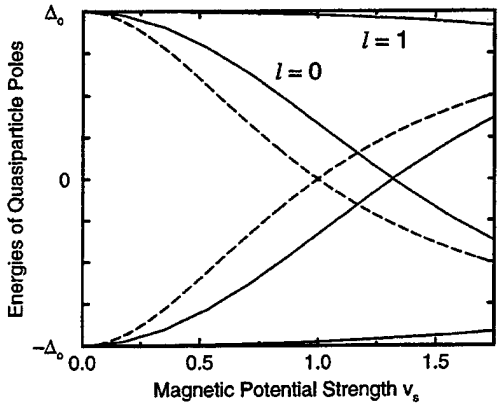

FIG. 1. Localized excited state poles for angular momentum channels $\ell = 0$ and 1 (solid lines). Dashed lines show results of Ref. [3]. At $v_s = v^*_{s0}$, the character of the $\ell = 0$ state changes from spin up to spin down.

$\det \mathbf{M}_\sigma(\omega) = 0$, then $\det \mathbf{M}_{-\sigma}(-\omega) = 0$, so the poles of $G_\sigma(\omega)$ must come in symmetric pairs ($\sigma = \pm 1/2$) around $\omega = 0$. The quasiparticle state for small v_s corresponding to these poles consists of an electron ($\omega > 0$) in the spin-up ($\uparrow$) band (the band attracted to the classical spin) and a hole ($\omega < 0$) in the spin-down ($\downarrow$) band. A hole in the down band has spin up and is attracted to the classical spin. Spin is a good quantum number for the quasiparticle, which is spin up. The spatially integrated spectral weight is one-half each for the electron and hole components.

As the potential strength increases, the excitation energy of each angular momentum state ℓ decreases, and then at some critical value ($v^*_{s\ell}$) begins to increase. For $v_s > v^*_s$ the *ground* state contains a spin-up quasiparticle bound to the classical spin [5]. The low-energy excitation now corresponds to removing that quasiparticle, which is a spin-down excitation. This qualitative behavior of the excitation energies can be extracted from the Shiba model [3], where the magnetic potential is modeled by a delta function at the impurity site. In Ref. [3] the zeros of $\mathbf{M}_\sigma(\omega)$ are found, neglecting the frequency symmetric component (whose significance is discussed below) of $\mathrm{Re}\, g(\mathbf{x},\mathbf{x}';\omega)$. These poles are also shown in Fig. 1.

The decrease in the quasiparticle energy by the classical spin is proportional to the overlap of the atomic-scale potential and the impurity state. The state is, aside from an r^{-2} falloff, extended over a volume whose linear scale is the coherence length. Thus the overlap, and consequently the quasiparticle's energy reduction, is proportional to $v_s\Delta_o$. When this energy exceeds the energy required to create a quasiparticle (Δ_o), the ground state contains a quasiparticle. Hence v^*_s is approximately independent of Δ_o [3], and is determined primarily by the normal-state properties of the superconductor.

In the normal state the spectral weight of the spin-up band at the Fermi energy has a peak at the origin, while that of the spin-down band is pushed away from the origin. In the superconductor this asymmetry is evident

in the quasiparticle spectral weights. Figure 2 shows the calculated angular momentum $\ell = 0$ spectral weights in the up and down bands for two values of v_s, indicating that the asymmetry of the spatial structure of the spectral weights becomes more pronounced with increasing v_s. Also shown are the $\ell = 1$ spectral weights for $v_s = 0.875$. The asymmetric localized-state spectral weights produce differential conductivities which are asymmetric as well. Figure 3 shows differential conductivities for $v_s = 7/8$ as a function of the voltage and the distance from the impurity. By $r = 5k_F^{-1}$ the spectrum has recovered to the homogeneous (bulk) spectrum. The differential conductivity farther away can be easily recovered by constructing the self-consistent $\mathbf{T}$ matrix, $\mathbf{V}(\mathbf{x}')\delta(\mathbf{x}' - \mathbf{x}'') + \mathbf{V}(\mathbf{x}')\mathbf{G}(\mathbf{x}', \mathbf{x}''; \omega)\mathbf{V}(\mathbf{x}'')$, directly from the dressed Green's functions.

The asymmetric behavior of the electronlike and holelike spectral weights due to the difference between the spin-up and spin-down band states does not emerge from the model of Ref. [3]. The Shiba model, due to the assumption of particle-hole symmetry implied by setting the symmetric real part of $g(\mathbf{0}, \mathbf{0}; \omega)$ to zero, predicts identical spatial dependences of the spectral weights for the up and down bands. As pointed out by Koster and Slater [23], proper treatment of the symmetric real part of $g(\mathbf{0}, \mathbf{0}; \omega)$ is essential for obtaining the local electronic properties around an impurity. The quantity $\mathrm{Re}\, g(\mathbf{0}, \mathbf{0}; \omega)$ is simply the Kramers-Kronig transform of the density of states. The spatially dependent form of $\mathrm{Re}\, g(\mathbf{x}, \mathbf{x}'; \omega)$ determines how the continuum states are distorted by the impurity potential to form the bound states. Neglecting the symmetric part of $\mathrm{Re}\, g(\mathbf{x}, \mathbf{x}'; \omega)$ corresponds to a particle-hole symmetric density of states around the Fermi energy. The potentials considered here are locally strong, and mix in states of the homogeneous superconductor with energies much farther from the Fermi surface than Δ_o. Often a benign approximation when bulk properties are being calculated, particle-hole symmetry leads to pathological properties when calculating local electronic structure.

We introduce a new parameter into the Shiba model, α, which is the ω-symmetric part of $\mathrm{Re}\langle g(\mathbf{0}, \mathbf{0}; \omega = 0)\rangle/\pi N_o$. The brackets indicate that $g(\mathbf{0}, \mathbf{x}; \omega = 0)$ has been averaged over a small volume given by the range of the potential modeled by the delta function. For $\alpha \neq 0$ the ratio for the localized quasiparticle of the spectral weight of the up band at the impurity, $A_\uparrow(\mathbf{0})$, to the spectral weight of the down band at the impurity, $A_\downarrow(\mathbf{0})$, is

$$\frac{A_\uparrow(\mathbf{0})}{A_\downarrow(\mathbf{0})} = \frac{1 + 2\alpha v_s + (1 + \alpha^2)v_s^2}{1 - 2\alpha v_s + (1 + \alpha^2)v_s^2}. \tag{7}$$

The introduction of α does not change the localized state energies qualitatively.

We now discuss the structure of $\Delta(\mathbf{x})$. Figure 4 shows $\delta\Delta(\mathbf{x})$'s for two values of v_s. While oscillating with wavelength $\sim \pi k_F^{-1}$, $\delta\Delta(\mathbf{x})$ falls off to a negligible potential within $10k_F^{-1}$. This justifies performing the numerical calculation in a sphere of that radius. A typical radial grid of 100 points provides a numerically robust solution. The self-consistent solution also depends on the value of $N_o\Delta_o/k_F^3$, which for niobium is 3.6×10^{-5} [26]. Relaxation of the order parameter on the atomic scale has also been seen in square-lattice calculations of the BdG equations for nonmagnetic impurities in quasi-two-dimensional d-wave superconductors [27], which should behave in a somewhat similar fashion to magnetic impurities in s-wave superconductors.

As shown in Fig. 4, for large values of v_s, $\Delta(\mathbf{x} = \mathbf{0}) < 0$. Sign changes in Δ, which could be seen in pair tunneling, have been suggested for magnetic impurities in

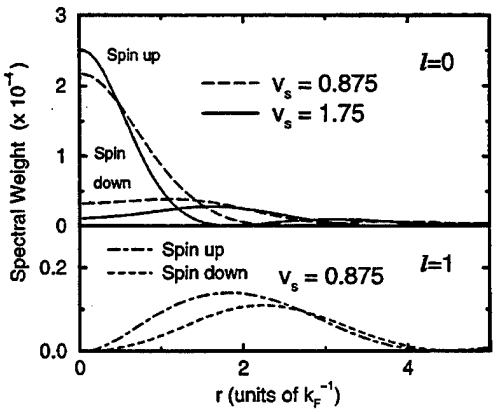

FIG. 2. Spectral weights for the $\ell = 0$ state's up-band component (electronlike for $v_s < v_s^*$) and down-band component (holelike for $v_s < v_s^*$) as a function of position for two values of the magnetic potential. Also shown are the spectral weights for the up and down bands for $\ell = 1$ for $v_s = 0.875$.

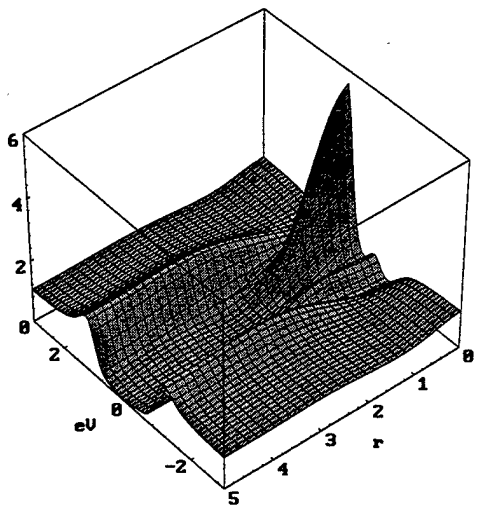

FIG. 3. Differential conductivity (dI/dV), relative to the normal metal as a function of the voltage (in units of Δ_o) and the distance from the impurity (in units of k_F^{-1}) for $v_s = 7/8$. The presence of the large peak near the origin on the positive-frequency side of the spectrum indicates that the impurity is not stronger than the critical strength ($v_s < v_{s0}^*$). $\beta = 7.5/\Delta_o$, which for niobium corresponds to $T \sim 2$ K.

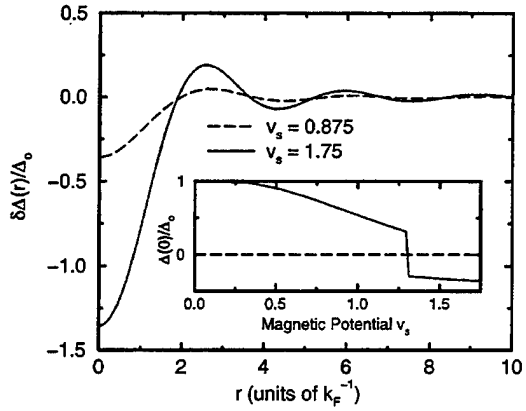

FIG. 4. Change in the local order parameter, $\delta\Delta(\mathbf{x})$, for two values of the magnetic potential. The change becomes negligible beyond $10k_F^{-1}$. Inset: Order parameter at the impurity, $\Delta(\mathbf{0})$, as a function of v_s, indicating a discontinuous change at v_{s0}^*.

the barriers of Josephson junctions [28]. Our sign change in $\Delta(\mathbf{0})$ occurs (at $T = 0$) precisely at v_{s0}^*. The symmetry of Eqs. (2)–(6) under $\omega \to -\omega$ and $s \to -s$ implies that $\mathrm{Im}\, F_\uparrow(\mathbf{r}, \mathbf{r}, \omega) = -\mathrm{Im}\, F_\downarrow(\mathbf{r}, \mathbf{r}, -\omega)$. As the pole in the spin-up band goes from electronlike ($\omega > 0$) to holelike ($\omega < 0$) and the pole in the spin-down band goes from holelike to electronlike, the contribution to $\Delta(\mathbf{0})$ from the localized state changes sign abruptly. $\Delta(\mathbf{0})$ as a function of v_s is shown in the inset of Fig. 4. At $T > 0$ the transition would be smoothed.

The behavior of $\Delta(\mathbf{0})$ as a function of v_s comes from the introduction at v_{s0}^* of a quasiparticle into the ground state of the system. The spin-up quasiparticle localized near the impurity in the ground state suppresses the local order parameter. Exciting the low-energy state (removing the spin-up quasiparticle) causes a pair to enter the condensate. We find that exciting the low-energy state for $v_s > v_{s0}^*$ *increases* $\Delta(\mathbf{0})$ and reduces the spin of the superconductor near the impurity. Typically the excitation of quasiparticles reduces $\Delta(\mathbf{x})$ (which is the case for $v_s < v_{s0}^*$).

We have calculated the electronic properties near a magnetic impurity embedded in a superconductor, and used these results to explain STM measurements around a magnetic atom on a surface. The asymmetry of the peak heights can arise from particle-hole asymmetry in the normal state of the superconductor. The recovery of the spectrum to its bulk structure within a few atomic spacings is due to the r^{-2} decay of the impurity state spectral weight, and the change in sign of the order parameter for sufficient v_s occurs because a quasiparticle is bound in the ground state. None of these aspects of the system change qualitatively at a surface. Thus the calculations presented here should have great value for the experimental (surface) configuration.

We wish to thank M. Salkola and A. V. Balatsky for pointing out Ref. [5] and clarifying Sakurai's picture of one $\ell = 0$ localized state and the transition at v_s^*. During review we have become aware of related work by M. Salkola, A. V. Balatsky, and J. R. Schrieffer [29]. We wish to acknowledge conversations with B. A. Jones and A. Yazdani. M. E. F. wishes to acknowledge the Office of Naval Research's Grant No. N00014-96-1-1012. J. M. B. wishes to acknowledge a N.R.C. Postdoctoral Fellowship.

[1] B. T. Matthias, H. Suhl, and E. Corenzwit, Phys. Rev. Lett. **1**, 92 (1958); C. Herring, Physica **24**, S 184 (1958).
[2] A. A. Abrikosov and L. P. Gor'kov, Zh. Eksp. Teor. Fiz. **39**, 1781 (1962) [Sov. Phys. JETP **12**, 1243 (1961)].
[3] H. Shiba, Prog. Theor. Phys. **40**, 435 (1968).
[4] A. I. Rusinov, Sov. Phys. JETP Lett. **9**, 85 (1969).
[5] A. Sakurai, Prog. Theor. Phys. **44**, 1472 (1970).
[6] O. Sakai *et al.*, J. Phys. Soc. Jpn. **62**, 318 (1993).
[7] W. Chung and M. Jarrell, Phys. Rev. Lett. **77**, 3621 (1996).
[8] F. Marsiglio, J. P. Carbotte, A. Puchkov, and T. Timusk, Phys. Rev. B **53**, 9433 (1996).
[9] R. Prange, Phys. Rev. **129**, 2495 (1963).
[10] J. P. Hurault, J. de Phys. **26**, 252 (1965).
[11] P. W. Anderson and H. Suhl, Phys. Rev. **116**, 898 (1959).
[12] T. Tsuzuki and T. Tsuneto, Prog. Theor. Phys. **37**, 1 (1967).
[13] R. Kummel, Phys. Rev. B **6**, 2617 (1972).
[14] P. Schlottmann, Phys. Rev. B **13**,1 (1976).
[15] M. F. Crommie, C. P. Lutz, and D. M. Eigler, Nature (London) **363**, 524 (1993); Y. Hasegawa and P. Avouris, Phys. Rev. Lett. **71**, 1071 (1993).
[16] J. M. Byers, M. E. Flatté, and D. J. Scalapino, Phys. Rev. Lett. **71**, 3363 (1993).
[17] J. D. Shore, M. Huang, A. T. Dorsey, and J. P. Sethna, Phys. Rev. Lett. **62**, 3089 (1989).
[18] F. Gygi and M. Schlüter, Phys. Rev. B **43**, 7609 (1991).
[19] H. F. Hess, R. B. Robinson, R. C. Dynes, J. M. Valles, Jr., and J. V. Waszicak, Phys. Rev. Lett. **62**, 214 (1990).
[20] Results have now appeared in A. Yazdani, B. A. Jones, C. P. Lutz, M. F. Crommie, and D. M. Eigler, Science **275**, 1767 (1997).
[21] See, e. g., P. G. de Gennes, *Superconductivity of Metals and Alloys* (Addison-Wesley, Reading, MA, 1989).
[22] E. W. Montroll and R. B. Potts, Phys. Rev. **100**, 525 (1955).
[23] G. F. Koster and J. C. Slater, Phys. Rev. **96**, 1208 (1954).
[24] T. Wolfram and J. Callaway, Phys. Rev. **130**, 2207 (1963).
[25] See A. A. Abrikosov, L. P. Gor'kov, and I. E. Dzyaloshinski, *Methods of Quantum Field Theory in Statistical Physics* (Dover, New York, 1963).
[26] $k_F = 1.18$ Å^{-1} and $\xi = 380$ Å.
[27] T. Xiang and J. M. Wheatley, Phys. Rev. B **51**, 11 721 (1995); M. Franz, C. Kallin, and A. J. Berlinsky, Phys. Rev. B **54**, R6897 (1996).
[28] See references in M. Sigrist and T. M. Rice, Rev. Mod. Phys. **67**, 503 (1995).
[29] M. Salkola, A. V. Balatsky, and J. R. Schrieffer, Phys. Rev. B (to be published).

Local electronic structure of defects in superconductors

Michael E. Flatté
Department of Physics and Astronomy, University of Iowa, Iowa City, Iowa 52242

Jeff M. Byers
Materials Physics, Naval Research Laboratory, Washington, D.C. 20375

(Received 16 December 1996)

The electronic structure near defects (such as impurities) in superconductors is explored using a fully self-consistent technique. This technique exploits the short-range nature of the impurity potential and of the induced change in the superconducting order parameter to calculate features in the electronic structure down to the atomic scale with unprecedented spectral resolution. Magnetic and nonmagnetic static impurity potentials are considered, as well as local alterations in the pairing interaction. Extensions to strong-coupling superconductors and superconductors with anisotropic order parameters are formulated. [S0163-1829(97)04537-2]

I. INTRODUCTION

Low-temperature superconductors almost always have a high concentration of nonmagnetic impurities. Even in the dirty limit, however, where the mean free path is shorter than the coherence length, superconductivity endures.[1] This phenomenon can be understood by generalizing BCS pairing[2] to be between degenerate Kramers-partnered states in a time-reversal invariant system.[3] Magnetic impurities, which do break time-reversal invariance, have more profound effects on the superconductor in dilute concentrations than nonmagnetic impurities, lowering the critical temperature T_c (Refs. 4–6) and producing localized states within the gap[7–13] which at sufficient concentrations hybridize to produce gaplessness.[14] In the course of the investigation of the effects of impurities on superconductivity during the last four decades, the primary emphasis has been the influence of impurities on bulk properties. These effects have been treated within a strong-coupling formalism (e.g., Ref. 15), but only very recently self-consistently and beyond the Born approximation.[16] The above work was primarily concerned with bulk or impurity-averaged characteristics and ignored the spatial structure of electronic properties near to the impurity.

Among the first local properties calculated in the vicinity of an impurity in a superconductor were the structures of screening clouds around a charged impurity[17,18] and a magnetic impurity[18,19] in a superconductor (characterized by exponentially decaying Friedel-like[20] oscillations). The oscillation of the order parameter around a magnetic impurity was first evaluated without self-consistency.[21–23] A self-consistent calculation was reported for the order parameter at the impurity and very far away for *weak* magnetic impurity potentials by Schlottmann,[24] and far away from nonmagnetic impurities by Fetter.[25]

Interest in local properties near impurities in superconductors has been revived by the capability of scanning tunneling microscopy (STM) to perform localized spectroscopic measurements. The differential conductivity measured at a point $\mathbf{x}$, voltage V, and temperature T can be related to the local density of states (LDOS) at the tip location as follows:

$$\frac{dI(\mathbf{x},V,T)}{dV}=\frac{e^2}{h}\int_{-\infty}^{\infty}d\omega\frac{\partial n_{\mathrm{STM}}(\omega)}{\partial\omega}\sum_{\sigma}\left(\frac{\mathrm{Im}\,G_{\sigma}(\mathbf{x},\mathbf{x};\omega)}{\pi}\right). \tag{1}$$

Here e is the charge of the electron and $n_{\mathrm{STM}}(\omega)$ is the Fermi function in the STM tip

$$n_{\mathrm{STM}}(\omega)=\left[1+\exp\left(\frac{\omega-eV}{k_BT}\right)\right]^{-1}. \tag{2}$$

The local density of states is proportional to the imaginary part of the retarded Green's function fully dressed by the interaction of the electronic system with the impurity.

The spatially dependent differential conductivity around a nonmagnetic impurity at the surface of a superconductor has been considered theoretically[26] for both isotropic and anisotropic order parameters. In Ref. 26 the impurity was modeled as a point defect, and spatial oscillations in the LDOS at various voltages were calculated. These oscillations are the superconductor's analog of oscillations in the LDOS created by step edges and defects on noble-metal surfaces.[27,28] The superconductor's LDOS oscillations would allow one to measure the anisotropy of the superconductor's order parameter. The conductance oscillations for voltages just above a gap minimum or maximum are strongly pronounced in the real-space directions corresponding to the momenta of the gap minimum and maximum. Calculations followed which considered sharp energy features in the scattering process, such as resonant states.[29,30] Nevertheless, an important assumption of these calculations has remained unchecked in detail, that the electronic distortions induced by the impurity are local, including the deformation of the order parameter. Self-consistent calculations using the Bogoliubov–de Gennes (BdG) equations[31] followed for two-dimensional systems,[32–35] but have been hampered by finite-size effects.

A magnetic impurity differs from a nonmagnetic impurity in that a localized state exists around it.[7–13,36] The first calculations of the LDOS of the localized and continuum states around a magnetic impurity were performed recently both with a simplified analytic model and numerically via the self-consistent technique[37] described in this paper. Calculations

of the LDOS of the localized state with angular momentum quantum number $\ell=0$ were performed with a slightly different analytic model and numerically in two dimensions via the self-consistent BdG equations.[38] These calculations were motivated by reports of experimental measurements around Mn and Gd atoms on a niobium surface. The experimental results, which have now appeared in Ref. 39, indicate: (1) discrete states are evident within the energy gap and the LDOS associated with them is asymmetric with voltage around $V=0$, and (2) the LDOS becomes indistinguishable from the bulk density of states within a distance greater than the Fermi wavelength but much less than the coherence length.

Another type of defect is a local change in the pairing interaction. The resulting spatially dependent order parameter can then distort the LDOS. An order-parameter suppression can even localize states, as in a vortex core.[40,41]

The local electronic properties of all of these defects can be calculated self-consistently from the Gor'kov equation[42] without further approximation with the technique introduced in Ref. 37. Our technique for calculating the electronic structure around a defect in a superconductor is related to the Koster-Slater inversion techniques for determining the local electronic structure of impurities in metals.[43,44] Since its original application to localized vibrational modes,[45] this algorithm has been applied to numerous problems including deep levels in semiconductors[46] and impurity states in magnets.[47] The Koster-Slater technique separates space around the defect into two regions: the near field and the far field. The far field is a region distant enough from the defect that the potential is insignificant and the order parameter has relaxed back to its homogeneous value. The near field is the region close to the defect where the potential is finite or the order parameter is distorted. In essence, the Gor'kov equation that determines the Green's functions of the inhomogeneous superconductor is inverted in the real-space region of the near field. This paper describes the technique in detail, expands on an analytic model introduced in Ref. 37 and reports several calculations of the properties of the defects described above.

In constrast to the Koster-Slater technique presented here, some other formalisms for inhomogeneous superconductivity, such as Ginzburg-Landau theory[48] or the Eilenberger equations,[49] treat the spatial degrees of freedom as coarse grained over the superconductor's coherence length. Coarse-grained approximations are not appropriate for considering electronic structure on the atomic scale near a defect. These approximations are not made, however, in deriving the BdG equations. These equations are generalized Schrödinger equations for the electron and hole wave functions of a quasiparticle, and are valid for a superconductor with an arbitrarily varying order parameter, only constrained by the validity of BCS theory.

Unfortunately, the BdG equations have significant practical difficulties as well. Despite qualitative success modeling STM measurements of a single vortex in superconducting $NbSe_2$,[50] calculations of the electronic structure[51–55] using the BdG equations are hampered by the difference in energy scales between the Fermi energy and the order parameter. Since the BdG equations are solved numerically for a finite system, the difficulty of the calculation is determined by the necessary spectral resolution. The key energy scale which must be resolved is the superconducting gap. Thus, the numerical difficulty increases as the ratio of the Fermi energy to the gap becomes large. Hence the band structure assumed for the superconductor must be somewhat unrealistic (for Refs. 54, 55 the Fermi wavelength was approximately 100 Å, which is inappropriately large[56]). This limitation extends to calculations of the interaction between a vortex and an impurity,[57] the characteristics of the vortex lattice,[58,59] and work on a nonmagnetic impurity[32–35] and a magnetic impurity[38] in a two-dimensional s-wave or d-wave superconductor. In contrast, the computational requirements of the Koster-Slater technique are determined by the range of the impurity potential, rather than the necessary spectral precision.

In Sec. II of this paper we first describe the BdG formalism for local defect potentials and then compare with the Koster-Slater formalism. Section III describes an analytic model, based on a δ-function potential, which reproduces some of the quantitative behavior of the numerical results. Section IV discusses the results of the numerical calculations for magnetic impurities, nonmagnetic impurities, impurities incorporating both magnetic and nonmagnetic potentials, and inhomogeneities in the pairing interaction. A heuristic picture of the electronic structure near these impurities will be presented here, and the calculations will be compared with the analytic model of Sec. III. Section V generalizes the formalism of Sec. II to the case of strong-coupling and anisotropically paired superconductors.

II. FORMALISM

A. Bogoliubov–de Gennes equations

To place our formalism in context we will contrast it with the BdG equations, which are Schrödinger-like equations for the electron and hole components of the quasiparticle wave functions $u(\mathbf{x})$ and $v(\mathbf{x})$, respectively. These are, for a free-electron band structure with mass m, the positive-energy (E) solutions to

$$\left[-\frac{(\hbar\nabla)^2}{2m}-E+V_0(\mathbf{x})+\sigma V_S(\mathbf{x})\right]u_\sigma(\mathbf{x})+\Delta(\mathbf{x})v_\sigma(\mathbf{x})=0,$$

$$\left[\frac{(\hbar\nabla)^2}{2m}-E-V_0(\mathbf{x})+\sigma V_S(\mathbf{x})\right]v_\sigma(\mathbf{x})+\Delta^*(\mathbf{x})u_\sigma(\mathbf{x})=0. \tag{3}$$

Here σV_S is a position-dependent, spin-dependent potential, such as one originating from an impurity with a classical spin. V_0 is a position-dependent nonmagnetic potential and $\Delta(\mathbf{x})$ is the inhomogeneous order parameter. $\Delta(\mathbf{x})$ can be chosen real since the defect potential is real.[60] The quantization direction of the electronic spins in the superconductor ($\sigma=\pm 1/2$) is chosen parallel to the classical spin. A classical spin has no quantum dynamics, and cannot flip the quasiparticle spin. Hence spin is a good quantum number for the quasiparticles and only two coupled equations [Eqs. (3)] are required. The combinations $\sigma V_S \pm V_0$ have physical significance: $\sigma V_S + V_0$ is the potential felt by an electron of spin σ, while $\sigma V_S - V_0$ is the potential felt by a hole of spin σ.

The spatially dependent order parameter is determined self-consistently:

$$\Delta(\mathbf{x})=\sum_{n\sigma}\gamma(\mathbf{x},E_{n\sigma})u_{n\sigma}(\mathbf{x})v^{*}_{n\sigma}(\mathbf{x})\tanh\left(\frac{E_{n\sigma}}{2k_BT}\right), \quad (4)$$

where n labels the states for each spin σ, T is the temperature, and k_B is Boltzmann's constant. $\gamma(\mathbf{x},E_{n\sigma})$ is the effective electron-electron interaction potential, which is

$$\gamma(\mathbf{x},E_{n\sigma})=\gamma_0, \quad E_{n\sigma}<\hbar\omega_D,$$
$$=0, \quad E_{n\sigma}>\hbar\omega_D. \quad (5)$$

For a spherically symmetric defect the wave functions are eigenstates of angular momentum with quantum numbers ℓ and m. Typically the defect is placed in a sphere of radius R with appropriate boundary conditions. The value of R is determined by the spectral resolution necessary for accurately evaluating Eq. (4) and the spectral width of features measurable by, for example, the STM. The typical complications resulting from approximating an infinite system by a finite-size system apply, such as discrete states above the energy gap and the heavy investment of computer time required for large values of R. For example, in the calculations for the vortex in $NbSe_2$,[54,55] $\epsilon_F/\Delta_0=32$ was the largest ratio of the Fermi energy to the homogeneous order parameter considered. This value is unrealistic, and is a result of inappropriately fitting the coherence length and upper critical field of $NbSe_2$ to a free-electron model. A more realistic band structure[56] has a bandwidth to energy gap ratio at least an order of magnitude greater, and a highly anisotropic Fermi velocity. Niobium has an $\epsilon_F/\Delta_0=705$, rendering its LDOS numerically inaccessible for most potentials V_S and V_0.

B. Koster-Slater inversion formalism

We now introduce a self-consistent method which works within a sphere whose radius is determined by the range of the defect's potential and utilizes the continuum spectrum of the homogeneous superconductor. In essence, we invert the Gor'kov equation in real space. The Gor'kov equation[42] for a defect in a superconductor can be written in the Nambu formalism[61] as

$$\int d\mathbf{x}''[\delta(\mathbf{x}-\mathbf{x}'')-\mathbf{g}(\mathbf{x},\mathbf{x}'';\omega)\mathbf{V}(\mathbf{x}'')]\mathbf{G}(\mathbf{x}'',\mathbf{x}';\omega)$$
$$=\mathbf{g}(\mathbf{x},\mathbf{x}';\omega), \quad (6)$$

where $\mathbf{g}$ is the homogeneous Green's function, $\mathbf{V}$ is the potential, and the inhomogeneous retarded Green's function,

$$\mathbf{G}(\mathbf{x},\mathbf{x}';\omega)=\begin{pmatrix} G_\uparrow(\mathbf{x},\mathbf{x}';\omega) & F(\mathbf{x},\mathbf{x}';\omega) \\ F^{*}(\mathbf{x},\mathbf{x}';-\omega) & -G^{*}_\downarrow(\mathbf{x},\mathbf{x}';-\omega)\end{pmatrix}. \quad (7)$$

The elements of this matrix are

$$G_\uparrow(\mathbf{x},\mathbf{x}';\omega)=-i\int_{-\infty}^{\infty}dt e^{i\omega t}\theta(t)\langle 0|\{\psi_\uparrow(\mathbf{x}';t),\psi^{\dagger}_\uparrow(\mathbf{x};0)\}|0\rangle, \quad (8)$$

$$F(\mathbf{x},\mathbf{x}';\omega)=-i\int_{-\infty}^{\infty}dt e^{i\omega t}\theta(t)\langle 0|\{\psi_\uparrow(\mathbf{x}';t),\psi_\downarrow(\mathbf{x};0)\}|0\rangle, \quad (9)$$

$$F^{*}(\mathbf{x},\mathbf{x}';-\omega)=-i\int_{-\infty}^{\infty}dt e^{i\omega t}\theta(t)$$
$$\times\langle 0|\{\psi^{\dagger}_\downarrow(\mathbf{x}';t),\psi^{\dagger}_\uparrow(\mathbf{x};0)\}|0\rangle, \quad (10)$$

$$-G^{*}_\downarrow(\mathbf{x},\mathbf{x}';-\omega)=-i\int_{-\infty}^{\infty}dt e^{i\omega t}\theta(t)$$
$$\times\langle 0|\{\psi^{\dagger}_\downarrow(\mathbf{x}';t),\psi_\downarrow(\mathbf{x};0)\}|0\rangle. \quad (11)$$

The explicit subscripts $\uparrow$ and $\downarrow$ do *not* refer to the spin of the excitation in the superconductor but rather to the spin band of the normal state used to construct the excitation. The key concept is that the spin-*up* band contains both *up* electrons and *down* holes just as the spin-*down* band contains both *down* electrons and *up* holes. The convention employed here is standard in the theory of semiconductors where a spin-up electron excited above the Fermi energy leaves a spin-down hole below the Fermi energy. This is convenient for magnetic potentials since if spin-up electrons are attracted to a magnetic impurity spin-down holes should be repelled by the impurity. In the presence of a single classical impurity spin, the quasiparticle spin is a good quantum number despite electron-hole mixing. Our convention determines the composition of a spin-up quasiparticle to be part spin-up electron and part spin-up hole, rather than part spin-up electron and part spin-down hole.

For $\omega>0$, $\mathbf{G}(\mathbf{x},\mathbf{x}';\omega)$ describes spin-up excitations, involving the mixing of electrons in the spin-up band with holes in the spin-down band. For $\omega<0$, $\mathbf{G}(\mathbf{x},\mathbf{x}';\omega)$ describes spin-down excitations, involving the mixing of electrons in the spin-down band with holes in the spin-up band. Since spin is a good quantum number it is not necessary to use a 4×4 formalism, such as that of Ref. 62. The notation here has been simplified and improved relative to Ref. 37.

The homogeneous Green's function is independent of σ, so

$$\mathbf{g}(\mathbf{x},\mathbf{x}';\omega)=\begin{pmatrix} g(\mathbf{x},\mathbf{x}';\omega) & f(\mathbf{x},\mathbf{x}';\omega) \\ f^{*}(\mathbf{x},\mathbf{x}';-\omega) & -g^{*}(\mathbf{x},\mathbf{x}';-\omega)\end{pmatrix}. \quad (12)$$

The potential

$$\mathbf{V}(\mathbf{x}'')=\begin{pmatrix} V_S(\mathbf{x}'')+V_0(\mathbf{x}'') & \delta\Delta(\mathbf{x}'') \\ \delta\Delta(\mathbf{x}'') & V_S(\mathbf{x}'')-V_0(\mathbf{x}'')\end{pmatrix}, \quad (13)$$

where $\delta\Delta(\mathbf{x})=\Delta(\mathbf{x})-\Delta_0$ and V_S, V_0, and $\Delta(\mathbf{x})$ have similar meaning above as in the BdG equations. The factor of one-half from the electron spin has been incorporated into the potential V_S. To be concrete, and without loss of generality, the spin direction attracted by the potential will be called spin up, and the spin direction repelled will be called spin down.[63] The self-consistency equation for the order parameter is

$$\delta\Delta(\mathbf{x})=\int_{-\infty}^{\infty}d\omega\,\gamma(\mathbf{x},\omega)n(\omega)\mathrm{Im}\,F(\mathbf{x},\mathbf{x};\omega)-\Delta_0, \quad (14)$$

where $n(\omega)$ is the Fermi occupation function at temperature T.

For a BCS superconductor with an isotropic gap in a parabolic band, for ω much smaller than the Fermi energy,

$$g(\mathbf{x},\mathbf{x}';\omega)=-\frac{\pi N_0}{k_F r}\,e^{-(\Delta_0^2-\omega^2)^{1/2}r/\pi\Delta_0\xi}\times\left(\cos k_F r+\frac{\omega}{\sqrt{\Delta_0^2-\omega^2}}\sin k_F r\right),$$

$$f(\mathbf{x},\mathbf{x}';\omega)=-\frac{\pi\Delta_0 N_0}{k_F r\sqrt{\Delta_0^2-\omega^2}}\,e^{-(\Delta_0^2-\omega^2)^{1/2}r/\pi\Delta_0\xi}\sin k_F r, \tag{15}$$

where $r=|\mathbf{x}-\mathbf{x}'|$ and N_0 is the density of states for each spin at the Fermi level. The coherence length $\xi=\hbar v_F/\pi\Delta_0$, where v_F is the Fermi velocity. These expressions are valid for ω above and below Δ_0 so long as the imaginary parts of both f and g are multiplied by sgn ω.

One strength of this formalism is its reliance on the short-range nature of the defect's potential. Solution of Eq. (6) requires inverting the frequency-dependent real-space matrix

$$\mathbf{M}(\mathbf{x},\mathbf{x}';\omega)=\delta(\mathbf{x}-\mathbf{x}')-\mathbf{g}(\mathbf{x},\mathbf{x}';\omega)\mathbf{V}(\mathbf{x}') \tag{16}$$

to obtain $\mathbf{G}(\mathbf{x},\mathbf{x}';\omega)$, so $\mathbf{G}=\mathbf{M}^{-1}\mathbf{g}$. The structure of $\mathbf{M}(\mathbf{x},\mathbf{x}';\omega)$ allows for a precise description of the difference between the near field and the far field. We require that the defect's potential $\mathbf{V}(\mathbf{x})$ is zero for $|\mathbf{x}|>R$. The space $|\mathbf{x}|>R$ belongs to the far field, whereas the space $|\mathbf{x}|\leq R$ belongs to the near field. We can then separate any real-space matrix $\mathbf{A}$ symbolically into four pieces:

$$\mathbf{A}=\begin{pmatrix}\mathbf{A}^{n\to n} & \mathbf{A}^{n\to f}\\ \mathbf{A}^{f\to n} & \mathbf{A}^{f\to f}\end{pmatrix}, \tag{17}$$

where n and f label the near-field region and far-field region, respectively. The particular example of $\mathbf{M}$ is block triangular:

$$\mathbf{M}=\begin{pmatrix}\mathbf{I}-\mathbf{g}^{n\to n}\mathbf{V} & 0\\ -\mathbf{g}^{f\to n}\mathbf{V} & \mathbf{I}\end{pmatrix},$$

$$\mathbf{M}^{-1}=\begin{pmatrix}(\mathbf{I}-\mathbf{g}^{n\to n}\mathbf{V})^{-1} & 0\\ \mathbf{g}^{f\to n}\mathbf{V}(\mathbf{I}-\mathbf{g}^{n\to n}\mathbf{V})^{-1} & \mathbf{I}\end{pmatrix}. \tag{18}$$

It is clear from Eq. (18) that the computational effort in inverting $\mathbf{M}$, and thus finding the inhomogeneous electronic structure, is entirely determined by the complexity of inverting $\mathbf{M}^{n\to n}$. The inhomogeneous Green's functions in the near and far fields are

$$\mathbf{G}^{n\to n}=(\mathbf{I}-\mathbf{g}^{n\to n}\mathbf{V})^{-1}\mathbf{g}^{n\to n}, \tag{19}$$

$$\mathbf{G}^{n\to f}=(\mathbf{I}-\mathbf{g}^{n\to n}\mathbf{V})^{-1}\mathbf{g}^{n\to f}, \tag{20}$$

$$\mathbf{G}^{f\to n}=\mathbf{g}^{f\to n}(\mathbf{I}-\mathbf{g}^{n\to n}\mathbf{V})^{-1}, \tag{21}$$

$$\mathbf{G}^{f\to f}=\mathbf{g}^{f\to f}+\mathbf{g}^{f\to n}\mathbf{V}(\mathbf{I}-\mathbf{g}^{n\to n}\mathbf{V})^{-1}\mathbf{g}^{n\to f}. \tag{22}$$

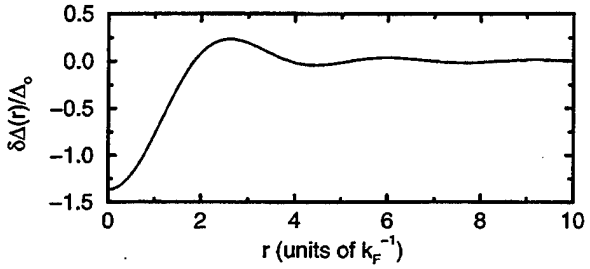

FIG. 1. Change in the local order parameter, $\delta\Delta(\mathbf{x})$, for a magnetic potential strength $v_s=\pi N_0|\int d\mathbf{x}V_S(\mathbf{x})|=1.75$ as a function of the distance from the impurity r. The change becomes negligible beyond $10k_F^{-1}$.

We thus obtain the useful result that the electronic structure in the far field is easily determined once the electronic structure in the near field is known. The connection to the T matrix formalism is straightforward, as from Eq. (22),

$$\mathbf{T}=\mathbf{V}(\mathbf{I}-\mathbf{g}^{n\to n}\mathbf{V})^{-1}. \tag{23}$$

Certain features of the above equations simplify their numerical implementation. Each angular momentum channel constitutes an independent block-diagonal submatrix in $\mathbf{M}(\omega)$. Since the bare Green's functions in Eqs. (15) have analytic expansions in spherical harmonics, $\mathbf{M}(\omega)$ can be calculated quickly. These expansions are detailed in the Appendix.

The value of R is governed by the longest-range potential. In this paper that is determined, not by the shorter-ranged magnetic and nonmagnetic potentials, but by the self-consistently determined $\delta\Delta(\mathbf{x})$. We model V_S and V_0 with Gaussians of radius k_F^{-1} and evaluate Eq. (14) at $T=0$. The $\delta\Delta(\mathbf{x})$ for $v_s=\pi N_0|\int d\mathbf{x}V_S(\mathbf{x})|=1.75$ and $v_0=\pi N_0|\int d\mathbf{x}V_0(\mathbf{x})|=0$ is shown in Fig. 1. While oscillating with wavelength $\sim\pi k_F^{-1}$, $\delta\Delta(\mathbf{x})$ falls off to a negligible potential within $10k_F^{-1}$. A typical radial grid of 100 points provides a numerically robust solution. The self-consistent solution depends on the value of

$$N_0\Delta_0/k_F^3=(2\pi^3\xi k_F)^{-1}=(4\pi^2\epsilon_F/\Delta_0)^{-1}, \tag{24}$$

which for niobium is 3.6×10^{-5} (Ref. 64). This is the single dimensionless parameter required to parametrize the free-electron model of a superconductor.

In contrast to the Koster-Slater technique described here, which exploits a physical distinction between the near field and the far field to accelerate the numerical calculation, the BdG equations treat the near field and the far field on the same level. A large R is desired for decent spectral resolution, but the possible size of R is limited by numerical constraints. Hence a numerical implementation of the BdG equations, by comparison, is typically slower and substantially less accurate than the Koster-Slater technique.

C. Connection to the Born approximation

In Ref. 26 it was argued that calculations within the Born approximation for the *spatial* structure of the $dI(\mathbf{r};V)/dV$ would remain accurate for strong potentials, so long as the potential was short ranged. In this section we explicitly make the connection between the result from the Born approxima-

tion and the result from the Koster-Slater technique in the limit that self-consistency can be ignored and that the size of the potential approaches a point.

In this limit Eq. (22) is

$$-\frac{1}{\pi}\sum_{\sigma}\ \mathrm{Im}\ G_{\sigma}(\mathbf{x},\mathbf{x};\omega)=-\frac{1}{\pi}\mathrm{Im}\{2g(\mathbf{x},\mathbf{x};\omega)+[\mathbf{g}(\mathbf{x},\mathbf{0};\omega)\mathbf{V}_{\mathrm{eff}}(\omega)\mathbf{g}(\mathbf{0},\mathbf{x};\omega)]_{11}-[\mathbf{g}^{*}(\mathbf{x},\mathbf{0};-\omega)\times\mathbf{V}^{*}_{\mathrm{eff}}(-\omega)\mathbf{g}^{*}(\mathbf{0},\mathbf{x};-\omega)]_{22}\},\tag{25}$$

where $\mathbf{V}_{\mathrm{eff}}(\omega)=\mathbf{V}[\mathbf{I}-\mathbf{g}(\mathbf{0},\mathbf{0};\omega)\mathbf{V}]^{-1}$. The inhomogeneous part of the right-hand side of Eq. (25) has the following form if the off-diagonal elements of $\mathbf{V}_{\mathrm{eff}}(\omega)$ can be ignored (this is appropriate when self-consistency is not important):

$$-\frac{1}{\pi}\mathrm{Im}\{([\mathbf{V}_{\mathrm{eff}}(\omega)]_{11}-[\mathbf{V}^{*}_{\mathrm{eff}}(-\omega)]_{22})(g(\mathbf{x},\mathbf{0},\omega)g(\mathbf{0},\mathbf{x},\omega)-f(\mathbf{x},\mathbf{0},\omega)f(\mathbf{0},\mathbf{x},\omega))\}.\tag{26}$$

In the Born approximation the Green's functions appear in the same combinations but the prefactor is the nonmagnetic potential V_0. Hence the spatially dependent features reported in Ref. 26, which are determined by the Green's-functions combinations, are qualitatively retained in our more complete model.

There would be no inhomogeneous structure for a magnetic potential in the Born approximation, however, since

$$\mathbf{V}_{\mathrm{eff}}(\omega)=\begin{pmatrix}V_S & 0\\ 0 & V_S\end{pmatrix},\tag{27}$$

so the distortions in the LDOS of the two spin directions are equal and opposite.

D. Self-consistent potentials

In addition to the self-consistent order parameter, self-consistent spin-dependent and charge-dependent potentials can also be constructed for $\mathbf{V}(\mathbf{x})$ using the calculated spatial structure of the spin $s(\mathbf{x})$ and charge $\rho(\mathbf{x})$ around the defect,

$$s(\mathbf{x})=\frac{1}{2}\int_{-\infty}^{\infty}d\omega n(\omega)\left(-\frac{\mathrm{Im}[G_{\uparrow}(\mathbf{x},\mathbf{x};\omega)-G_{\downarrow}(\mathbf{x},\mathbf{x};\omega)]}{\pi}\right),\tag{28}$$

$$\rho(\mathbf{x})=\sum_{\sigma}\int_{-\infty}^{\infty}d\omega n(\omega)\left(-\frac{\mathrm{Im}\ G_{\sigma}(\mathbf{x},\mathbf{x};\omega)}{\pi}\right).\tag{29}$$

Since these self-consistent quantities are unlikely to change much between the normal and superconducting state,[31] no calculations are reported for such potentials in this paper.

III. ANALYTIC SOLUTION OF THE POINT POTENTIAL

A. Magnetic and nonmagnetic point potentials

Approximating the local potential by a δ function

$$\mathbf{V}(\mathbf{x})=\mathbf{V}\delta(\mathbf{x})=\begin{pmatrix}V_S+V_0 & 0\\ 0 & V_S-V_0\end{pmatrix}\delta(\mathbf{x})\tag{30}$$

leads to a simple expression for Eq. (6),

$$\begin{pmatrix}1-g(\mathbf{0},\mathbf{0};\omega)(V_S+V_0) & -f(\mathbf{0},\mathbf{0};\omega)(V_S-V_0)\\ -f^{*}(\mathbf{0},\mathbf{0};-\omega)(V_S+V_0) & 1+g^{*}(\mathbf{0},\mathbf{0};-\omega)(V_S-V_0)\end{pmatrix}\times\mathbf{G}(\mathbf{0},\mathbf{0};\omega)=\mathbf{M}^{n\to n}(\omega)\mathbf{G}(\mathbf{0},\mathbf{0};\omega)=\mathbf{g}(\mathbf{0},\mathbf{0};\omega).\tag{31}$$

In principle $\mathbf{M}(\omega)$ can be found from the Green's functions in Eq. (15), however there is a divergence in the real part of $g(r;\omega)$ as $r\to 0$. This divergence is coped with in Ref. 8 by discarding the divergent piece. This approximation is essentially an assumption of *strict* particle-hole symmetry [not merely linearizing $\epsilon(k)$ around ϵ_F]. We now discuss the effects of this approximation on the local properties of the system in the *normal* state. The heuristics will be simpler for the normal state, but the conclusions also apply to the superconducting state.

B. Particle-hole symmetry in the normal state

In order to focus on the spin-dependent potential, the nonmagnetic potential will be set to zero. The normal-state properties can be obtained from Eq. (15) for $\Delta_0=0$. That yields a Green's function appropriate for an outgoing wave:

$$g(\mathbf{x},\mathbf{x}';\omega)=-\frac{\pi N_0}{k_F r}e^{ik_F r},\tag{32}$$

where ω is considered close to the Fermi surface so the change in momentum due to $\omega\neq 0$ is negligible. The *inhomogeneous* local density of states obtained for a δ-function potential using this Green's function is unphysical, since it diverges at $r=0$. Now we examine the local density of states when the divergent real part of g is ignored:

$$-\frac{1}{\pi}\mathrm{Im}\ G_{\sigma}(\mathbf{x},\mathbf{x};\omega)=N_0\left(1-\left[\frac{(\pi N_0 V_S)^2}{1+(\pi N_0 V_S)^2}\right]\frac{\sin^2 k_F r}{(k_F r)^2}\right).\tag{33}$$

This expression yields the pathological behavior that the local density of states near a spin-dependent potential is exactly the same for spin-up electrons as for spin-down electrons. A spatial response in the LDOS to a spin-dependent potential that is identical for up and down spin electrons *only* occurs for certain band structures with ϵ_F at special energies (e.g., half-filled tight-binding models). The local density of states for $v_s=\pi N_0|V_S|=0.1$ is plotted in Fig. 2 as a function of distance from the potential. Although it is somewhat distorted from its homogeneous value, it does not show the spin-dependent asymmetry of a more realistic model. An exact calculation for a Gaussian of range k_F^{-1} is also shown in Fig. 2 for comparison.

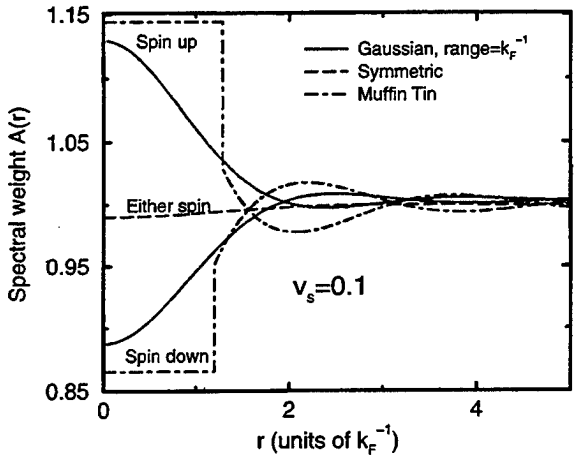

FIG. 2. Spectral weight in the normal state around a magnetic impurity with $v_s=0.1$ as a function of the distance from the impurity r. The solid lines are exact solutions for spin-up (attracted by the impurity) and spin-down (repelled by the impurity) electrons for a Gaussian potential of range k_F^{-1} in a metal with a free-electron dispersion relation. The dashed line, which is the same for both spin-up and spin-down electrons, is the calculated spectral weight for the particle-hole symmetric δ-function potential model. The dot-dashed line is the result for a δ-function potential calculated using the muffin-tin Green's functions. The muffin-tin Green's functions fix the pathological result of the symmetric model that the spectral weight is the same for spin-up and spin-down electrons. The muffin-tin parameter, $\alpha=0.704$, is determined by the range of the Gaussian potential and is therefore not a free parameter.

A more realistic approach to coping with the divergence in Eq. (32) without yielding the pathological result of Eq. (33) is to average the ω-symmetric real part of g over a range given by the assumed range of the potential. That yields a finite value for the local density of states at the potential, but does not control the behavior for small r. To perform that task, we consider a "muffin-tin" Green's function. This function has the form

$$g(\mathbf{x},\mathbf{x}';\omega)=-\frac{\pi N_0}{k_F r}e^{ik_F r}, \quad r>R_0$$
$$=-i\pi N_0-\pi\alpha, \quad r<R_0, \tag{34}$$

where α is the average of the ω-symmetric real part of g over the range of the potential, and R_0 is chosen so that the spatially integrated spectral weight of the Green's function is unchanged (as required by probability conservation). We show in Fig. 2 the local density of states calculated with this Green's function. In particular, the asymmetry in the response of spin-up electrons and spin-down electrons to a spin-dependent δ-function potential is governed by this phenomenological parameter α. The agreement with the exact solution is good at the origin and far from the impurity. The muffin-tin Green's function is discontinuous, unfortunately, but yields a better approximation of the response of the system than the particle-hole symmetric approximation (discarding the ω-symmetric real part of the Green's function).

It is also possible to generate an asymmetry between spin-up and spin-down electrons by adding a nonmagnetic potential v_0 *with* the v_s to parametrize the impurity, but still maintaining a particle-hole symmetric band structure. Since the response of a particle-hole symmetric system to a potential does not depend on the sign of that potential, the v_0 is required to distinguish between electrons and holes. A spin-up electron feels a potential v_s+v_0, whereas a spin-up hole feels a potential v_s-v_0. This additional nonmagnetic potential only breaks particle-hole symmetry locally (within the range of the potential), whereas for a realistic band structure the particle-hole symmetry is broken everywhere in the solid.

For a Gaussian potential with range a,

$$\alpha=\frac{2}{\sqrt{\pi}k_F a}\left[1+\sum_{n=2}^{\infty}\frac{1}{(2n-3)!!}\left(-\frac{(k_F a)^2}{2}\right)^{n-1}\right]. \tag{35}$$

For the Gaussian potentials numerically calculated in this paper, $a=k_F^{-1}$, so $\alpha=0.704$.

C. Self-consistency within the analytic model

As seen from Fig. 1, the distortion of the order parameter is short-ranged around an impurity. We may then consider the effect of the order-parameter distortion on the electronic structure to be parametrized by an effective δ-function potential $\delta\Delta\delta(\mathbf{x})$ similarly motivated to the δ-function potentials for the magnetic and nonmagnetic potentials. The potential $\mathbf{V}(\mathbf{x})$ is changed in the following way:

$$\mathbf{V}(\mathbf{x})=\mathbf{V}\delta(\mathbf{x})=\begin{pmatrix} V_S+V_0 & \delta\Delta \\ \delta\Delta & V_S-V_0 \end{pmatrix}\delta(\mathbf{x}). \tag{36}$$

The relative effect of the $\delta\Delta$ compared to the other two potentials is likely to be small for the potentials considered in this paper. Typically $N_0V_S/k_F^3\sim 1$ or $N_0V_0/k_F^3\sim 1$, and for a free-electron model of niobium $N_0\Delta_0/k_F^3=3.6\times10^{-5}$. Even for a small coherence length of $\xi=10k_F^{-1}$, $N_0\Delta_0/k_F^3=1.6\times10^{-3}$. For convenience we define $\delta_0=\pi N_0\delta\Delta$.

D. Energies of localized states in the superconductor

The energies of the localized states of angular momentum ℓ correspond to the positive energies $\omega_\ell=|\Omega|$, where

$$\det \mathbf{M}^{n\to n}(\Omega)=0, \tag{37}$$

and the solution is traced to the ℓ-channel block of $\mathbf{M}$ (see Appendix). For the analytic model, $\mathbf{M}^{n\to n}(\omega)$ is the matrix shown in Eq. (31), where $g(\mathbf{0},\mathbf{0};\omega)$ in the superconducting state is constructed similarly to that of the normal state,

$$g(\mathbf{0},\mathbf{0};\omega)=-\pi N_0\left(\alpha+\frac{\omega}{\sqrt{\Delta_0^2-\omega^2}}\right). \tag{38}$$

The anomalous Green's function is given by Eq. (15), since it does not have a divergence problem as $r\to0$,

$$f(\mathbf{0},\mathbf{0};\omega)=-\pi N_0\left(\frac{\Delta_0}{\sqrt{\Delta_0^2-\omega^2}}\right). \tag{39}$$

This analytic model only has localized states in the $\ell=0$ angular momentum channel, as expected for a δ-function potential. Those energies are

$$\omega_0=\left|\frac{v_s\delta_0\pm[(v_s\delta_0)^2-(v_s^2+\gamma^2)(\delta_0^2-\gamma^2)]^{1/2}}{v_s^2+\gamma^2}\right|\Delta_0, \tag{40}$$

where

$$\gamma=[(1+\alpha^2)(v_s^2-v_0^2-\delta_0^2)-2\alpha v_0-1]/2. \tag{41}$$

Equation (40) reduces to a result obtained by Shiba[8] when $v_0=\alpha=\delta_0=0$, a result obtained by Rusinov[9] when $\alpha=\delta_0=0$, a result obtained by us[37] when $v_0=\delta_0=0$, and a result obtained by Salkola, Balatsky, and Schrieffer[38] when $\alpha=0$.

One solution of Eq. (40) is a spin-up quasiparticle and the other is a spin-down quasiparticle. There may be only one real solution to Eq. (40); then only one $\ell=0$ localized state exists around the impurity. This occurs for large v_s. When $v_s=0$ the localized states are due to order-parameter suppression, and the energies of the two spin states are degenerate. This follows from time-reversal symmetry in the absence of a magnetic potential. For small v_s the two energies are split by an amount

$$\Delta\omega_0=\frac{2v_s\delta_0\Delta_0}{v_s^2+\gamma^2}. \tag{42}$$

E. Spectral weight asymmetry in the analytic model

A spin-up quasiparticle consists of amplitudes for a spin-up electron (electron in a spin-up state), and a spin-up hole (electron missing from a spin-down state). Therefore the spectral weight of a spin-up localized state will be divided between an electronlike pole in the spin-up band at $\omega=\omega_0$ [with weight $A_\uparrow(\mathbf{r};\omega_0)$] and a holelike pole in the spin-down band at $\omega=-\omega_0$ [with weight $A_\downarrow(\mathbf{r};-\omega_0)$]. These two types of excitation are independently resolvable by a scanning tunneling microscope, since at positive sample voltage relative to the tip the STM places electrons in the sample, whereas at negative sample voltage the STM places holes in the sample. We define the energy of the pole in the spin-up band to be $\omega_\uparrow$ and in the spin-down band to be $\omega_\downarrow$. Even though ω_0 is always positive, $\omega_\uparrow$ can be positive or negative, and $\omega_\uparrow=-\omega_\downarrow$.

The spatial structure of the spectral weights of the spin-up band and spin-down band components of the localized state are given by

$$\begin{aligned}
A_\sigma(\mathbf{r};\omega)&=\frac{\pi N_0\Delta_0}{2v_s}\delta(\omega-\omega_\sigma)\frac{\sqrt{\Delta_0^2-\omega^2}}{\Delta_0}\left[\frac{(v_0-v_s)\Delta_0^2+(v_0+v_s)\omega^2+(v_0+v_s)\alpha^2(\Delta_0^2-\omega^2)}{\Delta_0^2}\right.\\
&\left.+\frac{2(v_0+v_s)\alpha\omega\sqrt{\Delta_0^2-\omega^2}-(1+\alpha^2)(v_0^2-v_s^2)(\alpha(\Delta_0^2-\omega^2)+\omega\sqrt{\Delta_0^2-\omega^2})}{\Delta_0^2}\right], \qquad r<R_0\\
&=\frac{\pi N_0\Delta_0}{(k_Fr)^2}\frac{(\Delta_0^2-\omega^2)^{3/2}}{2v_s\Delta_0^3}\exp\left[-\frac{2r}{\pi\xi}\left(\frac{\sqrt{\Delta_0^2-\omega^2}}{\Delta_0}\right)\right]\delta(\omega-\omega_\sigma)\left[\left(v_s\frac{\Delta_0^2+\omega^2}{\Delta_0^2-\omega^2}-v_0+(v_s^2-v_0^2)\right.\right.\\
&\left.\times\left\{\alpha-\frac{\omega}{\sqrt{\Delta_0^2-\omega^2}}\right\}\right)\sin^2(k_Fr)+(v_s+v_0)\left(1+(v_s-v_0)\left\{\frac{\omega}{\sqrt{\Delta_0^2-\omega^2}}-\alpha\right\}\right)\cos^2(k_Fr)\\
&\left.+2(v_s+v_0)\left(v_0-v_s+[1-\alpha(v_0-v_s)]\frac{\omega}{\sqrt{\Delta_0^2-\omega^2}}\right)\sin(k_Fr)\cos(k_Fr)\right], \qquad r>R_0.
\end{aligned} \tag{43}$$

The above expression is set up for use as a muffin-tin Green's function. The construction of such a Green's function requires that the spectral weight integrates to one. However, ignoring the contribution from $r<R_0$, the above expression can be integrated over all space, and still yields one-half for the spin-up band and one-half for the spin-down band to order Δ_0/ϵ_F. Hence the quasiparticle is one-half electron and one-half hole. This provides additional confidence in the above expressions.

The frequency-integrated weight at the defect of the two types of excitation can be calculated within the analytic model, and is (for $\delta_0=0$)

$$\frac{A_\uparrow(\mathbf{r}=\mathbf{0})}{A_\downarrow(\mathbf{r}=\mathbf{0})}=\frac{1+2\alpha(v_0-v_s)+(1+\alpha^2)(v_0-v_s)^2}{1+2\alpha(v_0+v_s)+(1+\alpha^2)(v_0+v_s)^2}. \tag{44}$$

For a spin-down quasiparticle there is an electronlike pole in the spin-down band and a holelike pole in the spin-up band and the relative weight is still given by the expression above. This expression for $v_0=0$ was reported in Ref. 37.

In the following section these results are compared with numerical calculations of properties in the superconducting state *and* in the normal state.

IV. COMPARISON WITH NUMERICAL RESULTS AND DISCUSSION

A. Nonmagnetic impurity

Even strong nonmagnetic impurities at moderate concentrations will not suppress the critical temperature of a superconductor.[3] Nevertheless, it was recognized early on[25] that the local order parameter may be affected. In Ref. 25 the

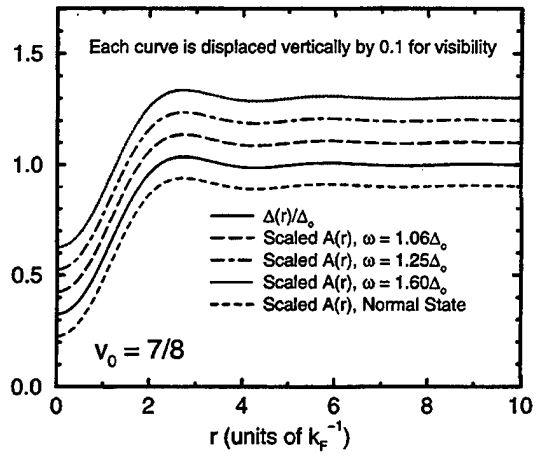

FIG. 3. Comparison of the spectral weight in the superconducting state at several frequencies to the spectral weight of the normal state and the spatial dependence of the order parameter. All of these curves are indistinguishable, but they have been displaced for better visibility. The spectral weights are normalized to their value at large distances from the impurity r, and the order parameter is normalized to the homogeneous order parameter Δ_0. This figure indicates that normal-state properties drive the spatially dependent features of the superconductor's spectrum.

effect of the nonmagnetic impurity was calculated in the far field by modeling the impurity potential with a phase shift. The phase shifts were evaluated for two models: a spherical square-well potential and a δ-shell potential. Self-consistency was ignored by only focusing on regions far from the impurity where the change in the order parameter is small compared to its homogeneous value. The order-parameter change due to the impurity was found to oscillate with the Fermi wavelength, and decay as r^{-2} for $r<\xi$. For $r>\xi$, expressions in Ref. 25 indicate a decay of r^{-3}.

Figure 3 shows the spectral weight $A(\mathbf{r};\omega)$ at several frequencies above the energy gap near a strong nonmagnetic impurity with a Gaussian potential of range k_F^{-1} and strength $v_0=7/8$, calculated self-consistently for a superconductor with $\xi k_F=449$ (a free-electron parametrization of niobium). The spectral weights are suppressed to approximately 30% of their homogeneous value at the center of the potential. Only continuum states are shown since no localized states were found for this potential. The curves showing the spectral weight have been displaced from each other so that they may be distinguished. Also shown displaced in Fig. 3 is the spectral weight in the normal state, normalized to the spectral weight in the homogeneous metal. *All* the quantities plotted in Fig. 3 are *identical* to the accuracy of the calculation. Figure 3 is an illustration of a relationship between the spectral weight in the normal state and the spectral weight in the superconducting state,

$$A(\mathbf{r};\omega)=\frac{A_n(\mathbf{r})}{2N_0}A_{sc}(\omega), \tag{45}$$

where $A_n(\mathbf{r})$ is the spectral weight in the inhomogeneous *normal* state for energies near the Fermi surface and $A_{sc}(\omega)$ is the *homogeneous* superconductor's spectral weight as a function of frequency. $2N_0$ is the normal state's spectral

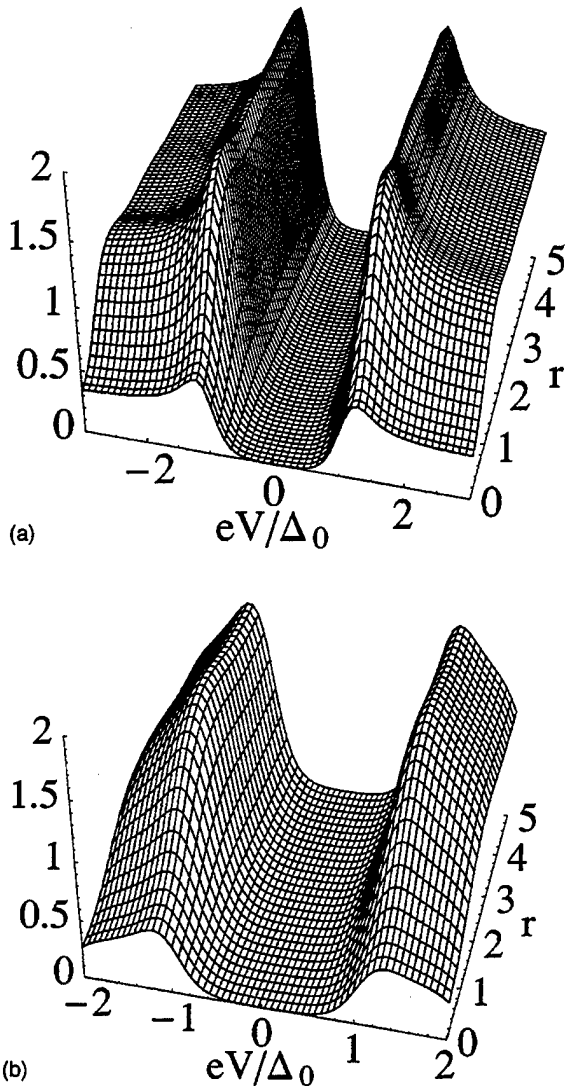

FIG. 4. Differential conductivity (LDOS) as a function of voltage and position calculated around a nonmagnetic impurity with $v_0=0.875$. The LDOS is normalized by the homogeneous DOS of the normal state. The spectrum is suppressed substantially in the vicinity of the impurity. The temperature is $0.13\Delta_0/k_B$, which for niobium corresponds to about 2 K. (a) A coherence length appropriate for niobium, $\xi k_F=449$. (b) A much shorter coherence length, $\xi k_F=10$.

weight far from the impurity. This expression is valid for small r and small ω, the regime of interest for STM on a superconductor. For ω of order Δ_0, Eq. (45) is valid for $r<\xi$.

We further illustrate the relationship of Eq. (45) in Fig. 4(a), which shows the LDOS for this nonmagnetic impurity normalized by the normal-state DOS, as a function of voltage and position calculated from Eq. (1) with $T=(0.13)\,\Delta_0/k_B$. This temperature corresponds to 2 K for niobium. There is no change in the energy *gap* due to this nonmagnetic potential. Figure 4(a) shows that it is merely the local amplitude of the spectral weight which is reduced—this would manifest itself in a locally reduced oscillator strength for an optical transition, or the reduction in the tun-

neling current for an STM, which is directly proportional to the LDOS shown in Fig. 4(a). Figure 4(b) is an identical calculation for a shorter coherence length, $\xi = 10k_F^{-1}$. There appears to be little difference, although here a localized state exists near the continuum.

Figures 3 and 4(a,b) show for the nonmagnetic impurity that the normal-state electronic structure determines the *spatial* dependence of the superconductor's $A(\mathbf{r};\omega)$ for all frequencies including near the energy gap. The potential strength of the impurity is orders of magnitude greater than Δ_0, and thus locally mixes in states far from the Fermi surface in the homogeneous metal. These states are required to construct probability densities which are suppressed by 70% near the impurity. The spatial structure of the spectral weight in the normal state is essentially identical to that seen in Fig. 3 over an energy range around the Fermi surface which is orders of magnitude greater than Δ_0.

Once the normal-state band structure has been distorted by the presence of the nonmagnetic impurity, superconductivity is a small perturbation within a narrower frequency range. The formation of the gap in the single-particle excitation spectrum in the superconducting state is characterized by the "mixing" of electron and hole amplitudes to form quasiparticles near the gap edge. These quasiparticles, therefore, are constructed from single-particle eigenstates of the metal which have already been strongly distorted by the impurity potential.

Equation (45) has important implications for spectroscopy on a superconductor, for one of the procedures for normalizing spectra taken at different lateral positions on a superconducting surface is to assume that the LDOS at a particular voltage much larger than Δ_0 is the same. This is an attempt to correct for possible changes in the tip-surface distance upon moving the tip laterally. A small change in the tip-surface distance can have a strong effect on the tunneling current. Unfortunately this procedure will prevent an experiment from seeing changes in the LDOS due to a nonmagnetic impurity, including the conductance oscillations described in Ref. 26.

We now discuss the properties of the order parameter. $\Delta(\mathbf{r})$ is self-consistently determined, and is shown in Fig. 3 for small r to be identical in spatial structure to the normal-state spectral weight,

$$\frac{\Delta(\mathbf{r})}{\Delta_0} = \frac{A_n(\mathbf{r})}{2N_0} = \frac{A(\mathbf{r};\omega)}{A_{sc}(\omega)}. \tag{46}$$

Since a nonmagnetic potential repulsive to electrons attracts holes, and $\Delta(\mathbf{r})$ depends equally on electron and hole amplitudes, one might expect a nonmagnetic potential to have little effect on the spatial dependence of the order parameter. However the allowable maximum spectral density of holes depends on the spectral density of the electron band where the holes reside, so if most electrons are excluded from the site, holes will be effectively excluded as well. To emphasize this point we note that the scaled anomalous spectral weight $\mathrm{Im}\, F(\mathbf{r},\mathbf{r};\omega)$ is identical to the scaled $A(\mathbf{r};\omega)$ for the frequencies shown in Fig. 3 [and for all relevant frequencies for the self-consistency equation Eq. (14)]. Since $\mathrm{Im}\, F(\mathbf{r},\mathbf{r};\omega)$ is proportional to the product of electron and hole amplitudes, and $A(\mathbf{r};\omega)$ is proportional to the electron amplitude squared, the spatial structure of the electron and hole spectral weights must be similar. They are, since the normal-state spectral weight $A_n(\mathbf{r};\omega)$ is roughly frequency independent around the Fermi energy over an energy range much greater than Δ_0.

We now comment on the lack of localized states near the nonmagnetic impurity for $\xi k_F = 449$ and the small binding energy of the quasiparticle for $\xi k_F = 10$. The suppression of the order parameter near the impurity may be considered to form an attractive off-diagonal potential which may bind quasiparticles. Localized states created by order-parameter suppression would be doubly degenerate, due to the two possible spin states [see Eq. (40)]. Since the quasiparticle is half hole and half electron, if the electron part is attracted and the hole part is repelled, one might expect the effects of such a nonmagnetic potential on the quasiparticle to cancel. However the binding energy of the localized state is an order of magnitude smaller [$\omega_0 = (1 - 2\times 10^{-4})\Delta_0$] than that found in Sec. IV D for a suppressed order parameter via pairing suppression. This may be explained by the well-known repulsive effect (quantum reflection) of a strong attractive potential on a quantum-mechanical particle. We find also that in the case of the magnetic impurity that a large enough nonmagnetic potential of either sign will suppress the binding of a quasiparticle to the impurity. We note here that the ratio of the nonmagnetic potential to the off-diagonal potential [$\delta\Delta(\mathbf{r})$] is much larger ($v_0/N_0\Delta_0 \sim 10^4$) than the ratios of the nonmagnetic potentials to the magnetic potentials considered below.

B. Magnetic impurity

Recently, we have presented calculations of the LDOS (and thus the differential conductivity in an STM experiment) in the vicinity of a magnetic impurity.[37] These calculations indicated that the spatial structure of the electron amplitude of the localized state differed strongly from the hole amplitude of the localized state. A further result was that the spectrum should recover to the homogeneous spectrum within a few atomic spacings. Similarly motivated calculations of the LDOS due to the $\ell = 0$ localized state have been presented since then,[38] although these calculations did not address the continuum LDOS. The two models used in Ref. 38 were (1) a δ-function model solved using particle-hole symmetric Green's functions, but not self-consistently, and (2) self-consistent calculations for a two-dimensional tight-binding s-wave superconductor within the BdG equations. The first method can only model the normal-state properties properly for a particle-hole symmetric band structure, such as at the Van Hove singularity in a two-dimensional tight-binding band structure. The second method must contend with numerical finite-size effects, which make it difficult to calculate the continuum states. A result obtained from the first method which is only true for special band structures is that the spatial structure of the electron and hole components of the quasiparticle are the same. The authors of Ref. 38 did raise the possibility of an additional nonmagnetic potential as a source of electron-hole amplitude asymmetry in the spatial structure of the localized state. We found[37] and will explore below that there is, for realistic band structures, electron-hole asymmetry without a nonmagnetic potential.[69]

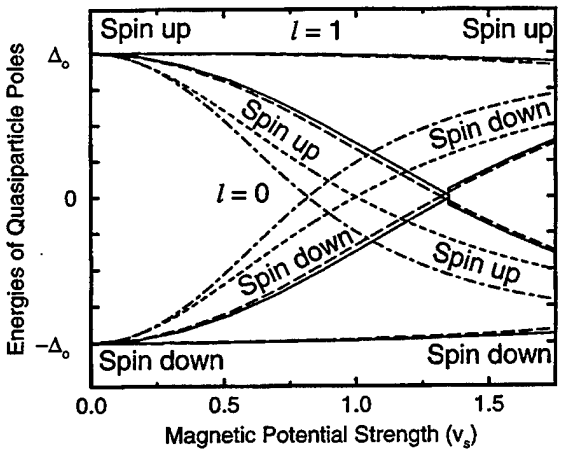

FIG. 5. Energies of the quasiparticle poles as a function of the magnetic potential strength v_s for the first two angular momentum states around the impurity. The spin-up and spin-down labels refer to the band that the excitation resides in—an excitation with negative energy (holelike) in a spin-up band is a spin-down hole. The solid line corresponds to $\xi k_F = 10$, the long-dashed line to $\xi k_F = 449$, the short dashed line to the symmetric model of Shiba, and the dot-dashed line to the result calculated with muffin-tin Green's functions and $\alpha = 0.704$. At a critical value of $v_s = v_{s0}^*$, the up poles cross to negative energies and the down poles cross to positive energies, indicating a change in the character of the ground state. The kink evident in the solid and long-dashed lines is real, and due to the discontinuous (at $T=0$) change in $\Delta(\mathbf{x})$ at v_{s0}^*. The unimportance of self-consistency can be gauged by the small difference between the short-coherence length result and the long-coherence length result.

1. Energy and character of localized states

We will begin with a discussion of the energies of the localized states around a magnetic impurity and the spin character of those states. Solutions to Eq. (37) can be evaluated numerically. Figure 5 shows the dependence of the energies of the localized state poles for the first two angular momentum channels on the strength of the magnetic potential. Results for a short coherence length ($\xi = 10k_F^{-1}$) are shown (solid line) as well as results for a long coherence length ($\xi = 449k_F^{-1}$). The localized quasiparticle state for small v_s is the spin state attracted to the classical spin, which we will label up ($\uparrow$).[63] As the potential strength increases, the excitation energy of each angular momentum state decreases. At some critical value $v_{s\ell}^*$ the localized state becomes a spin-down excitation, the energy changes abruptly, and then increases with increasing v_s. This behavior can be extracted from the analytic model [Eq. (40)] as well.

Evident from Eq. (7) is that the ℓ-channel electron pole involves entirely single-particle states within the spin-up band when the ℓ-channel solution to Eq. (37), $\Omega > 0$. This occurs for $v_s < v_{s\ell}^*$. However, for $\Omega < 0$ ($v_s > v_{s\ell}^*$), the electron pole involves entirely states within the spin-down band. The holelike pole always involves single-particle states in the opposite spin band from the electronlike pole. The source of the quasiparticle amplitude for the various poles is indicated in Fig. 5.

Also shown in Fig. 5 are the analytic results for the pole energies for $\alpha = 0$ (Ref. 8) and $\alpha = 0.704$. The muffin-tin model is no better than the particle-hole symmetric model in predicting the localized state energies. The muffin-tin model will prove more successful at predicting the spatial asymmetry between the electron and hole amplitudes of the localized state.

The unimportance of self-consistency for determining the energies of the localized states can be gauged by the small difference between the short-coherence length result and the long-coherence length result. The most important feature it determines in Fig. 5 is the size of the discontinuity in the localized state energy at v_{s0}^*. This discontinuity is due to a discontinuous change in the order parameter at this magnetic potential strength, a result pointed out in Ref. 37 which will be discussed more below.

As seen in Fig. 5, the value of v_{s0}^* is mostly independent of the value of the coherence length. We present the following justification of that observation. The decrease in the quasiparticle energy by the classical spin is proportional to the overlap of the atomic-scale potential and the impurity site. The state is, aside from a r^{-2} falloff, extended over a volume given by the range of the exponential envelope of the localized state [Eq. (43)], $R = \pi\xi/2\sqrt{1-(\omega_0/\Delta_0)^2}$. Thus the overlap, and consequently the quasiparticle's energy reduction, is proportional to $v_s\Delta_0$. When this energy exceeds the energy required to create a quasiparticle (Δ_0), the ground state contains a quasiparticle. Hence v_s^* is approximately independent of Δ_0, and is determined primarily by the normal-state properties of the superconductor.

A more complete interpretation of the energetic diagram of Fig. 5 requires an understanding of the threshold energy to create a pair of excitations, such as in an optical experiment. The pairing is suppressed local to the impurity since an up-spin electron is attracted to the impurity and its time-reversed partner, the down-spin electron, is repelled. Therefore, the energy needed to break a pair and create a localized quasiparticle with angular momentum ℓ in the vicinity of the magnetic impurity, when $v_s < v_{s\ell}^*$, is reduced from $2\Delta_0$ to $\Delta_0 + \omega_\ell$. One member of the broken pair is a delocalized spin-down quasiparticle at the gap edge (with energy Δ_0). The other member of the broken pair is a *localized* spin-up quasiparticle with energy ω_ℓ. For $v_s > v_{s\ell}^*$ there is a spin-up quasiparticle with angular momentum ℓ in the ground state of the superconductor.[65] An essential point about the ground state of a superconductor containing classical magnetic impurities is that at $T=0$ when $v_s < v_{s\ell}^*$ (for all ℓ) the ground state is composed entirely of paired electrons. When $v_s > v_{s\ell}^*$ for any ℓ then the $T=0$ ground state contains localized quasiparticles as well as pairs and there are new low-energy excitations including the reformation of a pair as well as the excitation of a localized quasiparticle to a higher energy localized or continuum state (which requires an energy less than any $\Delta_0 + \omega_\ell$).

2. Local density of states

We now focus on our results for the local density of states near the impurity. Figures 6(a), 6(b), and 6(c) show LDOS results for $v_s = 0.5$, 0.875, and 1.75 respectively. They show the state split off from the continuum, with a larger electronlike amplitude than holelike amplitude [Fig. 6(a)], and then lower in energy with an increased electron/hole asymmetry [Fig. 6(b)]. Finally the larger peak becomes holelike [Fig.

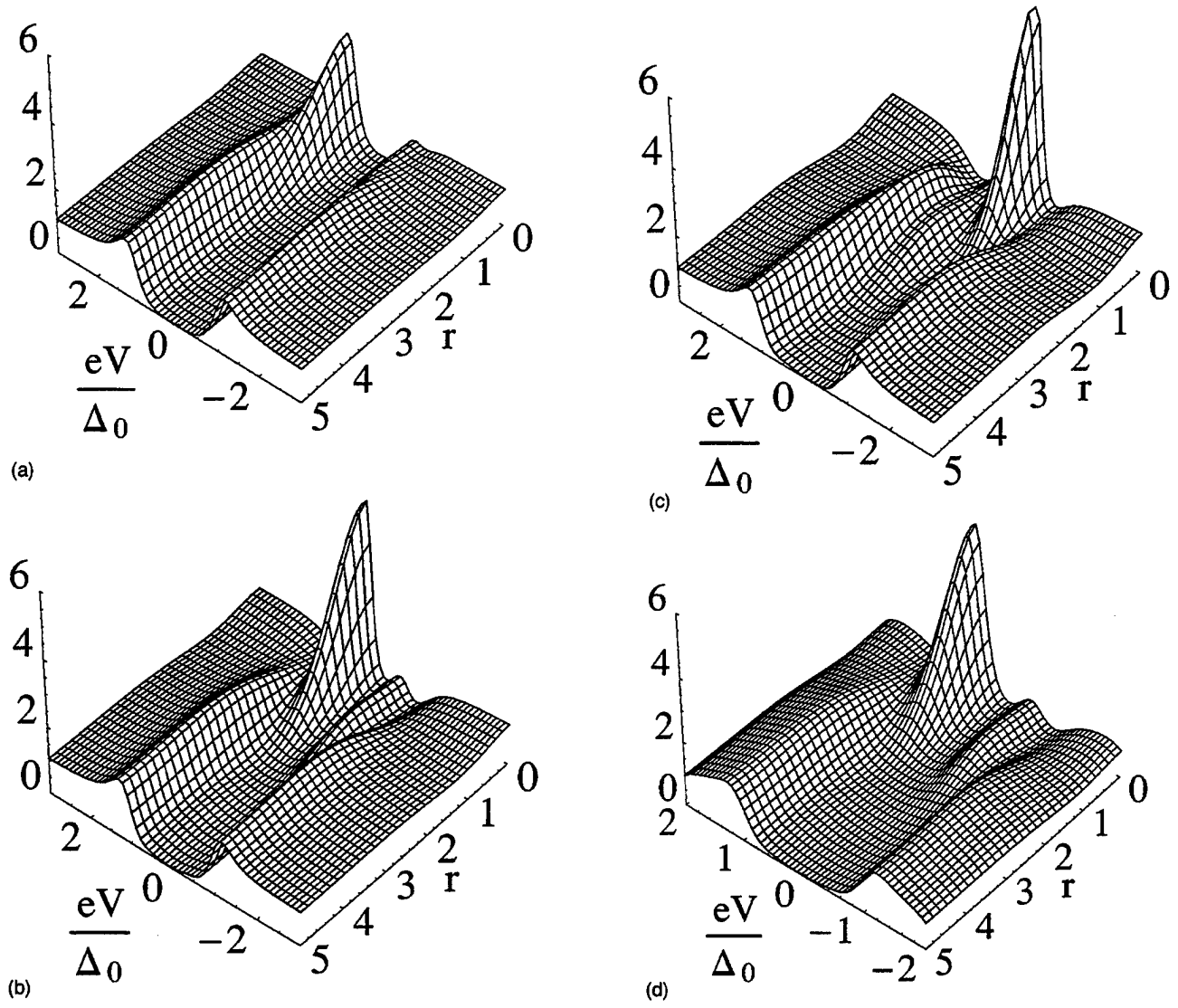

FIG. 6. Differential conductivity (LDOS) calculated around a magnetic impurity with (a) $v_s=0.5$, $\xi k_F=449$, (b) $v_s=0.875$, $\xi k_F=449$, (c) $v_s=1.75$, $\xi k_F=449$, (d) $v_s=0.875$, $\xi k_F=10$. All are calculated with $k_BT=0.13\Delta_0$ In the progression from (a) to (c) the asymmetry between the two peaks increases and the higher peak moves to lower energies, eventually becoming holelike. The LDOS is normalized by the normal-state's homogeneous DOS.

6(c)]. In all three cases the spectrum recovers to its bulk value within a few k_F^{-1}, due to the r^{-2} decay of the localized state (Eq. 43). The asymmetry between the electronlike and holelike peaks becomes more pronounced as v_s increases. We note that the larger peak is always associated with the spin-up band, whereas the other is associated with the spin-down band. Despite the apparent differences in peak size, the spatially integrated electron spectral weight of the quasiparticle is equal to the spatially integrated hole spectral weight. The localized quasiparticle is always half electron and half hole for all potentials examined here. For $v_s<v_{s0}^*$ the spin-up band amplitude is electronlike and the spin-down band amplitude is holelike. At v_{s0}^* (1.32 for a free-electron model of niobium), the spin-up component becomes holelike and the spin-down component becomes electronlike, as required by the change in the spin of the excitation.

Figure 6(d) shows the LDOS for a markedly different coherence length, $\xi=10k_F^{-1}$, and $v_s=0.875$. It is evaluated for the same value of Δ_0/k_BT as Figs. 6(a,b,c) and looks almost identical to Fig. 6(b). Since the localized state is broadened by temperature through Eq. (1), this is a manifestation of the proportionality of the spectral weight to $N_0\Delta_0$ [Eq. (43)]. Figure 7 shows the spectral weight at the origin for the $\ell=0$ state and for the $\ell=1$ state at its first maximum for $v_s=0.875$ as a function of the inverse of the coherence length, which is proportional to $N_0\Delta_0$. Figure 8 shows the spectral weight for $\xi=449k_F^{-1}$ as a function of v_s for the spin-up and spin-down poles at the origin for the $\ell=0$ state and at the first maximum for the $\ell=1$ state. It is clear that a nonmagnetic potential is not necessary to obtain an electron-hole asymmetry.

In Fig. 9 we show the asymmetry at the impurity as a function of v_s for two values of ξ—a long coherence length appropriate for niobium, and a short coherence length. From Fig. 7 it should be evident that the asymmetry is not sensitive to ξ. It is, however, predicted extremely well by the normal-state spin-up and spin-down band spectral weight asymmetry at the impurity (also shown in Fig. 9). We can therefore

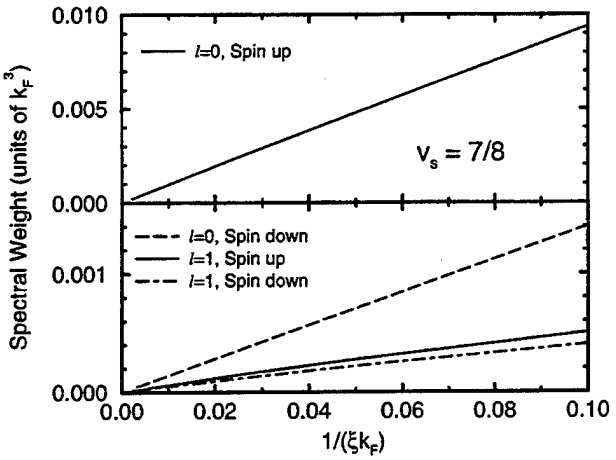

FIG. 7. Spectral weight at the impurity ($r=0$) for the first angular momentum channel, $\ell=0$, and at the first maximum for the second angular momentum channel, $\ell=1$, for poles in both the spin-up and spin-down bands, as a function of the inverse coherence length, showing a linear behavior. The magnetic potential strength is $v_s=0.875$.

conclude that as with the nonmagnetic impurity (Fig. 4), the spatial structure of the spectral weight of the localized state around a magnetic impurity is a normal-state property. We further show in Fig. 10 for $v_s=0.875$ the $\ell=0$, spin-up band and spin-down band projections of the normal-state spectral weight to compare with the localized state spin-up band and spin-down band spectral weights for two values of ξk_F. The normal-state and long-coherence length calculation are practically indistinguishable. The insets show $r^2A(r)$, which removes the rapid power-law decay of the state. The localized states for all angular momenta ℓ will decay as the power law r^{-2}. For the short-coherence length calculation the effect of an exponential envelope is also visible. In the analytic result the exponential envelope should have a range $R=\pi\xi/2\sqrt{1-(\omega_0/\Delta_0)^2}$, which corrects to better than 1%

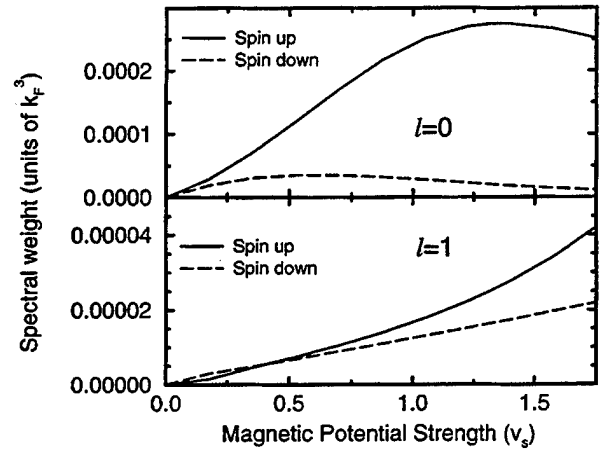

FIG. 8. Spectral weight at the impurity ($r=0$) for the $\ell=0$ channel for $\xi k_F=449$ as a function of magnetic potential strength for poles in both the spin-up and spin-down bands. The spectral weight in the spin-up band pole of the $\ell=0$ localized state saturates at large v_s. Also shown are the spectral weights at the first maximum for the $\ell=1$ localized states.

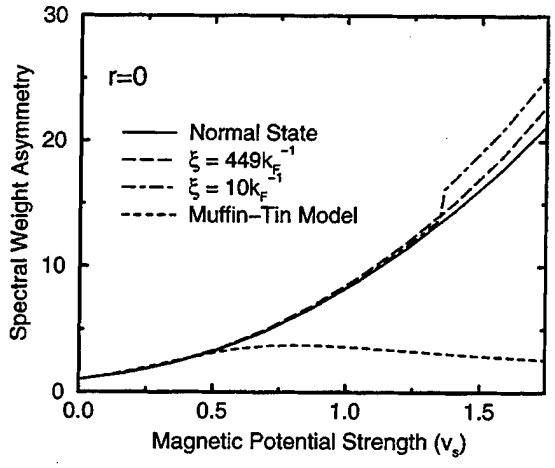

FIG. 9. Ratio of the spectral weight in the spin-up band and in the spin-down band at the impurity ($r=0$) as a function of magnetic potential strength. This is plotted for the normal-state $\ell=0$ projected Green's functions (solid line) as well as for the localized states for niobium ($\xi k_F=449$, long dashed line), for $\xi k_F=10$ (dot-dashed line), and for the muffin-tin model. The muffin-tin model is only successful for $v_s<0.5$, but that is due to a breakdown in describing the normal state. The normal-state electronic structure is a good predictor of the superconductor's electronic structure for the entire range of v_s.

the discrepancy in Fig. 10. The power-law falloff and exponential envelope can be seen directly from Eqs. (15) and (43).

We can summarize these comments with a general equation, similar in concept to that for the nonmagnetic impurity, Eq. (45). That is, for a localized quasiparticle state of spin σ', the spectral weight of a localized state with angular momentum ℓ would be

$$A_\sigma^{\sigma'}(\mathbf{r};\omega_\ell)=BA_{n\sigma}(\mathbf{r},\ell)\exp\left[-\left(\frac{2r}{\pi\xi}\right)\sqrt{1-\left(\frac{\omega_\ell}{\Delta_0}\right)^2}\right]\times\delta(\omega-\sigma\sigma'\omega_\ell), \tag{47}$$

where B is a normalization factor so that the spectral weight of the state integrates to one, and $A_{n\sigma}(\mathbf{r},\ell)$ is the angular momentum ℓ projection of the *normal*-state spectral weight in the spin σ band. We note that for small r there is an approximate relationship between the superconducting state's spectral weight and the normal state's spectral weight in each spin band,

$$\frac{1}{2E}\int_{-E}^{E}d\omega A_\sigma(\mathbf{r};\omega)=A_{n\sigma}(\mathbf{r}), \tag{48}$$

where $\Delta_0\ll E\ll\epsilon_F$. This, in connection with Eq. (47), implies a dependence on the normal-state structure of the continuum spectral weight around the magnetic impurity.

3. *Structure of the inhomogeneous order parameter*

We now return to the structure of $\Delta(\mathbf{x})$. This quantity, which is not directly observable, formed the focus of several investigations of the local structure around a magnetic impurity. The oscillation of the order parameter around a mag-

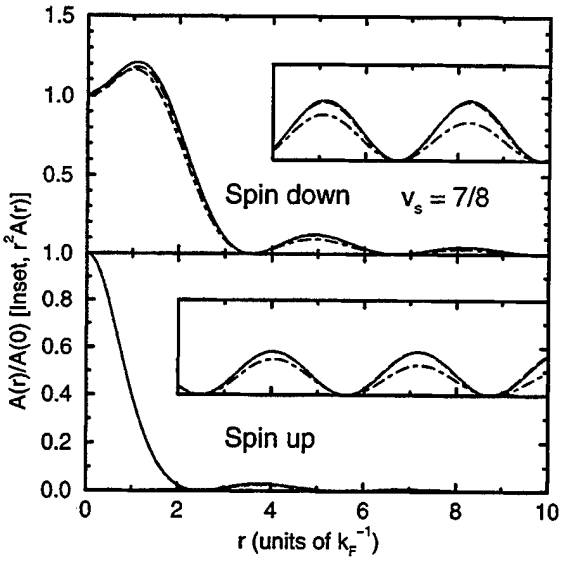

FIG. 10. Spectral weights for $\ell=0$ localized state in the up and down bands for $v_s=0.875$. The solid line is the normal state $\ell=0$ projected spectral weight, the long-dashed line is the localized state in a superconductor with $\xi k_F=449$, and the dot-dashed line is for $\xi k_F=10$. The inset shows the spectral weight multiplied by r^2 to remove the algebraic decay. The normal-state and long-coherence length results are practically indistinguishable. The deviation shown in the short-coherence length superconductor's spectral weight is fit to within 1% by the exponential decay factor described in the text. Hence the spatial structure of the spectral weight of the superconductor's localized state is well-predicted by the normal-state spectral weight.

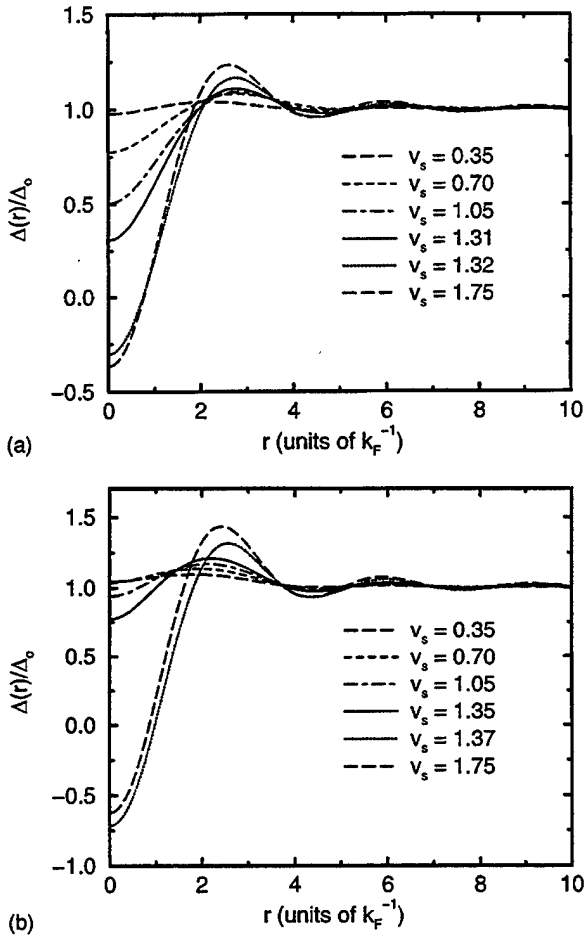

FIG. 11. Order parameters as a function of distance from the impurity r calculated for several magnetic potential strengths for (a) $\xi k_F=449$ and (b) $\xi k_F=10$. In both cases there is a discontinuous change in the order parameter when v_s passes through the critical strength v_{s0}^*.

netic impurity was first evaluated without self-consistency.[21–23] A self-consistent calculation of the order parameter at the impurity and very far away for *weak* impurity potentials was done by Schlottmann.[24]

As shown in Fig. 1, for large values of v_s, $\Delta(\mathbf{x}=\mathbf{0})<0$. Sign changes in Δ, as seen in pair tunneling, have been suggested for magnetic impurities in the barriers of Josephson junctions.[66–68] The sign change in $\Delta(\mathbf{0})$ occurs (at $T=0$) precisely at v_{s0}^*. Due to the spin and frequency symmetries of Eqs. (6)–(13), the anomalous spectral weight Im $F(\mathbf{r},\mathbf{r},\omega)$ associated with the spin-up pole is always equal and opposite to the anomalous spectral weight associated with the spin-down pole. As the pole in the spin-up band goes from electronlike ($\omega>0$) to holelike ($\omega<0$) and the pole in the spin-down band goes from holelike to electronlike the contribution to $\Delta(\mathbf{0})$ changes sign abruptly at $T=0$. The $\Delta(\mathbf{r})$ resulting from several values of v_s and two values of the coherence length are shown in Fig. 11(a,b). The discontinuity at v_{s0}^* is more pronounced for shorter coherence lengths since the localized state's spectral weight is more concentrated at the impurity [Eq. (47)]. $\Delta(\mathbf{0})$ as a function of v_s is shown in Fig. 12 for two values of the coherence length. At $T>0$ the transition would be smoothed somewhat.

The behavior of $\Delta(\mathbf{0})$ as a function of v_s comes from the introduction at v_{s0}^* of a quasiparticle into the ground state of the system. The spin-up quasiparticle localized near the impurity in the ground state suppresses the local order parameter. For time-reversal invariant potentials one cannot make $\Delta(\mathbf{r})$ negative by inserting a single quasiparticle, since the suppression from one quasiparticle is cancelled by the lack of suppression from its unexcited Kramers doublet partner. For a spin-dependent potential, however, the anomalous spectral weight near the impurity may be almost entirely contributed by the single low-energy localized state. When a quasiparticle is present in the ground state, the ground state has spin-$\frac{1}{2}$ up[65,38] and a negative $\Delta(\mathbf{r})$.[37] Exciting the low-energy state for $v_s>v_{s0}^*$ removes the spin-up quasiparticle, and therefore *increases* $\Delta(\mathbf{0})$, whereas excitation of quasiparticles typically reduces $\Delta(\mathbf{x})$ (which is the case for $v_s<v_{s0}^*$). Also, exciting the low-energy state alone *reduces* the total spin of the superconductor.

The behavior of $\Delta(\mathbf{r})$ for large r has not been evaluated numerically. We expect the contribution of the localized state to decay with a length determined by the exponential expression in Eq. (43), $R_{\rm loc}=\pi\xi/2\sqrt{1-(\omega_0/\Delta_0)^2}$. The contributions from the continuum states at a given ω have a ω-dependent spatial oscillation and decay as r^{-2}. When those contributions are integrated from Δ_0 to ω_D, one obtains a $r^{-3}\sin(r/R_{\rm cont})$ decay, where $R_{\rm cont}\sim\xi\Delta_0/\omega_D$. Since $R_{\rm loc}>R_{\rm cont}$ it would be possible to have first a $r^{-2}\exp(-r/R_{\rm loc})$ decay, followed by an oscillatory r^{-3} de-

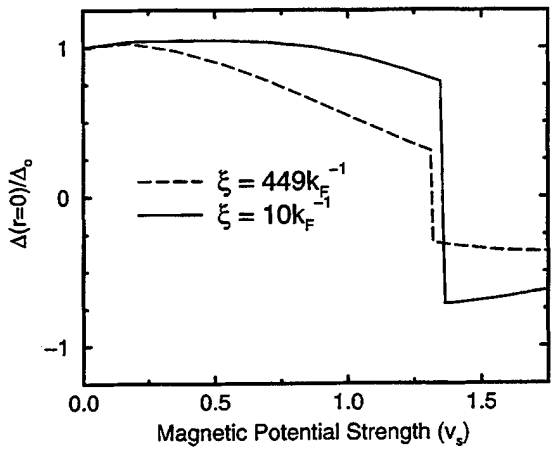

FIG. 12. Order parameters at the impurity ($r=0$) as a function of magnetic potential strength v_s for two values of the coherence length. The discontinuity in the order parameter at v_{s0}^* is much larger for the short-coherence-length superconductor.

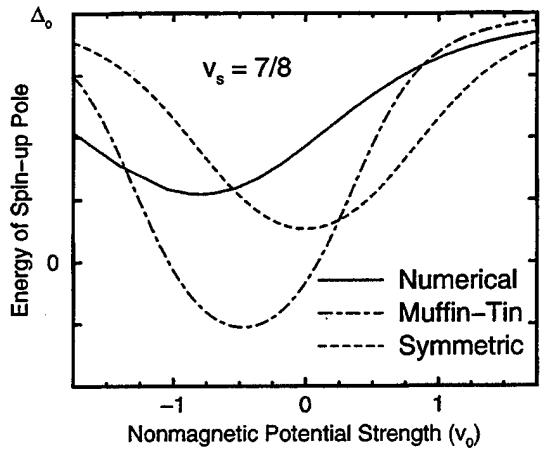

FIG. 14. The energy of the spin-up pole is shown as a function of nonmagnetic potential strength for $v_s=0.875$ and $\xi k_F=449$. The energy of the spin-down pole is just the negative of the energy of the spin-up pole. The analytic models do not perform particularly well in reproducing the pole energies, although the muffin-tin model does show a similar asymmetry around $v_0=0$ to the numerical calculations.

cay. The oscillatory r^{-3} decay was pointed out in Ref. 24. We emphasize that, although the order parameter appears to recover to its bulk value over a length scale much shorter than the coherence length, this is again a manifestation of the r^{-2} behavior of the normal and anomalous spectral weights. When $\delta\Delta(r)$ is multiplied by the surface area of the sphere at radius r, one finds that the order parameter's recovery length is on the order of the coherence length.

C. Combined magnetic and nonmagnetic potentials

We now discuss the addition of a nonmagnetic potential to the magnetic potential. It has been suggested[38] that introducing a v_0 with a v_s will provide electron-hole asymmetry. We find that it does change the asymmetry, which we show in Fig. 13 for a particular v_s, but that once again this is a normal-state property. The relationship between the normal-state spectral weights and the superconducting-state spectral weights of Eq. (47) still holds. Introducing v_0 also alters the localized-state energies [see Eq. (40)], which we show in Fig. 14 for $v_s=0.875$ and $\xi k_F=449$. The presence of a nonmagnetic potential may affect the value of v_{s0}^*.[38] We show in Fig. 15 a partial diagram of the ground state as a function of the parameters v_s and v_0 for $\xi k_F=449$. We note that the boundary between the two ground states is not shifted much

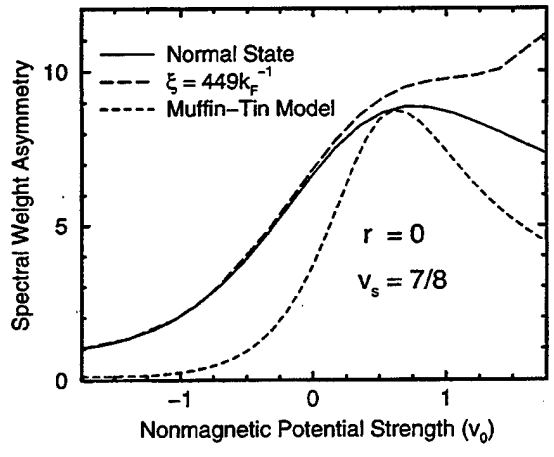

FIG. 13. Ratio of the spectral weight at the impurity in the spin-up band to the spin-down band for $v_s=0.875$ and $\xi k_F=449$ as the nonmagnetic potential v_0 varies. In a similar result to that seen in Fig. 9, the normal-state spectral weights are good predictors of the superconducting state's spectral weight. We note that the curves are not symmetrical around $v_0=0$, which results from a realistic band structure without particle-hole symmetry.

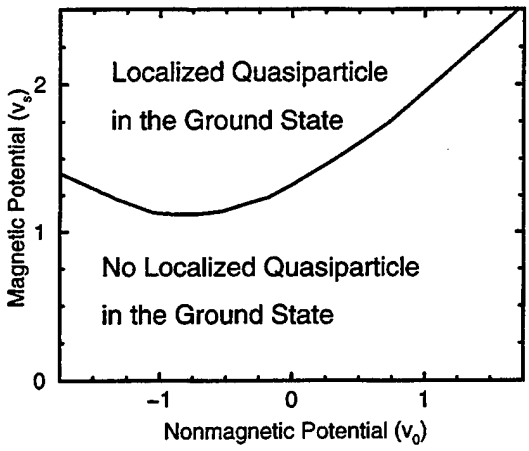

FIG. 15. Calculated boundary between two ground states around the magnetic impurity for $\xi k_F=449$. For a large enough magnetic impurity strength a quasiparticle is bound in the ground state. The minimum magnetic impurity strength depends on the nonmagnetic impurity strength. For still larger magnetic impurity strengths there would be ground states with more than one bound quasiparticle.

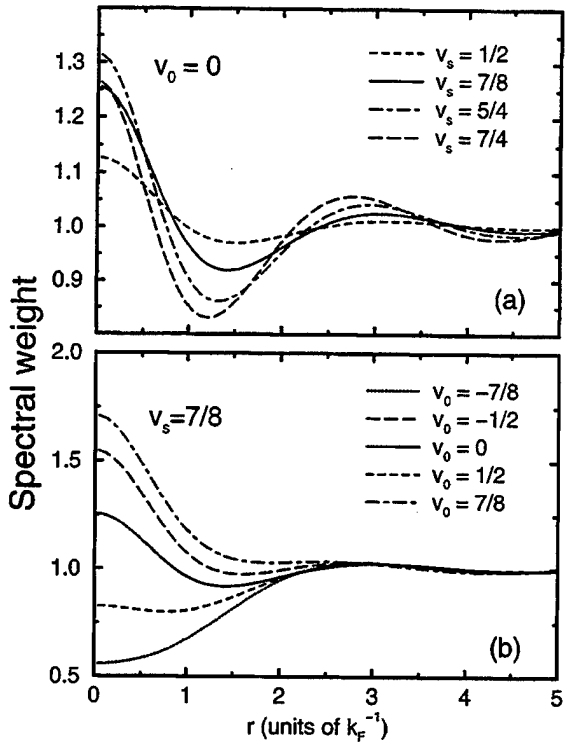

FIG. 16. Spectral weights in the normal state as functions of the distance from the impurity for several combinations of magnetic and nonmagnetic potentials (a) only a magnetic potential, and (b) a fixed magnetic potential $v_s = 0.875$ and a varying nonmagnetic potential. By making measurements around the impurity in the normal state (or integrating the superconductor's spectrum over a frequency much larger than Δ_0), information about the structure of the impurity may be obtained.

from $\xi k_F = 449$ to $\xi k_F = 10$, hence the condensation energy is not very significant in determining this boundary.

D. Connection to normal-state *dI/dV* spectra

The normal state may provide some guidance for attempts to extract impurity potentials in the superconducting state from STM measurements. Figure 16 shows *normal-state* dI/dV's for various potentials. These curves should also represent the frequency-averaged spectral weight measured in the superconducting state [see Eq. (48)].[70]

The enhancement or suppression of spectral weight near the origin is particularly sensitive to v_0. A measurement of this quantity, the energy of the localized state and the asymmetry of the electron and hole amplitudes at the impurity overconstrains v_0 and v_s, given an assumption of the shape of the potential. To extract information about the potential's detailed shape would require a fitting procedure using the differential conductivity at various positions. If, for some reason, the spin-down amplitude were too small to measure, it may remain possible to constrain the potential strength using the frequency-integrated spectral weight and the localized-state energy.

It seems appropriate to mention again the tendency to normalize spectra according to the LDOS measured at energies much larger than Δ_0. Since the normal-state LDOS near

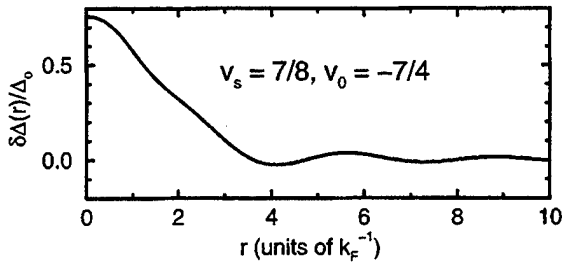

FIG. 17. The change in order parameter around an attractive nonmagnetic potential combined with a magnetic potential for $\xi k_F = 449$. The order parameter is larger at the impurity than in the homogeneous superconductor, yet there exists a localized state in the gap.

the impurity changes substantially in the presence of magnetic or nonmagnetic impurities, an experiment performed using such a normalization procedure would yield impurity parameters of questionable validity.

E. Relationship to Ginzburg-Landau theory

Although Ginzburg-Landau theory has a wide range of applicability, it fails to describe the electronic structure near these impurities. Shown in Fig. 17 is the order parameter for a mixed magnetic and nonmagnetic impurity ($v_s = 7/8$, $v_0 = -7/4$, and $\xi k_F = 449$). The order parameter is everywhere larger than in the homogeneous superconductor, however, the presence of a localized state within the gap indicates that superconductivity has been weakened around the impurity. Since the Ginzburg-Landau theory focuses on the order parameter and ignores the quasiparticle structure, a Ginzburg-Landau perspective would incorrectly predict an enhancement of superconductivity in the region.

F. Pairing suppression

The pairing potential, $\gamma(\mathbf{x})$ in Eq. (14), may also have spatial structure. When this parameter is changed it induces a

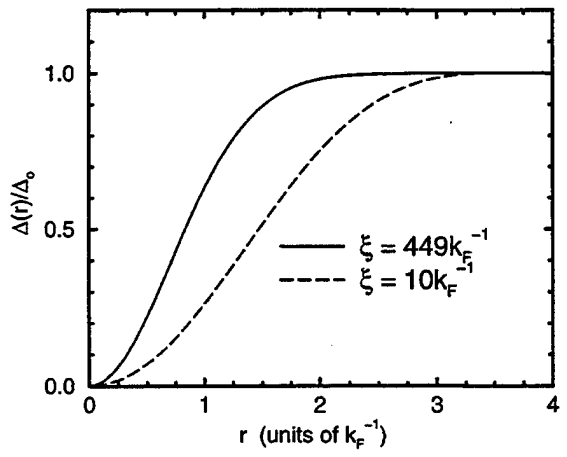

FIG. 18. Order parameter as a function of distance r from a defect with a suppressed pair potential, but no single-particle potential.

change in the order parameter which produces an off-diagonal potential felt by the quasiparticles. We set $v_s = v_0 = 0$ so that there is no magnetic or nonmagnetic potential to compete with the order-parameter change. Figure 18 shows the order parameter around a short-range suppression,

$$\gamma(\mathbf{x}) = [1 - e^{-(k_F r)^2}]\gamma_0 , \tag{49}$$

for two values of the coherence length. The order parameter is strongly suppressed and since $\gamma(\mathbf{0}) = 0$, $\Delta(\mathbf{0}) = 0$. For long coherence lengths, this change in the order parameter has no effect on the local density of states [shown in Fig. 19(a)]. It is possible to localize quasiparticle states, however, at shorter coherence lengths. These can produce features in the local density of states which are visible. One such case is shown in Fig. 19(b). The energy of the localized state is $\omega_0 = (1 - 4\times 10^{-3})\Delta_0$. Whereas a nonmagnetic potential changes the local density of states without significantly changing the energy gap, a pairing suppression has a very weak effect on both, especially in the long-coherence length limit.

V. STRONG-COUPLING AND ANISOTROPIC ORDER PARAMETERS

A few observations are in order concerning the extension of this formalism to systems where the homogeneous order parameter has important frequency or spatial structure. The Gor'kov equation [Eq. (6)] changes due to the more general form for the off-diagonal potential originating from the order parameter. Taking this opportunity to generalize,

$$\int d\mathbf{x}''d\mathbf{x}'''[\delta(\mathbf{x}-\mathbf{x}'')\delta(\mathbf{x}''-\mathbf{x}''') - \mathbf{g}(\mathbf{x},\mathbf{x}'';\omega)\mathbf{V}(\mathbf{x}'',\mathbf{x}''';\omega)]\mathbf{G}(\mathbf{x}''',\mathbf{x}';\omega) = \mathbf{g}(\mathbf{x},\mathbf{x}';\omega), \tag{50}$$

where

$$\mathbf{V}(\mathbf{x}'',\mathbf{x}''';\omega) = \begin{pmatrix} V_{e\uparrow}(\mathbf{x}'';\omega)\delta(\mathbf{x}''-\mathbf{x}''') & \delta\Delta(\mathbf{x}'',\mathbf{x}''';\omega) \\ \delta\Delta(\mathbf{x}'',\mathbf{x}''';\omega) & V_{h\uparrow}(\mathbf{x}'';\omega)\delta(\mathbf{x}''-\mathbf{x}''') \end{pmatrix}. \tag{51}$$

The diagonal terms are general potentials, possibly frequency-dependent, effective on spin-up electrons ($V_{e\uparrow}$) and spin-up holes ($V_{h\uparrow}$) for $\omega > 0$. Since this potential is diagonal in frequency, as is the Gor'kov equation, the frequency structure of the order parameter does not add any additional complication to numerically solving the Gor'kov equation. However, the addition of spatial structure to the pairing has added another integral over the volume to the Gor'kov equation, and thus dramatically increased the size of the matrix which needs to be inverted. Fortunately, the range of the order parameter in $|\mathbf{x}-\mathbf{x}'|$ is truncated by the range of the pairing interaction. For the isotropic-gap superconductor we have considered for most of this paper, the effective pairing interaction is modeled by a δ function in space. It is possible to obtain anisotropic order parameters, including the

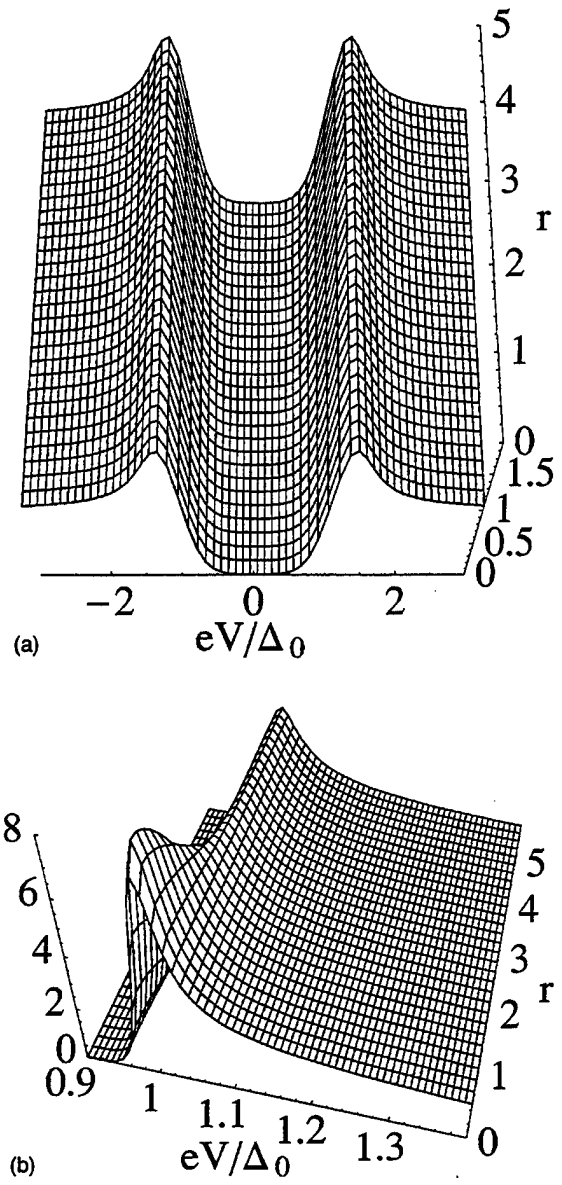

FIG. 19. Differential conductivity (LDOS), normalized by the normal-state's homogeneous DOS, around a defect with a suppressed pair potential, but no single-particle potential. (a) $\xi k_F = 449$, $k_B T = \Delta_0/7.5$—there is no evidence of any change in the spectrum due to the order parameter suppression shown in Fig. 18. (b) $\xi k_F = 10$, $k_B T = \Delta_0/100$—a localized state very near the continuum enhances the continuum edge seen in tunneling near the defect.

d-wave order parameters possibly appropriate for high-temperature superconductors, merely by considering pairing with nearest neighbors on a square tight-binding lattice. This model has been implemented with the BdG formalism for nonmagnetic impurities,[32–35] magnetic impurities,[38] and vortices[71] in d-wave superconductors. When formulated on a lattice the addition of nearest-neighbor pairing multiplies the rank of the matrix $\mathbf{M}^{n\to n}(\omega)$ by $1+z$, where z is the coordination number of the lattice.

The order parameter's frequency dependence complicates the self-consistency equation [Eq. (14)]. It must now be solved for each frequency:

$$\Delta(\mathbf{r},\mathbf{r}';\omega)Z(\mathbf{r},\mathbf{r}';\omega)=\int_{-\infty}^{\infty}d\epsilon n(\epsilon)[\mathrm{Re}\,F(\mathbf{r},\mathbf{r}';\epsilon)]\times(K_+(\mathbf{r},\mathbf{r}';\epsilon,\omega)-U_c),$$

$$\omega[1-Z(\mathbf{r},\mathbf{r}';\omega)]=\int_{-\infty}^{\infty}d\epsilon n(\epsilon)[\mathrm{Re}\,G(\mathbf{r},\mathbf{r}';\epsilon)]\times K_-(\mathbf{r},\mathbf{r}';\epsilon,\omega), \quad (52)$$

where $K_\pm$ are kernals of the pairing interaction and are different for each mechanism of superconductivity. They can be determined from the homogeneous solution. U_c is a Coulomb factor. Z, the quasiparticle weight, is solved for self-consistently. Incorporating these strong coupling effects allows a determination of the effect of the frequency dependence of the pairing interaction on the electronic structure around a defect. While selecting the particular location of the STM tip is similar to selecting the momentum of the quasiparticles of interest, selecting the STM voltage indicates which order-parameter frequency one wishes to probe.

VI. SUMMARY

The local electronic structure around a defect reflects both the properties of the defect and the medium it is embedded in. For a strong nonmagnetic or magnetic impurity in a superconductor, the distortion of the normal-state properties by the strong impurity plays a vital role in the response of the superconducting medium. The LDOS for the inhomogeneous superconductor can be related to the LDOS for the inhomogeneous normal metal via equations like Eqs. (45) and (47). In the case of a nonmagnetic impurity with no localized states around it, the LDOS for the inhomogeneous superconductor is merely the normalized LDOS for the inhomogeneous normal metal multiplied by the homogeneous superconductor's density of states. This should suggest some caution regarding the method used to normalize STM spectra taken at different places on a superconductor's surface.

For the case of a localized state (such as around a magnetic impurity) with angular momentum ℓ, the LDOS for the state is the angular-momentum-ℓ-projected LDOS of the inhomogeneous normal metal multiplied by a decaying exponential whose range is determined by the energy of the localized state. Since the spin-up band LDOS in the normal state differs from the spin-down band LDOS in the normal state, the electronlike pole of the localized quasiparticle will have different spatial structure than the holelike pole of the localized quasiparticle.

The self-consistent calculations described here have been performed with a powerful Koster-Slater technique which allows the Gor'kov equation to be solved in principle exactly. Although we have only presented calculations for weak-coupling isotropic order parameters within a free-electron model, we have formulated the extension of this technique to strong-coupling pairing and general band structures and order-parameter symmetries.

ACKNOWLEDGMENTS

We wish to thank C. M. Lieber for helpful conversations. M.E.F. wishes to acknowledge the Office of Naval Research's Grant No. N00014-96-1-1012. J.M.B. wishes to acknowledge financial support from the N.R.C.

APPENDIX

The expansion of the Green's functions of Eq. (15) suitable for a three-dimensional spherically symmetric situation are detailed here. The homogeneous Green's functions depend on $\mathbf{r}$ and $\mathbf{r}'$ through r, r', and $\cos\gamma=(\mathbf{r}\cdot\mathbf{r}')/rr'$. Then the Green's functions can be expanded in Legendre polynominals $P_\ell(\cos\gamma)$.

$$g(\mathbf{r},\mathbf{r}';\omega)=g(r,r',\cos\gamma;\omega)=\frac{2\ell+1}{4\pi}\sum_\ell g_\ell(r,r';\omega)P_\ell(\cos\gamma) \quad (A1)$$

and

$$g_\ell(r,r';\omega)=2\pi\int_{-1}^{1}P_\ell(x)g(r,r',x;\omega). \quad (A2)$$

Evaluating Eq. (A2) for both the normal and anomalous Green's functions of Eq. (15) yields

$$g_\ell(r,r';\omega)=-\frac{\pi^3}{\sqrt{rr'}}\left[i\left(1+\frac{\omega}{\sqrt{\omega^2-1}}\right)J_{\ell+1/2}(\{1+\sqrt{\omega^2-1}/\xi\}r^<)H^{(1)}_{\ell+1/2}(\{1+\sqrt{\omega^2-1}/\xi\}r^>)\right.$$
$$\left.-\left(1-\frac{\omega}{\sqrt{\omega^2-1}}\right)J_{\ell+1/2}(\{1-\sqrt{\omega^2-1}/\xi\}r^<)H^{(2)}_{\ell+1/2}(\{1-\sqrt{\omega^2-1}/\xi\}r^>)\right], \quad (A3)$$

$$f_\ell(r,r';\omega)=-\frac{i\pi^3}{\sqrt{rr'}}\frac{1}{\sqrt{\omega^2-1}}[J_{\ell+1/2}(\{1+\sqrt{\omega^2-1}/\xi\}r^<)H^{(1)}_{\ell+1/2}(\{1+\sqrt{\omega^2-1}/\xi\}r^>)$$
$$+J_{\ell+1/2}(\{1-\sqrt{\omega^2-1}/\xi\}r^<)H^{(2)}_{\ell+1/2}(\{1-\sqrt{\omega^2-1}/\xi\}r^>)], \quad (A4)$$

where J_ℓ, $H^{(1)}_\ell$, and $H^{(2)}_\ell$ are standard Bessel functions, $r^<$ ($r^>$) is the smaller (larger) of r and r', ω is in units of Δ_0 and r and r' are in units of k_F^{-1}. The Green's functions are in units of N_0.

The Gor'kov equation, Eq. (6), can now be written in a form diagonal in ℓ,

$$\mathbf{G}_\ell(r,r';\omega)=\mathbf{g}_\ell(r,r';\omega)+\int_0^\infty r_n^2dr_n\mathbf{g}_\ell(r,r_n;\omega)\mathbf{V}(r_n)\mathbf{G}_\ell(r_n,r';\omega). \quad (A5)$$

Thus the three-dimensional integral has been reduced to a one-dimensional radial integral. Since the numerical inversion procedure depends on inverting a matrix whose rank is proportional to the number of spatial points considered, this reduction to a one-dimensional integral dramatically increases the speed of this calculation over a calculation for a three-dimensional potential which is not spherically symmetric.

[1] M. Ma and P. A. Lee, Phys. Rev. B **32**, 5658 (1985).

[2] J. Bardeen, L. N. Cooper, and J. R. Schrieffer, Phys. Rev. **106**, 162 (1957); **108**, 1175 (1957).

[3] P. W. Anderson, Phys. Rev. Lett. **3**, 325 (1959).

[4] B. T. Matthias, H. Suhl, and E. Corenzwit, Phys. Rev. Lett. **1**, 92 (1958).

[5] C. Herring, Physica (Amsterdam) **24**, S 184 (1958).

[6] H. Suhl and B. T. Matthias, Phys. Rev. **114**, 977 (1959).

[7] L. Yu, Acta Phys. Sin. **21**, 75 (1965).

[8] H. Shiba, Prog. Theor. Phys. **40**, 435 (1968).

[9] A. I. Rusinov, JETP Lett. **9**, 85 (1969).

[10] J. Zittartz and E. Müller-Hartmann, Z. Phys. **232**, 11 (1970).

[11] E. Müller-Hartmann and J. Zittartz, Z. Phys. **234**, 58 (1970).

[12] E. Müller-Hartmann and J. Zittartz, Phys. Rev. Lett. **26**, 428 (1971).

[13] O. Sakai *et al.*, J. Phys. Soc. Jpn. **62**, 318 (1993).

[14] A. A. Abrikosov and L. P. Gor'kov, Zh. Eksp. Teor. Fiz. **39**, 1781 (1962) [Sov. Phys. JETP **12**, 1243 (1961)].

[15] F. Marsiglio, J. P. Carbotte, A. Puchkov, and T. Timusk, Phys. Rev. B **53**, 9433 (1996).

[16] M. Jarrell, D. S. Sivia, and B. Patton, Phys. Rev. B **42**, 4804 (1990); W. Chung and M. Jarrell, Phys. Rev. Lett. **77**, 3621 (1996).

[17] R. Prange, Phys. Rev. **129**, 2495 (1963).

[18] J. P. Hurault, J. Phys. (Paris) **26**, 252 (1965).

[19] P. W. Anderson and H. Suhl, Phys. Rev. **116**, 898 (1959).

[20] J. Friedel, Nuovo Cimento Suppl. **7**, 287 (1958).

[21] T. Tsuzuki and T. Tsuneto, Prog. Theor. Phys. **37**, 1 (1967).

[22] J. Heinrichs, Phys. Rev. **168**, 451 (1968).

[23] R. Kummel, Phys. Rev. B **6**, 2617 (1972).

[24] P. Schlottmann, Phys. Rev. B **13**, 1 (1976).

[25] A. L. Fetter, Phys. Rev. **140**, A1921 (1965).

[26] J. M. Byers, M. E. Flatté, and D. J. Scalapino, Phys. Rev. Lett. **71**, 3363 (1993).

[27] Y. Hasegawa and P. Avouris, Phys. Rev. Lett. **71**, 1071 (1993).

[28] M. F. Crommie, C. P. Lutz, and D. M. Eigler, Nature (London) **363**, 524 (1993).

[29] C. H. Choi, Phys. Rev. B **50**, 3491 (1994).

[30] M. I. Salkola, A. V. Balatsky, and D. J. Scalapino, Phys. Rev. Lett. **77**, 1841 (1996).

[31] See, e.g., P. G. de Gennes, *Superconductivity of Metals and Alloys* (Addison-Wesley, Reading, MA, 1989).

[32] T. Xiang and J. M. Wheatley, Phys. Rev. B **51**, 11 721 (1995).

[33] M. Franz, C. Kallin, and A. J. Berlinsky, Phys. Rev. B **54**, R6897 (1996).

[34] Y. Onishi, Y. Ohashi, Y. Shingaki, and K. Miyake, J. Phys. Soc. Jpn. **65**, 675 (1996).

[35] M. E. Flatté and J. M. Byers (unpublished).

[36] When the calculation is performed self-consistently, as will be described later in the paper, a very weakly localized state may exist around a nonmagnetic impurity.

[37] M. E. Flatté and J. M. Byers, Phys. Rev. Lett. **78**, 3761 (1997).

[38] M. Salkola, A. Balatsky, and J. R. Schrieffer, Phys. Rev. B **55**, 12 648 (1997).

[39] A. Yazdani, B. A. Jones, C. P. Lutz, M. F. Crommie, and D. M. Eigler, Science **275**, 1767 (1997).

[40] C. Caroli, P. G. de Gennes, and J. Matricon, Phys. Lett. **9**, 307 (1964).

[41] J. Bardeen, R. Kümmel, A. E. Jacobs, and L. Tewordt, Phys. Rev. **187**, 556 (1969).

[42] See, A. A. Abrikosov, L. P. Gor'kov, and I. E. Dzyaloshinski, *Methods of Quantum Field Theory in Statistical Physics* (Dover, New York, 1963).

[43] G. F. Koster and J. C. Slater, Phys. Rev. **95**, 1167 (1954).

[44] G. F. Koster and J. C. Slater, Phys. Rev. **96**, 1208 (1954).

[45] E. W. Montroll and R. B. Potts, Phys. Rev. **100**, 525 (1955).

[46] E.g., M. Jaros, *Deep Levels in Semiconductors* (Adam Hilger, Bristol, 1982).

[47] T. Wolfram and J. Callaway, Phys. Rev. **130**, 2207 (1963).

[48] V. L. Ginzburg and L. D. Landau, J. Exp. Theor. Phys. **20**, 1064 (1950).

[49] G. Eilenberger, Z. Phys. **214**, 195 (1968).

[50] H. F. Hess, R. B. Robinson, R. C. Dynes, J. M. Valles, Jr., and J. V. Waszczak, Phys. Rev. Lett. **62**, 214 (1990); J. Vac. Sci. Technol. A **8**, 450 (1990).

[51] J. D. Shore, M. Huang, A. T. Dorsey, and J. P. Sethna, Phys. Rev. Lett. **62**, 3089 (1989).

[52] A. W. Overhauser and L. L. Daemen, Phys. Rev. Lett. **62**, 1691 (1989).

[53] L. L. Daemen and A. W. Overhauser, Phys. Rev. B **40**, 10 778 (1989).

[54] F. Gygi and M. Schlüter, Phys. Rev. B **41**, 822 (1990).

[55] F. Gygi and M. Schlüter, Phys. Rev. B **43**, 7609 (1991).

[56] R. Corcoran, P. Meeson, Y. Onuki, P.-A. Probst, M. Springford, K. Takita, H. Harima, G. Y. Guo, and B. L. Gyorffy, J. Phys.: Condens. Matter **6**, 4479 (1994).

[57] F. Guinea and Yu. Pogorelov, Phys. Rev. Lett. **74**, 462 (1995).

[58] H. Hess, R. B. Robinson, and J. V. Waszczak, Phys. Rev. Lett. **64**, 2711 (1990).

[59] F. Gygi and M. Schlüter, Phys. Rev. Lett. **65**, 1820 (1990).

[60] Topological defects, such as vortices, can be different.

[61] See, J. R. Schrieffer, *Theory of Superconductivity* (Benjamin-Cummings, Reading, MA, 1983).

[62] V. Ambegaokar and A. Griffin, Phys. Rev. **137**, A1151 (1965).

[63] Unlike the case of a quantum spin, there is no qualitative difference between ferromagnetic and antiferromagnetic coupling for the classical spin. We therefore do not discuss the orientation of the impurity spin, but merely define a low-energy direction for the quasiparticle spin.

[64] $k_F = 1.18$ Å^{-1} for a free-electron model and $\xi = 380$ Å.

[65] A. Sakurai, Prog. Theor. Phys. **44**, 1472 (1970).

[66] B. I. Spivak and S. A. Kivelson, Phys. Rev. B **43**, 3740 (1991).

[67] S. V. Kuplevakhskii and I. I. Fal'ko, Fiz. Nizk. Temp. **10**, 691 (1984) [Sov. J. Low Temp. Phys. **10**, 361 (1984)].

[68]L. N. Bulaevski, V. V. Kuzii, and A. Sobyanin, Pis'ma Zh. Eksp. Teor. Fiz. **47**, 314 (1977) [JETP Lett. **25**, 290 (1977)].

[69]We note that, subsequent to Ref. 37, a calculation in Ref. 39 also found asymmetry without a nonmagnetic potential.

[70]This might be useful if there is a technical problem with making measurements in the normal state.

[71]P. I. Soininen, C. Kallin, and A. J. Berlinsky, Phys. Rev. B **50**, 13 883 (1994).

Impurity Effects on Quasiparticle c-Axis Planar Tunneling and STM Spectra in High-T_c Cuprates

Michael E. Flatté[1] and Jeff M. Byers[2]
[1]*Department of Physics and Astronomy, University of Iowa, Iowa City, Iowa 52242*
[2]*Materials Physics, Naval Research Laboratory, Washington, D.C. 20375*
(Received 8 December 1997)

We present self-consistent calculations of the electronic structure near strongly scattering impurities in cuprate superconductors described by a realistic band structure and order parameter magnitude. Energies and highly asymmetric line shapes of resonances, changes in gap-edge features, and local changes in the order parameter are determined for magnetic and nonmagnetic potentials. Experimental tunneling spectra are well fitted by calculations using a d-wave order parameter. The local density of states near such impurities is also calculated. [S0031-9007(98)06003-7]

PACS numbers: 74.50.+r, 73.20.Hb, 74.72.Bk

Planar tunneling provided a key tool for exploring the character of the superconducting state in low-temperature superconductors such as lead [1], and several measurements have been made in the high-temperature superconductors, principally on $YBa_2Cu_3O_{7-\delta}$ (YBCO) [2–4]. These measurements indicate (on YBCO) a greater density of states within the gap than consistent with the simple d-wave order parameter expected from angle-resolved photoemission spectroscopy [5] and Josephson π-junction [6] experiments. Theoretical examination of d-wave superconductors has shown that impurities can provide spectral weight within the gap, even at the chemical potential. Unfortunately calculations of resonant state effects in c-axis tunneling [7–9] which have the spectral resolution to resolve the resonances in energy [10] are quite limited. The band structures used were particle-hole symmetric with circular Fermi surfaces, order parameter self-consistency was ignored, and calculations were limited to resonances with energies $\Omega \ll \Delta_{\max}$, where $\Delta_{\max}$ is the order parameter maximum on the (normal) Fermi surface. The importance of a correct band structure has been established in recent calculations of T_c suppression [11] and photoemission spectral weights [12]. Furthermore in c-axis tunneling calculations only the effects of impurities on resonances were considered; the effects on features elsewhere in the spectrum, such as the gap edge, were ignored.

A complementary probe to planar tunneling is scanning tunneling spectroscopy (STS), which is best suited for exploring local properties at the surface of a sample. The *local* structure of impurities in superconductors with anisotropic order parameters has been the topic of increased investigation since two almost simultaneous events: the calculation of anisotropic structure in the local density of states (LDOS) around an impurity indicative of the order parameter symmetry and structure of the host superconductor [13], and the demonstration of the sensitivity of STS to the propagation properties of the host material around an impurity atom [14]. Recent work [15,16] has evaluated exactly the mean-field spatial structure of localized states [17–19] around classical (static, or elastic) magnetic impurities in superconductors with order parameters which are *isotropic* in the absence of impurities; this type of order parameter will be referred to as s wave. Such systems have recently been explored experimentally with STS [20]. Calculations in Refs. [15,16] are based on a Koster-Slater technique for finding the real-space Green's functions (and thus the LDOS). The submillivolt sub-Angstrom resolution of STS makes it the best tool for probing properties of an isolated impurity, and justifies the effort to calculate these local properties.

We present here the first calculations of c-axis planar tunneling spectra and local STS spectra on YBCO which use a correctly particle-hole asymmetric band structure, include a self-consistent determination of the order parameter, and produce spectra with essentially arbitrary energy resolution throughout the spectrum. The resonances are characterized by extremely asymmetric line shapes. We find, in contrast to previous work [8], that there are at least two resonances or localized states for a given magnetic potential or a given nonmagnetic potential for all anisotropic order parameters [21]. Hence the presence of a resonance around a nonmagnetic impurity is not *per se* an indication of a particular order parameter symmetry. We also calculate the ground state spin and order parameter as a function of impurity strength for several order parameters.

We further fit the (quite varied) planar tunneling results of three different experimental groups (shown in Fig. 1). None of the curves in Fig. 1 look like a typical clean d-wave superconductor's DOS. Nevertheless all four curves are fit by adding impurities of essentially the *same scattering strength* to a d-wave superconductor in different concentrations and assuming slightly different voltage resolutions. The experimental drop in differential conductance due to the gap structure is only about 30%; we interpret the large residual differential conductance as due to a metallic background originating from the copper-oxygen chains [22]. Note that these results are

 0031-9007/98/80(20)/4546(4)$15.00

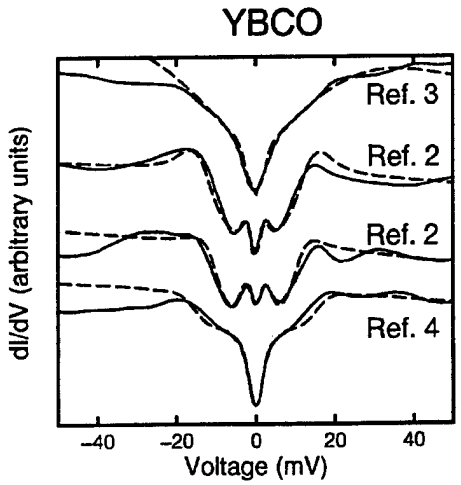

FIG. 1. Comparison of theoretical results (dashed lines) with measurements (solid lines) from Refs. [2–4]. The impurity parameters used were, from top down, $V_0 = 2t$, $n_i = 1.7\%$; $V_0 = 2.5t$, $n_i = 0.5\%$; $V_0 = 2.5t$, $n_i = 1.1\%$; and $V_0 = 2t$, $n_i = 1.4\%$.

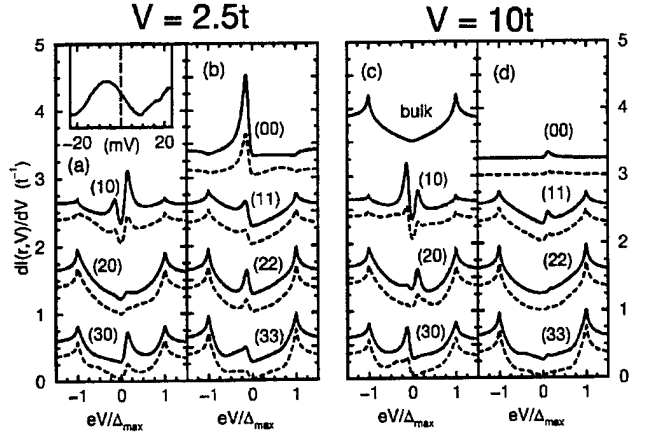

FIG. 2. Local differential conductance $[dI(r, V)/dV]$, relative to the normal metal for potentials of [(a) and (b)] $2.5t$ and [(c) and (d)] $10t$, shown as a function of the voltage. The series of curves are for different distances (sites on the square lattice) from the impurity. The solid lines are for nonmagnetic potentials and the dashed lines are for magnetic potentials. (a) and (c) show from one to three lattice spacings along the (10) direction from the impurity while (b) and (d) show from the origin to three lattice spacings along the (11) direction on the square lattice. An inset to (a) shows the measured STS spectrum on an oxygen vacancy (Ref. [22]). Also shown in (c) is the homogeneous (clean) tunneling spectrum.

also consistent with magnetic impurities in an s^*-wave superconductor at roughly double the concentration (the s^*-wave order parameter has the same magnitude as the d-wave one, but does not change sign). We believe that these impurities, which are present in concentrations on the order of 1% even in nominally clean samples, are oxygen vacancies near the surface of YBCO.

This view is supported by STS on the YBCO surface [22]. Our calculations of the LDOS at the impurity site agree with STS measurements [22] near oxygen vacancies on the YBCO surface. The LDOS is shown in Fig. 2 for magnetic and nonmagnetic impurities in a d-wave superconductor at sites near the impurity along the (10) direction and also along the (11) direction. Also shown is the measured LDOS at an oxygen vacancy [22]. At the impurity site there is no evidence of the gap features, and the spectrum is dominated by an asymmetric resonance. Immediately adjacent to the impurity the gap-edge feature begins to recover in strength. Whereas the DOS for potentials of $2.5t$ and $10t$ are roughly identical, and thus the results in Fig. 1 can be fitted with either potential strength, the LDOS at the impurity site is entirely holelike for $2.5t$ and electronlike for $10t$, where $t = 350$ meV is the nearest-neighbor hopping element for the band structure (described below). Since the measured LDOS at the oxygen vacancy is holelike, the potential strength of the oxygen vacancy must be $2–2.5t$. Although our surface model is incomplete (e.g., it does not include the copper-oxygen chains), supporting evidence is provided by STS [22] identification of a broad resonance at the oxygen vacancies for positive sample bias voltages around 700 meV, consistent with a potential of $2.5t$. We regard Figs. 1 and 2 as the principal results of this Letter.

The LDOS and DOS are calculated using an inversion procedure based on the Gor'kov equation. This procedure is similar to one used to calculate the local electronic structure near defects in isotropic s-wave superconductors [15,16]. The advantages of this technique over the alternative of finite-size diagonalization include (i) the Gor'kov equation for a static impurity is diagonal in frequency, so arbitrary frequency resolution is possible, (ii) the range of the inhomogeneous potential determines the numerical difficulty of calculating the spectra, and (iii) self-consistent potentials, such as the above order parameter variation or an on-site Coulomb repulsion, are easy to implement [23]. More details will be available in a forthcoming publication [24].

The Hamiltonian considered,

$$H = \sum_{(ij),\sigma} [-t_{ij} c^\dagger_{i\sigma} c_{j\sigma} + \Delta_{ij} c^\dagger_{i\uparrow} c^\dagger_{j\downarrow} + \Delta^*_{ij} c_{j\downarrow} c_{i\uparrow}] + V_S(c^\dagger_{0\uparrow} c_{0\uparrow} - c^\dagger_{0\downarrow} c_{0\downarrow}) + V_0(c^\dagger_{0\uparrow} c_{0\uparrow} + c^\dagger_{0\downarrow} c_{0\downarrow}), \quad (1)$$

includes a single-site potential which can be magnetic (V_S), nonmagnetic (V_0), or a combination of both. The homogeneous electronic structure has nearest- and next-nearest-neighbor hopping elements of $t = 350$ meV and $t' = -56$ meV, respectively, and a filling of 1.13. Only on-site and nearest-neighbor Δ_{ij} are nonzero, and $\Delta_{\max} = 25$ meV.

The numerical results presented in this Letter are obtained by inverting the Gor'kov equation, $\mathbf{G} = \mathbf{g} + \mathbf{gVG}$, for this Hamiltonian within a real-space region around the impurity beyond which the potential is negligible. Since the nonmagnetic and magnetic potentials are localized to a

single site, the only potential which is ignored outside this square is the off-diagonal potential (in the Nambu formalism) due to the local change in the order parameter. The Δ_{ij}'s are found self-consistently in the inversion process for the Gor'kov equation. Spectra outside this real-space region (typically a square 20 lattice spacings on a side) are constructed according to the generalized **T**-matrix equation: $\mathbf{G} = \mathbf{g} + \mathbf{gV}[\mathbf{I} - \mathbf{GV}]^{-1}\mathbf{g}$. The energy resolution of the calculations is $\Gamma = 0.35$ meV, and all spectral features presented here are much wider than Γ. Once **G** has been calculated throughout the region near the impurity, the LDOS, $A(i;\omega) = \sum_\sigma (-1/\pi)\,\mathrm{Im}\,G_\sigma(i,i;\omega)$, is straightforward to evaluate. Furthermore the DOS is obtained by spatially integrating the LDOS. The calculated energies of the resonances, identified by peaks in the DOS, are shown for nonmagnetic potentials in Fig. 3.

To obtain an analytic result with which to compare we find the zeros of the real part of the denominator of an approximate **T** matrix. The electronic structure of the homogeneous superconductor is parametrized with two frequency-independent parameters. The first, α, was introduced in Ref. [15] for s-wave superconductors, and parametrizes the particle-hole asymmetry of the band structure. The second, β, is approximately the square of the ratio of the root mean square average of the order parameter around the Fermi surface to its maximum value ($\Delta_{\max}$). $\beta = 1$ for s wave, and $\beta = 0$ for d wave. Order parameter variation due to the impurity potential is ignored. Defining dimensionless quantities $v_s = \pi N_0 V_S$ and $v_0 = \pi N_0 V_0$ [where N_0 is the density of states at the (normal) Fermi surface] we find resonances for the energies

$$\Omega = \left(\frac{R^2(\alpha,\beta,v_s,v_0)}{1 + R^2(\alpha,\beta,v_s,v_0)}\right)^{1/2}\Delta_{\max}, \tag{2}$$

where

$$R(\alpha,\beta,v_s,v_0) = \frac{v_s \pm \sqrt{v_s^2 - (1-\beta)(v_s^2 - v_0^2)[1 - 2v_0\alpha - (v_s^2 - v_0^2)(\beta+\alpha)]}}{(1-\beta)(v_s^2 - v_0^2)}. \tag{3}$$

Since $\Omega < \Delta_{\max}$ when R is finite, which it is for all *anisotropic* order parameters ($\beta < 1$), there always are two solutions to Eqs. (2) and (3) for anisotropic order parameters [21]. For the nonmagnetic case ($R = \sqrt{[(1-\alpha v_0)^2 + \beta v_0^2]/(1-\beta)v_0^2}$) resonances come in pairs due to the spin degree of freedom.

Resonance energies from the above expressions are shown in Fig. 3. The particle-hole asymmetry is due to the nonzero α; for $\alpha = 0$ the resonance energies are identical for $\pm v_s$. The main source of disagreement comes from the use of a standard method of finding resonances: solving for the zeros of the real part of the **T**-matrix denominator. This strategy is flawed for this system due to the strongly energy-dependent imaginary component of the **T**-matrix denominator.

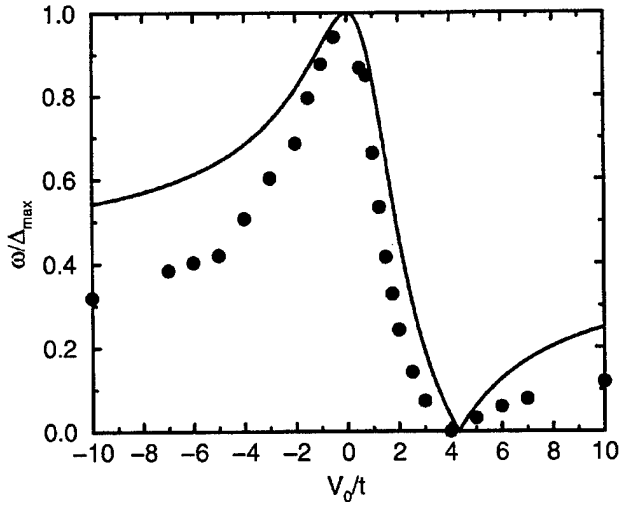

FIG. 3. Peak energies of resonant states created by a nonmagnetic impurity. Shown are the calculated results for a d-wave superconductor (circles) and an analytic model which includes particle-hole asymmetry [Eqs. (2) and (3)].

In contrast to the resonances for the d-wave system, resonances for nonmagnetic impurities in an s^*-wave system do not have lower energy than $\Omega = 0.77\Delta_{\max}$. Hence if the order parameter were s^* wave, in order to produce the results of Figs. 1 and 2, oxygen vacancies would have to behave as *magnetic* impurities.

The difference spectra for nonmagnetic and magnetic impurities in d-wave and s^*-wave superconductors are shown in Fig. 4. A difference spectrum is the change in the DOS due to the addition of one impurity. Shown are the reductions in the density of states near the gap feature, present even in the absence of resonances [Fig. 4(d)]. Spectral weight pulled to lower energies in the presence of the impurity exactly compensates for that taken from the gap feature. A resonance's line shape is much sharper on the low-energy side and broader on the high-energy side, due to the frequency-dependent DOS in the homogeneous superconductor. This also shifts the energy of the peak of a resonance.

Figure 5(a) shows for magnetic impurities the order parameter at the impurity, and in the inset [25] the total spin of the superconductor's ground state. In contrast to the isotropic s-wave case, where the order parameter at the impurity changes abruptly at some critical potential strength [15], for d wave the order parameter changes smoothly at all potentials, due to the finite width of the resonant state. For s wave this transition is characterized by the binding of a quasiparticle in the ground state [9,15,19], producing an abrupt change in the ground-state spin of the superconductor from 0 to 1/2. For the d-wave superconductor there is instead a cloud of quasiparticles near the impurity potential. The nonquantized behavior arises because there are quasiparticle states at the chemical

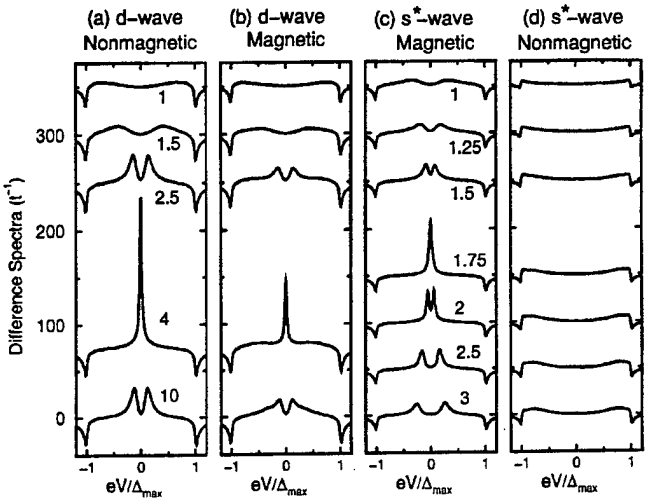

FIG. 4. Difference spectra (in units of t^{-1}) for (a) nonmagnetic and (b) magnetic impurities in a d-wave and (c) magnetic impurities and (d) nonmagnetic impurities in an s^*-wave superconductor. The numbers are the potential strengths in units of t, and are the same in (a) and (b), as well as for (c) and (d).

potential in the d-wave superconductor, but not in the s-wave superconductor.

The d-wave order parameter changes sign for sufficiently strong positive (electron repelling) nonmagnetic impurities [shown in Fig. 5(b)], but not for magnetic impurities or negative nonmagnetic impurities. The difference between positive and negative nonmagnetic impurities is due to the holelike character of the Fermi surface—a nonmagnetic potential which repels electrons attracts the holes to the impurity. The positive nonmagnetic impurity attracts twice as much hole weight (due to spin degeneracy) to the impurity as the magnetic impurity, so the order parameter suppression is greater. A change in the order parameter sign may affect the presence or absence of a Josephson π junction [26], should the coupling across an interface be near nonmagnetic impurities, such as in a rough junction.

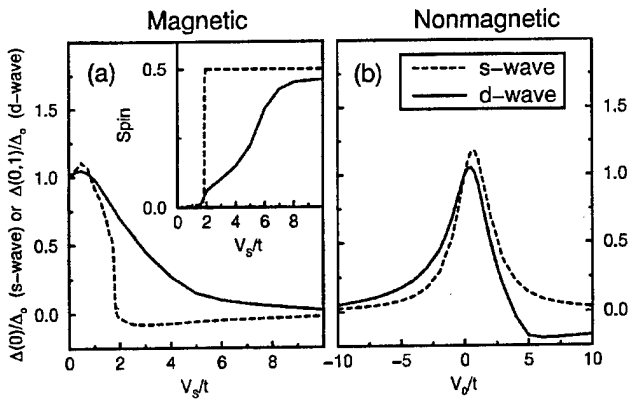

FIG. 5. Change in the order parameter at the impurity for (a) magnetic potentials, and (b) nonmagnetic potentials. Inset in (a) is the ground-state spin for magnetic potentials.

M. E. F. acknowledges Office of Naval Research Grant No. N00014-96-1-1012. J. M. B. acknowledges financial support from the N.R.C.

[1] W. L. McMillan and J. M. Rowell, Phys. Rev. Lett. **14**, 108 (1965).
[2] J. Geerk, X. X. Xi, and G. Linker, Z. Phys. B **73**, 329 (1988).
[3] I. Takeuchi, J. S. Tsai, Y. Shimakawa, T. Manako, and Y. Kubo, Physica (Amsterdam) **158C**, 83 (1989).
[4] M. Gurvitch *et al.*, Phys. Rev. Lett. **63**, 1008 (1989).
[5] B. O. Wells *et al.*, Phys. Rev. B **46**, 11 830 (1992); Z.-X. Shen *et al.*, Phys. Rev. Lett. **70**, 1553 (1993).
[6] D. A. Wollman *et al.*, Phys. Rev. Lett. **71**, 2134 (1993).
[7] C. H. Choi, Phys. Rev. B **50**, 3491 (1994).
[8] M. I. Salkola, A. V. Balatsky, and D. J. Scalapino, Phys. Rev. Lett. **77**, 1841 (1996).
[9] M. I. Salkola, A. V. Balatsky, and J. R. Schrieffer, Phys. Rev. B **55**, 12 648 (1997).
[10] Finite-size diagonalization calculations, while applied to more general situations, lack the necessary spectral resolution to resolve the resonances in energy for realistic order parameters. Examples of such calculations can be found in Ref. [9], as well as T. Xiang and J. M. Wheatley, Phys. Rev. B **51**, 11 721 (1995); M. Franz, C. Kallin, and A. J. Berlinsky, Phys. Rev. B **54**, R6897 (1996).
[11] R. Fehrenbacher, Phys. Rev. Lett. **77**, 1849 (1996).
[12] R. Fehrenbacher, Phys. Rev. B **54**, 6632 (1996).
[13] J. M. Byers, M. E. Flatté, and D. J. Scalapino, Phys. Rev. Lett. **71**, 3363 (1993).
[14] M. F. Crommie, C. P. Lutz, and D. M. Eigler, Nature (London) **363**, 524 (1993); Y. Hasegawa and P. Avouris, Phys. Rev. Lett. **71**, 1071 (1993).
[15] M. E. Flatté and J. M. Byers, Phys. Rev. Lett. **78**, 3761 (1997).
[16] M. E. Flatté and J. M. Byers, Phys. Rev. B (to be published).
[17] H. Shiba, Prog. Theor. Phys. **40**, 435 (1968).
[18] A. I. Rusinov, JETP Lett. **9**, 85 (1969).
[19] A. Sakurai, Prog. Theor. Phys. **44**, 1472 (1970).
[20] A. Yazdani, B. A. Jones, C. P. Lutz, M. F. Crommie, and D. M. Eigler, Science **275**, 1767 (1997).
[21] An isotropic order parameter superconductor has one localized state for a magnetic impurity, and zero for a nonmagnetic impurity (see Ref. [17]).
[22] H. L. Edwards *et al.*, Phys. Rev. Lett. **73**, 1154 (1994); **75**, 1387 (1995).
[23] A Coulomb repulsion term $Un_\uparrow n_\downarrow$ can always be written within mean-field theory as the sum of a magnetic and nonmagnetic potential, which must be self-consistently determined. $(U/2)[\langle n_\uparrow\rangle n_\downarrow + \langle n_\downarrow\rangle n_\uparrow] = (U/4)(\langle n\rangle n + \langle s\rangle s)$, where $s = n_\uparrow - n_\downarrow$ and $n = n_\uparrow + n_\downarrow$.
[24] M. E. Flatté and J. M. Byers, in Solid State Physics, edited by H. Ehrenreich and F. Spaepen (Academic Press, New York, to be published), Vol. 52.
[25] In the inset in Fig. 5(a) the order parameter has been increased by a factor of 3 to guarantee that all the distortion is within the considered far-field region.
[26] See references in M. Sigrist and T. M. Rice, Rev. Mod. Phys. **67**, 503 (1995).

Local Electronic Structure of Defects in Superconductors

Michael E. Flatté

Department of Physics and Astronomy

University of Iowa

Iowa City, Iowa 52242

Phone: (319) 335-0201

Fax: (319) 353-1115

E-mail: flatte@rashi.physics.uiowa.edu

Jeff M. Byers

Materials Physics

Naval Research Laboratory

Washington D.C. 20375

Phone: (202) 767-6147

Fax: (202) 767-1697

E-mail: byers@foucault.nrl.navy.mil

Contents

I. INTRODUCTION

1. The importance of defects in understanding homogeneous systems

Condensed matter physics is largely based on relating atomic-scale properties to macroscopic measurements. The probes available to the field have favored this approach. For instance, X-ray diffraction provides detailed information about the Fourier transform of lattice positions averaged over many lattice spacings. Such diffraction techniques have atomic-scale resolution only to the extent that structures are periodic, or, such as in the case of liquids, quasi-homogeneous. Macroscopic measurements (e.g. of thermodynamic quantities) are easiest to analyze in terms of homogeneous (clean) samples. Areas of intensive research have focused on making systems more and more homogeneous, primarily by removing defects from the crystalline matrix. As a result momentum-based perspectives have dominated condensed-matter theory, due to the nature of the available experimental techniques and the technological importance of clean crystalline structures.

The advent of scanning probe microscopies offers a new way to directly examine the local properties *without* a need for periodicity or homogeneity. Many materials of current interest are not periodic or homogeneous, and as a result momentum is *not* a good quantum number. Important examples include some solids, such as glasses, disordered alloys and amorphous silicon[1]. Examples of phenomena in these systems which are best described in real space include variable-range hopping, localization and long-range (RKKY) interactions. Soft condensed matter systems, such as polymers, membranes, or vortex phases in superconductors are also systems where momentum-based perspectives are often clumsy. The physics of entanglement of vortices or polymers, and of the constrained geometry of membranes, is more naturally explored in real space.

Additional important areas of interest where a local perspective is useful concern situa-

tions where translational symmetry is broken at an interface. In this category are real-space models of the proximity effect at the interface of a superconductor[2]. In semiconductor heterostructures, where interfaces are important, the dominant physical picture is a real-space based envelope function model[3]. Traditional information about such systems has involved that which can be measured far from the interface, such as the current through the structure. Local probes based on scanning tunneling microscopy (STM) have been used recently to probe the details of the proximity effect, such as the order parameter suppression induced by gold islands on a niobium surface[4,5].

Even when momentum is a good quantum number there are advantages to the real space viewpoint if interactions are localized. This is the case for Cooper pairs in a superconductor. Whereas the ordinary isotropic order parameter superconductor is usually modeled with an interaction of zero range, anisotropic superconductors are naturally modeled by interactions with finite but small range. An example is the $d_{x^2-y^2}$ order parameter believed to dominate in high-temperature superconductors, which can be produced by nearest-neighbor interactions on a square lattice.

Scanning probe microscopies place more of an emphasis on real space concepts and, thereby, help redefine what materials and situations are of interest. In this Chapter the focus will be on the ability of a scanning tunneling microscope to probe the local density of states in a superconductor when translational symmetry is broken. The pump-probe language of driven systems can be appropriated to understand this type of physical situation. Consider an impurity, step-edge, or grain boundary as a local pump which perturbs the otherwise homogeneous material; the STM in spectroscopic mode serves as a probe that examines the local response to reveal length-dependent properties on the atomic scale. Traditional techniques lose this information due to the inhomogeneous broadening of features in experimental data, thus driving the need for sample purity. In contrast, scanning probe microscopies use the pervasive inhomogeneity of real materials to their advantage.

An elegant example is the use of STM to measure the electronic structure near individual impurity atoms or step edges on noble-metal surfaces[6,7]. From information on the local electronic structure near these defects the dispersion relation of the surface state present on the *homogeneous* metal surface can be obtained.

The interplay of interactions and disorder has been a recurring theme in condensed matter physics. Here we will describe the use of the localized spectroscopic capabilities of STM to study how the best understood of interacting electron systems, a conventional low-T_c superconductor, responds to impurities. The local structure around an impurity if the superconductor has anisotropic pairing as in the high-T_c superconducting cuprates will also be presented. These are demonstrations of the use of real-space techniques to understand the localized spectroscopy of inhomogeneous superconductivity both for intrinsic interest and as an indicator of how STM and general scanning probe microscopies (SPM) may enhance the understanding of disordered correlated electron systems in the future.

2. Introduction to scanning tunneling microscopy

The scanning tunneling microscope[8–10] is an atomically sharp wire that can be positioned close enough to a surface for electrons to tunnel across the energy barrier constituted by the work function of the STM tip and sample surface. The tip can be scanned over the surface via a piezoelectric "walker" or other mechanical means. The STM current I is related to the tip height z and the tip-surface voltage V, by

$$I \propto e^{2\kappa z} \int d\omega n(\omega)[1 - n(w - eV)] \sum_{n,\sigma} |\psi_{n,\sigma}(\mathbf{x})|^2 \delta(\omega - E_n), \tag{1}$$

where e is the charge of the electron, $n(\omega)$ is the Fermi function in the sample and

$$n(\omega + eV) = n_{STM}(\omega) = \left[1 + \exp\left(\frac{\omega - eV}{k_B T}\right)\right]^{-1} \tag{2}$$

is the Fermi function in the STM tip. T is the temperature and k_B is Boltzmann's constant. The $\psi_{n,\sigma}(\mathbf{r})$ are the wavefunctions of the sample surface with E_n their corresponding energy eigenvalues and $\mathbf{x}$ is the position on the surface below the STM tip. With two out of the three quantities I, z and V fixed the third can imaged as a function of surface position $\mathbf{x}$. For our purposes the STM as a probe can be understood as operating in one of three modes: constant current, constant resistance, or constant height.

In the constant-current mode a feedback loop is maintained between the height and the current. The current is fixed by varying the height of the STM tip above the surface. A two-dimensional mapping of variation in height is the resulting data. If the voltage between the tip and surface is a large constant value (typically 500 mV to 2 V) a significant amount of the total density of states under the tip is sampled. When operating in this manner the height data can be interpreted as a topographic image of the surface. The STM is most often used in this mode due to the simplicity of the measurement and the direct interpretation of the data.

An additional powerful attribute of the STM is its ability to measure local spectra. One spectroscopic technique, the constant resistance mode, is to set the tip height based on a constant current at some relatively large voltage, then open the feedback loop (fixing the height) and measure the current as a function of voltage. This method has the advantage that when adatoms are present on the surface the tip height is adjusted up to prevent the tip from hitting them. Another spectroscopic method is the constant-height mode, which requires that the initial height be maintained without feedback throughout the measurement. This approach allows the current to be measured as a function of voltage as the tip is scanned across the surface. In either spectroscopic mode the differential conductance is obtained either by differentiating a collection of $I - V$ curves or through the use of more direct (and more accurate) lock-in techniques. Either of these modes of spectroscopic operation can be termed scanning tunneling spectroscopy (STS).

Tersoff and Hamann have identified the local density of states (LDOS) at the surface of the sample as the measured quantity in STS[11,12]. The differential conductance can be written at finite temperature in the following form which depends on the local density of states (LDOS) at the tip location:

$$\frac{dI(\mathbf{x},V,T)}{dV} \propto \int_{-\infty}^{\infty} d\omega \frac{\partial n_{STM}(\omega)}{\partial \omega} \sum_{\sigma n} |\psi_{n,\sigma}(\mathbf{x})|^2,$$
$$\propto \int_{-\infty}^{\infty} d\omega \frac{\partial n_{STM}(\omega)}{\partial \omega} \sum_{\sigma} \left(\frac{\mathrm{Im} G_\sigma(\mathbf{x},\mathbf{x};\omega)}{\pi} \right). \qquad (3)$$

The differential conductance is thus proportional to the imaginary part of the retarded Green's function fully dressed by the interaction of the electronic system with the impurity, which is the LDOS of the interacting system.

3. Atomic-scale structure in condensed electron systems

The traditional perspective on the importance of band structure on the properties of condensed electron systems is that only low-energy properties (such as the density of states at the Fermi level) are relevant. The argument for this perspective relies on small order parameter energies, typically of the order of meV, compared to the energy scale of important band structure features, typically of order eV.

Our purpose will be to extend this argument to inhomogeneous systems, where the energy scale of the inhomogeneity is very large compared to the order parameter energy. The new low-energy quantities of importance in the condensate are the low-energy LDOS of the inhomogeneous system. Due to the energy scale of the inhomogeneity, however, the low-energy LDOS depends on mixed-in high-energy features of the homogeneous material's band structure. This picture of inhomogeneous systems immediately suggests that caution must be exercised when making the common assumption that the electronic structure of a correlated electronic system is particle-hole symmetric. This assumption is usually as-

sociated with the observation that the electronic structure of the homogeneous system is particle-hole symmetric over the small energy range of interest (e.g. the energy scale of the order parameter or the temperature). The inhomogeneity, however, has a large energy scale, so the assumption of particle-hole symmetry in the homogeneous system produces serious errors in the low-energy LDOS of the inhomogeneous system.

Section 16 demonstrates the importance of the low-energy inhomogeneous electronic structure by using it to provide a direct way to visualize Anderson's argument for the stability of the superconducting state in the presence of nonmagnetic impurities. Superconductivity opens up a low-energy gap in the normal-state LDOS induced by the strong impurity, however neither the gap nor T_c is reduced. Section 17 extends this use of the normal-state LDOS to construct the superconductor's LDOS near a magnetic impurity. In a host superconductor with an anisotropic order parameter, however, the momentum-resolved density of quasiparticle states differs substantially from that of the normal state, so the connection between the normal-state and superconducting LDOS becomes less simple and direct.

4. The Koster-Slater technique

The local electronic properties of defects such as magnetic or nonmagnetic impurities in the superconductor can be calculated self-consistently from the Gor'kov equation[13] without further approximation with a new technique introduced in Refs. 14 and 15. This technique for calculating the electronic structure around a defect in a superconductor is related to the Koster-Slater inversion techniques for determining the local electronic structure of impurities in metals[16,17]. Since its original application to localized vibrational modes[18], this algorithm has been applied to numerous problems including deep levels in semiconductors[19] and impurity states in magnets[20].

The new Koster-Slater technique takes advantage of the short-ranged nature of the impu-

rity potential by formally separating space around the defect into two regions: the near field and the far field. The far field is a region distant enough from the defect that the potential is insignificant and the order parameter has relaxed back to its homogeneous value. The near field is the region close to the defect where the potential is finite or the order parameter is distorted. In essence, the Gor'kov equation that determines the Green's functions of the inhomogeneous superconductor is inverted in real space within the near field region.

5. Outline of this chapter

Section II provides a brief guide to the most important bulk characteristics of impurities in superconductors with either isotropic or anisotropic order parameters. Section III presents a survey of calculational techniques of the local properties of defects in superconductors, including coarse-grained approaches such as Ginzburg-Landau and Eilenberger theory, the quasiparticle-based method of the Bogoliubov-de Gennes equations, and the more recently developed Koster-Slater Green's function technique.

Section IV describes an analytic model, based on a delta-function potential, which reproduces some of the quantitative behavior obtained from the Koster-Slater calculations presented in Sections V and VI. For clarity when discussing the numerical calculations for various impurities, as well as heuristic pictures of the electronic structure near the impurities, the presentation has been separated into two sections depending on whether the order parameter is isotropic or anisotropic. Section V discusses the results of the numerical calculations for magnetic impurities, nonmagnetic impurities, impurities incorporating both magnetic and nonmagnetic potentials, and inhomogeneities in the pairing interaction, all in superconductors with isotropic order parameters, such as the low-temperature superconductors. Section VI discusses similar results for superconductors with anisotropic order parameters and quasi-two-dimensional electronic structure, characteristic of the high-

temperature superconductors. Comparisons with the analytic results of Section IV will be made in Sections V and VI. Section VII provides some very recent results for dynamical spins, which may be relevant to recent tunneling experiments on the edges of the high-temperature superconductor $YBa_2Cu_3O_{7-\delta}$.

II. BULK PROPERTIES OF DEFECTS IN SUPERCONDUCTORS

6. Models of the formation of a magnetic moment in a superconductor

The behavior of magnetic impurities in metals is a rich area in its own right, and the models developed there have been applied at various times to the problem of magnetic impurities in superconductors. The basic response of a superconductor to magnetic impurities is quite different than that of a metal. In a metal the magnetic moment of an impurity can disappear when that impurity atom is placed in a nonmagnetic host. Several models have been developed to describe this behavior. Excellent reviews of this topic are available in Refs. 21, 22. Here we merely provide a brief description suitable for conveying the richness and difficulty of the problem.

The model of Friedel[23] requires a strong scattering potential to generate a virtual bound state near the Fermi energy, and then a sufficiently strong exchange energy to induce a local magnetic moment. The Friedel Hamiltonian is

$$H = \sum_{\mathbf{k}s} E_{\mathbf{k}} n_{\mathbf{k}s} + J \sum_{\mathbf{k}ss'} \mathbf{S} \cdot c^{\dagger}_{\mathbf{k}s} \sigma_{ss'} c_{\mathbf{k}s'}, \tag{4}$$

where J is the exchange energy between the impurity spin and conduction electron spins. The condition for the formation of the local moment via ℓ-channel scattering[24],

$$2\epsilon_{ex}\rho_{\ell}(E_F) > 1, \tag{5}$$

is very similar to the Stoner condition for ferromagnetism. Here the exchange energy is equal to $-\frac{1}{2}n^2\epsilon_{ex}$, where n is the number of unpaired d electrons and $\rho_\ell(E_F)$ is the density of localized states in the virtual bound state.

The method of Anderson[25] relies on the now familiar model Hamiltonian,

$$H = \sum_\sigma E_d n_{ds} + U n_{d\uparrow} n_{d\downarrow} + \sum_{\mathbf{k}s} E_{\mathbf{k}} n_{\mathbf{k}s} + \sum_{\mathbf{k}s} \left[V_{d\mathbf{k}} c^\dagger_{\mathbf{k}s} c_{ds} + V^*_{\mathbf{k}d} c^\dagger_{ds} c_{\mathbf{k}s} \right]. \tag{6}$$

The hybridization between the conduction electrons and the d electrons introduces a non-magnetic resonant state at E_d when $U = 0$ with a linewidth

$$\Gamma = \pi \langle |V_{d\mathbf{k}}|^2 \rangle_{av} \rho(E). \tag{7}$$

When $U \neq 0$ the system can be magnetic or nonmagnetic depending on the relative values of Γ and U and the separation of E_d from the Fermi energy ϵ_F. A mean-field (Hartree-Fock) treatment of the Anderson model reveals the non-trivial "phase diagram" of Fig.1.

Although these models produce some sensible results, there are several drawbacks in their practical application. One of the key problems is the difficulty of measuring the required bare parameters of either model. Some of the bare quantities, such as U, can best be extracted from information on the electronic structure far from the Fermi surface. Unfortunately other electronic features can complicate the extraction of U from these measurements. As an example, metallic oxides have a lattice arrangement of d-orbitals, and their U can be extracted from photoemission spectroscopy[26]. The small additional signal from dilute magnetic impurities, however, cannot be distinguished. Given that the most common probes of electronic structure, i.e. thermodynamic or transport measurements, are only sensitive to the electronic structure near the Fermi energy, consistent information about all the parameters in the Anderson or Friedel model for a particular system can be hard to obtain.

A further problem concerns the importance of correlations within the local shell in the presence of more than one d electron. The Hartree-Fock theory is quite inadequate here,

and explanations based on Hund's rule must be introduced *ad hoc*. For impurity atoms with shells containing only one d electron or only missing one d electron, magnetic moments have been observed only at high impurity concentration. For shells with one or missing one f electron magnetic moments have been observed in hosts, but they appear fragile — vanishing under pressure[27] (increasing Γ). The loss of the moment appears to correlate with the movement of an electron from the f state to the conduction band (with a corresponding change in the Hartree-Fock potential). Thus even the one-electron or one-hole shells cannot be described well without taking into account aspects of the system ignored in the above models, such as the orbital moment, Hund's rules, and local effects like crystal fields[21].

7. Defects in isotropic order-parameter superconductors

The response of a superconductor to magnetic impurities is considerably more dramatic than that seen in metals. Matthias and co-workers noticed that magnetic impurities at a critical concentration of 1-2% could remove the characteristic gap in the density of states and at slightly higher concentrations all superconductivity vanished[28–30]. The first detailed model for magnetic impurities in a superconductor was based on inelastic scattering from the impurity treated within the Born approximation, namely Abrikosov-Gor'kov theory[31].

Before introducing Abrikosov-Gor'kov theory it is important to address the presence of nonmagnetic impurities. Low-temperature superconductors almost always have a high concentration of nonmagnetic impurities. Even in the dirty limit, however, where the elastic mean free path is shorter than the coherence length, superconductivity endures[32]. The differing effects of magnetic and nonmagnetic impurities are directly attributable to the time-reversal invariance of a superconducting condensate formed of electrons paired in spin singlets with an isotropic wavefunction. If the pair wavefunction is triplet as in He^3 or anisotropic as in high-T_c cuprate superconductors the distinction between the effects of

magnetic and nonmagnetic impurities is modified. The robustness of the superconductor to nonmagnetic impurities relies on the presence of Kramers doublets (pairs of degenerate states) in a time-reversal invariant system. The BCS pairing of states[33,34] of opposite momentum is then generalized to the pairing of two members of the Kramers doublet[35]. This argument only fails to the extent that the impurities destroy the normal-state metallic properties.

A magnetic impurity, which does break time-reversal symmetry, is described by a term $J(\mathbf{x})\mathbf{S}\cdot\sigma$ in the Hamiltonian. A complete treatment of this term includes the possibility of flipping the quasiparticle spin, and the resulting change in the impurity spin. Even in the simpler case of a normal metal a correct treatment of this situation is quite difficult. When the coupling J is antiferromagnetic, this effect can give rise to Kondo physics, which is beyond the scope of our treatment of impurity spins.

One of the common approximations is to ignore the quantum mechanical operator character of the impurity spin. The impurity can then be imagined as an inelastic spin-flipping scatterer. Within the Born approximation the effect of these impurities is to induce a finite width in any quasiparticle state. This treatment forms the basis of the popular Abrikosov-Gor'kov treatment[31] of magnetic impurities in superconductors. The effect of magnetic impurities is often referred to as pair-breaking, since an inelastic scattering event can transfer an energy greater than the order parameter Δ to a quasiparticle.

The introduction of a lifetime τ to the quasiparticle smoothes the gap edges at low concentrations, and eventually leads to gapless superconductivity. Fig. 2 below shows a series of calculated spectra for various $\alpha = [\tau\Delta]^{-1}$. In this model, as the impurity concentration is increased, the intra-gap states move from the gap edge deeper into the gap. The presence of these intra-gap states leads to a linear suppression of T_c with impurity concentration for low concentrations. A recent strong-coupling calculation[36] yields qualitatively similar results.

Intra-gap states form in quite a different way in the presence of a classical spin. In

this case a localized state is formed around each impurity with an energy determined by the strength of the spin-dependent potential. As the concentration of impurities increases, the individual localized states hybridize in a similar way to an impurity band in a semiconductor[37]. As the concentration increases the intra-gap band broadens until it fills the energy gap, leading to gapless superconductivity. Hence a model of gapless superconductivity is possible whether the spin is dynamic (and inelastically scatters the quasiparticle) or static (and elastically scatters the quasiparticle).

In the *classical* limit of the spin, $J(\mathbf{x}) \to 0$ and $S \to \infty$, while $J(\mathbf{x})S \to V_S(\mathbf{x})$. Since the amplitude of spin-flip scattering is proportional to $J(\mathbf{x})$, but not to S, in this limit the potential is spin-dependent, but does not flip the spin of the quasiparticles. We will always take the quantization direction of the superconducting electrons' spins to be parallel to the impurity spin, so the impurity term in the Hamiltonian will be $\sigma V_S(\mathbf{x})$. Thus the classical spin acts formally as a local magnetic field. The two most important qualitative differences between the Abrikosov-Gor'kov treatment and the treatment of the classical spin[38,37,39,40] are that (1) for the classical spin only elastic scattering is allowed, so the quasiparticle lifetimes are infinite in the absence of other phase-decohering processes, and (2) the classical spin model can be solved exactly even for strong potentials, while the treatment of inelastic properties beyond the Born approximation is extremely difficult.

The type of model appropriate for a particular magnetic impurity can be determined from two experimental quantities: the detailed concentration dependence of the critical temperature of the superconductor and the specific heat jump of the alloy at the superconducting transition relative to that of the host at its superconducting transition[41]. For moments whose characteristic fluctuation time is long ($\hbar\omega_o \ll \Delta$, where ω_o is the fluctuation frequency), and the impurity-conduction electron interaction (J) is weak the superconducting properties are well described by modeling the impurity with a classical spin. Such a system is Mn in niobium[42,43].

If the impurity-conduction electron interaction is antiferromagnetic, and is treated quantum mechanically, then for sufficiently low temperature there is a competition between the formation of a Kondo-like singlet between the impurity electron and a cloud of conduction electrons which compensate it, and the formation of a BCS singlet between conduction electrons. Such a system can demonstrate reentrant superconductivity, in which the system is superconducting between two finite temperatures T_{c1} and T_{c2}, but not at $T = 0$. Such a system is $LaAl_2$ with Ce impurities[44].

Considerable theoretical effort has been expended in exploring the interplay of the Kondo effect and superconductivity[45–48]. While there have been successes, such as the identification of an origin of reentrant superconductivity, the details of the Kondo effect in a superconductor should be considered an open problem. Part of the problem originates from the lack of good methods for tackling inhomogeneous frequency-dependent interacting systems. A recently developed tool for attacking such problems is dynamical mean field theory, and the quantum mechanical spin in a superconductor has been examined[49,50] with that technique.

The final category of behavior is for local moments with fast timescales. For such impurities the localized state can be treated as a broad (wider than the superconducting gap) resonance. The depression of T_c with n can be described by the following form,

$$\frac{T_c(n)}{T_c(0)} = e^{-\frac{An}{1-Dn}}, \tag{8}$$

where the parameters A and D depend on the parameters of the Anderson or Friedel models of the magnetic impurity. The origin of the suppression of T_c in this system is the reduction of the density of states at the Fermi level and the reduction of the effective attractive electron-electron interaction due to the Coulomb repulsion between electrons of opposite spin when they are both in the localized state.

8. Defects in anisotropic order-parameter superconductors

Extensive investigation in the high-temperature superconductors has explored the effect on the superconducting transition temperature of a wide variety of dopants. A review of this work is available in Ref. 51. As a general rule the critical temperature decreases linearly with dopant concentration, even at low concentrations. This set of results does not appear to be consistent with the robust nature of the low-temperature superconductors' critical temperature to nonmagnetic impurities. As discussed in Section 7, in low-temperature superconductors T_c decreases linearly with dopant density for magnetic impurities, but not for nonmagnetic impurities. The observation of linear decreases in the critical temperature with dopant concentration for a wide variety of dopants either leads one to the curious argument that almost all dopants act as magnetic impurities in the high-temperature superconductors, or that the order parameter is highly anisotropic. A particularly powerful example is the use of electron irradiation to displace oxygen atoms from the copper-oxygen planes[52] of $YBa_2Cu_3O_{7-\delta}$. The resulting defects do not have measurable local moments nor do they change the carrier concentration. Nevertheless, these nonmagnetic defects suppress the critical temperature to zero when merely 4.1% of the in-plane oxygen atoms have been displaced.

The observation that almost all impurities suppress T_c linearly should not be taken as an indication they all act the same. For example, the presence of Zn depresses T_c about three times more per impurity[53] than Ni. There is currently considerable controversy over both Ni and Zn concerning whether or not they should be treated as magnetic impurities or nonmagnetic impurities when placed in the copper-oxygen planes of high-temperature superconductors.

It has taken several years for the qualitative behavior of some thermodynamic quantities in clean high-temperature superconductors to be disentangled from the effects of impurities

on the superconductors. Essentially this has been achieved through the growth of extremely high quality samples, as well as the reproduction of earlier measurements through the addition of intentional doping. An impressive example of this type of work involves the magnetic penetration depth measured on $YBa_2Cu_3O_{7-\delta}$. Here twinned single crystals were intentionally doped with Zn and Ni impurities[54]. In the undoped samples[55], the penetration depth exhibits a linear dependence on the temperature, which is consistent with line nodes in the order parameter. The Zn doped samples showed a low-temperature T^2 behavior, followed by a crossover to linear T behavior at higher temperature. That nonmagnetic impurities induce the T^2 behavior can be viewed as support for an order parameter which averages to or close to zero around the Fermi surface. If the order parameter averaged to a sizable value around the Fermi surface, the disorder would tend to average the order parameter, leading to a low-temperature exponential behavior[56,57].

In order to obtain this T^2 dependence and crossover behavior it is crucial[58] to use strongly-scattering impurities rather than weakly-scattering ones, since concentrations of weakly-scattering impurities sufficient to generate this T^2 dependence also would destroy the superconducting state. Within the Born approximation, which applies for weakly scattering impurities, states very near the chemical potential (which affect the low-temperature properties of the system) must originate from the smoothing of the gap edge. When there are sufficient impurities to smooth the gap edge enough to place a substantial number of states at the chemical potential, superconductivity has already been destroyed. In contrast, strongly scattering impurities can put the intra-gap quasiparticle states predominately very near the chemical potential, where they affect the low-energy quasiparticle properties, but do not significantly damage T_c. The use of strongly scattering impurities has been an extremely fruitful direction in obtaining qualitative agreement between experiment and theory in the high-temperature superconductors.

III. TECHNIQUES FOR CALCULATING THE LOCAL PROPERTIES OF DEFECTS IN SUPERCONDUCTORS

Among the first local properties calculated in the vicinity of an impurity in a superconductor were the structures of screening clouds around a charged impurity[59,60] and a magnetic impurity[60,61] in a superconductor (characterized by exponentially-decaying Friedel-like[23] oscillations). The oscillation of the order parameter around a magnetic impurity was first evaluated without self-consistency[62–64]. A self-consistent calculation was reported for the order parameter at the impurity and very far away for *weak* magnetic impurity potentials by Schlottmann[65], and far away from nonmagnetic impurities by Fetter[66]. All of these calculations focused on ground-state properties of the system — this Chapter emphasizes the local properties of excited states as well.

9. Coarse-grained theories of local properties

Some formalisms for inhomogeneous superconductivity, such as Ginzburg-Landau theory[67] or the Eilenberger equations[68], treat the spatial degrees of freedom as coarse-grained over the superconductor's coherence length. This is sensible if the properties of interest are of that scale, such as the decay of the Gor'kov amplitude into a normal metal at an interface with a superconductor[2]. If the properties of interest have atomic-scale structure the Bogoliubov-de Gennes equations, or the Koster-Slater technique presented here, must be used.

The Ginzburg-Landau theory is based on the dependence of the free energy of the superconductor on the order parameter. It can be extremely useful to identify effects in a qualitative way, but since it only holds formally near T_c it has limited quantitative use at lower temperatures. Since it focuses on the order parameter, and the quasiparticles them-

selves do not directly appear in the theory, Ginzburg-Landau theory is not appropriate for addressing the details of localized states around magnetic impurities. The parameters of Ginzburg-Landau theory must either be set empirically from the behavior of macroscopic properties near T_c or they must be determined from a microscopic calculation. Such calculations have been performed in anisotropic order parameter superconductors[69,70]. As an additional concern, the Ginzburg-Landau theory does not produce the detailed information on the electronic structure necessary for calculating STM tunneling spectra.

The Eilenberger equations do contain information about the quasiparticles. They are obtained from the microscopic Gor'kov equations under the quasiclassical approximation that the gradients in the electron amplitudes due to the inhomogeneity are small. This approximation is not appropriate for situations where the electronic properties change considerably over a coherence length, or when a local potential is large compared to the order parameter. The Eilenberger equations have been applied to the electronic structure of the vortex core in s-wave superconductors[71,72], in anisotropic s-wave superconductors (specifically $NbSe_2$)[73], and in a d-wave superconductor[74]. In addition to lacking spatial information on the atomic scale, these treatments lack the ability to resolve the energies of quantized states within the vortex core (which can be picked out by STM[75,76]). This inability to resolve the energies of quantized states is a fundamental difficulty with the theory, since the quantized energies of the localized states can be considered to be determined by matching conditions on the quasiparticle wavefunction equations (BdG equations) at the boundaries of the system containing the vortex. They are thus intrinsically atomic-scale conditions.

Atomic-scale defects also have been investigated with the Eilenberger equations. Here the validity of the theory is even more in question, due to the strength of the potential. The electronic structure of a magnetic impurity[77] and the effect of pinning centers on vortices[78] are such examples. When the potential is large, such as in these cases, the Eilenberger equations are only appropriate for calculating properties far from the impurity.

10. Bogoliubov-de Gennes equations

The Bogoliubov-de Gennes equations are generalized Schrödinger equations for the electron and hole wavefunctions of a quasiparticle, and are valid for a superconductor with an arbitrarily-varying order parameter, only constrained by the validity of BCS theory. The inhomogeneous order parameter for an superconductor can also be determined self-consistently from these equations. Unfortunately, the BdG equations have significant practical difficulties.

Despite qualitative success modeling STM measurements of a single vortex in superconducting $NbSe_2$[75,76], calculations of the electronic structure[79–83] using the BdG equations are hampered by the difference in energy scales between the Fermi energy and the order parameter. Since the BdG equations are solved numerically for a finite system, the difficulty of the calculation is determined by the necessary spectral resolution. The key energy scale which must be resolved is the superconducting gap. Thus, the numerical difficulty increases as the ratio of the Fermi energy to the gap becomes large. For low-temperature superconductors the band structure assumed must be somewhat unrealistic (for Refs. 82 and 83 the Fermi wavelength in the calculation was approximately 100Å, which is too large[84] for $NbSe_2$). This limitation extends to calculations of a vortex's structure in a quasi-two-dimensional system with a square lattice[85], calculations of the interaction between a vortex and an impurity[86], the characteristics of the vortex lattice[87,88], and work on a nonmagnetic impurity[89–92] and a magnetic impurity[93] in a two-dimensional s-wave or d-wave superconductor. In contrast, the computational requirements of the Koster-Slater technique (to be described in Section 11) are determined by the range of the impurity potential, rather than the necessary spectral precision.

To place our new Koster-Slater formalism in context we will contrast it with the BdG equations. This Section, therefore, describes the BdG equations in several physical sit-

uations. The first is a three-dimensional continuum model of a superconductor with an isotropic order parameter. Following that description we explore a two-dimensional lattice model of a superconductor with an anisotropic order parameter. We conclude with a description of the additional formalism required in the presence of a magnetic field — and thus appropriate for the electronic structure of a vortex line.

The magnetic impurity will be modeled by a classical spin. The quantization direction of the electronic spins in the superconductor ($\sigma = \pm 1/2$) can therefore be chosen parallel to the classical spin, and spin is a good quantum number for the quasiparticles. The equations for parallel and antiparallel quasiparticle spins decouple, and we must therefore solve two equations, coupling electron and hole amplitudes of the same spin, rather than four equations coupling electron and hole amplitudes of both spins.

a. Three-dimensional continuum model with an isotropic order parameter

For a (normal-state) free electron band structure with mass m, the quasiparticles correspond to positive-energy (E) solutions to

$$\begin{aligned} \left[\frac{p^2}{2m} - \mu - E + V_0(\mathbf{x}) + \sigma V_S(\mathbf{x})\right] u_\sigma(\mathbf{x}) + \Delta(\mathbf{x}) v_\sigma(\mathbf{x}) &= 0, \\ \left[-\frac{p^2}{2m} + \mu - E - V_0(\mathbf{x}) + \sigma V_S(\mathbf{x})\right] v_\sigma(\mathbf{x}) + \Delta^*(\mathbf{x}) u_\sigma(\mathbf{x}) &= 0, \end{aligned} \tag{9}$$

where μ is the chemical potential and p is the operator $-i\hbar\nabla$. Here $\sigma V_S(\mathbf{x})$ is the position-dependent, spin-dependent potential of Section 7. $V_0(\mathbf{x})$ is a position-dependent nonmagnetic potential and $\Delta(\mathbf{x})$ is the inhomogeneous order parameter.

The spatially-dependent order parameter is determined self-consistently:

$$\Delta(\mathbf{x}) = \sum_{j\sigma} \gamma(\mathbf{x}, E_{j\sigma}) u_{j\sigma}(\mathbf{x}) v^*_{j\sigma}(\mathbf{x}) \left[1 - 2n(E_{j\sigma})\right],$$

$$= \sum_{j\sigma} \gamma(\mathbf{x}, E_{j\sigma}) u_{j\sigma}(\mathbf{x}) v^*_{j\sigma}(\mathbf{x}) \tanh\left(\frac{E_{j\sigma}}{2k_BT}\right), \tag{10}$$

where j labels the states for each spin σ. $\gamma(\mathbf{x}, E_{n\sigma})$ is the effective electron-electron interaction potential, which will usually be taken to be

$$\begin{aligned} \gamma(\mathbf{x}, E_{n\sigma}) &= \gamma_o \qquad E_{n\sigma} < \hbar\omega_D, \\ &= 0 \qquad E_{n\sigma} > \hbar\omega_D. \end{aligned} \tag{11}$$

These equations are derived under the assumption that the pairing potential has zero range (a delta function). A more general order parameter requires a pairing potential of greater than zero range. Furthermore, because the defect potential is real, $\Delta(\mathbf{x})$ may be chosen real. In contrast, the inhomogeneous order parameter for a vortex cannot be chosen to be real everywhere.

The combinations $\sigma V_S \pm V_0$ have straightforward physical significance: $\sigma V_S + V_0$ is the potential felt by an electron of spin σ, while $\sigma V_S - V_0$ is the potential felt by a hole of spin σ. The terms proportional to $\Delta(\mathbf{x})$, which couple $u(\mathbf{x})$ and $v(\mathbf{x})$ also have straightforward interpretations: they couple spin σ electrons to spin σ holes and vice versa. A spin σ electron can convert to a spin σ hole by putting a Cooper pair into the condensate (conserving particle number), and a spin σ hole can convert to a spin σ electron by pulling a Cooper pair from the condensate.

For a spherically-symmetric defect the wavefunctions are eigenstates of angular momentum with quantum numbers ℓ and m. Typically the defect is placed in a sphere of radius R with appropriate boundary conditions. For example, the wavefunctions may be set to zero at the boundary. Thus the solutions to Eq. (9) can be written as

$$\begin{pmatrix} u_{j\sigma,\ell m}(\mathbf{x}) \\ v_{j\sigma,\ell m}(\mathbf{x}) \end{pmatrix} = \sum_n \begin{pmatrix} U_{j\sigma,n\ell m} \\ V_{j\sigma,n\ell m} \end{pmatrix} j_\ell(k_{n\ell} r) Y_{\ell m}(\Omega), \tag{12}$$

where $j_\ell(k_{n\ell}R) = 0$. In this Ansatz Eq. (9) is a matrix equation relating all the $U_{n\ell m}$ and $V_{n\ell m}$ with fixed ℓ and m.

The size of the basis is partially determined by the number of $k_{n\ell}$'s necessary. The range of important $k_{n\ell}$ is centered around the Fermi surface, but extends above and below by energies comparable to the largest values of $V_0(\mathbf{x})$ and $V_S(\mathbf{x})$. Since these potentials have a characteristic scale of eV, this range is of the order of the bandwidth, and therefore is quite substantial. The other requirements on the eigenstates is that their energy separation should be small enough that Eq. (10), and the spectral width of features measurable by the STM, can be accurately evaluated. Otherwise, the finite-size effects on the spectrum will limit the accuracy of these quantities. The first condition, based on Eq. (10), requires that the level spacing must be much smaller than Δ_o (less than 1 meV for low-temperature superconductors). The second condition, based on resolving spectral features observable by STM, can be even more restrictive (less than 0.1 meV).

Operationally these conditions determine the minimum size R of the finite system which must be solved. The resulting computational requirements are so severe that such calculations have not been attempted for impurities. Attempts to evaluate similar equations for vortices (where the potential strengths are much smaller) will be discussed later in this Section.

b. Two-dimensional lattice model with a general order parameter

Consider now a case where the real-space locations are discrete. Such a lattice model is typically based on a tight-binding approach to the normal-state electronic properties. The focus here is on a square lattice, by virtue of its applicability to the high-temperature superconductors. The square lattice is considerably simpler than the real physical systems, and is intended to represent the important physics of the copper-oxygen planes[94]. The lattice sites are effectively the copper sites, which are arrayed in a square pattern within each copper-oxygen plane, with oxygen sites between nearest-neighbor coppers. The copper-

oxygen electronic structure can be described near the Fermi energy with an effective one-band tight-binding model.

A treatment of high-temperature superconductors also requires the consideration of general order parameters, for the evidence of anisotropic order parameters in high-temperature superconductors is overwhelming, supported by measurements of the magnetic penetration depth[55], angle-resolved photoemission[95–97], the critical current dependence of Josephson junctions[98], and the presence of a half-flux quantum in certain tricrystal rings[99]. A review of the current experimental support for various order parameter symmetries is available in Ref. 100.

The principal difference introduced by considering general order parameters in our model is the introduction of a second coordinate in the order parameter, $\Delta(\mathbf{x}, \mathbf{x}')$. The BdG equations now become

$$\begin{aligned}
&\left[\sigma V_S(\mathbf{R}_{ij}) + V_0(\mathbf{R}_{ij}) - \mu - E\right] u_\sigma(\mathbf{R}_{ij}) - \sum_{i'j'} t_{i-i',j-j'} u_\sigma(\mathbf{R}_{i'j'}) + \sum_{i'j'} \Delta(\mathbf{R}_{ij}, \mathbf{R}_{i'j'}) v_\sigma(\mathbf{R}_{i'j'}) = 0 \\
&\left[\sigma V_S(\mathbf{R}_{ij}) - V_0(\mathbf{R}_{ij}) + \mu - E\right] v_\sigma(\mathbf{R}_{ij}) + \sum_{i'j'} t_{i-i',j-j'} v_\sigma(\mathbf{R}_{i'j'}) + \sum_{i'j'} \Delta^*(\mathbf{R}_{ij}, \mathbf{R}_{i'j'}) u_\sigma(\mathbf{R}_{i'j'}) = 0.
\end{aligned} \tag{13}$$

Lattice locations are denoted by $\mathbf{R}_{ij}$, where i is the row and j is the column of the site. The expression for the inhomogeneous order parameter is

$$\Delta(\mathbf{R}_{ij}, \mathbf{R}_{kl}) = \frac{\gamma(|\mathbf{R}_{ij} - \mathbf{R}_{kl}|)}{2} \sum_{m\sigma} \left(u_{m\sigma}(\mathbf{R}_{ij}) v^*_{m\sigma}(\mathbf{R}_{kl}) + u_{m\sigma}(\mathbf{R}_{kl}) v^*_{m\sigma}(\mathbf{R}_{ij})\right) \left[1 - 2n(E_{m\sigma})\right], \tag{14}$$

where the sum m is over all the positive energy solutions to Eq. (13). Here $\gamma(R)$ is the effective electron-electron interaction potential. Unlike the effective potential considered in a superconductor with an isotropic order parameter, this interaction potential has finite range.

The number of parameters in Eq. (13) is reduced to simplify calculations. The model considered here includes nearest-neighbor and next-nearest neighbor hopping elements $t =$ 350meV and $t' = 56$meV. These values parametrize the normal-state band structure of $YBa_2Cu_3O_{7-\delta}$. More complete tight-binding parametrizations[101,102] are now available for $Bi_2Sr_2CaCu_2O_8$.

Further simplification occurs when the order parameter's range is limited. By allowing for on-site or nearest-neighbor pairing only we allow for both $d_{x^2-y^2}$ and anisotropic s-wave order parameters in addition to isotropic s-wave. Thus the sum over neighboring sites in Eq. (13) extends only to nearest neighbors for the order parameter. This restriction is more naturally guaranteed within the model by restricting the range of the pairing potential $\gamma(R)$. For the isotropic s-wave order parameter considered in the previous section, $\gamma(R)$ has the form of a delta function. For anisotropic order parameters we restrict $\gamma(R)$ to be non-zero only for $R = 0$ and for nearest-neighbor sites.

Direct diagonalization calculations based on Eq. (13) have been attempted[89–92]. The rank of the matrix to be inverted scales with the number of lattice sites. If we consider a physical square of sites of linear size d, the computation time scales as d^6. The approximate limit, based on CPU time and memory, for current high-end desk-top workstations is $d = 50$. A quantity of critical importance, then, is the amount of broadening required to smooth the spectrum obtained from the exact diagonalization of the finite cluster into a spectrum representative of the infinite system. Unfortunately, of course, the states of the finite cluster are distributed over the entire band-width of the infinite system, instead of near the gap edge where good resolution is desired. The distribution of the states is highly nonuniform due to symmetry-induced degeneracies. We find that the broadening factor necessary to obtain a spectrum which does not clearly show the influence of finite-size effects is at least $\Gamma \sim 4t/d$.

In order to accurately resolve the gap edge we need $\Gamma \ll \Delta_{max}$, where Δ_{max} is the

maximum value of the order parameter on the Fermi surface. Since even for the largest possible currently accessible values of d, $\Gamma \sim 0.1t$, gaps cannot be accurately resolved unless $\Delta_{max} \sim t$. Even for the high-temperature superconductors, which have large order parameters, this is unrealistically large by over a factor of ten. We show in Fig. 3(a,b) the density of states in the presence of a realistic $d_{x^2-y^2}$ gap in a high-temperature superconductor. Figure 3(a) shows the spectrum over a broad energy range, while Fig. 3(b) shows a closeup view of the energy gap region, where the spectrum is unbroadened (solid line) and broadened by $\Gamma = 0.1t$ (dashed line).

c. Vortices in isotropic superconductors

The electronic structure of a superconductor in the neighborhood of a vortex can be determined from the above equations if the influence of the vector potential is also considered. In the presence of a vortex, the potential present in the Bogoliubov-de Gennes equations comes from two self-consistent quantities: the order parameter, as above, and the vector potential $\mathbf{A}(\mathbf{x})$. The new Bogoliubov-de Gennes equations are

$$\begin{aligned}\left[\frac{(\mathbf{p}-\frac{e}{c}\mathbf{A}(\mathbf{x}))^2}{2m} - \mu - E + V_0(\mathbf{x}) + \sigma V_S(\mathbf{x})\right] u_\sigma(\mathbf{x}) + \Delta(\mathbf{x}) v_\sigma(\mathbf{x}) &= 0, \\ \left[-\frac{(\mathbf{p}+\frac{e}{c}\mathbf{A}(\mathbf{x}))^2}{2m} + \mu - E - V_0(\mathbf{x}) + \sigma V_S(\mathbf{x})\right] v_\sigma(\mathbf{x}) + \Delta^*(\mathbf{x}) u_\sigma(\mathbf{x}) &= 0.\end{aligned} \tag{15}$$

where $\mathbf{A}(\mathbf{x})$ is determined by first calculating the current,

$$\begin{aligned}\mathbf{j}(\mathbf{x}) = \frac{e\hbar}{2mi}\sum_{n\sigma}\Bigg[& n(E_{n\sigma}) u^*_{n\sigma}\left(\nabla - \frac{ie}{\hbar c}\mathbf{A}(\mathbf{x})\right) u_{n\sigma} + \\ & \{1 - n(E_{n\sigma})\} v_{n\sigma}(\mathbf{x})\left(\nabla - \frac{ie}{\hbar c}\mathbf{A}(\mathbf{x})\right) v^*_{n\sigma} - \text{H.c.}\Bigg],\end{aligned} \tag{16}$$

and then calculating $\mathbf{A}(\mathbf{x})$ from

$$\nabla \times \nabla \times \mathbf{A}(\mathbf{x}) = \frac{4\pi}{c}\mathbf{j}(\mathbf{x}). \tag{17}$$

A self-consistent solution of these equations is obtained by repeatedly solving Eq. (15) and calculating $\Delta(\mathbf{x})$ and $\mathbf{A}(\mathbf{x})$ using Eqs. (10), (16), and (17), and reinserting them into Eq. (15) until convergence is attained.

Caroli *et al.*[103] showed that the suppressed order parameter in the vicinity of the vortex core allowed for the presence of localized states. The suppressed order parameter was assumed to heal over a coherence length, and the localized states were found. Later work by Bardeen *et al.*[104] treated the order parameter self-consistently within a variational calculation. Motivated by the STM measurements of Hess *et al.*[75,76], Shore *et al.* calculated the LDOS of the vortex core bound states, assuming a particular form for the order parameter. Gygi and Schlüter[83], were the first to directly solve Eqs. (15)-(17) in a homogeneous medium with cylindrical symmetry (around the vortex core) and calculate both the self-consistent order parameter and the LDOS.

Since the system of interest in Ref. 83 was $NbSe_2$, the electronic structure was assumed to be quasi-two-dimensional with a free-electron like dispersion in the planes. The cylindrical symmetry allows us to write solutions of Eq. (15) with well-defined angular momentum around the vortex core,

$$\begin{aligned} u(\mathbf{x}) &= u_{n\mu k_z}(\rho)\mathrm{e}^{i(\mu-1/2)\theta}\mathrm{e}^{ik_z z}, \\ v(\mathbf{x}) &= v_{n\mu k_z}(\rho)\mathrm{e}^{i(\mu+1/2)\theta}\mathrm{e}^{ik_z z}, \end{aligned} \tag{18}$$

where n is a radial quantum number, $\mu = \nu + 1/2$ (where ν is an odd integer), and k_z is the momentum parallel to the vortex line. Equations (15)-(17) simplify if the gauge is chosen[103] where $\Delta(\mathbf{x}) = |\Delta(\rho)|\mathrm{e}^{-i\theta}$. In this gauge, for cylindrical symmetry, the vector potential has the form

$$\mathbf{A}(\mathbf{x}) = A_\theta(\rho)\hat{\mathbf{e}}_\theta. \tag{19}$$

The BdG equations are then solved separately for each value of μ and k_z. Results from these calculations will be compared in at the end of this Section with results for impurities.

d. Vortices in superconductors with anisotropic order parameters

Cylindrical symmetry, which rendered numerically tractable the vortex problem in an isotropic order parameter superconductor, is not appropriate for the high-temperature superconductors with their anisotropic order parameters. Instead further approximations to the vortex problem are required. All attempts using the BdG equations[69,105] to date have relied on the observation that the vortex core size is considerably smaller than the London penetration depth. By considering a region of the material of a size much greater than the core, but much smaller than the London penetration depth, it is possible to consider the vector potential to be very small. Since the form of the vector potential for $\xi < \rho < \lambda$ is proportional to $\lambda^{-2}\ln(\lambda/\rho)$, and the screening current is proportional[106] to λ^{-2}, this approximation corresponds to the $\lambda \to \infty$ limit, and has been referred to as the extreme type II limit.

This approximation eliminates the need to calculate self-consistently $\mathbf{j}(\mathbf{x})$ and $\mathbf{A}(\mathbf{x})$, and eliminates $\mathbf{A}(\mathbf{x})$ from Eq. (15). In Ref. 69, the resulting equations were solved in a quadrant with the center of the core at one corner. The presence of the vortex was enforced by establishing the proper matching conditions between the solution at the vertical and horizontal edges containing the center of the vortex. The same computational problems connected with solving for the order parameter exist for the vortex as for the impurity. This has either been finessed by taking an unrealistically large value[105] for Δ_o, or by ignoring the "spiky" nature of the sum in Eq. (10) and not showing the density of states[69].

e. Comparison of BdG calculations for impurities and vortices

A principal computational distinction between the vortex problem and the impurity problem has to do with the strength of the defect potential. In the case of the vortex the potentials, coming from the $\mathbf{A}(\mathbf{x})$ terms and the $\Delta(\mathbf{x})$ terms in Eq. (15) are of the scale of meV. In contrast the potentials $V_0(\mathbf{x})$ and $V_S(\mathbf{x})$ are of the scale of eV. It is not possible to choose a coarser energy level spacing for the impurity, however, because the separation between the energies of the eigenstates must be considerably less than Δ_o for both the impurity and vortex in order to accurately evaluate Eq. (10).

The BdG equations are hard to evaluate even with the smaller potential of the vortex. For example, in the calculations for the vortex in $NbSe_2$[82,83], $\epsilon_F/\Delta_o = 32$ was the largest ratio of the Fermi energy to the homogeneous order parameter considered. This value is a result of fitting the coherence length and upper critical field of $NbSe_2$ to a free-electron model. A more realistic band structure[84] has a bandwidth to energy gap ratio at least an order of magnitude greater, and a highly anisotropic Fermi velocity. Niobium has an $\epsilon_F/\Delta_o = 705$, rendering its LDOS numerically inaccessible for most potentials V_S and V_0.

The energy scales are greater for the impurity potential than the vortex, but the spatial extent of the order parameter suppression is much greater for the vortex than for the impurity. Figure 4 shows the order parameter as a function of distance from the vortex core, as calculated in Ref. 83. The length scale of the relaxation of the order parameter to its bulk value is of order ξ. Figure 5 shows the same situation for an impurity, as calculated with the Koster-Slater method described in the next section. For this calculation V_S and V_0 are Gaussians of radius k_F^{-1}. The $\delta\Delta(\mathbf{x})$ for $v_s = \pi N_o |\int d\mathbf{x} V_S(\mathbf{x})| = 1.75$ and $v_0 = \pi N_o |\int d\mathbf{x} V_0(\mathbf{x})| = 0$ is shown in Fig. 5. While oscillating with wavelength $\sim \pi k_F^{-1}$, $\delta\Delta(\mathbf{x})$ falls off to a negligible potential within $10k_F^{-1}$. Thus, the effective range of the potential arising from the distorted order parameter is much greater for the vortex. The two types

of inhomogeneities clearly have different computational requirements; the vortex requires a better treatment of length scales beyond ξ, while the impurity requires a better treatment of energy scales far exceeding Δ_o. There also exist problems which share both elements of difficulty, of which the most notable is evaluating the pinning potential of an impurity for a vortex.

11. Koster-Slater inversion formalism

a. Three-dimensional continuum model with isotropic order parameter

We now introduce a self-consistent method which works within a sphere whose radius is determined by the range of the defect's potential and utilizes the continuum spectrum of the homogeneous superconductor. Our presentation of this method will largely follow Ref. 15. In essence, we invert the Gor'kov equation in real space. The Gor'kov equation[13] for a defect in a superconductor can be written in the Nambu formalism[107] as:

$$\int d\mathbf{x}'' \left[\delta(\mathbf{x}-\mathbf{x}'') - \mathbf{g}(\mathbf{x},\mathbf{x}'';\omega)\mathbf{V}(\mathbf{x}'')\right]\mathbf{G}(\mathbf{x}'',\mathbf{x}';\omega) = \mathbf{g}(\mathbf{x},\mathbf{x}';\omega) \tag{20}$$

where $\mathbf{g}$ is the homogeneous Green's function, $\mathbf{V}$ is the potential, and the inhomogeneous retarded Green's function,

$$\mathbf{G}(\mathbf{x},\mathbf{x}';\omega) = \begin{pmatrix} G_\uparrow(\mathbf{x},\mathbf{x}';\omega) & F(\mathbf{x},\mathbf{x}';\omega) \\ F^\dagger(\mathbf{x},\mathbf{x}';-\omega) & -G_\downarrow^\dagger(\mathbf{x},\mathbf{x}';-\omega) \end{pmatrix}. \tag{21}$$

If the potential can spin-flip scatter quasiparticles a 4×4 formalism must be used[108]. Here the assumption remains that the spin is classical (no inelastic dynamics and no spin flipping), and the quantization direction in the superconductor is chosen parallel to the impurity spin. The elements of the matrix in Eq. (21) are

$$G_\uparrow(\mathbf{x},\mathbf{x}';\omega) = -i\int_{-\infty}^{\infty} dt e^{i\omega t}\theta(t)\langle 0|\{\psi_\uparrow(\mathbf{x}';t),\psi_\uparrow^\dagger(\mathbf{x};0)\}|0\rangle, \tag{22}$$

$$F(\mathbf{x},\mathbf{x}';\omega) = -i\int_{-\infty}^{\infty} dt e^{i\omega t}\theta(t)\langle 0|\{\psi_\uparrow(\mathbf{x}';t),\psi_\downarrow(\mathbf{x};0)\}|0\rangle, \tag{23}$$

$$F^\dagger(\mathbf{x},\mathbf{x}';-\omega) = -i\int_{-\infty}^{\infty} dt e^{i\omega t}\theta(t)\langle 0|\{\psi_\downarrow^\dagger(\mathbf{x}';t),\psi_\uparrow^\dagger(\mathbf{x};0)\}|0\rangle, \tag{24}$$

$$-G_\downarrow^\dagger(\mathbf{x},\mathbf{x}';-\omega) = -i\int_{-\infty}^{\infty} dt e^{i\omega t}\theta(t)\langle 0|\{\psi_\downarrow^\dagger(\mathbf{x}';t),\psi_\downarrow(\mathbf{x};0)\}|0\rangle. \tag{25}$$

The explicit subscripts $\uparrow$ and $\downarrow$ do *not* refer to the spin of the excitation in the superconductor but rather to the spin band of the normal state used to construct the excitation. The key concept is that the spin-*up* band contains both *up* electrons and *down* holes just as the spin-*down* band contains both *down* electrons and *up* holes. The convention employed here is standard in the theory of semiconductors where a spin-up electron excited above the Fermi energy leaves a spin-down hole below the Fermi energy. This is convenient for magnetic potentials since if spin-up electrons are attracted to a magnetic impurity spin-down holes should be repelled by the impurity. In the presence of a single classical impurity spin, the quasiparticle spin is a good quantum number despite electron-hole mixing. Our convention determines the composition of a spin-up quasiparticle to be part spin-up electron and part spin-up hole, rather than part spin-up electron and part spin-down hole.

For $\omega > 0$, $\mathbf{G}(\mathbf{x},\mathbf{x}';\omega)$ describes spin-up excitations, including the mixing of electrons in the spin-up band with holes in the spin-down band. For $\omega < 0$, $\mathbf{G}(\mathbf{x},\mathbf{x}';\omega)$ describes spin-down excitations, including the mixing of electrons in the spin-down band with holes in the spin-up band. By calculating $\mathbf{G}(\mathbf{x},\mathbf{x}';\omega)$ for all ω, information about both spin-up and spin-down quasiparticles is obtained.

The homogeneous Green's function is independent of the spin σ, so

$$\mathbf{g}(\mathbf{x},\mathbf{x}';\omega) = \begin{pmatrix} g(\mathbf{x},\mathbf{x}';\omega) & f(\mathbf{x},\mathbf{x}';\omega) \\ f^\dagger(\mathbf{x},\mathbf{x}';-\omega) & -g^\dagger(\mathbf{x},\mathbf{x}';-\omega) \end{pmatrix}. \tag{26}$$

The potential,

$$\mathbf{V}(\mathbf{x}'') = \begin{pmatrix} V_S(\mathbf{x}'') + V_0(\mathbf{x}'') & \delta\Delta(\mathbf{x}'') \\ \delta\Delta(\mathbf{x}'') & V_S(\mathbf{x}'') - V_0(\mathbf{x}'') \end{pmatrix}, \tag{27}$$

where $\delta\Delta(\mathbf{x}) = \Delta(\mathbf{x}) - \Delta_o$ and V_S, V_0, and $\Delta(\mathbf{x})$ have similar meaning above as in the BdG equations. The factor of one-half from the electron spin magnitude has been incorporated into the potential V_S. The self-consistency equation for the order parameter is

$$\delta\Delta(\mathbf{x}) = \int_{-\infty}^{\infty} d\omega\gamma(\mathbf{x},\omega)n(\omega)\mathrm{Im}\left[F(\mathbf{x},\mathbf{x};\omega) - F(\mathbf{x},\mathbf{x};-\omega)\right] - \Delta_o. \tag{28}$$

An error in this equation in Ref. 15 has been corrected in Eq. (28).

To be concrete, and without loss of generality, the spin direction attracted by the potential will be called spin up, and the spin direction repelled will be called spin down. Unlike the case of the quantum spin, there is no qualitative difference between ferromagnetic and antiferromagnetic coupling for the classical spin. We therefore do not discuss the orientation of the impurity spin, but merely define a low-energy direction for the quasiparticle spin.

For a BCS superconductor with an isotropic gap in a parabolic band, for ω much smaller than the Fermi energy, the analytic forms for the homogeneous Green's functions are

$$\begin{aligned} g(\mathbf{x},\mathbf{x}';\omega) &= -\frac{\pi N_o}{k_F r}\mathrm{e}^{-(\Delta_o^2-\omega^2)^{\frac{1}{2}}r/\pi\Delta_o\xi}\left(\cos k_F r + \frac{\omega}{\sqrt{\Delta_o^2-\omega^2}}\sin k_F r\right), \\ f(\mathbf{x},\mathbf{x}';\omega) &= -\frac{\pi\Delta_o N_o}{k_F r\sqrt{\Delta_o^2-\omega^2}}\mathrm{e}^{-(\Delta_o^2-\omega^2)^{\frac{1}{2}}r/\pi\Delta_o\xi}\sin k_F r, \end{aligned} \tag{29}$$

where $r = |\mathbf{x} - \mathbf{x}'|$ and N_o is the density of states for each spin at the Fermi level. The coherence length $\xi = \hbar v_F/\pi\Delta_o$, where v_F is the Fermi velocity. These expressions are valid for ω above and below Δ_o so long as the imaginary parts of both f and g are multiplied by $\mathrm{sgn}\omega$.

One strength of this formalism is its reliance on the short-range nature of the impurity's potential. Solution of Eq. (20) requires inverting the frequency-dependent real-space matrix

$$\mathbf{M}(\mathbf{x},\mathbf{x}';\omega) = \delta(\mathbf{x}-\mathbf{x}') - \mathbf{g}(\mathbf{x},\mathbf{x}';\omega)\mathbf{V}(\mathbf{x}') \tag{30}$$

to obtain $\mathbf{G}(\mathbf{x},\mathbf{x}';\omega)$, so $\mathbf{G} = \mathbf{M}^{-1}\mathbf{g}$. The structure of $\mathbf{M}(\mathbf{x},\mathbf{x}';\omega)$ allows for a precise description of the difference between the *near* field and the *far* field. We require that the impurity's potential $\mathbf{V}(\mathbf{x})$ is zero for $|\mathbf{x}| > R$. The space $|\mathbf{x}| > R$ belongs to the far field, whereas the space $|\mathbf{x}| \leq R$ belongs to the near field. We can then separate any real-space matrix $\mathbf{A}$ symbolically into four pieces:

$$\mathbf{A} = \begin{pmatrix} \mathbf{A}^{n\to n} & \mathbf{A}^{n\to f} \\ \mathbf{A}^{f\to n} & \mathbf{A}^{f\to f} \end{pmatrix} \tag{31}$$

where n and f label the near field region and far field region, respectively. The particular example of $\mathbf{M}$ is block-triangular:

$$\mathbf{M} = \begin{pmatrix} \mathbf{I} - \mathbf{g}^{n\to n}\mathbf{V} & 0 \\ -\mathbf{g}^{f\to n}\mathbf{V} & \mathbf{I} \end{pmatrix}, \qquad \mathbf{M}^{-1} = \begin{pmatrix} (\mathbf{I} - \mathbf{g}^{n\to n}\mathbf{V})^{-1} & 0 \\ \mathbf{g}^{f\to n}\mathbf{V}(\mathbf{I} - \mathbf{g}^{n\to n}\mathbf{V})^{-1} & \mathbf{I} \end{pmatrix}. \tag{32}$$

It is clear from Eq. (32) that the computational effort in inverting $\mathbf{M}$, and thus finding the inhomogeneous electronic structure, is entirely determined by the complexity of inverting $\mathbf{M}^{n\to n}$. The inhomogeneous Green's functions in the near and far fields are:

$$\mathbf{G}^{n\to n} = (\mathbf{I} - \mathbf{g}^{n\to n}\mathbf{V})^{-1}\mathbf{g}^{n\to n} \tag{33}$$

$$\mathbf{G}^{n\to f} = (\mathbf{I} - \mathbf{g}^{n\to n}\mathbf{V})^{-1}\mathbf{g}^{n\to f} \tag{34}$$

$$\mathbf{G}^{f\to n} = \mathbf{g}^{f\to n}(\mathbf{I} - \mathbf{g}^{n\to n}\mathbf{V})^{-1} \tag{35}$$

$$\mathbf{G}^{f\to f} = \mathbf{g}^{f\to f} + \mathbf{g}^{f\to n}\mathbf{V}(\mathbf{I} - \mathbf{g}^{n\to n}\mathbf{V})^{-1}\mathbf{g}^{n\to f} \tag{36}$$

We thus obtain the useful result that the electronic structure in the far field is easily determined once the electronic structure in the near field is known. The connection to the $\mathbf{T}$-matrix formalism is straightforward, as from Eq. (36),

$$\mathbf{T} = \mathbf{V}(\mathbf{I} - \mathbf{g}^{n\to n}\mathbf{V})^{-1} \tag{37}$$

Certain features of the above equations simplify their numerical implementation. For spherical symmetry each angular momentum channel constitutes an independent block-diagonal submatrix in $\mathbf{M}(\omega)$. Since the bare Green's functions in Eqs. (29) have analytic expansions in spherical harmonics, $\mathbf{M}(\omega)$ can be calculated quickly. These expansions are detailed in the Appendix.

The value of R is governed by the longest-range potential. For the impurities considered here that is determined, not by the shorter-ranged magnetic and nonmagnetic potentials, but by the self-consistently determined $\delta\Delta(\mathbf{x})$. Figure 5 showed the order parameter around an impurity evaluated from Eq. (28) at $T = 0$. A typical radial grid of 100 points provides a numerically robust solution. While oscillating with wavelength $\sim \pi k_F^{-1}$, $\delta\Delta(\mathbf{x})$ falls off to a negligible potential within $10k_F^{-1}$. The self-consistent solution depends on the value of

$$N_o\Delta_o/k_F^3 = (2\pi^3\xi k_F)^{-1} = (4\pi^2\epsilon_F/\Delta_o)^{-1}, \tag{38}$$

which for a free-electron model of niobium ($k_F = 1.18\text{Å}^{-1}$ and $\xi = 380\text{Å}$) is 3.6×10^{-5}. This is the single dimensionless parameter required to parametrize the free-electron model of a superconductor.

In contrast to the Koster-Slater technique described here, which exploits a physical distinction between the near field and the far field to accelerate the numerical calculation, the BdG equations treat the near field and the far field on the same level. A large R is desired for decent spectral resolution, but the possible size of R is limited by computational constraints. Hence a numerical implementation of the BdG equations, by comparison, is typically slower and substantially less accurate than the Koster-Slater technique.

b. Two-dimensional lattice model for general order parameters

For the quasi-two-dimensional tight-binding model of a superconductor appropriate for high-temperature superconductors, the lattice formulation of the Gor'kov equation must be

used.

$$\sum_{i'j'k'l'} \left[\delta_{ij,i'j'}\delta_{kl,k'l'} - \mathbf{g}(\mathbf{R}_{ij},\mathbf{R}_{i'j'};\omega)\mathbf{V}(\mathbf{R}_{i'j'},\mathbf{R}_{k'l'})\right]\mathbf{G}(\mathbf{R}_{k'l'},\mathbf{R}_{kl};\omega) = \mathbf{g}(\mathbf{R}_{ij},\mathbf{R}_{kl};\omega), \quad (39)$$

where ij, kl, $i'j'$, and $k'l'$ label lattice sites, $\mathbf{g}(\mathbf{R}_{ij},\mathbf{R}_{kl};\omega)$ is the Green's function of the homogeneous superconductor, $\mathbf{V}(\mathbf{R}_{ij},\mathbf{R}_{kl})$ is the self-consistent inhomogeneous potential, and $\mathbf{G}(\mathbf{R}_{ij},\mathbf{R}_{kl};\omega)$ is the Green's function of the superconductor fully dressed by interactions with the impurity. Eq. (39) is written in implicit Nambu form,

$$\mathbf{G}(\mathbf{R}_{ij},\mathbf{R}_{kl};\omega) = \begin{pmatrix} G_\uparrow(\mathbf{R}_{ij},\mathbf{R}_{kl};\omega) & F(\mathbf{R}_{ij},\mathbf{R}_{kl};\omega) \\ F^\dagger(\mathbf{R}_{ij},\mathbf{R}_{kl};\omega) & -G_\downarrow^\dagger(\mathbf{R}_{ij},\mathbf{R}_{kl};-\omega) \end{pmatrix} \quad (40)$$

and

$$\mathbf{V}(\mathbf{R}_{ij},\mathbf{R}_{kl}) = \begin{pmatrix} V_e(\mathbf{R}_{ij},\mathbf{R}_{kl}) & \delta\Delta(\mathbf{R}_{ij},\mathbf{R}_{kl}) \\ \delta\Delta(\mathbf{R}_{ij},\mathbf{R}_{kl}) & V_h(\mathbf{R}_{ij},\mathbf{R}_{kl}) \end{pmatrix}. \quad (41)$$

V_e and V_h are the potentials felt by a spin-up electron and spin-up hole, respectively, and $\delta\Delta(\mathbf{R}_{ij},\mathbf{R}_{kl})$ must be self-consistently determined from

$$\delta\Delta(\mathbf{R}_{ij},\mathbf{R}_{kl}) = \frac{\gamma(|\mathbf{R}_{ij}-\mathbf{R}_{kl}|)}{2}\int_{-\infty}^{\infty} n(\omega)\mathrm{Im}(F(\mathbf{R}_{ij},\mathbf{R}_{kl};\omega) + F(\mathbf{R}_{kl},\mathbf{R}_{ij};\omega) \\ -F(\mathbf{R}_{ij},\mathbf{R}_{kl};-\omega) - F(\mathbf{R}_{kl},\mathbf{R}_{ij};-\omega)) - \Delta_o(\mathbf{R}_{ij},\mathbf{R}_{kl}). \quad (42)$$

Here $\Delta_o(\mathbf{R}_{ij},\mathbf{R}_{kl})$ is the homogeneous order parameter. For an isotropic s-wave superconductor, $\gamma(R) = \gamma\delta_{R0}$, while for our model of an anisotropic s-wave or $d_{x^2-y^2}$ superconductor $\gamma(R) \doteq \gamma$ when the distance R corresponds to a nearest-neighbor distance.

The electron and hole potentials also have two spatial position labels. For the typical magnetic and nonmagnetic potentials, as described in in the above description of isotropic order parameter superconductors, the two positions would be the same (e.g. $V_S(\mathbf{R}_{ij})\delta_{ik}\delta_{jl}$). An example of a physically relevant two-position potential is a local change in the hopping matrix elements.

c. Self-consistent potentials

In addition to the self-consistent order parameter, self-consistent spin-dependent and charge-dependent potentials can also be constructed for $\mathbf{V}(\mathbf{x})$ using the calculated spatial structure of the spin $s(\mathbf{x})$ and charge $\rho(\mathbf{x})$ around the defect,

$$s(\mathbf{x}) = \frac{1}{2}\int_{-\infty}^{\infty} d\omega n(\omega)\left(-\frac{\mathrm{Im}\left[G_{\uparrow}(\mathbf{x},\mathbf{x};\omega) - G_{\downarrow}(\mathbf{x},\mathbf{x};\omega)\right]}{\pi}\right) \tag{43}$$

$$\rho(\mathbf{x}) = e\sum_{\sigma}\int_{-\infty}^{\infty} d\omega n(\omega)\left(-\frac{\mathrm{Im}G_{\sigma}(\mathbf{x},\mathbf{x};\omega)}{\pi}\right). \tag{44}$$

Since these self-consistent quantities are not expected to change appreciably between the normal and superconducting state[2], no calculations are reported for such potentials here.

d. Strong-coupling order parameters

A few observations are in order concerning the extension of this formalism to systems where the homogeneous order parameter has important frequency structure. The Gor'kov equation (Eq. (20)) changes due to the more general form for the off-diagonal potential originating from the order parameter.

$$\int d\mathbf{x}''d\mathbf{x}'''\left[\delta(\mathbf{x}-\mathbf{x}'')\delta(\mathbf{x}''-\mathbf{x}''') - \mathbf{g}(\mathbf{x},\mathbf{x}'';\omega)\mathbf{V}(\mathbf{x}'',\mathbf{x}''';\omega)\right]\mathbf{G}(\mathbf{x}''',\mathbf{x}';\omega) = \mathbf{g}(\mathbf{x},\mathbf{x}';\omega) \tag{45}$$

where

$$\mathbf{V}(\mathbf{x}'',\mathbf{x}''';\omega) = \begin{pmatrix} V_{e\uparrow}(\mathbf{x}'';\omega)\delta(\mathbf{x}''-\mathbf{x}''') & \delta\Delta(\mathbf{x}'',\mathbf{x}''';\omega) \\ \delta\Delta(\mathbf{x}'',\mathbf{x}''';\omega) & V_{h\uparrow}(\mathbf{x}'';\omega)\delta(\mathbf{x}''-\mathbf{x}''') \end{pmatrix}. \tag{46}$$

General frequency dependence is included in Eqs. (45) and (46). The diagonal terms are the possibly energy-dependent potentials effective on spin-up electrons ($V_{e\uparrow}$) and spin-up holes ($V_{h\uparrow}$) for $\omega > 0$. Since this potential is diagonal in frequency, as is the Gor'kov equation, the frequency structure of the order parameter does not add any additional complication to numerically solving the Gor'kov equation.

The order parameter's frequency dependence complicates the self-consistency equation (Eq. (28)). It must now be solved for each frequency self-consistently with the quasiparticle weight Z:

$$\Delta(\mathbf{r},\mathbf{r}';\omega)Z(\mathbf{r},\mathbf{r}';\omega) = \int_{-\infty}^{\infty} d\epsilon n(\epsilon)\left[\mathrm{Re}F(\mathbf{r},\mathbf{r}';\epsilon)\right]\left(K_{+}(\mathbf{r},\mathbf{r}';\epsilon,\omega) - U_c\right),$$
$$\omega\left[1 - Z(\mathbf{r},\mathbf{r}';\omega)\right] = \int_{-\infty}^{\infty} d\epsilon n(\epsilon)\left[\mathrm{Re}G(\mathbf{r},\mathbf{r}';\epsilon)\right] K_{-}(\mathbf{r},\mathbf{r}';\epsilon,\omega), \qquad (47)$$

where $K_{\pm}$ are kernals of the pairing interaction and are different for each mechanism of superconductivity. They can be determined from the homogeneous solution. U_c is a Coulomb factor. Incorporating these strong coupling effects allows a determination of the effect of the frequency-dependence of the pairing interaction on the electronic structure around a defect. While selecting the particular location of the STM tip is similar to selecting the momentum of the quasiparticles of interest, selecting the STM voltage indicates which order parameter frequency is probed.

e. Dynamical spins

The ability to model dynamical spins without creating an intractable numerical problem is an additional advantage of the Koster-Slater Green's function technique. As mentioned in Section 7, there are several levels of approximation which are of interest for dynamical spins. The most complete model, which is required to obtain effects such as the Kondo effect, will accurately treat inelastic scattering, spin-flipping, and the quantum nature of the impurity spin.

The next level of approximation would allow for spin flipping and inelastic scattering. A model which could include spin flipping would need to be based on a 4×4 matrix formalism[108] containing the simultaneous coupled equations of motion for electrons and holes of *both* spins. A major complication additionally introduced by inelastic processes, however, is that the

Gor'kov equation, Eq. (20), is no longer diagonal in frequency. Inhomogeneous Green's functions for all ω are coupled to each other by inelastic processes.

In order to make the infinite set of coupled equations that result more tractable we model the time dependence of the dynamic spin with a harmonic potential of frequency ω_o, such as,

$$V_S(\mathbf{x},t) = V_S(\mathbf{x})\cos(\omega_o t). \tag{48}$$

The frequency ω_o is taken to be characteristic of the spin motion. Energy transfer to and from the superconductor is only possible in units of ω_o. The more general form of Eq. (20) is now

$$\int d\mathbf{x}''\left[\delta(\mathbf{x}-\mathbf{x}'') - \mathbf{g}(\mathbf{x},\mathbf{x}'';\omega)\mathbf{V}(\mathbf{x}'';n\omega_o)\right]\mathbf{G}(\mathbf{x}'',\mathbf{x}';\omega,\omega+n\omega_o) = \mathbf{g}(\mathbf{x},\mathbf{x}';\omega)\delta_{n0}, \tag{49}$$

where in the 4×4 formalism the inhomogeneous retarded Green's function,

$$\mathbf{G}(\mathbf{x},\mathbf{x}';\omega) = \begin{pmatrix} G_\uparrow(\mathbf{x},\mathbf{x}';\omega) & F(\mathbf{x},\mathbf{x}';\omega) & 0 & 0 \\ F^\dagger(\mathbf{x},\mathbf{x}';\omega) & -G_\downarrow^\dagger(\mathbf{x},\mathbf{x}';-\omega) & 0 & 0 \\ 0 & 0 & G_\downarrow(\mathbf{x},\mathbf{x}';\omega) & F(\mathbf{x},\mathbf{x}';-\omega) \\ 0 & 0 & F^\dagger(\mathbf{x},\mathbf{x}';-\omega) & -G_\uparrow^\dagger(\mathbf{x},\mathbf{x}';-\omega) \end{pmatrix}, \tag{50}$$

and the potential, $\mathbf{V}(\mathbf{x};\omega)$, is

$$\begin{pmatrix} V_{Sz}(\mathbf{x};\omega)+V_0(\mathbf{x};\omega) & \delta\Delta(\mathbf{x}) & V_{Sx}(\mathbf{x};\omega)+iV_{Sy}(\mathbf{x};\omega) & 0 \\ \delta\Delta(\mathbf{x}) & V_{Sz}(\mathbf{x};\omega)-V_0(\mathbf{x};\omega) & 0 & V_{Sx}(\mathbf{x};\omega)+iV_{Sy}(\mathbf{x};\omega) \\ V_{Sx}(\mathbf{x};\omega)-iV_{Sy}(\mathbf{x};\omega) & 0 & -V_{Sz}(\mathbf{x};\omega)+V_0(\mathbf{x};\omega) & \delta\Delta(\mathbf{x}) \\ 0 & V_{Sx}(\mathbf{x};\omega)-iV_{Sy}(\mathbf{x};\omega) & \delta\Delta(\mathbf{x}) & -V_{Sz}(\mathbf{x};\omega)-V_0(\mathbf{x};\omega) \end{pmatrix}. \tag{51}$$

Our numerical results will rely on further approximations as well. By setting $V_{Sx} = V_{Sy} = 0$ we remove the complication of mixing the quasiparticle spins, thus retaining spin as

a good quantum number and reducing our problem to the 2×2 Nambu formalism. The time dependence of the potential will be assumed to be $\cos(\omega_o t)$, making the potential couple only "nearest neighbor" Green's functions in frequency space. Despite these apparently serious approximations the key known feature of dynamic spins in superconductors, the zero bias anomaly (ZBA) in tunneling, is obtained in our calculations if the timescale of the spin is fast enough.

IV. ANALYTIC SOLUTION OF THE POINT POTENTIAL

The formalism described above is extremely powerful for working with short-range potentials within mean-field theory. It has the additional advantage of yielding some analytic results for more approximate models. The main feature these models share is that the potential has zero range — it is a point. Such a model for the potential, when coupled with a carefully chosen analytic expression for the Green's function, can yield simple analytic expressions for the energies and LDOS of localized states or resonances around impurities in a superconductor.

Analytic expressions for the Green's functions are typically limited to continuum models. A continuum model of the electronic structure, however, when combined with a delta function potential, may yield pathological results. We first explore such an analytic model and the resulting pathologies through the response of a normal metal to a spin-dependent point potential. $\mathrm{Re}g(\mathbf{x}, \mathbf{x}'; \omega = 0)$ diverges as $r = |\mathbf{x} - \mathbf{x}'| \to 0$, and sensible results are not possible unless a nondivergent Green's function is used. It is quite common in such a situation (e.g. Ref. 37) to set $\mathrm{Re}g(\mathbf{x}, \mathbf{x}'; \omega = 0) = 0$. The δ-function potential, however, should be considered a mathematical convenience, and successful use of a δ-function potential is based on the ability to reproduce with it the results of more realistic potentials. Calculations of *local* electronic properties near a δ-function impurity fail using this approximation for the Green's

function. As an example, a calculation using $\mathrm{Re}g(\mathbf{x},\mathbf{x}';\omega=0)=0$ for all positions within the range of the potential yields the same LDOS for both spin-up and spin-down electrons around a potential which attracts spin-up electrons and repels spin-down electrons.

Once this flaw in standard calculations is pointed out, an approximate Green's function which does not yield such pathologies is introduced and the resulting LDOS are analyzed. The $\mathrm{Re}g(0,\mathbf{x};\omega=0)$ is averaged over the range of a physical potential to yield a single parameter α, which depends on the details of the band structure. This example illuminates the importance of a correct understanding of a band structure's effects on local properties.

Section 13 treats the isotropic order parameter superconductor, obtaining the energies of localized states. The model and results are applicable to three dimensions or two dimensions — the details of the band structure are again absorbed into the phenomenological quantity α. The LDOS of localized states is obtained for the special case of a three-dimensional system with a (normal-state) free-electron dispersion relation.

Section 14 addresses the situation where the order parameter is anisotropic. First it is demonstrated that for any anisotropic order parameter there are always at least two intra-gap resonances or localized states associated with a magnetic or nonmagnetic impurity. Subsequently the energies of the intra-gap resonances are determined for an analytic approximation to the Green's functions in a two-dimensional superconductor with a $d_{x^2-y^2}$ order parameter.

The presentation of the point potential concludes in Section 15 with a quite different focus, an examination of the LDOS at a fixed frequency. In the limit that the potential is a point the spatial structure of the LDOS depends on the relative magnitude of two spatially dependent functions which depend only on the Green's functions of the homogeneous superconductor — one which depends on the normal Green's function $g(\mathbf{x},\mathbf{x}';\omega)$ and the other which depends on the anomalous Green's function $f(\mathbf{x},\mathbf{x}';\omega)$. The relative magnitude of these two functions is determined in part by the potential strength of the impurity. Due

to the similarities in the spatial structure of $g(\mathbf{x},\mathbf{x}';\omega)$ and $f(\mathbf{x},\mathbf{x}';\omega)$, the spatial structure of the LDOS is often still given by the Born approximation (weak-scattering) result.

12. Particle-hole symmetry in the normal state

In the limit $\Delta_o \to 0$ the Green's functions of the normal metal can be recovered from Eq. (29). In particular, the anomalous Green's function $f(\mathbf{x},\mathbf{x}';\omega) = 0$. For a three-dimensional free-electron metal the normal Green's function is appropriate for an outgoing wave:

$$g(\mathbf{x},\mathbf{x}';\omega) = -\frac{\pi N_o}{k_F r} e^{ik_F r}, \tag{52}$$

where ω is considered close to the Fermi surface so the change in momentum due to $\omega \neq 0$ is negligible.

When Δ_o and $f(\mathbf{x},\mathbf{x}';\omega)$ vanish, the 2×2 matrix equation of Eq. (20) becomes diagonal. In order to focus on the spin-dependent potential, the nonmagnetic potential will be set to zero. For a spin-dependent delta-function potential the two resulting equations are

$$[1 - g(\mathbf{0},\mathbf{0};\omega)V_S]\, G_\uparrow(\mathbf{0},\mathbf{0};\omega) = g(\mathbf{0},\mathbf{0};\omega), \tag{53}$$

$$[-1 - g^*(\mathbf{0},\mathbf{0};-\omega)V_S]\, G^*_\downarrow(\mathbf{0},\mathbf{0};-\omega) = -g^*(\mathbf{0},\mathbf{0};-\omega). \tag{54}$$

Taking the complex conjugate of Eq. (54) and changing $-\omega$ to ω yields the clearer equation

$$[1 + g(\mathbf{0},\mathbf{0};\omega)V_S] G_\downarrow(\mathbf{0},\mathbf{0};\omega) = g(\mathbf{0},\mathbf{0};\omega). \tag{55}$$

These equations are not well defined for the Green's function of Eq. (52), since the real part of the Green's function diverges at $r = 0$. A common method of coping with this problem is to ignore the real part of g. This approximation is essentially an assumption of a *strict* particle-hole symmetry (not merely linearizing $\epsilon(k)$ around ϵ_F). We can write

$$\mathrm{Re}g(\mathbf{x},\mathbf{x}';\omega) = \int \frac{A(\mathbf{k};\epsilon)e^{i\mathbf{k}\cdot(\mathbf{x}-\mathbf{x}')}}{\omega-\epsilon+i\delta} d\mathbf{k}d\epsilon, \tag{56}$$

where $A(\mathbf{k};\epsilon)$ is the momentum-resolved density of states with a given energy ϵ. In order for $\mathrm{Re}g(\mathbf{x},\mathbf{x}';\omega=0)$ to vanish for all r, we require $A(\mathbf{k};\epsilon) = A(\mathbf{k};-\epsilon)$ for all $\mathbf{k}$ and ϵ. It is this particle-hole symmetry in the momentum-resolved density of states which produces pathological results in the spatially-resolved density of states in the presence of an impurity.

The LDOS calculated with this approximate Green's function around a spin-dependent delta-function potential is

$$-\frac{1}{\pi}\mathrm{Im}G_\sigma(\mathbf{x},\mathbf{x};\omega) = N_o\left(1-\left[\frac{(\pi N_o V_S)^2}{1+(\pi N_o V_S)^2}\right]\frac{\sin^2 k_F r}{(k_F r)^2}\right). \tag{57}$$

This expression yields the pathological behavior that the local density of states near a spin-dependent potential is exactly the same for spin-up electrons as for spin-down electrons. The local density of states for $v_s = \pi N_o|V_S| = 0.1$ is plotted in Figure 6 as a function of distance from the potential. Although it is somewhat distorted from its homogeneous value, it does not show the spin-dependent asymmetry of a more realistic model. An exact calculation for a Gaussian of range k_F^{-1} is also shown in Figure 6 for comparison.

A more realistic approach to coping with the divergence in Eq. (52) without yielding the pathological result of Eq. (57) is to average the ω-symmetric real part of g over a range given by the assumed range of the potential. That yields a finite value for the local density of states at the potential, but does not control the behavior for small r. To perform that task, we consider a "muffin-tin" Green's function. This function has the form

$$\begin{aligned} g(\mathbf{x},\mathbf{x}';\omega) &= -\frac{\pi N_o}{k_F r}e^{ik_F r} \qquad && r > R_o \\ &= -i\pi N_o - \pi\alpha \qquad && r < R_o \end{aligned} \tag{58}$$

where α is the average of the ω-symmetric real part of g over the range of the potential, and R_o is chosen so that the spatially-integrated spectral weight of the Green's function

is unchanged (as required by probability conservation). We show in Figure 6 the local density of states calculated with this Green's function. In particular, the asymmetry in the response of spin-up electrons and spin-down electrons to a spin-dependent delta-function potential is governed by this phenomenological parameter α. The agreement with the exact solution is good at the origin and far from the impurity. The muffin-tin Green's function is discontinuous, unfortunately, but yields a better approximation of the response of the system than the particle-hole symmetric approximation (discarding the ω-symmetric real part of the Green's function).

For a Gaussian potential with range a,

$$\alpha = \frac{2}{\sqrt{\pi} k_F a} \left(1 + \sum_{n=2}^{\infty} \frac{1}{(2n-3)!!} \left(-\frac{(k_F a)^2}{2} \right)^{n-1} \right). \tag{59}$$

For the Gaussian potentials numerically calculated in this paper, $a = k_F^{-1}$, so $\alpha = 0.704$.

It is also possible to generate an asymmetry between spin-up and spin-down electrons by adding a nonmagnetic potential v_0 *with* the v_s to parametrize the impurity, but still maintaining a particle-hole symmetric band structure. Since the response of a particle-hole symmetric system to a potential does not depend on the sign of that potential, the v_0 is required to distinguish between electrons and holes. A spin-up electron feels a potential $v_s + v_0$, whereas a spin-up hole feels a potential $v_s - v_0$. This additional nonmagnetic potential only breaks particle-hole symmetry locally (within the range of the potential), whereas for a realistic band structure the particle-hole symmetry is broken everywhere in the solid.

13. Magnetic and nonmagnetic point potentials in a superconductor with an isotropic order parameter

a. Gor'kov equations and self-consistency

Approximating the local potential by a delta function,

$$\mathbf{V}(\mathbf{x}) = \mathbf{V}\delta(\mathbf{x}) = \begin{pmatrix} V_S + V_0 & 0 \\ 0 & V_S - V_0 \end{pmatrix} \delta(\mathbf{x}) \tag{60}$$

leads to a simple expression for Eq. (20),

$$\begin{pmatrix} 1 - g(\mathbf{0},\mathbf{0};\omega)(V_S + V_0) & -f(\mathbf{0},\mathbf{0};\omega)(V_S - V_0) \\ -f^*(\mathbf{0},\mathbf{0};-\omega)(V_S + V_0) & 1 + g^*(\mathbf{0},\mathbf{0};-\omega)(V_S - V_0) \end{pmatrix} \mathbf{G}(\mathbf{0},\mathbf{0};\omega) = \mathbf{M}^{n\to n}(\omega)\mathbf{G}(\mathbf{0},\mathbf{0};\omega)$$
$$= \mathbf{g}(\mathbf{0},\mathbf{0};\omega). \tag{61}$$

In principle $\mathbf{M}(\omega)$ can be found from the Green's functions in Eq. (29), however the same divergence in the real part of $g(r;\omega)$ as $r \to 0$ which is present in the normal state is present in the superconducting state. This divergence is coped with in Ref. 37 by discarding the divergent piece. This strategy, however, yields the same pathologies in the superconducting state as were found in the normal state. Below we will introduce appropriate Green's functions for the superconducting state. First, however, our definition of the potential $\mathbf{V}$ in this model will be extended to include a crude form of self consistency.

As seen from Figure 5, the distortion of the order parameter is short-ranged around an impurity. We may then consider the effect of the order-parameter distortion on the electronic structure to be parametrized by an effective delta-function potential $\delta\Delta\delta(\mathbf{x})$ similarly motivated to the delta-function potentials for the magnetic and nonmagnetic potentials. The potential $\mathbf{V}(\mathbf{x})$ is changed in the following way:

$$\mathbf{V}(\mathbf{x}) = \mathbf{V}\delta(\mathbf{x}) = \begin{pmatrix} V_S + V_0 & \delta\Delta \\ \delta\Delta & V_S - V_0 \end{pmatrix} \delta(\mathbf{x}). \tag{62}$$

The relative effect of the $\delta\Delta$ compared to the other two potentials is likely to be small for the potentials considered in this paper. Typically $N_o V_S/k_F^3 \sim 1$ or $N_o V_0/k_F^3 \sim 1$, and for a free-electron model of niobium $N_o\Delta_o/k_F^3 = 3.6 \times 10^{-5}$. Even for a small coherence length of $\xi = 10k_F^{-1}$, $N_o\Delta_o/k_F^3 = 1.6 \times 10^{-3}$. For convenience we define $\delta_0 = \pi N_o \delta\Delta$.

b. Energies and character of localized states in the superconductor

The energies of the localized states of angular momentum ℓ correspond to the positive energies $\omega_\ell = |\Omega|$, where

$$\det \mathbf{M}^{n\to n}(\Omega) = 0, \tag{63}$$

and the solution is traced to the ℓ-channel block of $\mathbf{M}$ (see Appendix). For the analytic model, $\mathbf{M}^{n\to n}(\omega)$ is the matrix shown in Eq. (61), where $g(\mathbf{0},\mathbf{0};\omega)$ in the superconducting state is constructed similarly to that of the normal state,

$$g(\mathbf{0},\mathbf{0};\omega) = -\pi N_o \left(\alpha + \frac{\omega}{\sqrt{\Delta_o^2 - \omega^2}}\right). \tag{64}$$

The anomalous Green's function is given by Eq. (29), since it does not have a divergence problem as $r \to 0$,

$$f(\mathbf{0},\mathbf{0};\omega) = -\pi N_o \left(\frac{\Delta_o}{\sqrt{\Delta_o^2 - \omega^2}}\right). \tag{65}$$

This analytic model only has localized states in the $\ell = 0$ angular momentum channel, as expected for a delta-function potential. Those energies are

$$\omega_o = \left|\frac{v_s\delta_0 \pm \left[(v_s\delta_0)^2 - (v_s^2+\gamma^2)(\delta_0^2-\gamma^2)\right]^{1/2}}{v_s^2+\gamma^2}\right|\Delta_o \tag{66}$$

where

$$\gamma = \left[(1+\alpha^2)(v_s^2 - v_0^2 - \delta_0^2) - 2\alpha v_0 - 1\right]/2. \tag{67}$$

Eq. (66) reduces to a result obtained by Shiba[37] when $v_0 = \alpha = \delta_0 = 0$, a result obtained by Rusinov[39] when $\alpha = \delta_0 = 0$, a result obtained by us[14] when $v_0 = \delta_0 = 0$, and a result obtained by Salkola, Balatsky and Schrieffer[93] when $\alpha = 0$.

The energies of Eq. (66) correspond to a spin-up quasiparticle and a spin-down quasiparticle. However, there may be only one real energy; then only one $\ell = 0$ localized state exists around the impurity, as occurs for a magnetic impurity ($v_0 = \delta_0 = 0$). When $v_s = 0$ the localized states are due to order parameter suppression, and the energies of the two spin states are degenerate. This follows from time-reversal symmetry in the absence of a magnetic potential. For small v_s the two energies are split by an amount

$$\Delta\omega_o = \frac{2v_s\delta_o\Delta_o}{v_s^2 + \gamma^2}. \tag{68}$$

c. Spectral weight asymmetry in the analytic model

The spatial structure of the spectral weight as a function of the distance r from the impurity will now be addressed. A spin-up quasiparticle consists of amplitudes for a spin-up electron (electron in a spin-up state), and a spin-up hole (electron missing from a spin-down state). Therefore the spectral weight of a spin-up localized state will be divided between an electron-like pole in the spin-up band at $\omega = \omega_o$ (with weight $A_\uparrow(r;\omega_o)$) and a hole-like pole in the spin-down band at $\omega = -\omega_o$ (with weight $A_\downarrow(r;-\omega_o)$). These two types of excitation are independently resolvable by a scanning tunneling microscope since at positive sample voltage relative to the tip, the STM places electrons in the sample, whereas at negative sample voltage the STM places holes in the sample. We define the energy of the pole in the spin-up band to be $\omega_\uparrow$ and in the spin-down band to be $\omega_\downarrow$. Even though ω_o is always positive, $\omega_\uparrow$ can be positive or negative, and $\omega_\uparrow = -\omega_\downarrow$.

The spatial structure of the spectral weights of the spin-up band and spin-down band components of the localized state are given by

$$A_\sigma(r;\omega) = \frac{\pi N_o \Delta_o}{2v_s}\delta(\omega-\omega_\sigma)\frac{\sqrt{\Delta_o^2-\omega^2}}{\Delta_o}\Bigg[\frac{(v_0-v_s)\Delta_o^2+(v_0+v_s)\omega^2+(v_0+v_s)\alpha^2(\Delta_o^2-\omega^2)}{\Delta_o^2}$$
$$+\frac{2(v_0+v_s)\alpha\,\omega\sqrt{\Delta_o^2-\omega^2}-(1+\alpha^2)(v_0^2-v_s^2)\left(\alpha(\Delta_o^2-\omega^2)+\omega\sqrt{\Delta_o^2-\omega^2}\right)}{\Delta_o^2}\Bigg],$$
$$r < R_o$$
$$= \frac{\pi N_o \Delta_o}{(k_F r)^2}\frac{(\Delta_o^2-\omega^2)^{\frac{3}{2}}}{2v_s\Delta_o^3}\mathrm{e}^{-\frac{2r}{\pi\xi}\left(\frac{\sqrt{\Delta_o^2-\omega^2}}{\Delta_o}\right)}\delta(\omega-\omega_\sigma)\times$$
$$\Bigg[\left(v_s\frac{\Delta_o^2+\omega^2}{\Delta_o^2-\omega^2}-v_0+(v_s^2-v_o^2)\left\{\alpha-\frac{\omega}{\sqrt{\Delta_o^2-\omega^2}}\right\}\right)\sin^2(k_F r)$$
$$+(v_s+v_0)\left(1+(v_s-v_0)\left\{\frac{\omega}{\sqrt{\Delta_o^2-\omega^2}}-\alpha\right\}\right)\cos^2(k_F r)$$
$$+2(v_s+v_0)\left(v_0-v_s+[1-\alpha(v_0-v_s)]\frac{\omega}{\sqrt{\Delta_o^2-\omega^2}}\right)\sin(k_F r)\cos(k_F r)\Bigg],$$
$$r > R_o \qquad (69)$$

The above expression is set up for use as a muffin-tin Green's function. The construction of such a Green's function requires that the spectral weight integrates to one. However, ignoring the contribution from $r < R_o$, the above expression can be integrated over all space, and still yields one-half for the spin-up band and one-half for the spin-down band to order Δ_o/ϵ_F. Note that an intra-gap quasiparticle in an isotropic order parameter superconductor must be one-half electron and one-half hole.

The frequency-integrated weight at the defect of the two types of excitation can be calculated within the analytic model, and is (for $\delta_0 = 0$)

$$\frac{A_\uparrow(r=0)}{A_\downarrow(r=0)} = \frac{1+2\alpha(v_0-v_s)+(1+\alpha^2)(v_0-v_s)^2}{1+2\alpha(v_0+v_s)+(1+\alpha^2)(v_0+v_s)^2} \qquad (70)$$

For a spin-down quasiparticle there is an electron-like pole in the spin-down band and a hole-like pole in the spin-up band and the relative weight is still given by the expression above. This expression for $v_0 = 0$ was reported in Ref. 14.

In Sec 17 these results are compared with numerical calculations of properties in the

superconducting state *and* in the normal state.

14. Anisotropic order parameters

a. A general result for anisotropic order parameters

In anisotropic superconductors a finite density of states remains within the energy "gap". In particular, for a *d*-wave order parameter the density of states remains finite down to the chemical potential. An intra-gap state can hybridize with this continuum of quasiparticles within the gap, producing a *resonance* rather than a localized state.

With a few additional approximations it can be shown that there are always at least two resonant energies for both magnetic and nonmagnetic potentials for an anisotropic superconductor. The first approximation is that impurity-induced variations in the order parameter can be neglected. A further approximation involves the condition for a resonant state, when Re[detM] = 0. For anisotropic superconductors, where there is a finite density of states within Δ_{max} of the chemical potential, detM can have an imaginary part. This part produces a width in the resonance, and it can be argued that the resonance is poorly defined if the width is much greater than Δ_{max}. This problem is complicated by the frequency dependence of Im[detM], which can distort the shape and peak energy of the resonances. These complexities are set aside here as simpler situations are considered.

The Gor'kov equation is

$$[1 - g(\omega)V_e][1 + g^*(\omega)V_h] - f^2(\omega)V_eV_h = \mathrm{detM}. \tag{71}$$

We separate the particle-hole symmetric part of the Green's function from that which is not particle-hole symmetric by assuming the following form for $g(\omega)$:

$$g(\omega) = N_o(\alpha + \tilde{g}(\omega)). \tag{72}$$

Here $\tilde{g}(\omega) = -\tilde{g}^*(-\omega)$. In order to parametrize the anisotropy of the order parameter in a way still suitable to our analytic model we can make the approximation

$$f^2(\omega) = \beta(\omega) N_o^2 (\tilde{g}^2(\omega) + 1). \tag{73}$$

$\beta(\omega)$ is thus a measure of the gap anisotropy. Two special cases yield simple frequency-independent values for $\beta(\omega)$, (1) isotropic s-wave ($\beta = 1$) and (2) d-wave ($\beta = 0$). Using the appropriate dimensionless quantities in our lattice situation, $v_s = \pi N_o V_S$ and $v_0 = \pi N_o V_0$, we can express the conditions for resonant states.

Resonances for magnetic potentials exist when

$$\tilde{g}(\omega) = \left[1 \pm \sqrt{v_s^2(\alpha^2 + \beta)(1 - \beta) + \beta}\right] / (1 - \beta) v_s, \tag{74}$$

and for nonmagnetic potentials when

$$\tilde{g}(\omega) = \pm \sqrt{[(1 - \alpha v_0)^2 + \beta v_0^2] / (1 - \beta) v_0^2}. \tag{75}$$

Since $\mathrm{Re}\tilde{g}(\omega)$ varies from $+\infty$ to $-\infty$ between $\omega = -\Delta_{max}$ and $\omega = \Delta_{max}$, and since for all order parameters except isotropic s-wave $0 \leq \beta(\omega) < 1$ for ω sufficiently close to Δ_{max}, there always are solutions to Eqs. (74) and (75). For the nonmagnetic case solutions come in pairs due to the spin degree of freedom. Note that the degeneracy of the two solutions for the magnetic potential for a particle-hole symmetric d-wave model ($\alpha = \beta = 0$), which was pointed out in Ref. 93 and linked to the point-group of the lattice, is actually not directly related to the spatial symmetry of the superconductor.

b. Energies of resonances for a two-dimensional d-wave superconductor

A d-wave superconductor is a special case of the above results, and one which is likely relevant to high temperature superconductors. The on-site anomalous Green's function vanishes, hence $\beta(\omega) = 0$. Salkola, *et al.*[109] have derived the form of the ordinary Green's

function for the order parameter $\Delta(\phi) = \Delta_{max} \cos 2\phi$, where ϕ is the angle of the momentum from the (10) direction. They obtain

$$G_0(\omega) = -(2\epsilon/\pi)\left[\mathrm{sgn}(\omega)K(\sqrt{1-\epsilon^2}) + iK(\epsilon)\right], \tag{76}$$

for $\epsilon = |\omega|/\Delta_{max} < 1$. K is the complete elliptic integral of the first kind. Solutions to Eq. (75) for $\alpha = 0$ to logarithmic accuracy are given by[110]

$$\Omega_0 = \frac{\Delta_{max}}{2N_F V_0 \ln(8N_F V_0)}, \tag{77}$$

with a linewidth

$$\Gamma = \frac{\pi\Omega_0}{2\ln(8N_F V_0)}. \tag{78}$$

15. Connection to the Born approximation

In Ref. 111 it was argued that calculations within the Born approximation for the *spatial* structure of the $dI(\mathbf{r};V)/dV$ would remain accurate for strong potentials, so long as the potential was short-ranged. In this section we explicitly make the connection between the result from the Born approximation and the result from the Koster-Slater technique in the limit that self-consistency can be ignored and that the size of the potential approaches a point.

In this limit Eq. (36) is

$$-\frac{1}{\pi}\sum_\sigma \mathrm{Im}G_\sigma(\mathbf{x},\mathbf{x};\omega) = -\frac{1}{\pi}\mathrm{Im}\Big\{2g(\mathbf{x},\mathbf{x};\omega) + [\mathbf{g}(\mathbf{x},\mathbf{0};\omega)\mathbf{V}_{\mathbf{eff}}(\omega)\mathbf{g}(\mathbf{0},\mathbf{x};\omega)]_{11} - [\mathbf{g}^*(\mathbf{x},\mathbf{0};-\omega)\mathbf{V}^*_{\mathbf{eff}}(-\omega)\mathbf{g}^*(\mathbf{0},\mathbf{x};-\omega)]_{22}\Big\}, \tag{79}$$

where $\mathbf{V}_{eff}(\omega) = \mathbf{V}[\mathbf{I} - \mathbf{g}(\mathbf{0},\mathbf{0};\omega)\mathbf{V}]^{-1}$. The inhomogeneous part of the right-hand side of Eq. (79) has the following form if the off-diagonal elements of $\mathbf{V}_{\mathbf{eff}}(\omega)$ can be ignored (this is appropriate when self-consistency is not important):

$$-\frac{1}{\pi}\mathrm{Im}\Big\{\left([\mathbf{V_{eff}}(\omega)]_{11}-[\mathbf{V_{eff}}^*(-\omega)]_{22}\right)g(\mathbf{x},\mathbf{0},\omega)g(\mathbf{0},\mathbf{x},\omega)$$
$$-\left([\mathbf{V_{eff}}^*(-\omega)]_{11}-[\mathbf{V_{eff}}(\omega)]_{22}\right)f(\mathbf{x},\mathbf{0},\omega)f(\mathbf{0},\mathbf{x},\omega)\Big\} \tag{80}$$
$$=C_1(\omega)g(\mathbf{x},\mathbf{0},\omega)g(\mathbf{0},\mathbf{x},\omega)-C_2(\omega)f(\mathbf{x},\mathbf{0},\omega)f(\mathbf{0},\mathbf{x},\omega). \tag{81}$$

The functions $C_1(\omega)$ and $C_2(\omega)$ depend on the potential strength and the frequency, but *not* on the position. In Ref. 111 the differential conductance near a a nonmagnetic impurity in the Born approximation was found to depend on the spatial Green's functions in the same combinations as Eq. (81), with $C_1(\omega) = C_2(\omega) = V_0$.

The spatial structure of the LDOS in Eq. (81) depends sensitively on the order parameter anisotropy, and particularly the momenta of the minima and maxima of the order parameter on the Fermi surface. In the real-space directions corresponding to these momenta the LDOS is enhanced. Figures 7(a,b) show the spatial structure of the differential conductance calculated in the Born approximation for a voltage just above Δ_{max} for (a) an isotropic order parameter and (b) a $d_{x^2-y^2}$ order parameter. The normal-state electronic structure is assumed to be that of a quasi-two-dimensional free-electron gas, and the length units are k_F^{-1}. Enhancements of the LDOS along the real-space directions corresponding to gap nodes also have been found at low voltages. Figure 7(c) shows the enhancement of the LDOS at a voltage much less than Δ_{max} along directions rotated 45^o from those in Fig. 7(b). The enhancement of the LDOS along these directions, corresponding to nodes in momentum space of the $d_{x^2-y^2}$ order parameter, occurs because most quasiparticles at low energies have group velocities perpendicular to the Fermi surface near the locations of nodes. This feature was pointed out generally in Ref. 111.

The argument was made in Ref. 111 that the spatial structure calculated in the Born approximation was essentially the same as that obtained in the strong potential limit. The derivation at the beginning of this section justifies these arguments so long as $C_1(\omega)$ is not too different from $C_2(\omega)$. In a later calculation Choi[112] found these two prefactors to

be similar for voltages above Δ_{max} for strongly scattering potentials as well as for weakly scattering potentials, but he did not consider the interesting case of scattering from an intra-gap resonance.

There are two major qualitative changes in the LDOS introduced by a strong potential. One is the relative amplitude of the LDOS at different *frequencies* (due to resonances or localized states). The other is the relative amplitude of $C_1(\omega)$ and $C_2(\omega)$, which can differ substantially from the Born approximation result when ω is near a resonance.

The case for a magnetic potential is slightly different. For a purely magnetic potential there would be no inhomogeneous structure in the LDOS within the Born approximation, since

$$\mathbf{V_{eff}}(\omega) = \begin{pmatrix} V_S & 0 \\ 0 & V_S \end{pmatrix}, \tag{82}$$

so the distortions in the LDOS of the two spin directions are equal and opposite. For a stronger magnetic potential, since $[\mathbf{V_{eff}}(\omega)]_{11} \neq [\mathbf{V_{eff}}^*(-\omega)]_{22}$, the LDOS would be spatially inhomogeneous, and would have similar spatial structure as for the nonmagnetic impurity.

V. IMPURITIES IN SUPERCONDUCTORS WITH ISOTROPIC ORDER PARAMETERS

16. Nonmagnetic impurity

Even strong nonmagnetic impurities at moderate concentrations will not suppress the critical temperature of a superconductor with an isotropic order parameter[35]. Nevertheless, it was recognized early on[66] that the local order parameter may be affected. In Ref. 66 the effect of the nonmagnetic impurity was calculated in the far field by modeling the impurity potential with a phase shift. The phase shifts were evaluated for two models: a

spherical square-well potential and a delta-shell potential. Self-consistency was ignored by only focusing on regions far from the impurity where the change in the order parameter is small compared to its homogeneous value. The order parameter change due to the impurity was found to oscillate with the Fermi wavelength, and decay as r^{-2} for $r < \xi$. For $r > \xi$, expressions in Ref. 66 indicate a decay of r^{-3}.

Figure 8 shows the spectral weight $A(r;\omega)$ at several frequencies above the energy gap near a strong nonmagnetic impurity with a Gaussian potential of range k_F^{-1} and strength $v_0 = 7/8$, calculated self-consistently for a superconductor with $\xi k_F = 449$ (a free-electron parametrization of niobium). The spectral weights are suppressed to approximately 30% of their homogeneous value at the center of the potential. Only continuum states are shown since no localized states were found for this potential. The curves showing the spectral weight have been displaced from each other so that they may be distinguished. Also shown displaced in Fig. 8 is the spectral weight in the normal state, normalized to the spectral weight in the homogeneous metal. *All* the quantities plotted in Fig. 8 are *identical* to the accuracy of the calculation. Fig. 8 is an illustration of a relationship between the spectral weight in the normal state and the spectral weight in the superconducting state,

$$A(r;\omega) = \frac{A_n(r)}{2N_o} A_{sc}(\omega) \tag{83}$$

where $A_n(r)$ is the spectral weight in the inhomogeneous *normal* state for energies near the Fermi surface and $A_{sc}(\omega)$ is the *homogeneous* superconductor's spectral weight as a function of frequency. $2N_o$ is the normal state's spectral weight far from the impurity. This expression is valid for small r and small ω, the regime of interest for STM on a superconductor. For ω of order Δ_o, Eq. (83) is valid for $r \ll \xi$.

We further illustrate the relationship of Eq. (83) in Figure 9(a), which shows the LDOS for this nonmagnetic impurity, normalized by the normal-state density of states, as a function of voltage and position calculated from Eq. (3) with $T = 0.13\Delta_o/k_B$. This temperature

corresponds to 2K for niobium. There is no change in the energy *gap* due to this nonmagnetic potential. Figure 9(a) shows that it is merely the local amplitude of the spectral weight which is reduced — this would manifest itself in a locally reduced oscillator strength for an optical transition, or the reduction in the tunneling current for an STM, which is directly proportional to the LDOS shown in Figure 9(a). Figure 9(b) is an identical calculation for a shorter coherence length, $\xi = 10k_F^{-1}$. There appears to be little difference, although here a localized state exists near the continuum.

Figures 8 and 9(a,b) show for the nonmagnetic impurity that the normal-state electronic structure determines the *spatial* dependence of the superconductor's $A(r;\omega)$ for all frequencies including near the energy gap. The potential strength of the impurity is orders of magnitude greater than Δ_o, and thus locally mixes in states far from the Fermi surface in the homogeneous metal. These states are required to construct probability densities which are suppressed by 70% near the impurity. The spatial structure of the spectral weight in the normal state is essentially identical to that seen in Fig. 8 over an energy range around the Fermi surface which is orders of magnitude greater than Δ_o.

Once the normal-state electronic structure has been distorted by the presence of the nonmagnetic impurity, superconductivity is a small perturbation within a narrower frequency range. The formation of the gap in the single-particle excitation spectrum in the superconducting state is characterized by the "mixing" of electron and hole amplitudes to form quasiparticles near the gap edge. These quasiparticles, therefore, are constructed from eigenstates of the metal which have already been strongly distorted by the impurity potential.

Equation (83) has important implications for spectroscopy on a superconductor, for one of the procedures for normalizing spectra taken at different lateral positions on a superconducting surface is to assume that the LDOS at a particular voltage much larger than Δ_o is the same. This is an attempt to correct for possible changes in the tip-surface distance upon moving the tip laterally. A small change in the tip-surface distance can have a strong

effect on the tunneling current. Unfortunately this procedure will prevent an experiment from seeing changes in the LDOS due to a nonmagnetic impurity, including the conductance oscillations described in Ref. 111.

We now discuss the properties of the order parameter. $\Delta(r)$ is self-consistently determined, and is shown in Fig. 8 for small r to be identical in spatial structure to the normal-state spectral weight,

$$\frac{\Delta(r)}{\Delta_o} = \frac{A_n(r)}{2N_o} = \frac{A(r;\omega)}{A_{sc}(\omega)}. \tag{84}$$

Since a nonmagnetic potential repulsive to electrons attracts holes, and $\Delta(r)$ depends equally on electron and hole amplitudes, one might expect a nonmagnetic potential to have little effect on the spatial dependence of the order parameter. However the allowable maximum spectral density of holes depends on the spectral density of the electron band where the holes reside, so if most electrons are excluded from the site, holes will be effectively excluded as well. To emphasize this point we note that the scaled anomalous spectral weight $\mathrm{Im}F(\mathbf{r},\mathbf{r};\omega)$ is identical to the scaled $A(r;\omega)$ for the frequencies shown in Fig. 8 (and for all relevant frequencies for the self-consistency equation Eq. (28)). Since $\mathrm{Im}F(\mathbf{r},\mathbf{r};\omega)$ is proportional to the product of electron and hole amplitudes, and $A(r;\omega)$ is proportional to the electron amplitude squared, the spatial structure of the electron and hole spectral weights must be similar. They are, since the normal-state spectral weight $A_n(r;\omega)$ is roughly frequency independent around the Fermi energy over an energy range much greater than Δ_o.

We now comment on the lack of localized states near the nonmagnetic impurity for $\xi k_F = 449$ and the small binding energy of the quasiparticle for $\xi k_F = 10$. The suppression of the order parameter near the impurity may be considered to form an attractive off-diagonal potential which may bind quasiparticles. Localized states created by order-parameter suppression would be doubly degenerate, due to the two possible spin states (see Eq.(66)). If the electron part is attracted and the hole part is repelled, one might expect the effects of a

nonmagnetic potential on the localized quasiparticle to cancel, since a localized quasiparticle is half hole and half electron. However the binding energy of the localized state is an order of magnitude smaller ($\omega_o = (1-2\times10^{-4})\Delta_o$) than that found in Section 20 for a suppressed order parameter via pairing suppression. This may be explained by the well-known repulsive effect (quantum reflection) of a strong attractive potential on a quantum-mechanical particle. We find also that in the case of the magnetic impurity that a large enough nonmagnetic potential of either sign will suppress the binding of a quasiparticle to the impurity. We note here that the ratio of the nonmagnetic potential to the off-diagonal potential ($\delta\Delta(\mathbf{r})$) is much larger ($v_0/N_o\Delta_o \sim 10^4$) than the ratios of the nonmagnetic potentials to the magnetic potentials considered below.

17. Magnetic impurity

Recently, we have presented calculations of the LDOS (and thus the differential conductance in an STM experiment) in the vicinity of a magnetic impurity[14]. These calculations indicated that the spatial structure of the electron amplitude of the localized state differed strongly from the hole amplitude. A further result was that the spectrum should recover to the homogeneous spectrum within a few atomic spacings. Similarly motivated calculations of the LDOS due to the $\ell = 0$ localized state have been presented since then[93], although these calculations did not address the continuum LDOS. The two models used in Ref. 93 were (1) a δ-function model solved using particle-hole symmetric Green's functions, but not self-consistently, and (2) self-consistent calculations for a two-dimensional tight-binding s-wave superconductor within the BdG equations. The first method can only model the normal-state properties properly for a particle-hole symmetric band structure, such as at the Van Hove singularity in a two-dimensional tight-binding band structure. The second method must contend with numerical finite-size effects, which make it difficult to calcu-

late the continuum states. A result obtained from the first method which is only true for special band structures is that the spatial structure of the electron and hole components of the quasiparticle are the same. The authors of Ref. 93 did raise the possibility of an additional nonmagnetic potential as a source of electron-hole amplitude asymmetry in the spatial structure of the localized state. We found[14] and will explore below that there is, for realistic band structures, electron-hole asymmetry without a nonmagnetic potential.

a. Energy and character of localized states

We will begin with a discussion of the energies of the localized states around a magnetic impurity and the spin character of those states. Solutions to Eq. (63) can be evaluated numerically. Figure 10 shows the dependence of the energies of the localized state poles for the first two angular momentum channels on the strength of the magnetic potential. Results for a short coherence length ($\xi = 10k_F^{-1}$) are shown (solid line) as well as results for a long coherence length ($\xi = 449k_F^{-1}$). The localized quasiparticle state for small v_s is the spin state attracted to the classical spin, which we will label up ($\uparrow$). As the potential strength increases, the excitation energy of each angular momentum state decreases. At some critical value $v_{s\ell}^*$ the localized state becomes a spin-down excitation, the energy changes abruptly, and then increases with increasing v_s. This behavior can be extracted from the analytic model (Eq. (66)) as well.

Evident from Eq. (21) is that the ℓ-channel electron pole involves entirely single-particle states within the spin-up band when the ℓ-channel solution to Eq. (63), $\Omega > 0$. This occurs for $v_s < v_{s\ell}^*$. However, for $\Omega < 0$ ($v_s > v_{s\ell}^*$)), the electron pole involves entirely states within the spin-down band. The hole-like pole always involves single-particle states in the opposite spin band from the electron-like pole. The source of the quasiparticle amplitude for the various poles is indicated in Fig. 10.

Also shown in Figure 10 are the analytic results for the pole energies for $\alpha = 0$ (Ref. 37) and $\alpha = 0.704$. The muffin-tin model is no better than the particle-hole symmetric model in predicting the localized state energies. The muffin-tin model will prove more successful at predicting the spatial asymmetry between the electron and hole amplitudes of the localized state.

The unimportance of self-consistency for determining the energies of the localized states can be gauged by the small difference between the short-coherence length result and the long-coherence length result. The most important feature it determines in Fig. 10 is the size of the discontinuity in the localized state energy at v_{s0}^*. This discontinuity is due to a discontinuous change in the order parameter at this magnetic potential strength, a result pointed out in Ref. 14 which will be discussed more below.

As seen in Fig. 10, the value of v_{s0}^* is mostly independent of the value of the coherence length. We present the following justification of that observation. The decrease in the quasiparticle energy by the classical spin is proportional to the overlap of the atomic-scale potential and the impurity site. The state is, aside from a r^{-2} falloff, extended over a volume given by the range of the exponential envelope of the localized state (Eq. (69)), $R = \pi\xi/2\sqrt{1-(\omega_o/\Delta_o)^2}$. Thus the overlap, and consequently the quasiparticle's energy reduction, is proportional to $v_s\Delta_o$. When this energy exceeds the energy required to create a quasiparticle (Δ_o), the ground state contains a quasiparticle. Hence v_s^* is approximately independent of Δ_o, and is determined primarily by the normal-state properties of the superconductor.

A more complete interpretation of the energetic diagram of Fig. 10 requires an understanding of the threshold energy to create a pair of excitations, such as in an optical experiment. The pairing is suppressed local to the impurity since an up-spin electron is attracted to the impurity and its time-reversed partner, the down-spin electron, is repelled. Therefore, the energy needed to break a pair and create a localized quasiparticle with an-

gular momentum ℓ in the vicinity of the magnetic impurity, when $v_s < v_{s\ell}{}^*$, is reduced from $2\Delta_o$ to $\Delta_o + \omega_\ell$. One member of the broken pair is a delocalized spin-down quasiparticle at the gap edge (with energy Δ_o). The other member of the broken pair is a *localized* spin-up quasiparticle with energy ω_ℓ. For $v_s > v_{s\ell}^*$ there is a spin-up quasiparticle with angular momentum ℓ in the ground state of the superconductor[40]. An essential point about the ground state of a superconductor containing classical magnetic impurities is that at $T = 0$ when $v_s < v_{s\ell}{}^*$ (for all ℓ) the ground state is composed entirely of paired electrons. When $v_s > v_{s\ell}{}^*$ for any ℓ then the $T = 0$ ground state contains localized quasiparticles as well as pairs and there are new low-energy excitations including the re-formation of a pair as well as the excitation of a localized quasiparticle to a higher energy localized or continuum state (which requires an energy less than any $\Delta_o + \omega_\ell$).

The spin in the ground state of the superconductor can be calculated if some care is taken. In order to obtain good results for the ground-state spin the magnetization density of states must be calculated over the entire portion of the band which lies beneath the chemical potential. This calculation is easier in the two-dimensional lattice model, so results will be presented from there. Figure 11 shows the *integrated* magnetization density of states,

$$S(\epsilon) = \frac{1}{2}\int_{-\infty}^{\epsilon} d\omega \int d\mathbf{x} \mathrm{Im}\left[G_\uparrow(\mathbf{x},\mathbf{x};\omega) - G_\downarrow(\mathbf{x},\mathbf{x};\omega)\right], \tag{85}$$

in an isotropic superconductor for (a) $v_s < v_{s0}$ and (b) $v_s > v_{s0}$. The magnetization density of states is integrated from below the band edge to an energy ϵ. The spin of the ground state corresponds to the value when $\epsilon = \mu$, where μ is the chemical potential (taken here to be $\mu = 0$). The two potentials of Fig. 11(a,b) differ by about 10%, yet clearly for Fig. 11(a) the ground-state spin is zero, and for Fig. 11(b) the ground-state spin is 1/2. These values are indicated on the figure by dashed lines. The contributions to the integrated spin from around $-3.5t$ and around $4.5t$ correspond, respectively, to the bound state of the attracted spin direction and the antibound state of the repelled spin direction.

b. Local density of states

We now focus on our results for the local density of states near the impurity. Figures 12(a), 12(b), and 12(c) show LDOS results for $v_s = 0.52$, 0.875, and 1.75 respectively. They show the state split off from the continuum, with a larger electron-like amplitude than hole-like amplitude (12(a)), and then lower in energy with an increased electron/hole asymmetry (12(b)). Finally the larger peak becomes hole-like (12(c)). In all three cases the spectrum recovers to its bulk value within a few k_F^{-1}, due to the r^{-2} decay of the localized state (Eq. 69). The asymmetry between the electron-like and hole-like peaks becomes more pronounced as v_s increases. We note that the larger peak is always associated with the spin-up band, whereas the other is associated with the spin-down band. Despite the apparent differences in peak size, the spatially integrated electron spectral weight of the quasiparticle is equal to the spatially integrated hole spectral weight. The localized quasiparticle is always half electron and half hole for all potentials examined here. For $v_s < v_{s0}^*$ the spin-up band amplitude is electron-like and the spin-down band amplitude is hole-like. At v_{s0}^* (1.32 for a free-electron model of niobium), the spin-up component becomes hole-like and the spin-down component becomes electron-like, as required by the change in the spin of the excitation.

Figure 12(d) shows the LDOS for a markedly different coherence length, $\xi = 10k_F^{-1}$, and $v_s = 0.875$. It is evaluated for the same value of Δ_o/k_BT as Figs. 12(abc) and looks almost identical to Fig. 12(b). Since the localized state is broadened by temperature through Eq. (3), this is a manifestation of the proportionality of the spectral weight to $N_o\Delta_o$ (Eq. (69)). Figure 13 shows the spectral weight at the origin for the $\ell = 0$ state and for the $\ell = 1$ state at its first maximum for $v_s = 0.875$ as a function of the inverse of the coherence length, which is proportional to $N_o\Delta_o$. Figure 14 shows the spectral weight for $\xi = 449k_F^{-1}$ as a function of v_s for the spin-up and spin-down poles at the origin for the $\ell = 0$ state and at the first maximum for the $\ell = 1$ state. It is clear that a nonmagnetic potential is not necessary

to obtain an electron-hole asymmetry.

In Figure 15 we show the asymmetry at the impurity as a function of v_s for two values of ξ — a long coherence length appropriate for niobium, and a short coherence length. From Figure 13 it should be evident that the asymmetry is not sensitive to ξ. It is, however, predicted extremely well by the normal-state spin-up and spin-down band spectral weight asymmetry at the impurity (also shown in Figure 15). We can therefore conclude that as with the nonmagnetic impurity (Figure 9), the spatial structure of the spectral weight of the localized state around a magnetic impurity is a normal-state property. We further show in Figure 16 for $v_s = 0.875$ the $\ell = 0$, spin-up band and spin-down band projections of the normal-state spectral weight to compare with the localized state spin-up band and spin-down band spectral weights for two values of ξk_F. The normal-state and long-coherence length calculation are practically indistinguishable. The insets show $r^2 A(r)$, which removes the rapid power-law decay of the state. The localized states for all angular momenta ℓ will decay as the power law r^{-2}. For the short-coherence length calculation the effect of an exponential envelope is also visible. In the analytic result the exponential envelope should have a range $R = \pi\xi/2\sqrt{1-(\omega_o/\Delta_o)^2}$, which corrects to better than 1% the discrepancy in Figure 16. The power-law fall-off and exponential envelope can be seen directly from Eq. (29) and Eq. (69).

We can summarize these comments with a general equation, similar in concept to that for the nonmagnetic impurity, Eq. (83). That is, for a localized quasiparticle state of spin σ', the spectral weight of a localized state with angular momentum ℓ would be

$$A_\sigma^{\sigma'}(r;\omega_\ell) = BA_{n\sigma}(r,\ell)\mathrm{e}^{-\left(\frac{2r}{\pi\xi}\right)\sqrt{1-\left(\frac{\omega_\ell}{\Delta_o}\right)^2}}\delta(\omega - \sigma\sigma'\omega_\ell), \tag{86}$$

where B is a normalization factor so that the spectral weight of the state integrates to one, and $A_{n\sigma}(r,\ell)$ is the angular-momentum ℓ projection of the *normal*-state spectral weight in the spin σ band. We note that for small r there is an approximate relationship between the

superconducting state's spectral weight and the normal state's spectral weight in each spin band,

$$\frac{1}{2E}\int_{-E}^{E} d\omega A_\sigma(r;\omega) = A_{n\sigma}(r), \tag{87}$$

where $\Delta_o \ll E \ll \epsilon_F$. This, in connection with Eq. (86), implies a dependence on the normal-state structure of the continuum spectral weight around the magnetic impurity.

c. Recent experimental results

Recent experimental results on the local spectra of single atoms placed on the (110) surface of niobium[113] indicate: (1) discrete states are evident within the energy gap and the LDOS associated with them is asymmetric with voltage around $V = 0$, and (2) the LDOS becomes indistinguishable from the bulk density of states within a distance greater than the Fermi wavelength but much less than the coherence length. Figure 17 shows these STM difference spectra. Three different atoms were placed on the surface: manganese (Mn), gadolinium (Gd), and silver (Ag). Niobium is an isotropic-order parameter superconductor, so the behavior of magnetic and nonmagnetic impurities should be different. The Ag atom is not expected to show any magnetic behavior, while the d electrons of Mn and the f electrons of Gd may produce local moments. It is known that Mn has a local moment in bulk Nb[42,43]. Due to the differences in coordination, however, the exchange interaction of such an atom placed on the surface will not be the same, and hence it was not known whether they would produce a local moment.

The difference spectra of Fig. 17 is obtained in the following way: the tip is positioned at the given distance from the center of the impurity, and the height of the tip is adjusted until the resistance of the junction is 10^7 ohms at a voltage of 10 mV. Then the tunneling spectrum taken with a similarly normalized junction far from the impurity is subtracted.

As pointed out in Section 16, this procedure discards any uniform suppression of the local density of states over this (narrow) voltage range. A nonmagnetic impurity produces such a uniform suppression, and so the difference spectra obtained near the silver atom indicate no change from the bulk spectrum.

A quite different situation is found for the Mn and Gd atoms. Near the impurity the difference spectra indicate a suppression of the gap-edge density of states and an enhancement of the intra-gap density of states. It is particularly noteworthy that the spectra are extremely particle-hole asymmetric. These qualitative results are consistent with the results of Sec 17, reported in Ref. 14 and elaborated in Ref. 15. The later theoretical work of Ref. 93 and Ref. 113 is also consistent.

An attempt was made in Ref. 113 to model the experimental results with a spherical square-well potential for the impurity, and a free-electron normal-state band structure for niobium. The results of that comparison for the difference spectrum measured directly on top of the Mn atom are shown in Fig. 18. The agreement shown here is actually somewhat marginal, since the energy and height of the large hole-like peak can be fit by adjusting the range of the square-well and the strength of the spin-dependent potential. The width of the peak is determined by the temperature. The remaining feature of the spectrum is the relative height of the electron-like and hole-like peaks, which is not well fit. A more flexible model, with less trivial position-dependence of the spin-dependent potential, is able to better fit the experimental results. There are more serious problems, however, with this strategy, which are now described.

The authors of Ref. 113 argue that the Mn impurity on the Nb surface is a strong impurity, based primarily on the hole-like nature of the larger peak in the difference spectrum of Fig. 18. The actual value of the exchange integral they extract is $J = 4\text{eV}$, which is considerably stronger than the $J = 2.7\text{eV}$ of a Mn atom in the bulk[43]. This appears unlikely, since the lower coordination number of an atom on the surface would lead to a

weaker exchange interaction. The unlikely large value of J is due to the assumed electronic structure of niobium in Ref. 113. Far from having a normal-state free-electron dispersion, niobium has a d band at the Fermi energy which is more than half filled. These d-band states are most likely to interact with the d-state of Mn. Since this d band is more than half filled, the carriers which predominately interact with the impurity spin are holes. We reconsider the arguments of Section 17 in the light of a normal-state Fermi surface which is hole-like. For weak impurities, the state near the continuum is predominately hole-like near the impurity. When a quasiparticle falls into the ground state, and thus the impurity is strong, the large quasiparticle peak is electron-like. This is the opposite of the situation for an electron-like Fermi surface. Therefore a large hole-like peak near the impurity is indicative of a *weak* impurity, rather than a strong impurity.

In order to make further progress in a detailed comparison between theory and experiment it appears necessary to perform a calculation based on a more appropriate model of the niobium electronic structure. Such models are available within pseudopotential theory, and work is underway in this direction.

d. Structure of the inhomogeneous order parameter

We now return to the structure of $\Delta(\mathbf{x})$. This quantity, which is not directly observable, formed the focus of several investigations of the local structure around a magnetic impurity. The oscillation of the order parameter around a magnetic impurity was first evaluated without self-consistency[62–64]. A self-consistent calculation of the order parameter at the impurity and very far away for *weak* impurity potentials was done by Schlottmann[65].

As shown in Figure 5, for large values of v_s, $\Delta(r = 0) < 0$. Sign changes in Δ, as seen in pair tunneling, have been suggested for magnetic impurities in the barriers of Josephson junctions[114–117]. The sign change in $\Delta(0)$ occurs (at $T = 0$) precisely at v_{s0}^*. Due to the

spin and frequency symmetries of Eqs. (20-27), the anomalous spectral weight $\mathrm{Im}F(\mathbf{r},\mathbf{r},\omega)$ associated with the spin-up pole is always equal and opposite to the anomalous spectral weight associated with the spin-down pole. As the pole in the spin-up band goes from electron-like ($\omega > 0$) to hole-like ($\omega < 0$) and the pole in the spin-down band goes from hole-like to electron-like the contribution to $\Delta(0)$ changes sign abruptly at $T = 0$. The $\Delta(r)$ resulting from several values of v_s and two values of the coherence length are shown in Figure 19(a,b). The discontinuity at v_{s0}^* is more pronounced for shorter coherence lengths since the localized state's spectral weight is more concentrated at the impurity (Eq. (86)). $\Delta(0)$ as a function of v_s is shown in Figure 20 for two values of the coherence length. At $T > 0$ the transition would be smoothed somewhat.

The behavior of $\Delta(0)$ as a function of v_s comes from the introduction at v_{s0}^* of a quasiparticle into the ground state of the system. The spin-up quasiparticle localized near the impurity in the ground state suppresses the local order parameter. For time-reversal invariant potentials one cannot make $\Delta(r)$ negative by inserting a single quasiparticle, since the suppression from one quasiparticle is cancelled by the lack of suppression from its unexcited Kramers doublet partner. For a spin-dependent potential, however, the anomalous spectral weight near the impurity may be almost entirely contributed by the single low-energy localized state. When a quasiparticle is present in the ground state, the ground state has spin-$\frac{1}{2}$ up[40] and a negative $\Delta(r)$[14]. Exciting the low-energy state for $v_s > v_{s0}^*$ removes the spin-up quasiparticle, and therefore *increases* $\Delta(0)$, whereas excitation of quasiparticles typically reduces $\Delta(\mathbf{x})$ (which is the case for $v_s < v_{s0}^*$). Also, exciting the low-energy state alone, such as in a tunneling experiment, *reduces* the total spin of the superconductor.

The behavior of $\Delta(r)$ for large r has not been evaluated numerically. We expect the contribution of the localized state to decay with a length determined by the exponential envelope in Eq. (69), $R_{loc} = \pi\xi/2\sqrt{1-(\omega_o/\Delta_o)^2}$. The contributions from the continuum states at a given ω have a ω-dependent spatial oscillation and decay as r^{-2}. When those

contributions are integrated from Δ_o to ω_D, one obtains a $r^{-3}\sin(r/R_{cont})$ decay, where $R_{cont} \sim \xi\Delta_o/\omega_D$. Since $R_{loc} > R_{cont}$ it would be possible to have first a $r^{-2}\exp(-r/R_{loc})$ decay, followed by an oscillatory r^{-3} decay. The oscillatory r^{-3} decay was pointed out in Ref. 65. We emphasize that, although the order parameter appears to recover to its bulk value over a length scale much shorter than the coherence length, this is again a manifestation of the r^{-2} behavior of the normal and anomalous spectral weights. When $\delta\Delta(r)$ is multiplied by the surface area of the sphere at radius r, one finds that the order parameter's recovery length is on the order of the coherence length.

18. Combined magnetic and nonmagnetic potentials

We now discuss the addition of a nonmagnetic potential to the magnetic potential. It has been suggested[93] that introducing a v_0 with a v_s will provide electron-hole asymmetry. We find that it does change the asymmetry, which we show in Figure 21 for a particular v_s, but that once again this is a normal-state property. The relationship between the normal-state spectral weights and the superconducting-state spectral weights of Eq. (86) still holds. Introducing v_0 also alters the localized-state energies (see Eq. (66)), which we show in Figure 22 for $v_s = 0.875$ and $\xi k_F = 449$. The presence of a nonmagnetic potential may affect the value of v_{s0}^*[93]. We show in Figure 23 a partial diagram of the ground state as a function of the parameters v_s and v_0 for $\xi k_F = 449$. We note that the boundary between the two ground states is not shifted much from $\xi k_F = 449$ to $\xi k_F = 10$, hence the order parameter energy is not very significant in determining this boundary.

19. Connection to normal-state dI/dV spectra

The normal state may provide some guidance for attempts to extract impurity potentials in the superconducting state from STM measurements. Figure 24 shows *normal-state*

dI/dV's for various potentials. These curves should also represent the frequency-averaged spectral weight measured in the superconducting state (see Eq. (87)).

The enhancement or suppression of spectral weight near the origin is particularly sensitive to v_0. A measurement of this quantity, the energy of the localized state and the asymmetry of the electron and hole amplitudes at the impurity overconstrains v_0 and v_s, given an assumption of the shape of the potential. To extract information about the potential's detailed shape would require a fitting procedure using the differential conductance at various positions. If, for some reason, the spin-down amplitude were too small to measure, it may be possible to constrain the potential strength using the frequency-integrated spectral weight and the localized-state energy.

It seems appropriate to mention again the tendency to normalize spectra according to the LDOS measured at energies much larger than Δ_o. Since the normal-state LDOS near the impurity changes substantially in the presence of magnetic or nonmagnetic impurities, an experiment performed using such a normalization procedure would yield impurity parameters of questionable validity.

20. Pairing suppression

The pairing potential, $\gamma(\mathbf{x})$ in Eq. (28), may also have spatial structure. When this parameter is changed it induces a change in the order parameter which produces an off-diagonal potential felt by the quasiparticles. We set $v_s = v_0 = 0$ so that there is no magnetic or nonmagnetic potential to compete with the order parameter change. Figure 25 shows the order parameter around a short-range suppression,

$$\gamma(\mathbf{x}) = \left[1 - \mathrm{e}^{-(k_F r)^2}\right] \gamma_o, \tag{88}$$

for two values of the coherence length. The order parameter is strongly suppressed and since $\gamma(\mathbf{0}) = 0$, $\Delta(\mathbf{0}) = 0$. For long coherence lengths, this change in the order parameter has

no effect on the local density of states (shown in Figure 26(a)). It is possible to localize quasiparticle states, however, at shorter coherence lengths. These can produce features in the local density of states which are visible. One such case is shown in Figure 26(b). The energy of the localized state is $\omega_o = (1 - 4 \times 10^{-3})\Delta_o$. Whereas a nonmagnetic potential changes the local density of states without significantly changing the energy gap, a pairing suppression has a very weak effect on both, especially in the long-coherence length limit.

21. Comparison of local electronic structure near impurities with that near vortices

As pointed out in Section 10, the vortex has a weak potential, on the scale of meV, extended over a long distance, of order ξ. The impurity, however, has a strong potential, on the order of eV, extended over a short distance, of order Å. Localized excited states are found in both cases, but several qualitative differences should be described. Whereas even for a strong potential the impurity induces one well-localized state, and possibly a few more very weakly bound states, the vortex localizes states over a volume of order ξ. The quasiparticle excitation energies in a superconductor with an isotropic order parameter are shown in Fig. 27 as a function of angular momentum. Just as in an atomic system, the expectation value of the distance from the vortex core increases with increasing angular momentum. Thus the quasiparticles at greater and greater distances are more and more weakly localized. The states above 1.2 meV are in the continuum, but appear at definite energies due to the finite size of the system.

The position-dependence of quasiparticle energies implies that STM tunneling spectra taken close to the vortex core will show well-localized states within the gap. As the distance from the core increases the position of the quasiparticle states within the gap gets closer to the gap edge. Fig. 28 shows the calculated differential conductance for several different distances from the vortex core, showing this characteristic feature of the intra-gap states.

STM measurements around a magnetic impurity are quite different. Since there is usually only one localized state the intra-gap energy of the state will not change with distance — but the magnitude of the LDOS will change.

VI. IMPURITIES IN SUPERCONDUCTORS WITH ANISOTROPIC ORDER PARAMETERS

Several experiments, including photoemission[95–97], Josephson edge and corner tunneling devices[98], and tricrystal rings[99] strongly indicate that the order parameter in high-temperature superconductors is anisotropic. The above experiments also support the $d_{x^2-y^2}$ order parameter, while other experiments[118] indicate the order parameter in some crystals may be d+s, or some other anisotropic combination.

Results for the local electronic structure of impurities in $d_{x^2-y^2}$ superconductors will be presented here. The normal-state electronic structure of the superconductor will be taken to be a one-band two-dimensional tight-binding model, based on the properties of the copper-oxygen planes in these high-temperature superconducting compounds[94]. The nearest-neighbor and next-nearest neighbor hopping elements are chosen to be $t = 350$meV and $t' = 56$meV, respectively, while the chemical potential (which determines the doping) is $\mu = 0$.

22. Energy and character of resonances

An important distinction between isotropic and anisotropic order parameters (particularly order parameters which vanish at places on the Fermi surface) is that in a superconductor with an anisotropic order parameter a finite density of states remains within the energy "gap". In the case of an order parameter which vanishes at places on the Fermi surface, there is a finite density of states down to zero energy within the energy gap. Hence

any impurity-associated localized state within the gap can hybridize with the continuum of quasiparticle states within the gap. The resulting impurity feature will be a resonance, rather than the pure localized state of Section 17.

To illustrate this we first show[119] in Fig. 29 the energies of the resonances in a $d_{x^2-y^2}$ superconductor for nonmagnetic potentials with strength v_0. These energies Ω, which are identified by peaks in the DOS within our calculations, are shown along with the analytic calculations from Ref. 93 (see also Section 14). These analytic calculations are based on a particle-hole symmetric expression for the homogeneous Green's functions, and so are the same for $\pm v_0$.

A further problem, however, is that these analytic calculations are based on the standard method of identifying resonances: setting the real part of the **T**-matrix denominator zero and using the remaining imaginary part to determine the width. This method was used to derive Eq. (75) of Section 14, which applies to superconductors with asymmetric band structures and order parameter anisotropy. Results from Eq. (75), shown on Fig. 29, do agree better with the numerical results, although they still differ by 50% for $\Omega > 0.3\Delta_{max}$. Results obtained using the exact numerical Green's functions in detM, and solving for Re[detM]$= 0$, do not differ qualitatively from those obtained from Eq. (75).

A useful comparison with the $d_{x^2-y^2}$ system is to a system where the order parameter is the absolute value of the $d_{x^2-y^2}$ order parameter. This order parameter, referred to as an s^*-wave order parameter, has the same magnitude as the d-wave order parameter, but does not change sign. In contrast to the resonances for the d-wave system, resonances for nonmagnetic impurities in the s^*-wave system do not have lower energy than $\Omega = 0.77\Delta_{max}$. Hence if the order parameter were s^*-wave, in order to produce low-energy resonances, the impurities would have to be magnetic.

The differential DOS for nonmagnetic and magnetic impurities in a $d_{x^2-y^2}$ superconductor and an s^*-wave superconductor with the same gap magnitude are shown in Fig. 30. The

differential DOS is the change in the DOS due to the addition of one impurity. Shown are the reductions in the density of states near the gap feature. Spectral weight pulled to lower energies in the presence of the impurity exactly compensates for that taken from the gap feature. A resonance's lineshape is much sharper on the low-energy side and broader on the high-energy side, due to the frequency-dependent DOS in the homogeneous superconductor. This also shifts the energy of the peak of a resonance.

Each resonance for the nonmagnetic impurity has a spin degeneracy. For a magnetic impurity there are typically two resonances, but at different energies since the superconductor is not particle-hole symmetric. For the d-wave superconductor, where $\beta = 0$, the energies of the two resonances for a magnetic impurity of strength v_s are expected to correspond to the same energies as those of a nonmagnetic impurity of strength $+v_s$ and a nonmagnetic impurity of strength $-v_s$. These resonances are quite difficult to disentangle unambiguously from the numerical results, so our focus will be on nonmagnetic impurities.

23. Local density of states

In order to describe the LDOS it is important to connect the LDOS calculated at points on the two-dimensional lattice,

$$A(\mathbf{R}_{ij};\omega) = -\frac{1}{\pi}\sum_{\sigma} \mathrm{Im}G_{\sigma}(\mathbf{R}_{ij},\mathbf{R}_{ij};\omega), \tag{89}$$

to the LDOS of the real continuous system. Implied in our lattice description is the existence of Wannier functions at each lattice site in the superconductor. The continuous LDOS is then the product of the lattice LDOS with these Wannier functions,

$$A(\mathbf{r};\omega) = \sum_{ij} A(\mathbf{R}_{ij};\omega)|\phi(\mathbf{r}-\mathbf{R}_{ij})|^2, \tag{90}$$

where $\phi(\mathbf{r})$ is the Wannier function associated with the single effective tight-binding band of a homogeneous copper-oxygen plane. If $\phi(\mathbf{r})$ is well-localized to an individual copper site,

only one term in the sums over i and j will contribute, greatly simplifying the result. The differential conductance is proportional to the LDOS of Eq. (90), so there is the following relationship between the differential conductance and the lattice LDOS:

$$\frac{dI}{dV}(\mathbf{r}, V) \propto \int_{-\infty}^{\infty} d\omega \frac{\partial n_{STM}(\omega)}{\partial \omega} \sum_{ij} A(\mathbf{R}_{ij}; \omega) |\phi(\mathbf{r} - \mathbf{R}_{ij})|^2. \tag{91}$$

The LDOS at the impurity site for an isotropic order parameter superconductor is shown in Fig. 31(a) for several magnetic impurity strengths V_S. Since the band-structure filling is over half, the carriers are holes. As described in Section 17, when the carriers are holes, for weak impurity potentials the large peak at the impurity is hole-like. As the potential strength increases the large peak moves towards the chemical potential, and eventually to the electron-like continuum edge. Figure 31(b) shows the LDOS at a nonmagnetic impurity site for a $d_{x^2-y^2}$ superconductor for several potential strengths. In contrast to Fig. 31(a), only a hole-like peak is seen at smaller potentials, and for a large potential the peak is entirely electron-like. Figure 31(c) is for a magnetic impurity in the $d_{x^2-y^2}$ superconductor, and indicates that the size of the large peak is about half the size as for a nonmagnetic impurity. An additional structure is evident on the electron-like side of the spectrum, which is due to the other intra-gap resonance (see Eqs. (74) and (75)). The two resonances of the nonmagnetic impurity are degenerate, and correspond to the two spin directions. The two resonances of the magnetic impurity, however, in general occur at quite different energies.

We now show in Fig. 32 the LDOS for magnetic and nonmagnetic impurities in a $d_{x^2-y^2}$ superconductor at sites along a direction from the impurity along the (10) direction and also along the (11) direction. At the impurity site there is no evidence of the gap features, and the spectrum is dominated by an asymmetric resonance which is hole-like for $V = 2.5t$ and electron-like for $V = 10t$. The result for $V = 2.5t$ is in rough agreement with STS measurements[120,121] near oxygen vacancies on the $YBa_2Cu_3O_{7-\delta}$ surface, also shown. Immediately adjacent to the impurity the gap edge feature begins to recover in strength.

Whereas the DOS for potentials of $2.5t$ and $10t$ are roughly identical (Fig. 30), the LDOS at the impurity site is entirely hole-like for $2.5t$ and electron-like for $10t$. Although our surface model is incomplete (e.g. it does not include the copper-oxygen chains), supporting evidence is provided by STS[120,121] identification of a broad resonance at the oxygen vacancies for positive sample bias voltages around 700 meV, consistent with a potential of $2.5t$.

We now consider the spatial structure of the LDOS at specific voltages. In Section 15 the spatial structure of the LDOS was explored for s-wave and $d_{x^2-y^2}$ superconductors with cylindrical Fermi surfaces. Figure 33 shows the LDOS for $V = 2.5t$ at (a) the hole-like peak and (b) and the electron-like peak of the resonance. For this potential the LDOS peak at the impurity site is entirely hole-like. In addition the LDOS along the diagonals away from the impurity vanishes for the electron-like peak of the resonance.

In Section 15 it was pointed out that the spatial structure of the LDOS depends on the relative magnitude of two functions — one depending on the normal Green's function and one on the anomalous Green's function. In the Born approximation the two functions have approximately the same magnitude. The situation is completely different for Fig. 33(a,b), for the two voltages shown correspond to the hole-like and electron-like LDOS of a resonance which is entirely hole-like at the impurity. As a result, the hole-like LDOS of the resonance has the spatial structure of $g(\mathbf{x}, \mathbf{0}; \omega)g(\mathbf{0}, \mathbf{x}; \omega)$, while the electron-like LDOS has the spatial structure of $f(\mathbf{x}, \mathbf{0}; \omega)f(\mathbf{0}, \mathbf{x}; \omega)$. The different spatial structure of these two functions is the origin of the different spatial structure apparent in Fig. 33(a,b). The vanishing of the electron-like resonance LDOS along the diagonals occurs because the anomalous Green's function $f(\mathbf{0}, \mathbf{x}; \omega)$ vanishes (by symmetry) for all energies for $\mathbf{x}$ along diagonals. The normal Green's function does not vanish along those diagonals, so the hole-like resonance LDOS has a pronounced density of states along the diagonals.

We note that such atomic-scale aspects of the LDOS would not be produced in a calculation which coarse-grained the electronic structure, such as the Eilenberger equations.

These features are also not extractable from the Born approximation, since they require knowledge of whether the resonance is hole-like or electron-like at the impurity site. Born approximation calculations for the LDOS at low energies (Fig. 7(c)) do reproduce the rough angular structure far from the impurity. The enhancement of the LDOS along the diagonals of the square lattice is a result of a larger density of states of quasiparticles with group velocity along the diagonals at low energies.

Figure 33(c) shows the LDOS for a voltage just exceeding the order parameter maximum. Oscillations along the four directions corresponding to gap maxima are clearly present, and are *reductions* of the LDOS. This is the origin of the spectral weight which is pulled into the intra-gap region and becomes (in part) the intra-gap resonances. Again, these features are also evident in the Born approximation calculations (Fig. 7(b)). Figure 33(d) shows the LDOS around such an impurity in the normal state, indicating that while the enhancements along (10) or (11) directions are not present in the normal state, the structure on the smaller spatial scale is quite similar. The anisotropy of the order parameter serves to amplify or suppress the spatial features which already exist in the normal state.

24. Local distortion of the order parameter

a. Character of the ground state

Fig. 34(a) shows for magnetic impurities the order parameter at the impurity, and in the inset the total spin of the superconductor's ground state. In contrast to the isotropic s-wave case, where the order parameter at the impurity changes abruptly at some critical potential strength[14], for d-wave the order parameter changes smoothly at all potentials, due to the finite width of the resonant state. For s-wave this transition is characterized by the binding of a quasiparticle in the ground state[40,14,93], producing an abrupt change in

the ground-state spin of the superconductor from 0 to 1/2. For the d-wave superconductor there is instead a cloud of quasiparticles near the impurity potential. The non-quantized behavior arises because there are quasiparticle states at the chemical potential in the d-wave superconductor, but not in the s-wave superconductor.

The d-wave order parameter changes sign for sufficiently strong positive (electron repelling) nonmagnetic impurities (shown in Fig. 34(b)), but not for magnetic impurities or negative nonmagnetic impurities. The difference between positive and negative nonmagnetic impurities is due to the hole-like character of the Fermi surface — a nonmagnetic potential which repels electrons attracts the holes to the impurity. The positive nonmagnetic impurity attracts twice as much hole weight (due to spin degeneracy) to the impurity as the magnetic impurity, so the order parameter suppression is greater. A change in the order parameter sign may affect the presence or absence of a Josephson π-junction[114–117], should the coupling across an interface be near nonmagnetic impurities, such as in a rough junction.

b. Presence of other local order parameter symmetries near the impurity

The symmetry properties of the order parameter near a localized impurity with the symmetry of the lattice are somewhat subtle. In the model used here of nearest-neighbor pairing the order parameter is associated with the nearest-neighbor bonds between lattice sites rather than the sites themselves on the square lattice. An order parameter symmetry, however, is associated with a site; four symmetries are allowed, depending on the relative sign and magnitude of the four nearest-neighbor bonds emanating from a site. These four are:

$$\Delta_s(\mathbf{R}_{ij}) = \Delta(\mathbf{R}_{ij},\mathbf{R}_{i,j+1}) + \Delta(\mathbf{R}_{ij},\mathbf{R}_{i,j-1}) + \Delta(\mathbf{R}_{ij},\mathbf{R}_{i+1,j}) + \Delta(\mathbf{R}_{ij},\mathbf{R}_{i-1,j}), \tag{92}$$

$$\Delta_d(\mathbf{R}_{ij}) = \Delta(\mathbf{R}_{ij},\mathbf{R}_{i,j+1}) + \Delta(\mathbf{R}_{ij},\mathbf{R}_{i,j-1}) - \Delta(\mathbf{R}_{ij},\mathbf{R}_{i+1,j}) - \Delta(\mathbf{R}_{ij},\mathbf{R}_{i-1,j}), \tag{93}$$

$$\Delta_{p_x}(\mathbf{R}_{ij}) = \Delta(\mathbf{R}_{ij},\mathbf{R}_{i,j+1}) - \Delta(\mathbf{R}_{ij},\mathbf{R}_{i,j-1}), \tag{94}$$

$$\Delta_{p_y}(\mathbf{R}_{ij}) = \Delta(\mathbf{R}_{ij}, \mathbf{R}_{i-1,j}) - \Delta(\mathbf{R}_{ij}, \mathbf{R}_{i+1,j}). \tag{95}$$

These order parameters will be referred to as local order parameter symmetries. p_x and p_y symmetries are not typically considered, for they are associated with triplet pairing in a homogeneous superconductor.

In an inhomogeneous superconductor, however, these other symmetries naturally arise. Consider a bond-related order parameter $\Delta(\mathbf{R}_{ij}, \mathbf{R}_{i,j+1})$ which decreases as j increases. This is naturally described by an induced p_x component of the order parameter. The explanation of its presence in singlet pairing is that the system is not homogeneous. Consider a general form for the nearest-neighbor bond-related order parameter in an inhomogeneous superconductor,

$$\Delta(\mathbf{R}, \mathbf{R}+\delta) = \sum_i F_i(\mathbf{R})\Delta_i(\delta), \tag{96}$$

where i labels the symmetry of the local order parameter component and F_i is a spatially-dependent order parameter amplitude (not the Gor'kov amplitude). The condition for singlet pairing is that

$$\Delta(\mathbf{R}, \mathbf{R}+\delta) = \Delta(-\mathbf{R}, -\mathbf{R}-\delta), \tag{97}$$

where $\mathbf{R}$ can be measured from any site of symmetry. In the homogeneous superconductor $F_i(\mathbf{R})$ is spatially uniform and any site is a site of symmetry, so $\Delta_i(\delta) = \Delta_i(-\delta)$, eliminating p_x and p_y symmetry. In the *inhomogeneous* superconductor, however, the only site of symmetry is the site where the impurity is located. Thus the condition of Eq. (97) is satisfied for p_x and p_y symmetry if $F_i(\mathbf{R}) = -F_i(-\mathbf{R})$. The local odd parity of $\Delta_i(\delta)$ is compensated for by an odd-parity amplitude $F_i(\mathbf{R})$.

When a superconducting transition occurs the system condenses with a particular symmetry of the order parameter. That symmetry creates other conditions on the amplitudes

of the various local order parameter symmetries. For example, if the symmetry is $d_{x^2-y^2}$ an additional condition exists around a site of symmetry,

$$\Delta(\mathbf{R}_{ij}, \mathbf{R}_{i,j+1}) = -\Delta(\mathbf{R}_{ji}, \mathbf{R}_{j+1,i}). \tag{98}$$

Here again the site of symmetry is the impurity site. From Eq. (98) conditions on the spatial amplitudes of the local order parameter symmetries can be derived, such as $F_d(\mathbf{R}_{ij}) = F_d(\mathbf{R}_{ji})$ and $F_s(\mathbf{R}_{ij}) = -F_s(\mathbf{R}_{ji})$. The spatial amplitude of the local d-wave order parameter symmetry is s-like, whereas that of the local s-wave order parameter symmetry is d-like. Furthermore, $F_{p_x}(\mathbf{R}_{ij}) = -F_{p_y}(\mathbf{R}_{ji})$. These features derived from symmetry can be seen in Fig. 35(a-d) which shows the spatial amplitude of the local order parameter symmetries.

In some early work the p_x and p_y components were neglected (e.g., Ref. 69). The results of Ref. 69 are not strictly incorrect, however, for every bond is shared by two sites ($\Delta(\mathbf{R}, \mathbf{R}+\delta) = \Delta(\mathbf{R}+\delta, \mathbf{R})$). Hence the description outlined above is overcomplete. The problem with neglecting p_x and p_y components in favor of s and d is that reconstructing the bond-related order parameter from $F_s(\mathbf{R})$ and $F_d(\mathbf{R})$ becomes a non-local problem. Another strategy would be to associate two bonds with each site and calculate symmetric and antisymmetric combinations of these two bonds. This method, however, loses the connection between the local order parameter components and the symmetries of the lattice. A more elegant solution would consider the order parameter amplitudes to be defined on every other site. In particular, this procedure does not cause difficulties when one attempts to use the results obtained from this microscopic model to obtain coefficients for an effective Ginzburg-Landau model.

The presence of other local order parameter symmetries around the impurity can be considered a natural result of inhomogeneity, and particularly of gradients in the bond-related order parameter of the superconductor. Consideration of the symmetry of the inhomogeneous system around the impurity site allows one to derive detailed relationships among the

spatial amplitudes of these new local order parameter symmetries.

25. Planar tunneling

The detailed results obtained from calculations of the local properties of the electronic structure can also assist in understanding macroscopic measurements, such as planar tunneling spectra. The planar tunneling dI/dV is proportional to the DOS, so the local information is lost. As a result, the strongly particle-hole asymmetric STM dI/dV spectra of Fig. 32 are averaged to produce a planar dI/dV spectrum which is essentially particle-hole symmetric.

We fit the (quite varied) planar tunneling results of three different experimental groups[122–124] (shown in Fig. 36). None of the curves in Fig. 36 look like a typical clean d-wave superconductor's DOS. Nevertheless all four curves are fit by adding impurities of essentially the *same scattering strength* to a $d_{x^2-y^2}$ superconductor in different concentrations and assuming slightly different voltage resolutions. The experimental drop in differential conductance due to the gap structure is only about 30%; we interpret the large residual differential conductance as due to a metallic background originating from the copper-oxygen chains[120,121]. Note that these results are also consistent with magnetic impurities in an s^*-wave superconductor at roughly double the concentration. We believe that these impurities are oxygen vacancies near the surface of $YBa_2Cu_3O_{7-\delta}$, which are present in concentrations on the order of 1% even in nominally fully oxygenated samples[125–127].

Whereas the DOS for potentials of $2.5t$ and $10t$ are roughly identical, and thus the results in Fig. 36 can be fit with either potential strength, the LDOS at the impurity site is entirely hole-like for $2.5t$ and electron-like for $10t$. Since the measured LDOS at the oxygen vacancy is hole-like, the potential strength of the oxygen vacancy must be $2 - 2.5t$. This is an excellent example of the value of coordinating results from STS with results from bulk measurements. The planar tunneling measurements would not be sufficient to

distinguish between two possible scattering strengths, but by probing the local properties of the individual impurity with STS it is possible to make this determination.

VII. BRIEF DISCUSSION OF RECENT RESULTS FOR DYNAMICAL SPINS

In the previous section remarkable agreement was achieved between experimental and theoretical results on planar tunneling spectra by assuming the presence of a finite concentration of strongly scattering nonmagnetic impurities. The experimental planar tunneling spectra from Refs. 122–124 are characteristic of tunneling into the c-axis surface in $YBa_2Cu_3O_{7-\delta}$. Due to the layered structure of $YBa_2Cu_3O_{7-\delta}$, these surfaces are quite special.

Tunneling into a surface whose normal has any component in the ab plane are quite different, and are characterized by the presence of a zero-bias anomaly. The traditional interpretation of this zero-bias anomaly is due to the presence at these surfaces of dynamical magnetic impurities. A model of noninteracting quantum spins present in the interface[128,129] does generate this zero-bias anomaly.

Recently considerable interest has been generated by the observation that, in the absence of a magnetic field, and at sufficiently low temperatures, the zero-bias anomaly splits into two distinct peaks[130]. This behavior is not consistent with a model based on noninteracting spins, in which a magnetic field is required for splitting the zero-bias anomaly. The anomaly is also split by a magnetic field, but if it were due to noninteracting spins the splitting would be characterized by a large g-factor at low fields. Furthermore the splitting saturates at large fields. One new explanation which has been proposed of this effect is the presence of a subdominant order parameter which splits a zero-bias anomaly arising from an Andreév surface bound state. Details of this theory can be found in Ref. 131, and it will not be discussed in detail here.

We find that the experimental observations from Ref. 130 can be incorporated into a model of dynamical magnetic impurities at the surface if the impurities interact with each other. These dynamical magnetic impurities would most likely be uncompensated copper spins, and appear to be present at all interfaces in $YBa_2Cu_3O_{7-\delta}$ except when $YBa_2Cu_3O_{7-\delta}$ is c-axis cleaved (parallel to the copper-oxygen planes). At sufficiently low temperatures the spin-spin interactions cause the spin dynamics to freeze out, and the spins behave essentially as static spins. The DOS from static spins has already been discussed in detail in Section 22, and is characterized by two peaks symmetric around the chemical potential. At higher temperatures when the timescale of the dynamics of the impurity spins is fast, the zero-bias anomaly is present, just as if the impurities were not interacting. As the temperature is lowered, however, the timescale of motion of the impurity spins increases and the tunneling spectra will show the splitting of the zero-bias anomaly. Within this model the presence of the anomalous g-factor is due to the interactions among the spins, and is not surprising in a system which resembles a spin glass.

Figure 37 indicates the differential DOS from an impurity calculated for various timescales of the impurity spin. The impurity potential is $V_S = 3t$. For a fast timescale (large ω_o) there is spectral weight centered at the chemical potential. As the spin slows down, and thus ω_o decreases, the spin begins to appear approximately static and the characteristic double-peak spectrum of the static magnetic impurity reappears. We emphasize that the explanation in terms of dynamical spins is consistent with all currently published experimental observations.

This is an area of considerable current interest, and further experimental probes of the interface region will be required to determine whether our explanation based on dynamical spins, the explanation of Ref. 131, or some other explanation is correct. Probes which are likely to be sensitive to the Andreév surface current are those sensitive to current flow, such as scanning SQUIDs, while a detailed probe of the surface with an STM would be most

useful to determine the role of spins.

VIII. SUMMARY

The local electronic structure around an defect reflects both the properties of a defect and the medium in which it is embedded. For a strong nonmagnetic or magnetic impurity in a superconductor, the distortion of the normal-state properties by the strong impurity plays a vital role in the response of the superconducting medium. For an isotropic gap superconductor the LDOS for the inhomogeneous superconductor can be related to the LDOS for the inhomogeneous normal metal via equations like Eq. (83) and Eq. (86). In the case of a nonmagnetic impurity with no localized states around it, the LDOS for the inhomogeneous superconductor is merely the normalized LDOS for the inhomogeneous normal metal multiplied by the homogeneous superconductor's density of states. This should suggest some caution regarding the method used to normalize STM spectra taken at different places on a superconductor's surface.

For the case of a localized state (such as around a magnetic impurity) with angular momentum ℓ, the LDOS for the state is the angular-momentum-ℓ-projected LDOS of the inhomogeneous normal metal multiplied by a decaying exponential whose range is determined by the energy of the localized state. Since the spin-up band LDOS in the normal state differs from the spin-down band LDOS in the normal state, the electron-like pole of the localized quasiparticle will have different spatial structure than the hole-like pole of the localized quasiparticle.

For an impurity embedded in a host with an anisotropic order parameter, the anisotropy of the host produces rich spatial structure in the LDOS around the impurity. This structure includes the four-fold "cross" pattern which should be apparent for voltages just above the gap maximum of a d-wave superconductor as well as the 45^o rotated cross pattern at low

voltages. It also includes the variation in the relative heights of the electron-like and hole-like components of a resonant state. Resonant states in d-wave superconductors appear to explain the typical planar tunneling curves, and also may explain the recently observed splitting of the zero-bias anomaly on the ab edges of $YBa_2Cu_3O_{7-\delta}$.

The self-consistent calculations described here have been performed with a new, powerful, Koster-Slater technique which allows the Gor'kov equation to be solved in principle exactly. We note that technique should be generalizable to any condensed electronic system where mean field theory is a good approximation. The order parameter will have different physical meanings and the self-consistency conditions are likely to have somewhat different forms, but the general technique itself should survive. It is extremely well suited for STM probes of condensed electronic systems, for its strength is in determining the short-length scale, low-energy properties of the system.

ACKNOWLEDGMENTS

We wish to thank C.M. Lieber for helpful conversations. We also wish to thank the authors of Ref. 83 and Ref. 113 for providing figure originals.

M.E.F. wishes to acknowledge the Office of Naval Research's Grant No. N00014-96-1-1012. J.M.B. wishes to acknowledge an N.R.C. Postdoctoral Fellowship.

APPENDIX

The expansion of the Green's functions of Eq. (29) suitable for a three-dimensional spherically symmetric situation are detailed here. The homogeneous Green's functions depend on $\mathbf{r}$ and $\mathbf{r}'$ through r, r', and $\cos\gamma = (\mathbf{r}\cdot\mathbf{r}')/rr'$. Then the Green's functions can be expanded in Legendre polynominals $P_\ell(\cos\gamma)$.

$$g(\mathbf{r},\mathbf{r}';\omega) = g(r,r',\cos\gamma;\omega) = \frac{2\ell+1}{4\pi}\sum_{\ell} g_\ell(r,r';\omega)P_\ell(\cos\gamma) \tag{99}$$

and

$$g_\ell(r,r';\omega) = 2\pi\int_{-1}^{1} P_\ell(x)g(r,r',x;\omega). \tag{100}$$

Evaluating Eq. (100) for both the normal and anomalous Green's functions of Eq. (29) yields

$$\begin{aligned} g_\ell(r,r';\omega) = -\frac{\pi^3}{\sqrt{rr'}}\Bigg[& i\left(1+\frac{\omega}{\sqrt{\omega^2-1}}\right) J_{\ell+\frac{1}{2}}(\{1+\sqrt{\omega^2-1}/\xi\}r^<)H^{(1)}_{\ell+\frac{1}{2}}(\{1+\sqrt{\omega^2-1}/\xi\}r^>) \\ & -\left(1-\frac{\omega}{\sqrt{\omega^2-1}}\right) J_{\ell+\frac{1}{2}}(\{1-\sqrt{\omega^2-1}/\xi\}r^<)H^{(2)}_{\ell+\frac{1}{2}}(\{1-\sqrt{\omega^2-1}/\xi\}r^>)\Bigg] \end{aligned} \tag{101}$$

$$\begin{aligned} f_\ell(r,r';\omega) = -\frac{i\pi^3}{\sqrt{rr'}}\frac{1}{\sqrt{\omega^2-1}}\Big[& J_{\ell+\frac{1}{2}}(\{1+\sqrt{\omega^2-1}/\xi\}r^<)H^{(1)}_{\ell+\frac{1}{2}}(\{1+\sqrt{\omega^2-1}/\xi\}r^>) \\ & +J_{\ell+\frac{1}{2}}(\{1-\sqrt{\omega^2-1}/\xi\}r^<)H^{(2)}_{\ell+\frac{1}{2}}(\{1-\sqrt{\omega^2-1}/\xi\}r^>)\Big] \end{aligned} \tag{102}$$

where J_ℓ, $H^{(1)}_\ell$, and $H^{(2)}_\ell$ are standard Bessel functions, $r^<$ ($r^>$) is the smaller (larger) of r and r', ω is in units of Δ_o and r and r' are in units of k_F^{-1}. The Green's functions are in units of N_o.

The Gor'kov equation, Eq. (20), can now be written in a form diagonal in ℓ,

$$\mathbf{G}_\ell(r,r';\omega) = \mathbf{g}_\ell(r,r';\omega) + \int_0^\infty r_n^2 dr_n \mathbf{g}_\ell(r,r_n;\omega)\mathbf{V}(r_n)\mathbf{G}_\ell(r_n,r';\omega). \tag{103}$$

Thus the three-dimensional integral has been reduced to a one-dimensional radial integral. Since the numerical inversion procedure depends on inverting a matrix whose rank is proportional to the number of spatial points considered, this reduction to a one-dimensional integral dramatically increases the speed of this calculation over a calculation for a three-dimensional potential which is not spherically symmetric.

REFERENCES

[1] See, e.g. *La Matiere mal condenseé (Ill-condensed matter)*, ed. R. Balian, R. Maynard, and G. Toulouse, North-Holland, New York, (1979).

[2] See, e. g., P. G. de Gennes, *Superconductivity of Metals and Alloys*, Addison-Wesley, Reading, MA (1989).

[3] G. Bastard, in *Proceedings of the NATO Advanced Study Institute on Molecular Beam Epitaxy in Heterostructures, Erice, Italy, 1983,* ed. L. L. Chang and K. Ploog Martinus-Nijhoff, Dordrecht (1984), p. 381.

[4] S. H. Tessmer, D. J. Van Harlingen, J. W. Lyding, *Phys. Rev. Lett.* **70**, 3135 (1993).

[5] S. H. Tessmer, M. B. Tarlie, D. J. Van Harlingen, D. L. Maslov, and P. M. Goldbart, *Phys. Rev. Lett.* **77**, 924 (1996).

[6] M.F. Crommie, C.P. Lutz, and D.M. Eigler, *Nature (London)* **363**, 524 (1993).

[7] Y. Hasegawa and P. Avouris, *Phys. Rev. Lett.* **71**, 1071 (1993).

[8] G. Binning and H. Rohrer, *Helv. Phys. Acta* **55**, 726 (1982).

[9] G. Binnig, H. Rohrer, Ch. Gerber, and E. Weibel, *Phys. Rev. Lett.* **49**, 57 (1982).

[10] G. Binnig and H. Rohrer, *IBM J. Res. Develop.* **30**, 355 (1986).

[11] J. Tersoff and D. R. Hamann, *Phys. Rev. B* **31**, 805 (1985).

[12] P. K. Hansma and J. Tersoff, *J. Appl. Phys.* **61**, R1 (1987).

[13] see A. A. Abrikosov, L. P. Gor'kov, and I. E. Dzyaloshinski, *Methods of Quantum Field Theory in Statistical Physics*, Dover, New York, (1963).

[14] M. E. Flatté and J. M. Byers, *Phys. Rev. Lett.* **78**, 3761 (1997).

[15] M. E. Flatté and J. M. Byers, *Phys. Rev. B* **56**, 11213 (1997).

[16] G.F. Koster and J.C. Slater, *Phys. Rev.* **95**, 1167 (1954).

[17] G.F. Koster and J.C. Slater, *Phys. Rev.* **96**, 1208 (1954).

[18] E. W. Montroll and R.B. Potts, *Phys. Rev.* **100**, 525 (1955).

[19] e.g. M. Jaros, *Deep Levels in Semiconductors* Adam Hilger, Bristol (1982).

[20] T. Wolfram and J. Callaway, *Phys. Rev.* **130**, 2207 (1963).

[21] D. K. Wohlleben and B. R. Coles in *Magnetism V*, ed. H. Suhl, Academic Press, New York (1973), p. 3.

[22] A. Blandin in *Magnetism V*, ed. H. Suhl, Academic Press, New York (1973), p. 57.

[23] J. Friedel, *Nuovo Cimento Suppl.* **7**, 287 (1958).

[24] A. Blandin and J. Friedel, *J. Phys. Radium* **20**, 160 (1959).

[25] P. W. Anderson, *Phys. Rev.* **124**, 41 (1961).

[26] J. Zaanen, G. A. Sawatzky and J. W. Allen, *Phys. Rev. Lett.* **55**, 418 (1985).

[27] M. B. Maple, J. Wittig, and K. S. Kim, *Phys. Rev. Lett.* **23**, 1375 (1969).

[28] B. T. Matthias, H. Suhl, and E. Corenzwit, *Phys. Rev. Lett.* **1**, 92 (1958).

[29] C. Herring, *Physica* **24**, S 184 (1958).

[30] H. Suhl and B. T. Matthias, *Phys. Rev.* **114**, 977 (1959).

[31] A. A. Abrikosov and L. P. Gor'kov, *Zh. Eksp. Teor. Fiz.* **39**, 1781 (1962) (*Soviet Phys. JETP* **12**, 1243 (1961)).

[32] M. Ma and P.A. Lee, *Phys. Rev. B* **32**, 5658 (1985).

[33] J. Bardeen, L. N. Cooper, and J. R. Schrieffer, *Phys. Rev.* **106**, 162 (1957).

[34] J. Bardeen, L. N. Cooper, and J. R. Schrieffer, *Phys. Rev.* **108**, 1175 (1957).

[35] P.W. Anderson, *Phys. Rev. Lett.* **3**, 325 (1959).

[36] F. Marsiglio, J.P. Carbotte, A. Puchkov, and T. Timusk, *Phys. Rev. B* **53**, 9433 (1996).

[37] H. Shiba, *Prog. Theor. Phys.* **40**, 435 (1968).

[38] L. Yu, *Acta Physica Sinica* **21**, 75 (1965).

[39] A. I. Rusinov, *Soviet Phys. JETP Letters* **9**, 85 (1969).

[40] A. Sakurai, *Prog. Theor. Phys.* **44**, 1472 (1970).

[41] M. B. Maple in *Moment Formation in Solids*, ed. W. J. L. Buyers, Plenum, New York (1984), p. 1.

[42] D. S. Buchanan, A. Roy, D. M. Ginsberg, and J. E. Cunningham, *Phys. Rev. B* **29**, 2469 (1984).

[43] A. Roy, D. S. Buchanan, D. J. Holmgren, and D. M. Ginsberg, *Phys. Rev. B* **31**, 3003 (1985).

[44] S. D. Bader, N. E. Phillips, M. B. Maple, and C. A. Luengo, *Solid State Commun.* **16**, 1263 (1975).

[45] J. Zittartz and E. Müller-Hartmann, *Z. Physik* **232**, 11 (1970).

[46] E. Müller-Hartmann and J. Zittartz, *Z. Physik* **234**, 58 (1970).

[47] E. Müller-Hartmann and J. Zittartz, *Phys. Rev. Lett.* **26**, 428 (1971).

[48] O. Sakai, Y. Shimizu, H. Shiba, and K. Satori, *J. Phys. Soc. Japan* **62**, 3181 (1993).

[49] M. Jarrell, D.S. Sivia, and B. Patton, *Phys. Rev. B* **42**, 4804 (1990).

[50] W. Chung and M. Jarrell, *Phys. Rev. Lett.* **77**, 3621 (1996).

[51] K. Westerhold and B. von Hedt, *J. Low Temp. Phys.* **95**, 123 (1994).

[52] J. Giapintzakis, D. M. Ginsberg, M. A. Kirk, and S. Ockers, *Phys. Rev. B* **50**, 15967 (1994).

[53] E. R. Ulm, J.-T. Kim, T. R. Lemberger, S. R. Foltyn, and X. Wu, *Phys. Rev. B* **51**, 9193 (1995).

[54] D. A. Bonn, S. Kamal, K. Zhang, R. Liang, D. J. Baar, E. Klein, and W. N. Hardy, *Phys. Rev. B* **50**, 4051 (1994).

[55] W. N. Hardy, D. A. Bonn, D. C. Morgan, R. Liang, and K. Zhang, *Phys. Rev. Lett.* **70**, 3999 (1993).

[56] L. S. Borkowski and P. J. Hirschfeld, *Phys. Rev. B* **49**, 15404 (1994).

[57] R. Fehrenbacher and M. Norman, *Phys. Rev. B* **50**, 3495 (1994).

[58] P. J. Hirschfeld and N. Goldenfeld, *Phys. Rev. B* **48**, 4219 (1993).

[59] R. Prange, *Phys. Rev.* **129**, 2495 (1963).

[60] J. P. Hurault, *Journal de Physique* **26**, 252 (1965).

[61] P.W. Anderson and H. Suhl, *Phys. Rev.* **116**, 898 (1959).

[62] T. Tsuzuki and T. Tsuneto, *Prog. Theor. Phys.* **37**, 1 (1967).

[63] J. Heinrichs, *Phys. Rev.* **168**, 451 (1968).

[64] R. Kummel, *Phys. Rev B* **6**, 2617 (1972).

[65] P. Schlottmann, *Phys. Rev. B* **13**, 1 (1976).

[66] A.L. Fetter, *Phys. Rev.* **140**, A1921 (1965).

[67] V. L. Ginzburg and L. D. Landau, *J. Exptl. Theoret. Phys. (USSR)* **20**, 1064 (1950).

[68] G. Eilenberger, *Z. Phys.* **214**, 195 (1968).

[69] P. I. Soininen, C. Kallin, and A. J. Berlinsky, *Phys Rev. B* **50**, 13883 (1994).

[70] M. Franz, C. Kallin, P. I. Soininen, A. J. Berlinsky, and A. L. Fetter, *Phys. Rev. B* **53**, 5795 (1996).

[71] W. Pesch and L. Kramer, *J. Low Temp. Phys.* **15**, 367 (1974).

[72] U. Klein, *J. Low Temp. Phys.* **69**, 1 (1987).

[73] N. Hayashi, M. Ichioka, and K. Machida, *Phys. Rev. Lett.* **77**, 4074 (1996).

[74] M. Ichioka, N. Hayashi, N. Enomoto, and K. Machida, *Phys. Rev. B* **53**, 15316 (1996).

[75] H. F. Hess, R. B. Robinson, R. C. Dynes, J. M. Valles, Jr., and J. V. Waszicak, *Phys. Rev. Lett.* **62**, 214 (1990).

[76] H. F. Hess, R. B. Robinson, R. C. Dynes, J. M. Valles, Jr., and J. V. Waszicak, *J. Vac. Sci. Tchnol. A* **8**, 450 (1990).

[77] P. Muzikar, *Phys. Rev. B* **43**, 10201 (1991).

[78] E. V. Thuneberg, J. Kurkijärvi, and D. Rainer, *Phys. Rev. B* **29**, 3913 (1984).

[79] J. D. Shore, M. Huang, A. T. Dorsey and J. P. Sethna, *Phys. Rev. Lett.* **62**, 3089 (1989).

[80] A. W. Overhauser and L. L. Daemen, *Phys. Rev. Lett.* **62**, 1691 (1989).

[81] A. W. Overhauser and L. L. Daemen, *Phys. Rev. B* **40**, 10778 (1989).

[82] F. Gygi and M. Schlüter, *Phys. Rev. B* **41**, 822 (1990).

[83] F. Gygi and M. Schlüter, *Phys. Rev. B* **43**, 7609 (1991).

[84] R. Corcoran, P. Meeson, Y. Onuki, P.-A. Probst, M. Springford, K. Takita, H. Harima, G.Y. Guo, and B.L. Gyorffy. *J. Phys. Condens. Matter* **6**, 4479 (1994).

[85] Y.-D. Zhu, F. C. Zhang, and M. Sigrist, *Phys. Rev. B* **51**, 1105 (1995).

[86] F. Guinea and Yu. Pogorelov, *Phys. Rev. Lett.* **74**, 462 (1995).

[87] H. Hess, R. B. Robinson, and J. V. Waszczak, *Phys. Rev. Lett.* **64**, 2711 (1990).

[88] F. Gygi and M. Schlüter, *Phys. Rev. Lett.* **65**, 1820 (1990).

[89] T. Xiang and J.M. Wheatley, *Phys. Rev. B* **51**, 11721 (1995).

[90] M. Franz, C. Kallin, and A.J. Berlinsky, *Phys. Rev. B* **54**, R6897 (1996).

[91] Y. Onishi, Y. Ohashi, Y. Shingaki and K. Miyake, *J. Phys. Soc. Japan* **65**, 675 (1996).

[92] M.E. Flatté and J.M. Byers, unpublished.

[93] M. Salkola, A. Balatsky, and J.R. Schrieffer, *Phys. Rev. B* **55**, 12648 (1997).

[94] G. Burns, *High-temperature superconductivity: an introduction*, Academic Press, San Diego, CA (1992).

[95] D. S. Dessau, B. O. Wells, Z.-X. Shen, W. E. Spicer, A. J. Arko, R. S. List, D. B. Mitzi, and A. Kapitulnik, *Phys. Rev. Lett.* **66**, 2160 (1991).

[96] Z. X. Shen, D. S. Dessau, B. O. Wells, D. M. King, W. E. Spicer, A. J. Arko, D. Marshall, L. W. Lombardo, A. Kapitulnik, P. Dickinson, S. Doniach, J. DiCarlo, A. G. Loeser, and C. H. Park, *Phys. Rev. Lett.* **70**, 1553 (1993).

[97] Z.-X. Shen and D. S. Dessau, *Phys. Rep.* **253**, 1 (1995).

[98] D. A. Wollman, D. J. Van Harlingen, W. C. Lee, D. M. Ginsberg, and A. J. Leggett, *Phys. Rev. Lett.* **71**, 2134 (1993).

[99] C. C. Tsuei, J. R. Kirtley, C. C. Chi, L. S. Yu-Jahnes, A. Gupta, T. Shaw, J. Z. Sun, and M. B. Ketchen, *Phys. Rev. Lett.* **73**, 593 (1994).

[100] J. Annett, N. Goldenfeld, and A. J. Leggett, in *Physical Properties of High Temperature Superconductors Volume 5*, ed. D. M. Ginsberg, World Scientific, Singapore (1996).

[101] R. Fehrenbacher and M. R. Norman, *Phys. Rev. Lett.* **74**, 3884 (1995).

[102] M. R. Norman, M. Randeria, H. Ding, and J. C. Campuzano, *Phys. Rev. B* **52**, 615 (1995).

[103] C. Caroli, P. G. de Gennes, and J. Matricon, *Phys. Lett.* **9**, 307 (1964).

[104] J. Bardeen, R. Kümmel, A.E. Jacobs, and L. Tewordt, *Phys. Rev.* **187**, 556 (1969).

[105] Y. Wang and A. H. MacDonald, *Phys. Rev. B* **52**, 3876 (1995).

[106] A. L. Fetter and P. C. Hohenberg, in *Superconductivity*, ed. R. D. Parks, Marcel Dekker, Inc., New York (1969).

[107] see J. R. Schrieffer, *Theory of Superconductivity*, Benjamin-Cummings, Reading (1983).

[108] V. Ambegaokar and A. Griffin, *Phys. Rev.* **137**, A1151 (1965).

[109] M.I. Salkola, A.V. Balatsky, and D.J. Scalapino, *Phys. Rev. Lett.* **77**, 1841 (1996).

[110] A. V. Balatsky, M. I. Salkola, and A. Rosengren, *Phys. Rev. B* **51**, 15547 (1995).

[111] J.M. Byers, M.E. Flatté, D.J. Scalapino, *Phys. Rev. Lett.* **71**, 3363 (1993).

[112] C.H. Choi, *Phys. Rev. B* **50**, 3491 (1994).

[113] A. Yazdani, B. A. Jones, C.P. Lutz, M.F. Crommie, and D. M. Eigler, *Science*, **275**, 1767 (1997).

[114] B.I. Spivak and S.A. Kivelson, *Phys. Rev. B* **43**, 3740 (1991).

[115] S. V. Kuplevakhskii and I. I. Fal'ko, *Fiz. Nizk. Temp.* **10**, 691 (1984) [*Sov. J. Low Temp. Phys.* **10**, 361 (1984)].

[116] L. N. Bulaevski, V. V. Kuzii, and A. Sobyanin, Pis'ma *Zh. Eksp. Teor. Fiz.* **47**, 314 (1977), [*JETP Lett.* **25**, 290 (1977)].

[117] See references in M. Sigrist and T.M. Rice, *Rev. Mod. Phys.* **67**, 503 (1995).

[118] K. A. Kouznetsov, A. G. Sun, B. Chen, A. S. Katz, S. R. Bahcall, J. Clarke, R. C. Dynes, D. A. Gajewski, S. H. Han, M. B. Maple, J. Giapintzakis, J.-T. Kim, and D. M. Ginsberg, *Phys. Rev. Lett.* **79**, 3050 (1997).

[119] M. E. Flatté and J. M. Byers, to be published.

[120] H. L. Edwards, A. L. Barr, J. T. Markert, and A. L. de Lozanne, *Phys. Rev. Lett.* **73**, 1154 (1994).

[121] H. L. Edwards, D. J. Derro, A. L. Barr, J. T. Markert, and A. L. de Lozanne, *Phys. Rev. Lett.* **75**, 1387 (1995).

[122] J. Geerk, X. X. Xi and G. Linker, *Z. Phys. B* **73**, 329 (1988).

[123] I. Takeuchi, J. S. Tsai, Y. Shimakawa, T. Manako, and Y. Kubo, *Physica C* **158**, 83 (1989).

[124] M. Gurvitch, J. M. Valles, Jr., A. M. Cucolo, R. C. Dynes, J. P. Garno, L. F. Schneemeyer,

and J. V. Waszczak, *Phys. Rev. Lett.* **63**, 1008 (1989).

[125] E. F. Skelton, A. R. Drews, M. S. Osofsky, S. B. Qadri, J. Z. Hu, T. A. Vanderah, J. L. Teng, and R. L. Greene, *Science* **263**, 1416 (1994)

[126] V. M. Browning, E. F. Skelton, M. S. Osofsky, S. B. Qadri, J. Z. Hu, L. W. Finger, and P. Caubet, *Phys. Rev. B* **56**, 2860 (1997).

[127] S. B. Qadri, E. F. Skelton, P. R. Broussard, V. C. Cestone, M. S. Osofsky, V. M. Browning, M. E. Reeves, W. Prusseit, *Thin Solid Films* **308**, 420 (1997).

[128] J. A. Appelbaum, *Phys. Rev.* **154**, 633 (1967)

[129] J. A. Appelbaum and L. Y. L. Shen, *Phys. Rev. B* **5**, 544 (1972).

[130] M. Covington, M. Aprili, E. Paraoanu, L. H. Greene, F. Xu, J. Zhu, and C. A. Mirkin, *Phys. Rev. Lett.* **79**, 277 (1997); Erratum **79**, 2598 (1997).

[131] M. Fogelstrom, D. Rainer, and J. A. Sauls, *Phys. Rev. Lett.* **79**, 281 (1997); Erratum **79**, 2754 (1997).

FIGURES

FIG. 1. The "phase diagram" of the Anderson model in a mean-field (Hartree-Fock) treatment as a function of the separation of the d-orbital energy from the Fermi energy and the width of the resonant state. Regions where the d-orbital is magnetic or nonmagnetic are indicated. [After Ref. 25.]

FIG. 2. The ratio of the density of states in the superconductor to that of the normal metal in a paramagnetic alloy as a function of the excitation frequency. The parameter $\alpha = [\tau\Delta]^{-1}$ is a a measure of the linewidth of the quasiparticles. [From Ref. 108.]

FIG. 3. (a) The density of states in a quasi-two-dimensional superconductor with a $d_{x^2-y^2}$ order parameter. The nearest-neighbor hopping matrix element, $t = 350$ meV, while the next-nearest-neighbor hopping matrix element, $t' = -56$ meV. The order parameter $\Delta_{max} = 25$ meV. The broadening introduced in order to evaluate the density of states is $\Gamma = 0.3$ meV. (b) A close-up view of the "gap" region (solid line). The dashed line shows the result of broadening by $\Gamma = 0.1t = 35$ meV. This severe broadening is required to smooth out the finite-size effects in the BdG calculations.

FIG. 4. The self-consistently evaluated order parameter near a vortex calculated with the BdG equations. For this system, the coherence length (as defined as the distance over which the order parameter relaxes to its bulk value) $\xi = 206$ atomic units (a.u.) [From Ref 83.]

FIG. 5. Change in the local order parameter, $\delta\Delta(\mathbf{x})$, for a magnetic potential strength $v_s = \pi N_o |\int d\mathbf{x} V_S(\mathbf{x})| = 1.75$ as a function of the distance from the impurity r. The change becomes negligible beyond $10k_F^{-1}$. [From Ref. 15.]

FIG. 6. Spectral weight in the normal state around a magnetic impurity with $v_s = 0.1$ as a function of the distance from the impurity r. The solid lines are exact solutions for spin-up (attracted by the impurity) and spin-down (repelled by the impurity) electrons for a Gaussian potential of range k_F^{-1} in a metal with a free-electron dispersion relation. The dashed line, which is the same for both spin-up and spin-down electrons, is the calculated spectral weight for the particle-hole symmetric delta-function potential model. The dot-dashed line is the result for a delta-function potential calculated using the muffin-tin Green's functions. The muffin-tin Green's functions fix the pathological result of the symmetric model that the spectral weight is the same for spin-up and spin-down electrons. The muffin-tin parameter, $\alpha = 0.704$, is determined by the range of the Gaussian potential and is therefore not a free parameter. [From Ref. 15.]

FIG. 7. Differential conductance, normalized to the normal metal's homogeneous differential conductance, near a nonmagnetic impurity ($V_0 N_o = 1$) in a superconductor. The length scale is set by k_F^{-1} and the coherence length is $10k_F^{-1}$. The range of the intensity is from -0.1 (black) to 0.1 (white). (a) Isotropic order parameter, voltage of $1.1\Delta_{max}$. (b) $d_{x^2-y^2}$ order parameter, voltage of $1.1\Delta_{max}$. (c) $d_{x^2-y^2}$ order parameter, voltage of $0.1\Delta_{max}$. For (c) the result has been multiplied by the radius to enhance the oscillatory features far from the impurity. [(a) and (b) from Ref. 111.]

FIG. 8. Comparison of the spectral weight in the superconducting state at several frequencies to the spectral weight of the normal state and the spatial dependence of the order parameter. All of these curves are indistinguishable, but they have been displaced for better visibility. The spectral weights are normalized to their value at large distances from the impurity r, and the order parameter is normalized to the homogeneous order parameter Δ_o. This figure indicates that normal-state properties drive the spatially-dependent features of the superconductor's spectrum. [From Ref. 15.]

FIG. 9. Differential conductance (LDOS) as a function of voltage and position calculated around a nonmagnetic impurity with $v_0 = 0.875$. The LDOS is normalized by the homogeneous DOS of the normal state. The spectrum is suppressed substantially in the vicinity of the impurity. The temperature is $0.13\Delta_o/k_B$, which for niobium corresponds to about 2K. (a) A coherence length appropriate for niobium, $\xi k_F = 449$. (b) A much shorter coherence length, $\xi k_F = 10$. [From Ref. 15.]

FIG. 10. Energies of the quasiparticle poles as a function of the magnetic potential strength v_s for the first two angular momentum states around the impurity. The spin-up and spin-down labels refer to the band that the excitation resides in — an excitation with negative energy (hole-like) in a spin-up band is a spin-down hole. The solid line corresponds to $\xi k_F = 10$, the long-dashed line to $\xi k_F = 449$, the short dashed line to the symmetric model of Shiba, and the dot-dashed line to the result calculated with muffin-tin Green's functions and $\alpha = 0.704$. At a critical value of $v_s = v_{s0}^*$, the up poles cross to negative energies and the down poles cross to positive energies, indicating a change in the character of the ground state. The kink evident in the solid and long-dashed lines is real, and due to the discontinuous (at $T = 0$) change in $\Delta(\mathbf{x})$ at v_{s0}^*. The unimportance of self-consistency can be gauged by the small difference between the short-coherence length result and the long-coherence length result. [From Ref. 15.]

FIG. 11. Magnetization density of states integrated from below the band edge to ϵ. The ground-state spin of the system corresponds to the value at zero energy (the chemical potential). The potential for (a) is below the critical potential strength v_{s0}^*, so the ground state spin is zero, while the potential for (b) is above v_{s0}^*, so the ground state spin is 1/2.

FIG. 12. Differential conductance (LDOS) calculated around a magnetic impurity with (a) $v_s = 0.5$, $\xi k_F = 449$, (b) $v_s = 0.875$, $\xi k_F = 449$, (c) $v_s = 1.75$, $\xi k_F = 449$, (d) $v_s = 0.875$, $\xi k_F = 10$. All are calculated with $k_B T = 0.13\Delta_o$. In the progression from (a) to (c) the asymmetry between the two peaks increases and the higher peak moves to lower energies, eventually becoming hole-like. The LDOS is normalized by the normal-state's homogeneous density of states. [From Ref. 15.]

FIG. 13. Spectral weight at the impurity ($r = 0$) for the first angular momentum channel, $\ell = 0$, and at the first maximum for the second angular momentum channel, $\ell = 1$, for poles in both the spin-up and spin-down bands, as a function of the inverse coherence length, showing a linear behavior. The magnetic potential strength is $v_s = 0.875$. [From Ref. 15.]

FIG. 14. Spectral weight at the impurity ($r = 0$) for the $\ell = 0$ channel for $\xi k_F = 449$ as a function of magnetic potential strength for poles in both the spin-up and spin-down bands. The spectral weight in the spin-up band pole of the $\ell = 0$ localized state saturates at large v_s. Also shown are the spectral weights at the first maximum for the $\ell = 1$ localized states. [From Ref. 15.]

FIG. 15. Ratio of the spectral weight in the spin-up band and in the spin-down band at the impurity ($r = 0$) as a function of magnetic potential strength. This is plotted for the normal state $\ell = 0$ projected Green's functions (solid line) as well as for the localized states for niobium ($\xi k_F = 449$, long dashed line), for $\xi k_F = 10$ (dot-dashed line), and for the muffin-tin model. The muffin-tin model is only successful for $v_s < 0.5$, but that is due to a breakdown in describing the normal state. The normal-state electronic structure is a good predictor of the superconductor's electronic structure for the entire range of v_s. [From Ref. 15.]

FIG. 16. Spectral weights for the $\ell = 0$ localized state in the up and down bands for $v_s = 0.875$. The solid line is the normal state $\ell = 0$ projected spectral weight, the long-dashed line is the localized state in a superconductor with $\xi k_F = 449$, and the dot-dashed line is for $\xi k_F = 10$. The inset shows the spectral weight multiplied by r^2 to remove the algebraic decay. The normal-state and long-coherence length results are practically indistinguishable. The deviation shown in the short-coherence length superconductor's spectral weight is fit to within 1% by the exponential decay factor described in the text. Hence the spatial structure of the spectral weight of the superconductor's localized state is well-predicted by the normal state spectral weight. [From Ref. 15.]

FIG. 17. Experimental STM difference spectra taken near single Gd, Mn, and Ag atoms on the (110) surface of niobium. [Reprinted with permission from A. Yazdani, B. A. Jones, C.P. Lutz, M.F. Crommie, and D. M. Eigler, *Science*, **275**, 1767 (1997). Copyright 1997 American Association for the Advancement of Science.]

FIG. 18. Comparison of experimental STM difference spectrum at the Mn impurity and model calculation using spherical square well magnetic potential and a free-electron band structure for niobium. [Reprinted with permission from A. Yazdani, B. A. Jones, C.P. Lutz, M.F. Crommie, and D. M. Eigler, *Science*, **275**, 1767 (1997). Copyright 1997 American Association for the Advancement of Science.]

FIG. 19. Order parameters as a function of distance from the impurity r calculated for several magnetic potential strengths for (a) $\xi k_F = 449$ and (b) $\xi k_F = 10$. In both cases there is a discontinuous change in the order parameter when v_s passes through the critical strength v_{s0}^*. [From Ref. 15.]

FIG. 20. Order parameters at the impurity ($r = 0$) as a function of magnetic potential strength v_s for two values of the coherence length. The discontinuity in the order parameter at v_{s0}^* is much larger for the short-coherence-length superconductor. [From Ref. 15.]

FIG. 21. Ratio of the spectral weight at the impurity in the spin-up band to the spin-down band for $v_s = 0.875$ and $\xi k_F = 449$ as the nonmagnetic potential v_0 varies. In a similar result to that seen in Fig. 15, the normal-state spectral weights are good predictors of the superconducting state's spectral weight. We note that the curves are not symmetrical around $v_0 = 0$, which results from a realistic band structure without particle-hole symmetry. [From Ref. 15.]

FIG. 22. The energy of the spin-up pole is shown as a function of nonmagnetic potential strength for $v_s = 0.875$ and $\xi k_F = 449$. The energy of the spin-down pole is just the negative of the energy of the spin-up pole. The analytic models do not perform particularly well in reproducing the pole energies, although the muffin-tin model does show a similar asymmetry around $v_0 = 0$ to the numerical calculations. [From Ref. 15.]

FIG. 23. Calculated boundary between two ground states around the magnetic impurity for $\xi k_F = 449$. For a large enough magnetic impurity strength a quasiparticle is bound in the ground state. The minimum magnetic impurity strength depends on the nonmagnetic impurity strength. For still larger magnetic impurity strengths there would be ground states with more than one bound quasiparticle. [From Ref. 15.]

FIG. 24. Spectral weights in the normal state as functions of the distance from the impurity for several combinations of magnetic and nonmagnetic potentials (a) only a magnetic potential, and (b) a fixed magnetic potential $v_s = 0.875$ and a varying nonmagnetic potential. By making measurements around the impurity in the normal state (or integrating the superconductor's spectrum over a frequency much larger than Δ_o), information about the structure of the impurity may be obtained. [From Ref. 15.]

FIG. 25. Order parameter as a function of distance r from a defect with a suppressed pair potential, but no single-particle potential. [From Ref. 15.]

FIG. 26. Differential conductance (LDOS), normalized by the normal-state's homogeneous DOS, around a defect with a suppressed pair potential, but no single-particle potential. (a) $\xi k_F = 449$, $k_B T = 0.13\Delta_o$ — there is no evidence of any change in the spectrum due to the order parameter suppression shown in Fig. 25. (b) $\xi k_F = 10$, $k_B T = \Delta_o/100$ — a localized state very near the continuum enhances the continuum edge seen in tunneling near the defect. [From Ref. 15.]

FIG. 27. Quasiparticle excitation energies for positive μ calculated at $T = 3$K for $NbSe_2$. [From Ref. 83.]

FIG. 28. Normalized tunneling conductance spectra calculated at various distances from the center of the vortex line. Distances are indicated in atomic units. [From Ref. 83.]

FIG. 29. Peak energies of resonant states created by a non-magnetic impurity. Shown are the calculated results for a $d_{x^2-y^2}$ superconductor (circles) and the analytic model of Ref. 93 (dot-dashed line). The solid line is a modified pole theory from Eq. (75). [From Ref. 119.]

FIG. 30. Difference spectra (in units of t^{-1}) for (a) non-magnetic and (b) magnetic impurities in a $d_{x^2-y^2}$ and (c) magnetic impurities and (d) non-magnetic impurities in an s^*-wave superconductor. The numbers are the potential strengths in units of t, and are the same in (a) and (b), as well as for (c) and (d). [From Ref. 119.]

FIG. 31. LDOS at the impurity location in a two-dimensional lattice model. (a) Isotropic order parameter superconductor and magnetic impurity with potential strength (from top down) $V_S = .1$, 1.5, 2, 2.5, and 3 in units of the nearest-neighbor hopping matrix element t. (b) $d_{x^2-y^2}$ order parameter superconductor and non-magnetic impurity with potential strength (from top down) $V_0 = 2$, 3, 4, and 10 in units of t. (c) Same as (b), but for a magnetic impurity.

FIG. 32. Local differential conductance $(dI(r,V)/dV)$, relative to the normal metal for potentials of [(a) and (b)] $2.5t$ and [(c) and (d)] $10t$, shown as a function of the voltage. The series of curves are for different distances (sites on the square lattice) from the impurity. The solid lines are for non-magnetic potentials and the dashed lines are for magnetic potentials. [(a) and (c)] show from one to three lattice spacings along the (10) direction from the impurity while [(b) and (d)] show from the origin to three lattice spacings along the (11) direction on the square lattice. An inset to (a) shows the measured STS spectrum on an oxygen vacancy (Ref. 120, 121). Also shown in (c) is the homogeneous (clean) tunneling spectrum. [From Ref. 119.]

FIG. 33. Spatial structure of the LDOS for fixed voltages. The potential is nonmagnetic with strength $2.5t$. (a) $eV = -0.14\Delta_{max}$ and (b) $eV = 0.14\Delta_{max}$, corresponding to the hole-like and electron-like peaks of the resonant state, respectively. (c) $eV = 1.03\Delta_{max}$, showing a four-fold "cross" pattern, and (d) the LDOS around this impurity in the normal state.

FIG. 34. Change in the order parameter at the impurity for (a) magnetic potentials, and (b) nonmagnetic potentials. Inset of (a) is the ground-state spin for magnetic potentials. For the inset the order parameter has been increased by a factor of three to guarantee that all the distortion is within the considered far-field region. [From Ref. 119.]

FIG. 35. Change in the spatial amplitude of local order parameter symmetries as a function of position around the impurity. The potential is nonmagnetic with strength $2.5t$. (a) d-wave, (b) s-wave, (c) p_x-wave, and (d) p_y-wave local order parameter symmetries are shown.

FIG. 36. Comparison of theoretical results (dashed lines) with measurements (solid lines) from Refs. 122–124. The impurity parameters used were, from top down, $V_0 = 2t$, $n_i = 1.7\%$, $V_0 = 2.5t$, $n_i = 0.5\%$, $V_0 = 2.5t$, $n_i = 1.1\%$, and $V_0 = 2t$, $n_i = 1.4\%$. [From Ref. 119.]

FIG. 37. Differential density of states due to a dynamical impurity with a frequency ω_o and potential $V_S = 3t$. For a fast timescale (large ω_o) there is spectral weight centered at the chemical potential. As the spin slows down, and thus ω_o decreases, the spin begins to appear approximately static and the characteristic double-peak spectrum of the static magnetic impurity reappears.

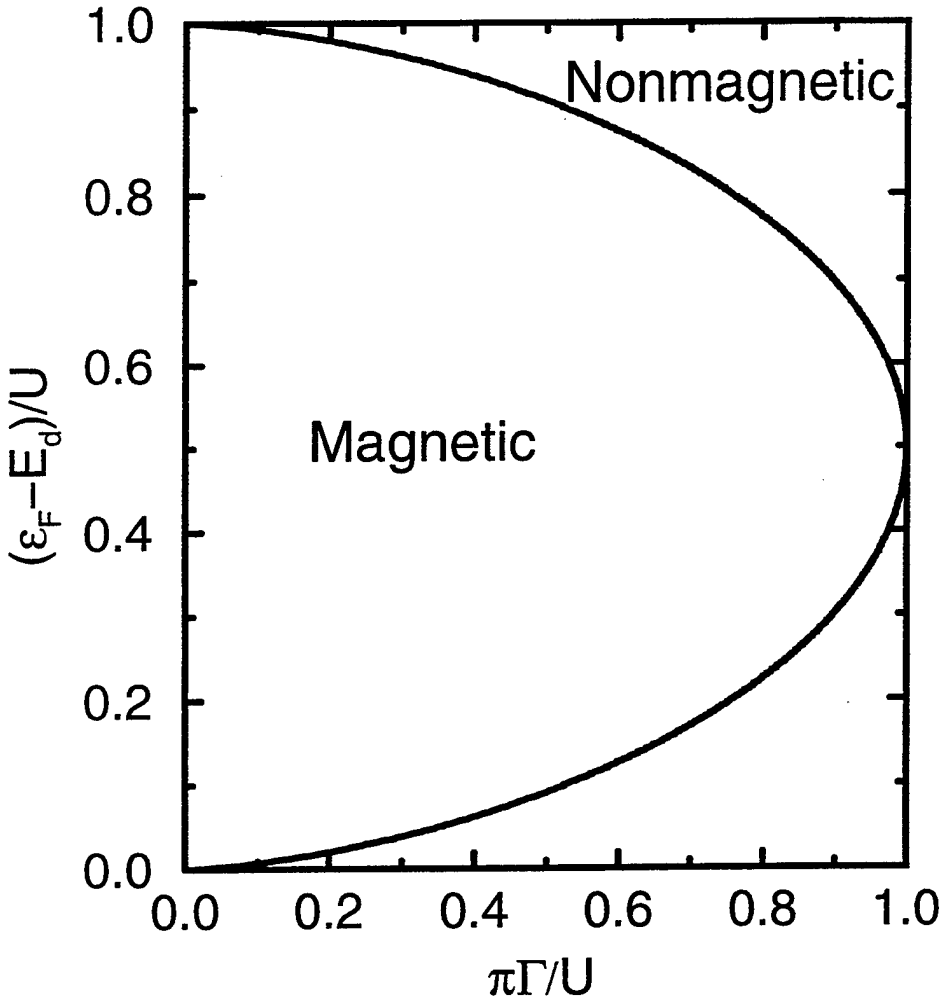

Figure 1, Flatte and Byers, "Local Electronic Structure of Defects in Superconductors", Solid State Physics Volume 52.

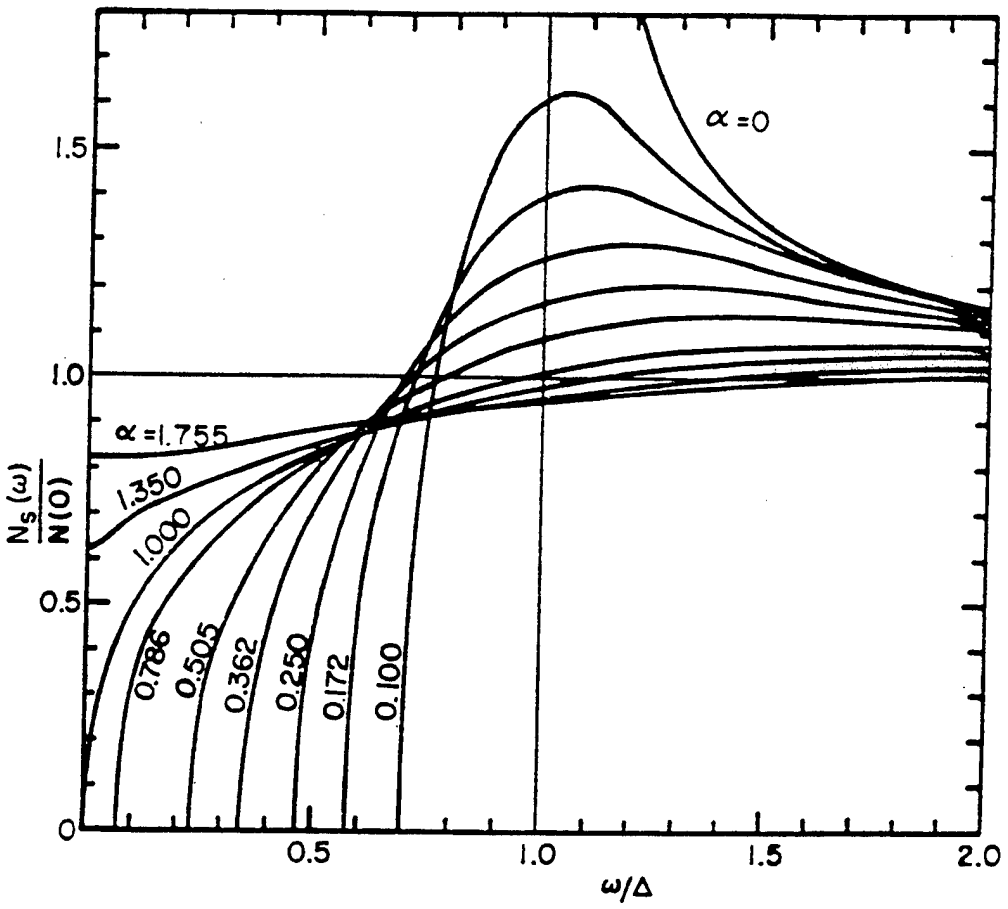

Figure 2. Flatté and Byers, "Local Electronic Structure of Defects in Superconductors," Solid State Physics Vol 52.

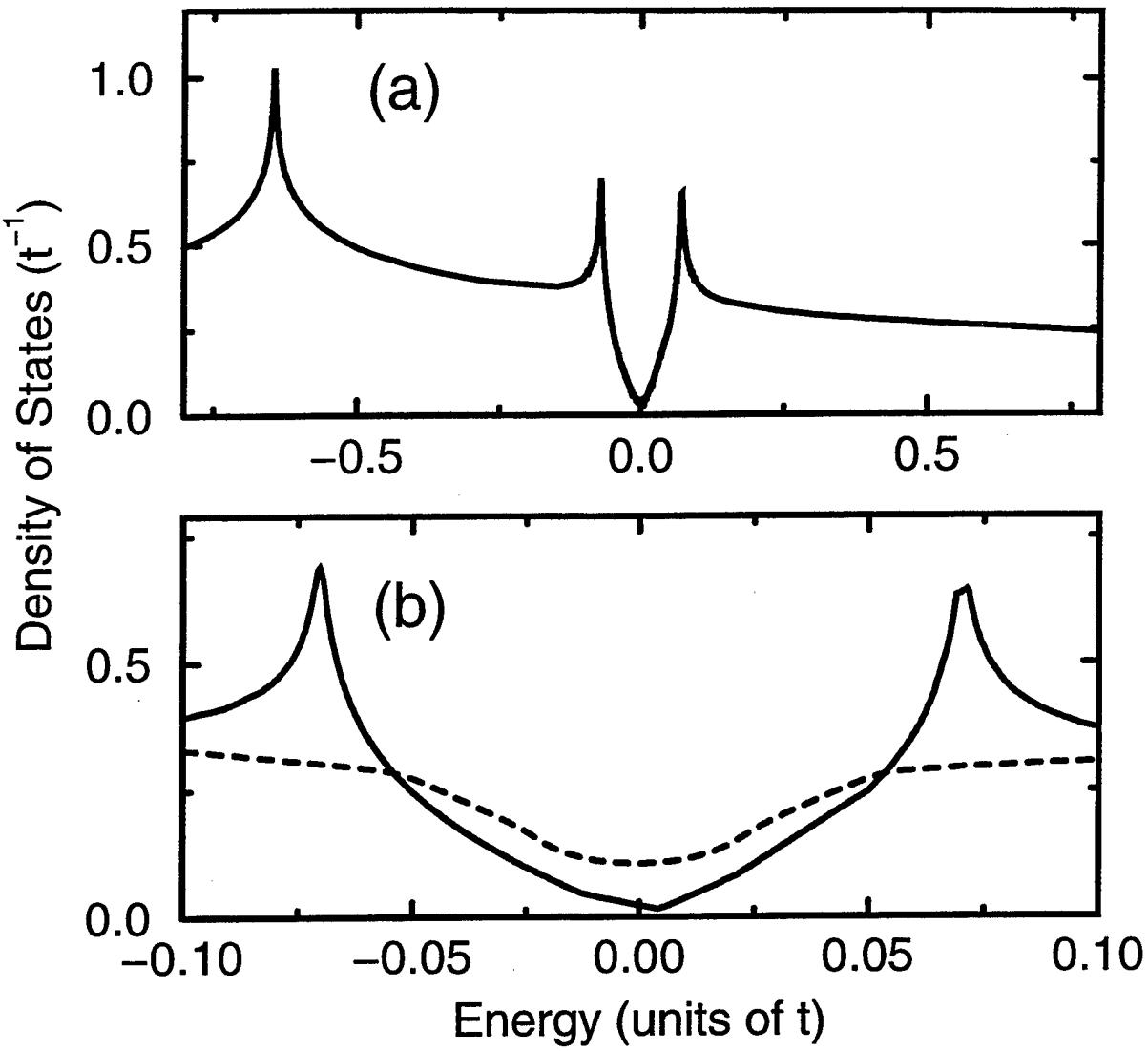

Figure 3, Flatte and Byers, "Local Electronic Structure of Defects in Superconductors", Solid State Physics Volume 52.

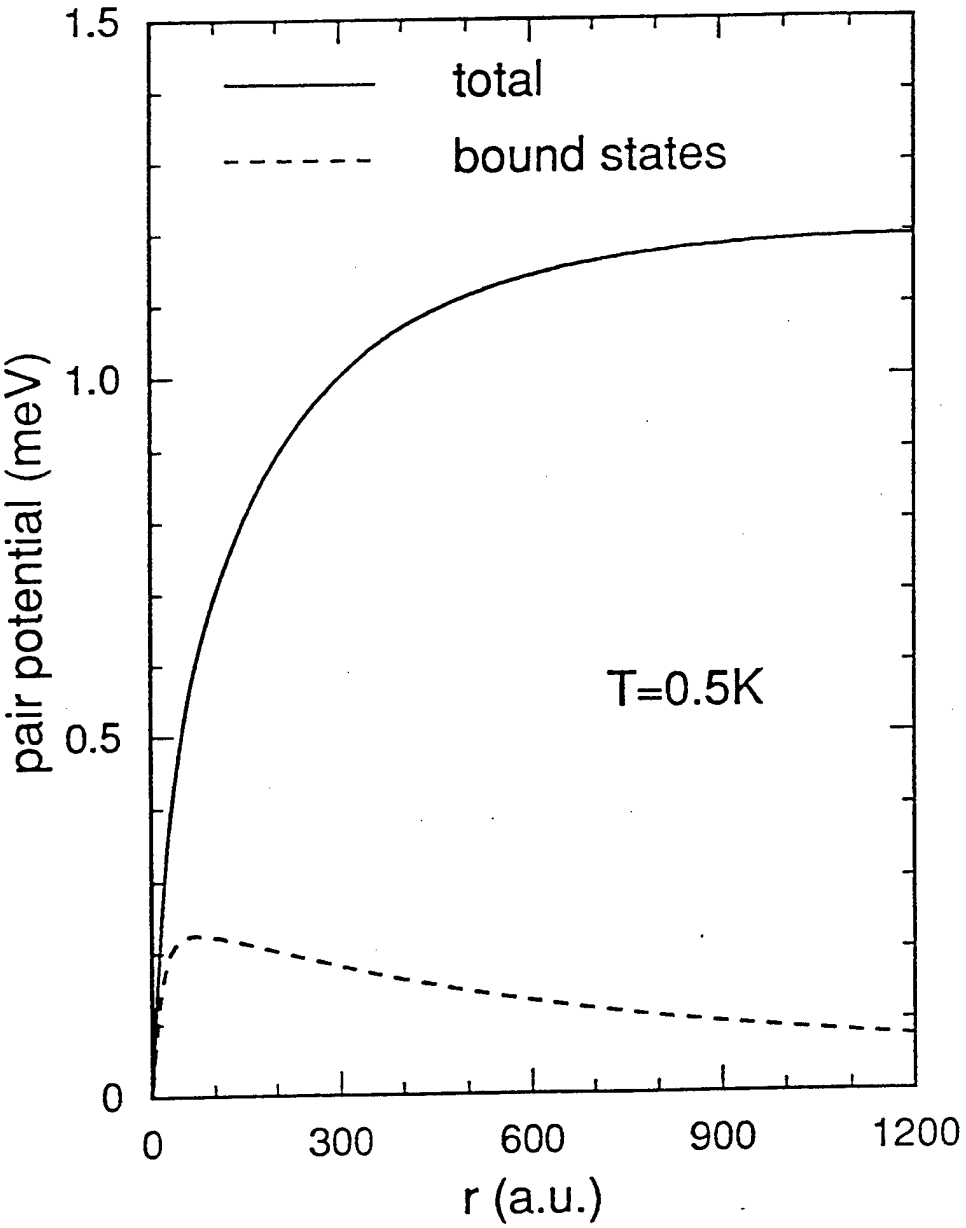

Figure 4, Flatté and Byers, "Local Electronic Structure of Defects in Superconductors", Solid State Physics Volume 52.

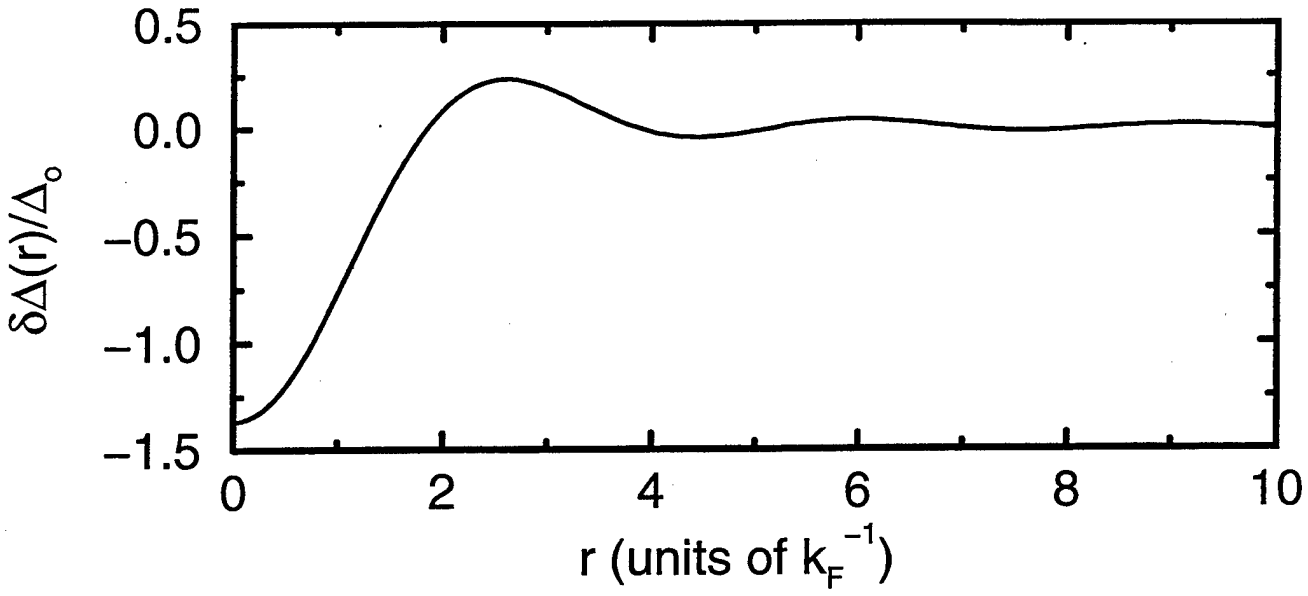

Figure 5, Flatte and Byers, "Local Electronic Structure of Defects in Superconductors", Solid State Physics Volume 52.

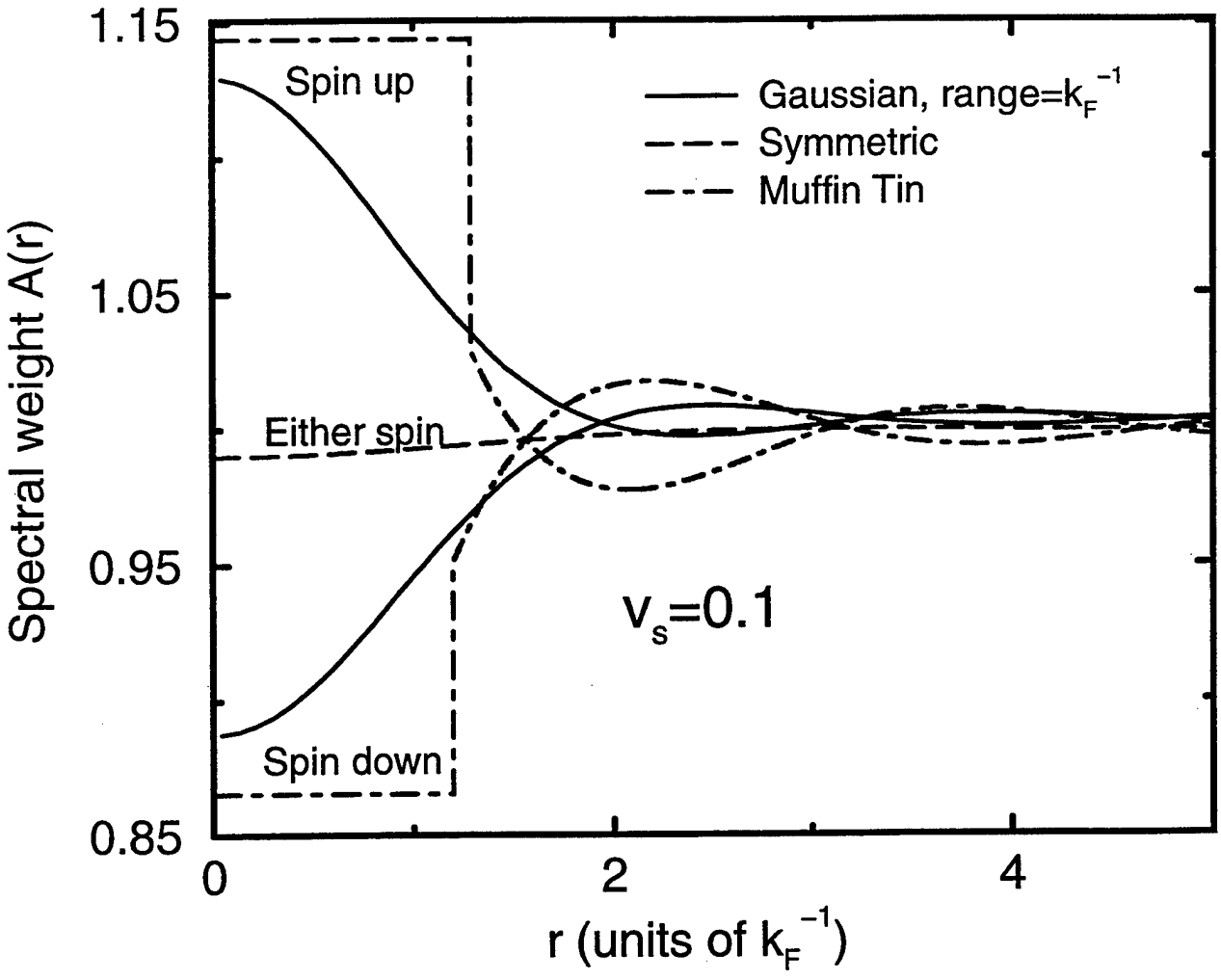

Figure 6, Flatte and Byers, "Local Electronic Structure of Defects in Superconductors", Solid State Physics Volume 52.

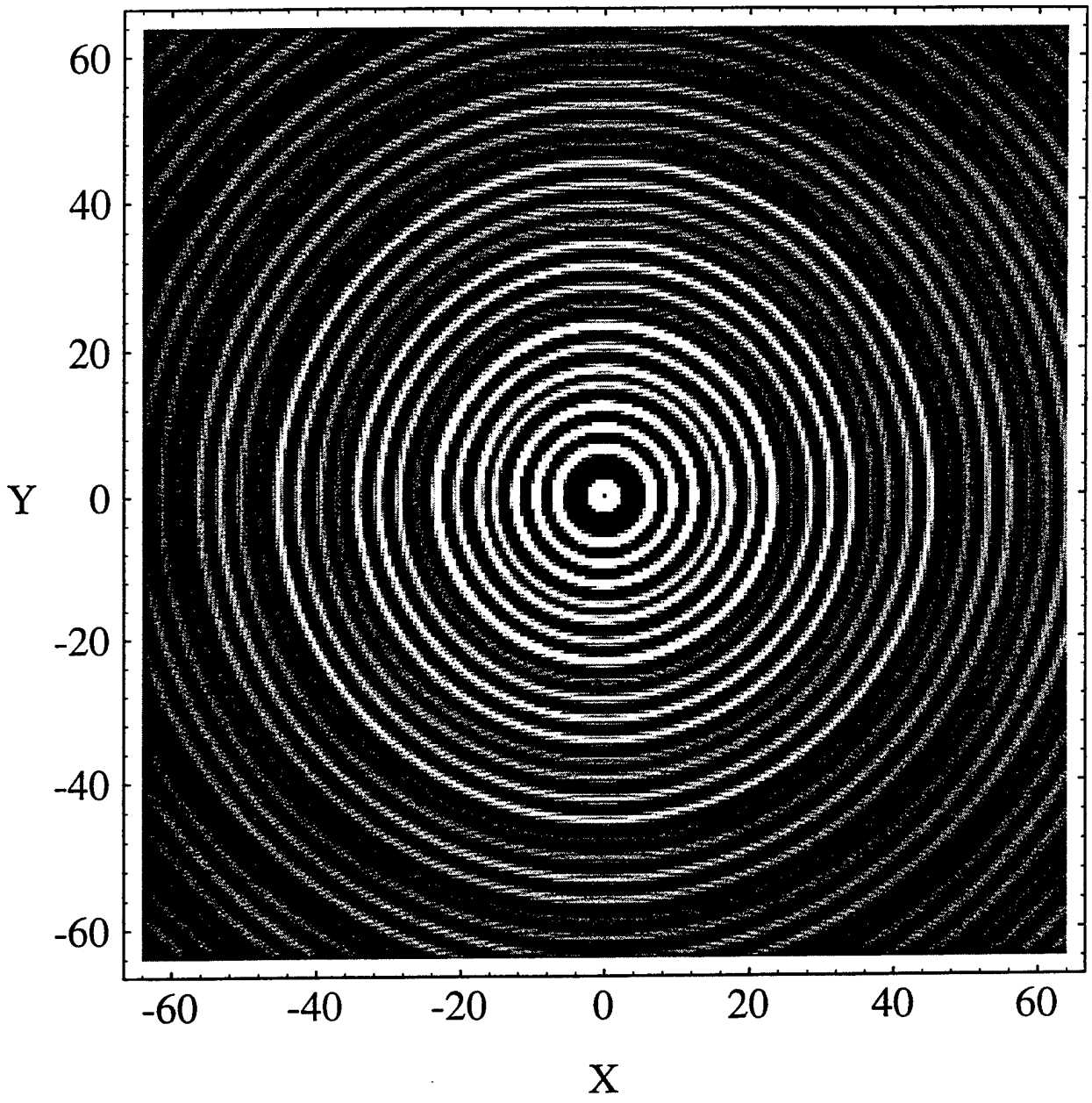

Figure 7(a), Flatté and Byers, "Local Electronic Structure of Defects in Superconductors", Solid State Physics Volume 52.

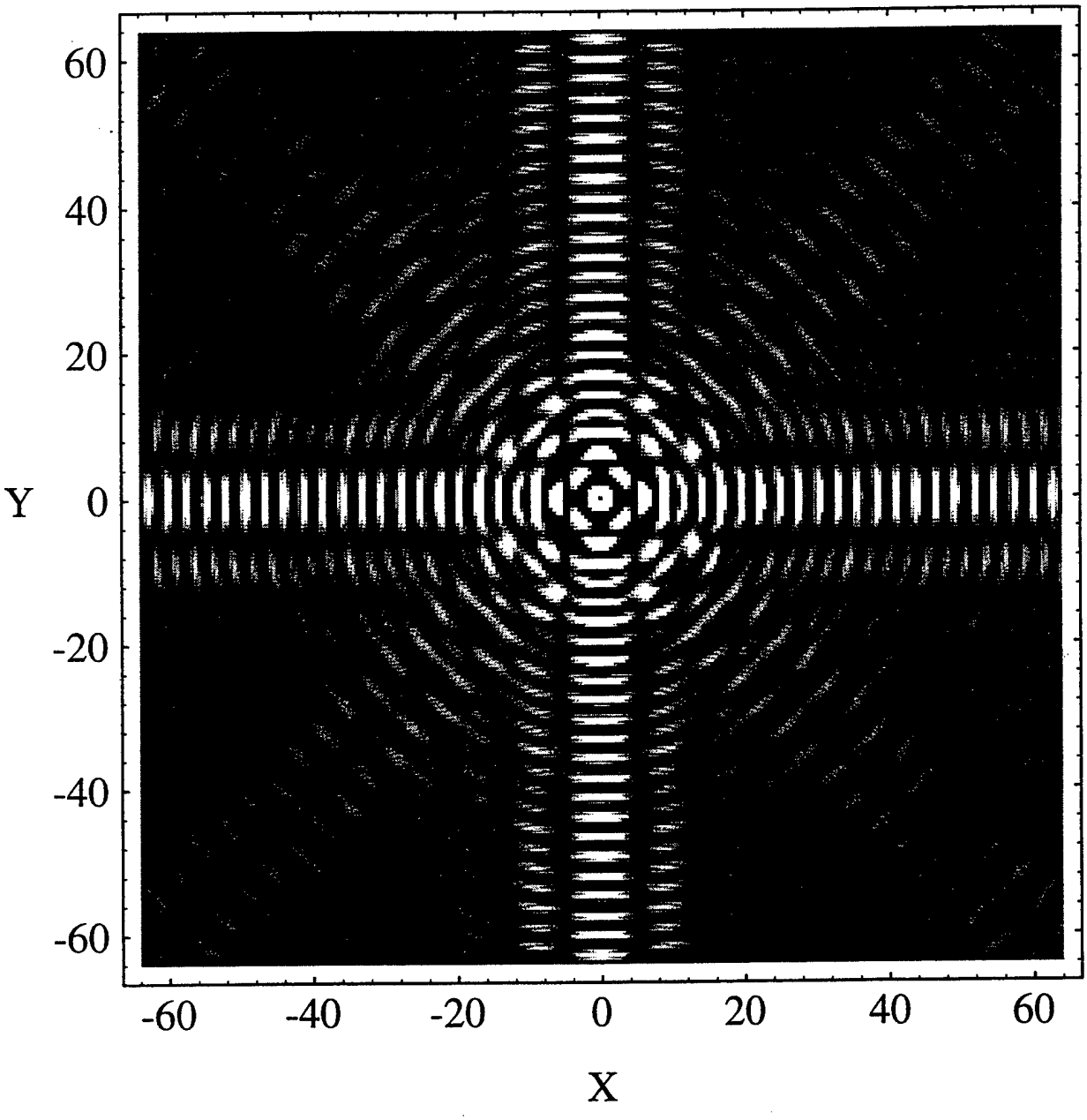

Figure 7(b), Flatté and Byers, "Local Electronic Structure of Defects in Superconductors", Solid State Physics Volume 52.

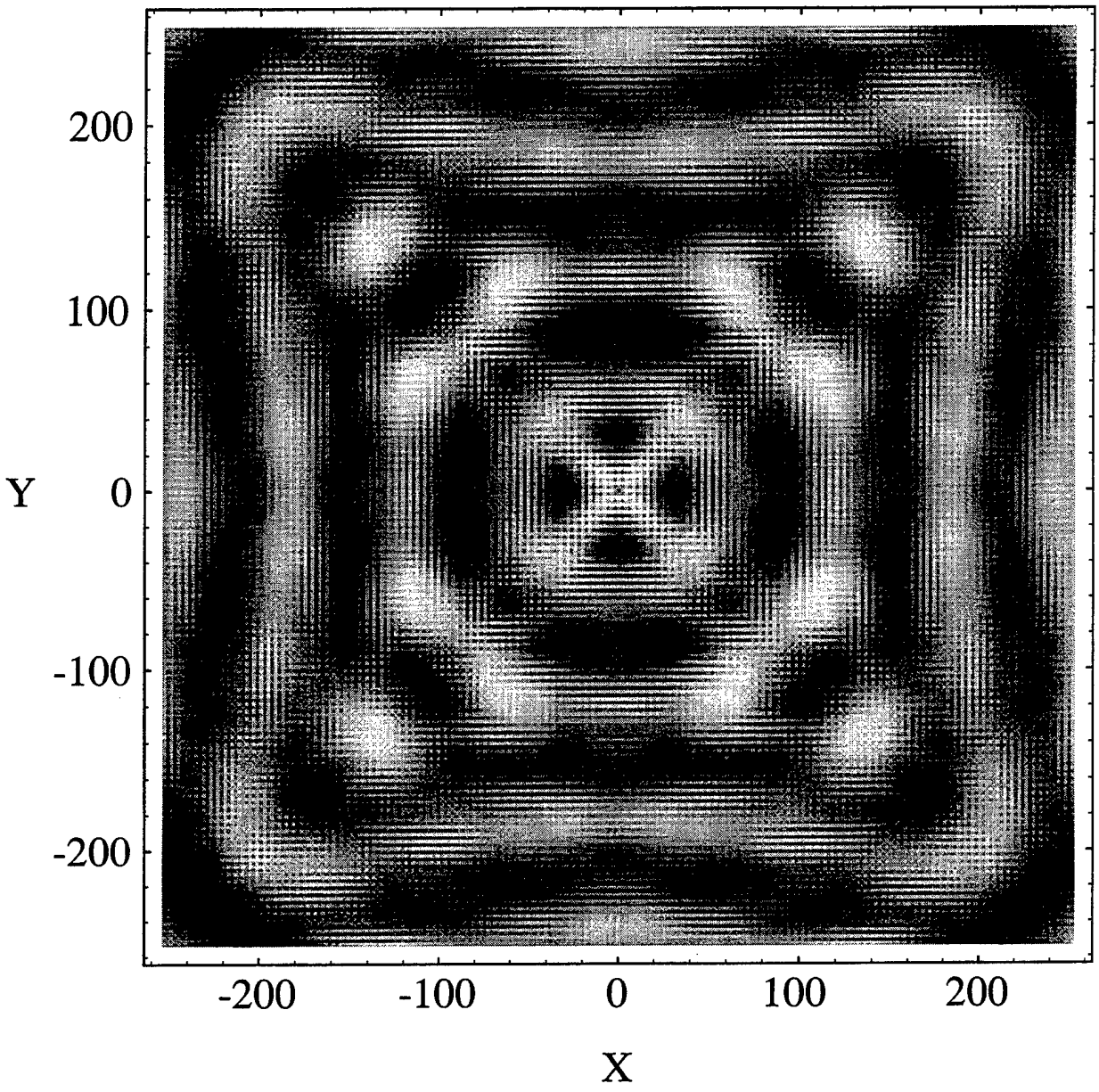

Fig. 7(c)

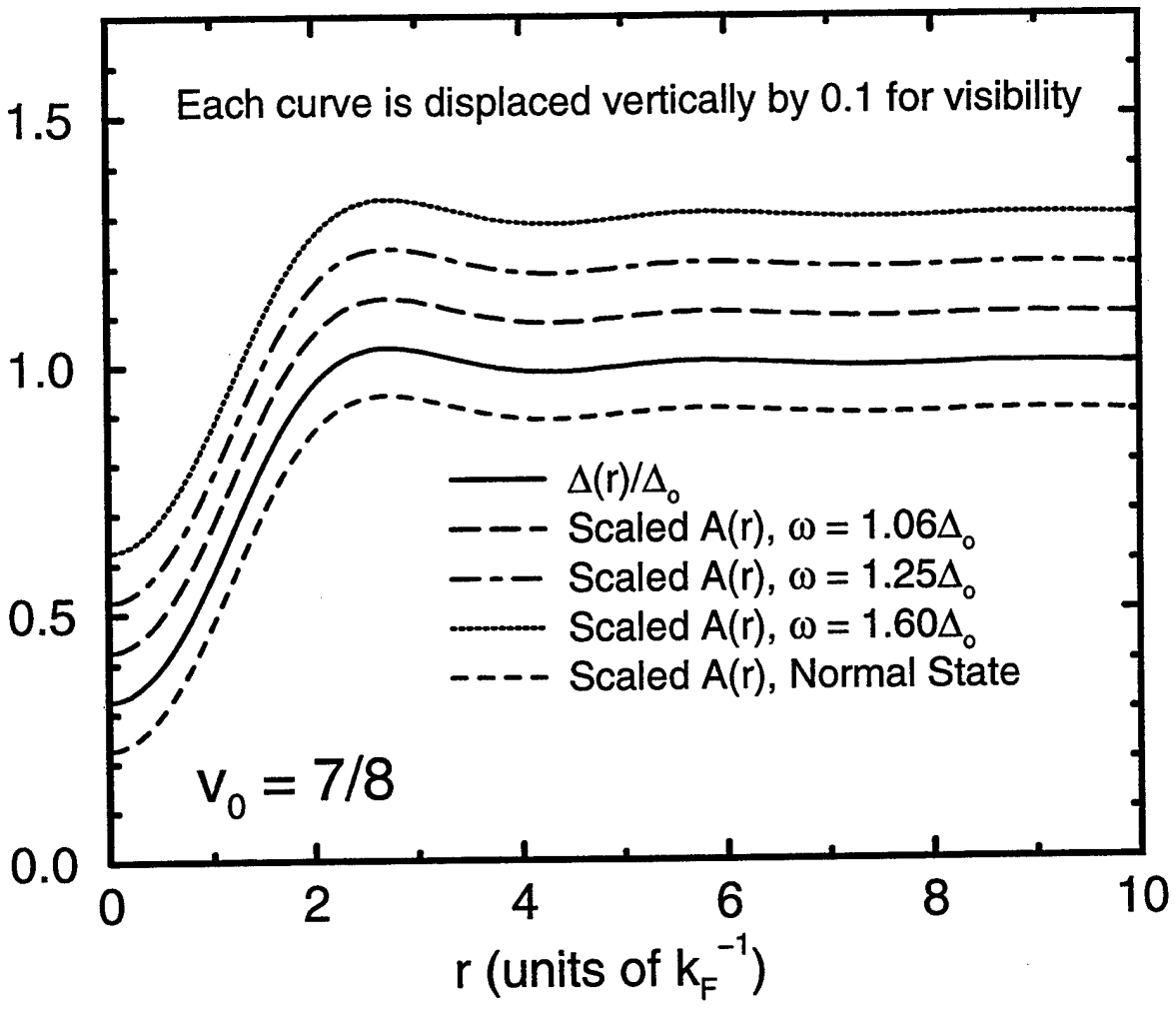

Figure 8, Flatte and Byers, "Local Electronic Structure of Defects in Superconductors", Solid State Physics Volume 52.

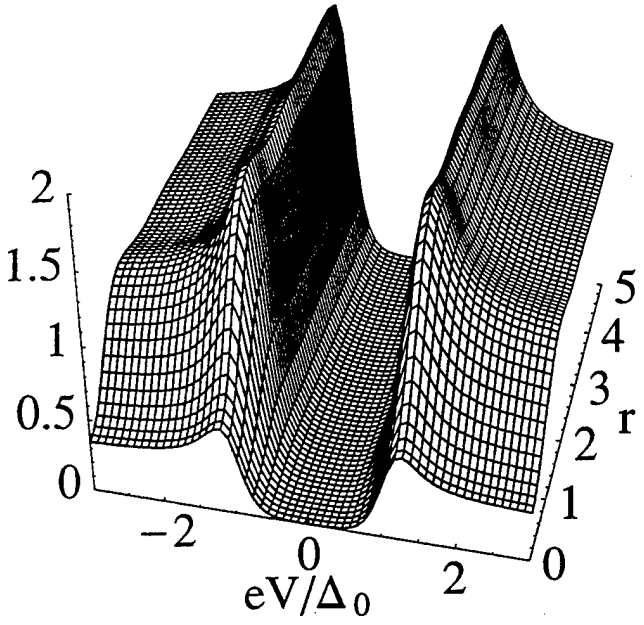

Figure 9(a), Flatte and Byers, "Local Electronic Structure of Defects in Superconductors," Solid State Physics Volume 52

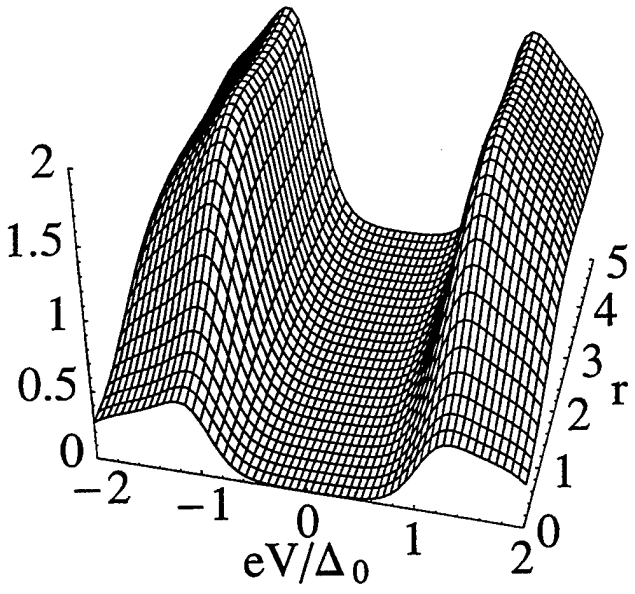

Figure 9(b), Flatté and Byers, "Local Electronic Structure of Defects in Superconductors," Solid State Physics Volume 52.

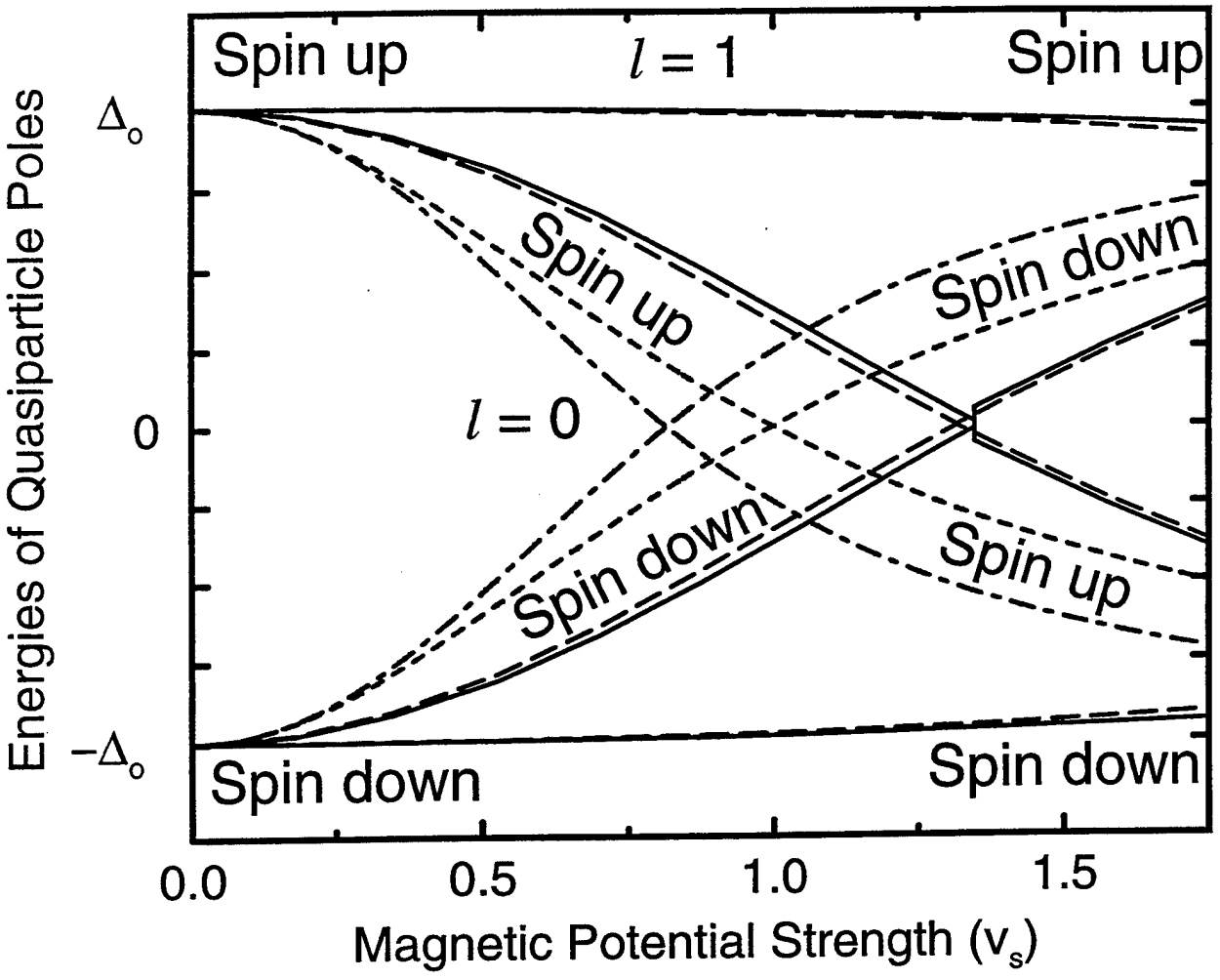

Figure 10, Flatte and Byers, "Local Electronic Structure of Defects in Superconductors", Solid State Physics Volume 52.

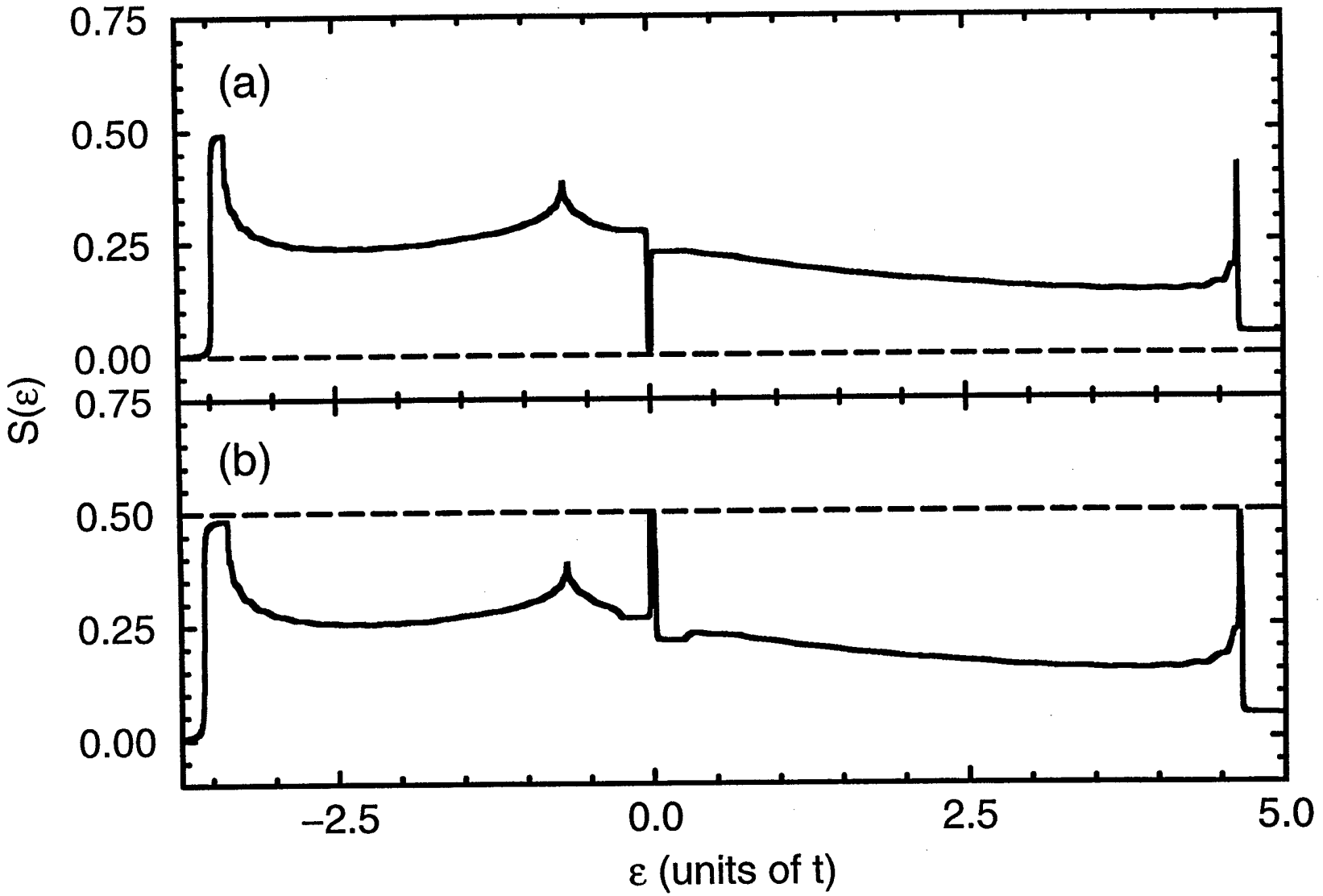

Figure 11, Flatte and Byers, "Local Electronic Properties of Defects in Superconductors", Solid State Physics Volume 52.

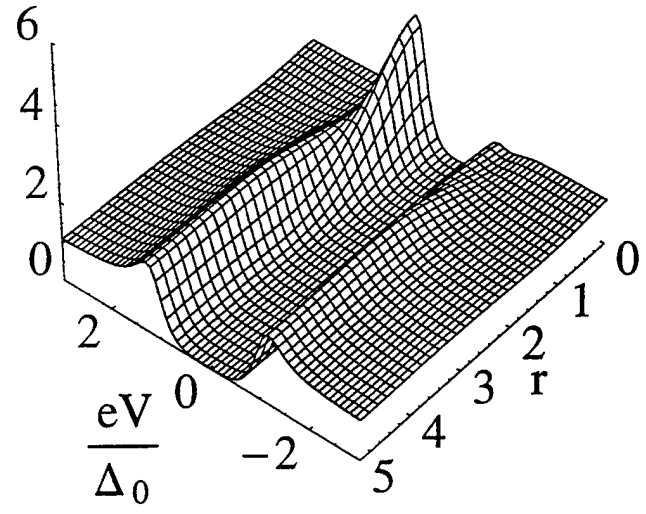

Figure 12(a), Flatte and Byers, "Local Electronic ~~Properties~~ Structure of Defects in Superconductors", Solid State Physics Volume 52.

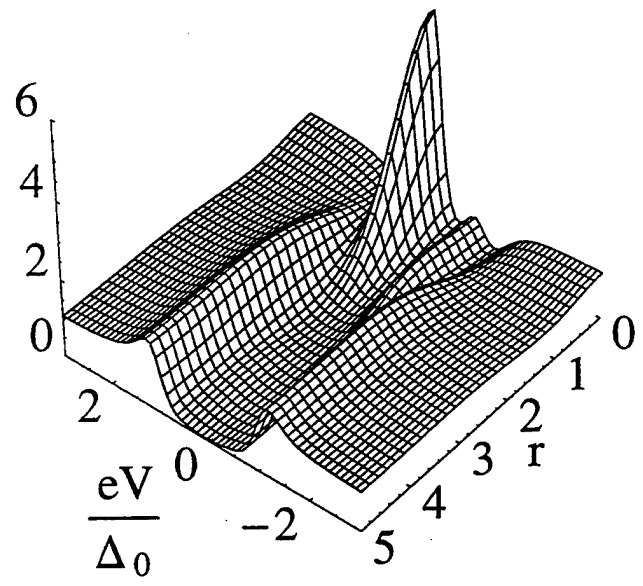

Figure 12(b), Flatté and Byers, "Local Electronic Structure of Defects in Superconductors", Solid State Physics Volume 52.

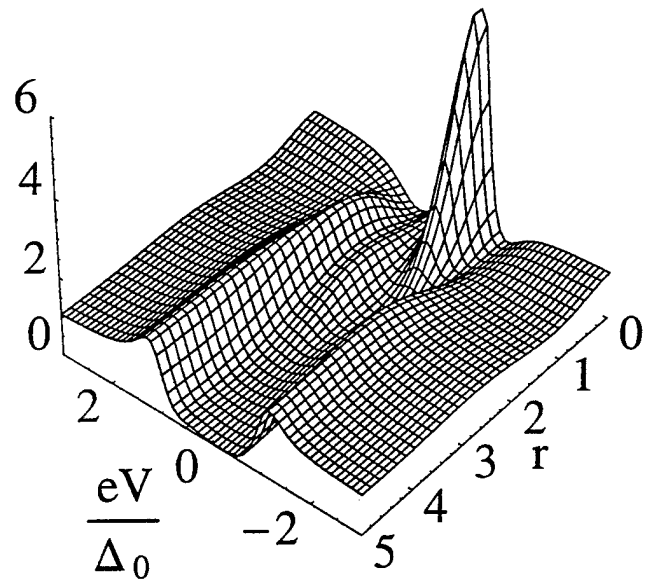

Figure 12(c), Flatté and Byers, "Local Electronic Structure of Defects in Superconductors", Solid State Physics Volume 52.

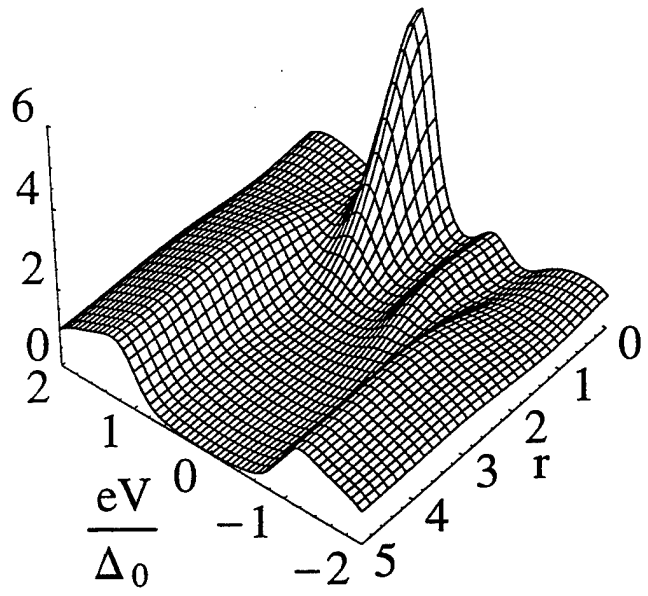

Figure 12(d), Flatté and Byers, "Local Electronic Structure of Defects in Superconductors," Solid State Physics Volume 52.

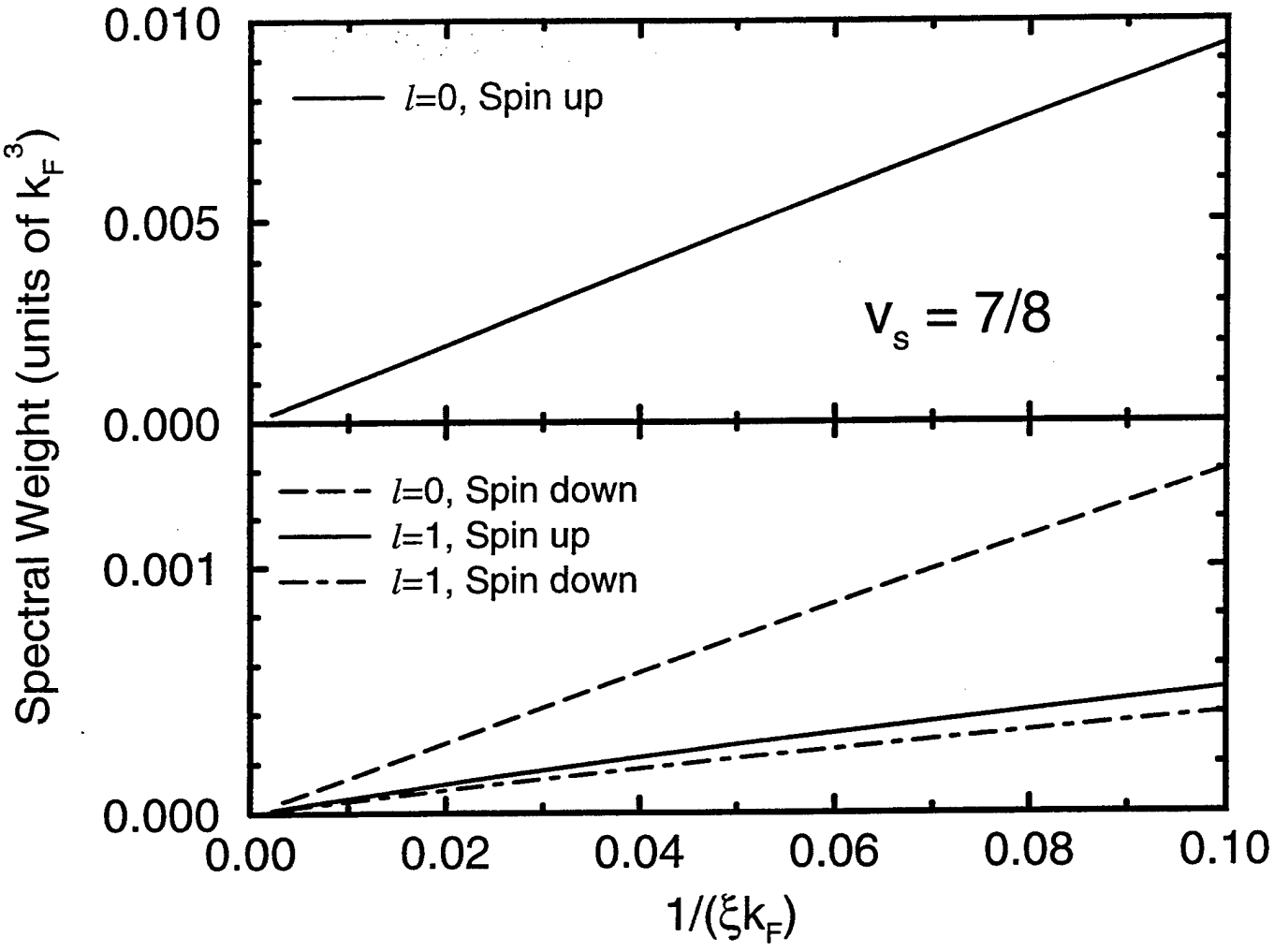

Figure 13, Flatte and Byers, "Local Electronic Structure of Defects in Superconductors", Solid State Physics Volume 52.

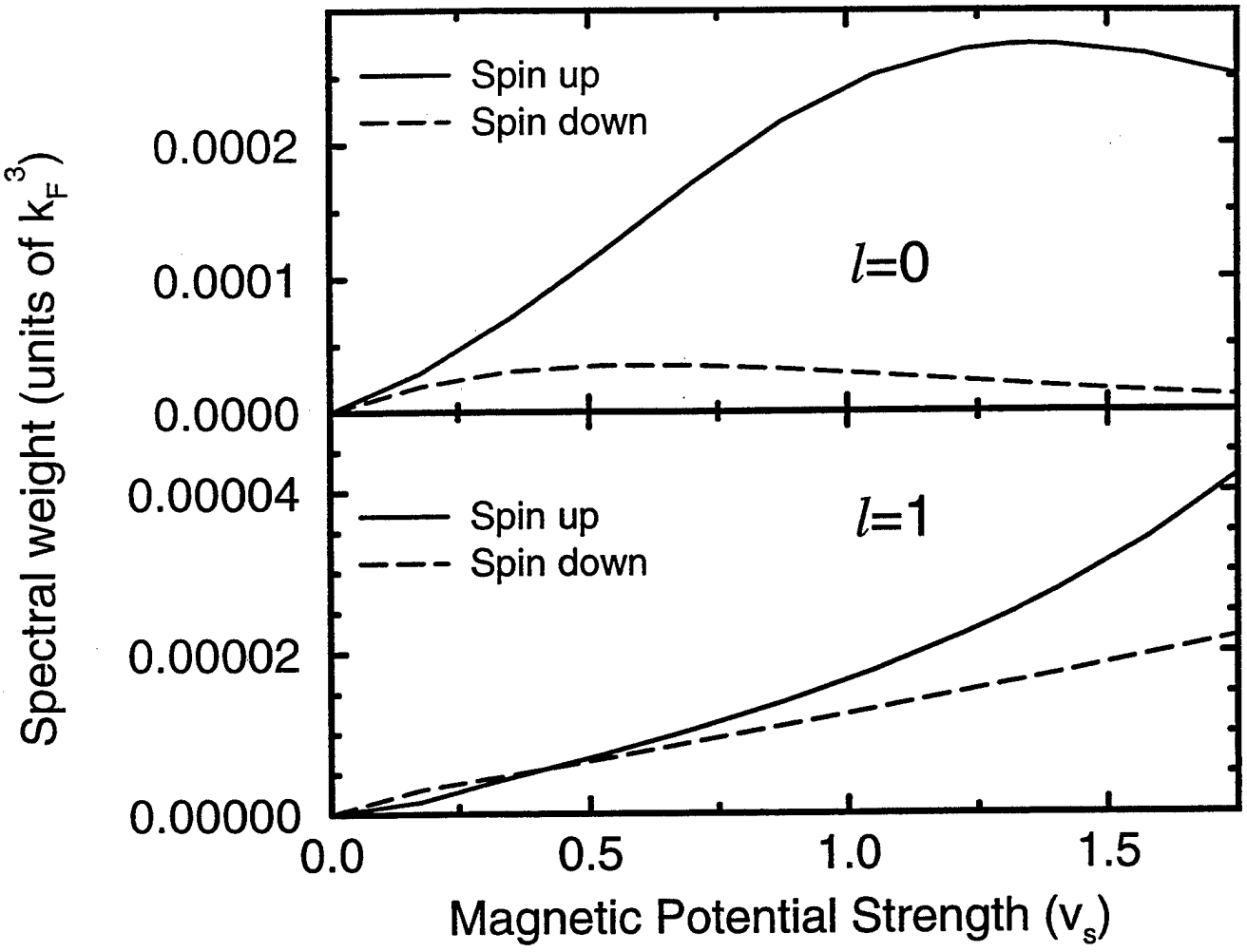

Figure 14, Flatte and Byers, "Local Electronic Structure of Defects in Superconductors", Solid State Physics Volume 52.

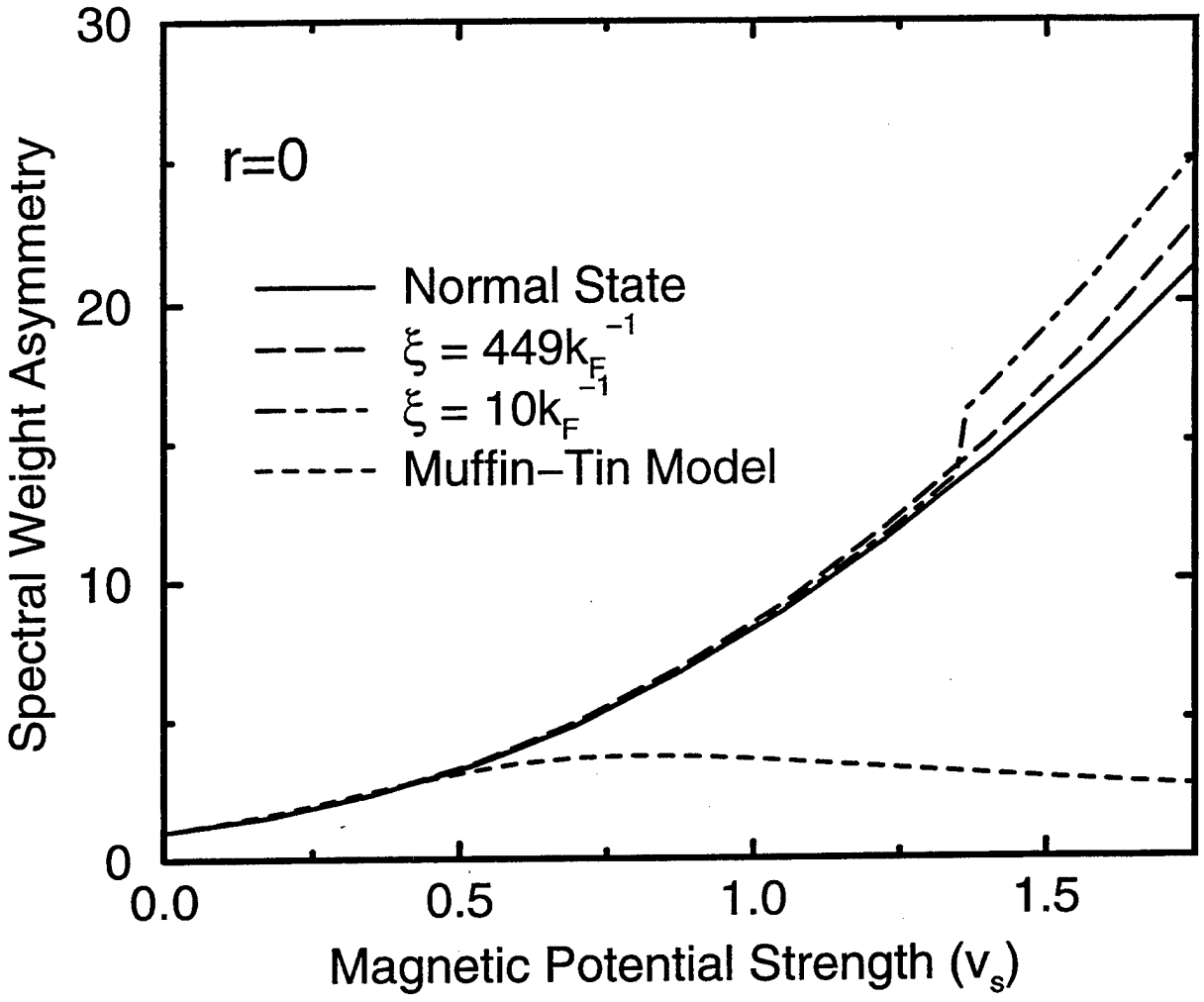

Figure 15, Flatte and Byers, "Local Electronic Structure of Defects in Superconductors", Solid State Physics Volume 52.

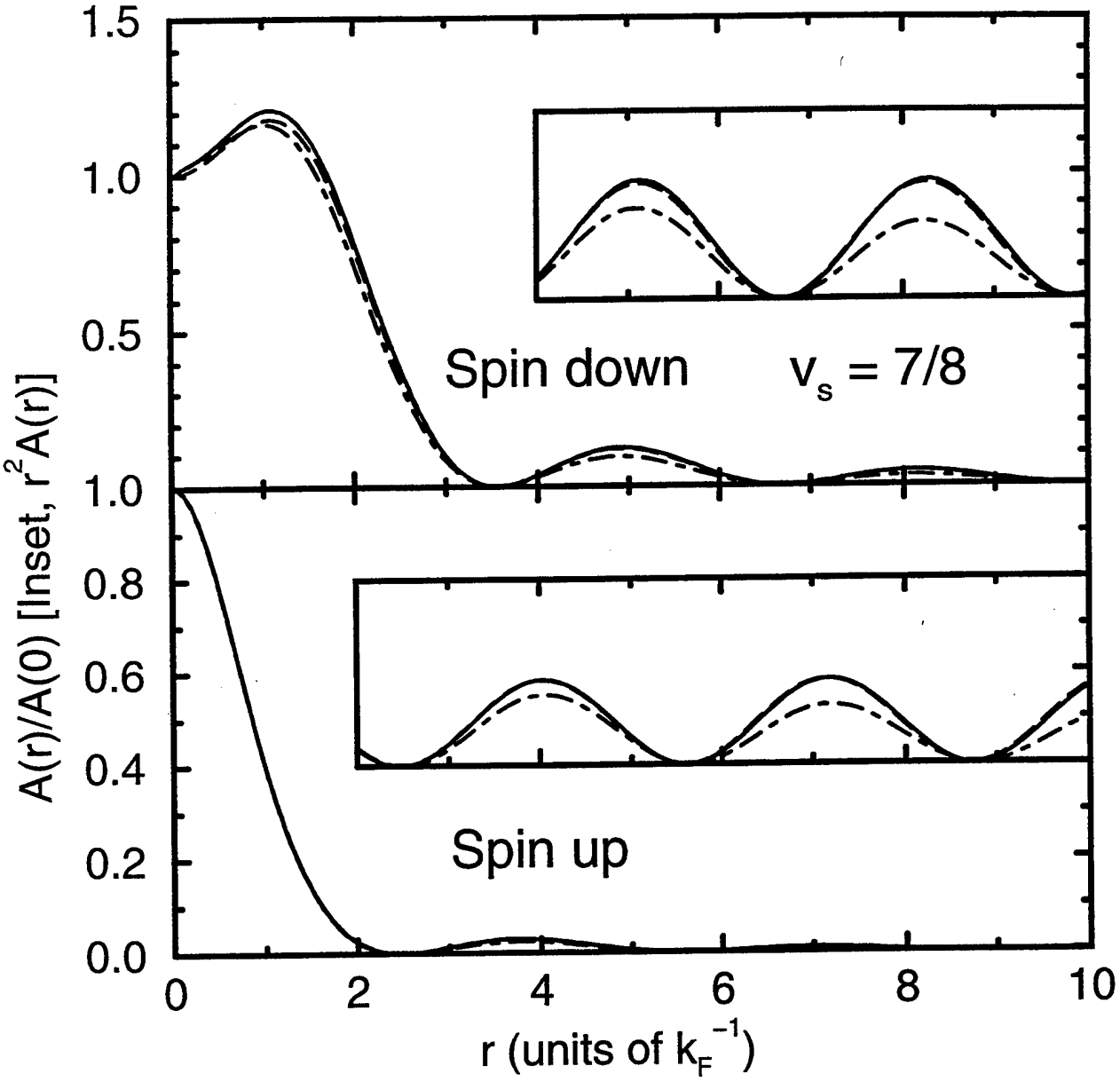

Figure 16, Flatte and Byers, "Local Electronic Structure of Defects in Superconductors", Solid State Physics Volume 52.

Figure 2

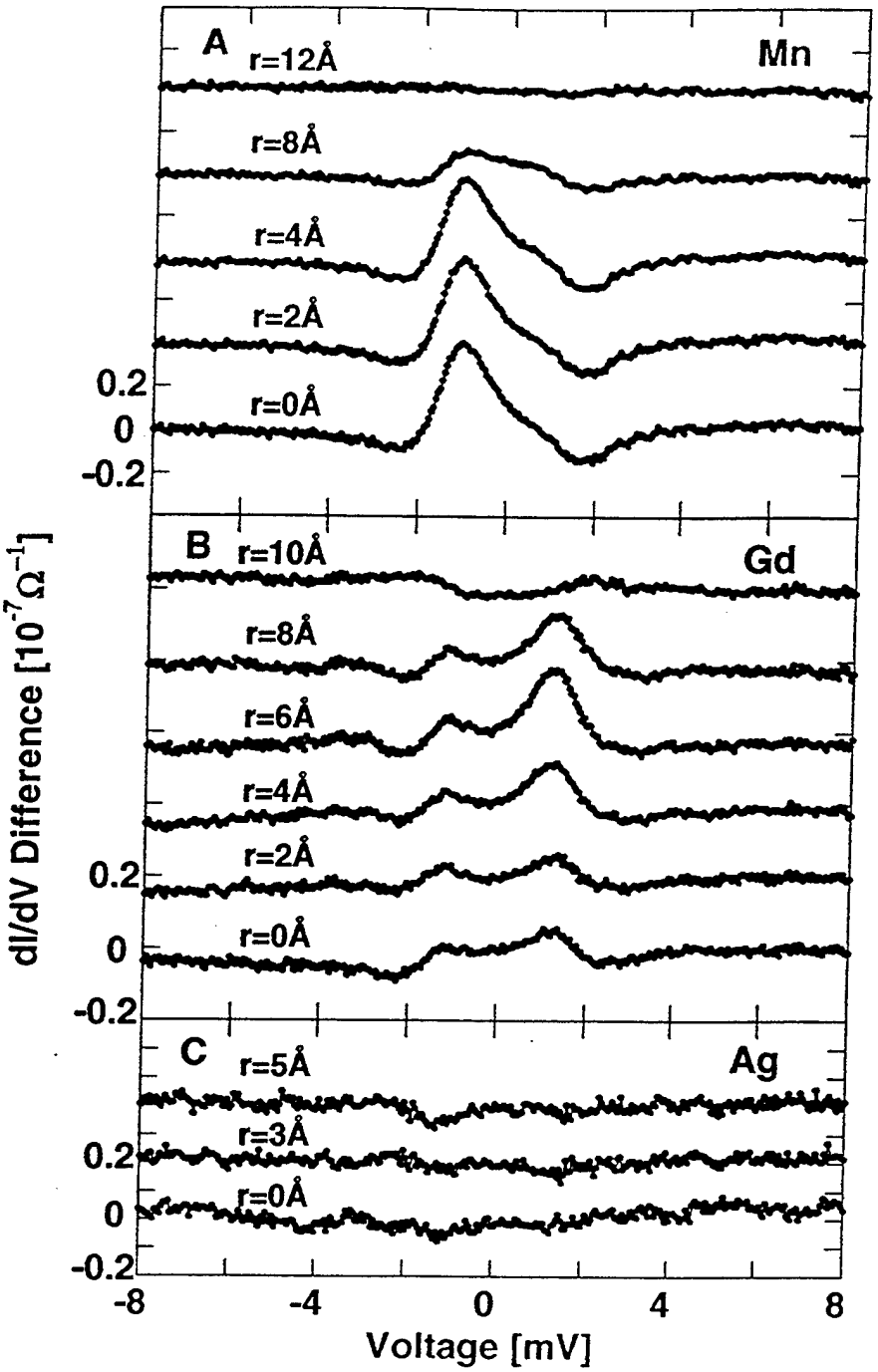

Figure 17, Flatté and Byers, "Local Electronic Structure of Defects in Superconductors", Solid State Physics Volume 52.

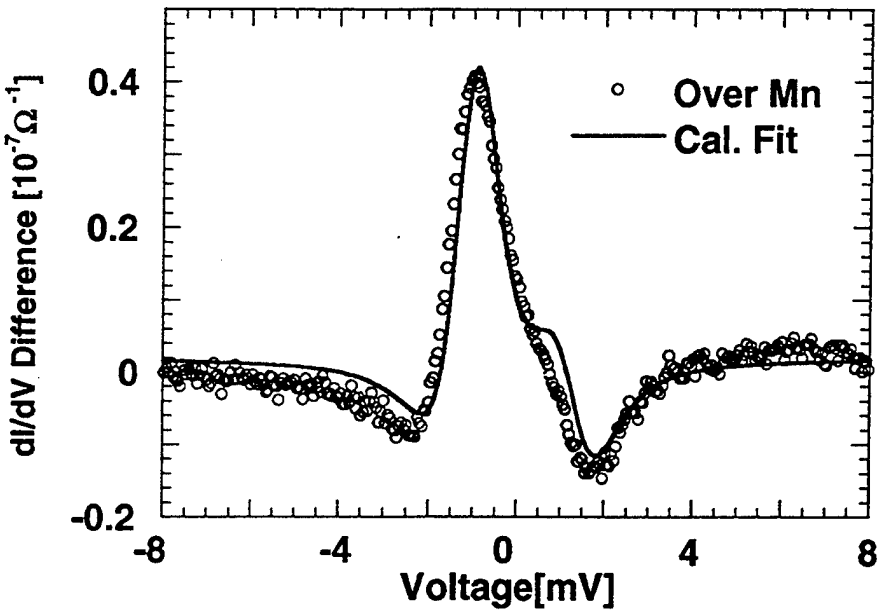

Figure 18, Flatté and Byers, "Local Electronic Structure of Defects in Superconductors," Solid State Physics Vol. 52.

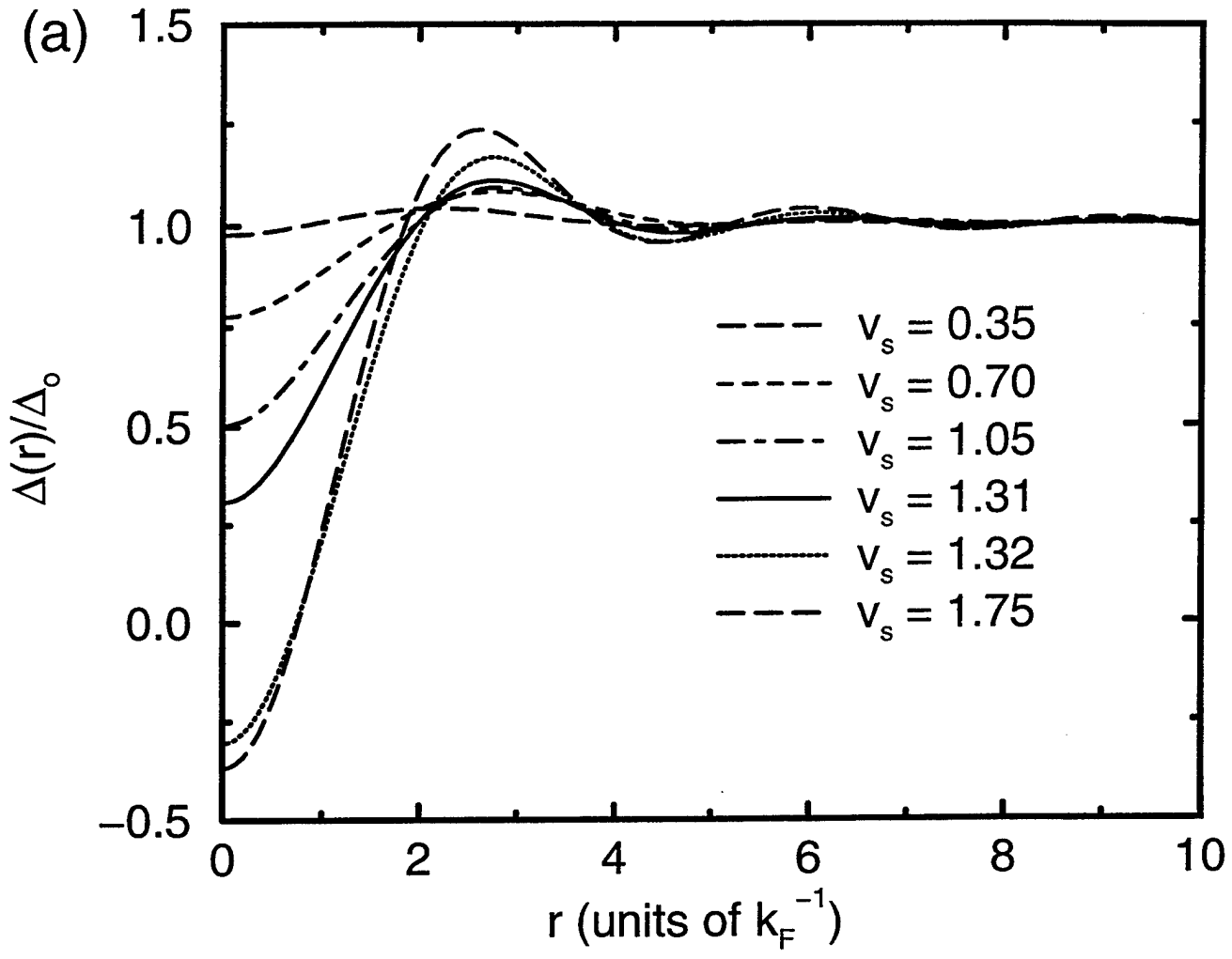

Figure 19(a), Flatte and Byers, "Local Electronic Structure of Defects in Superconductors", Solid State Physics Volume 52.

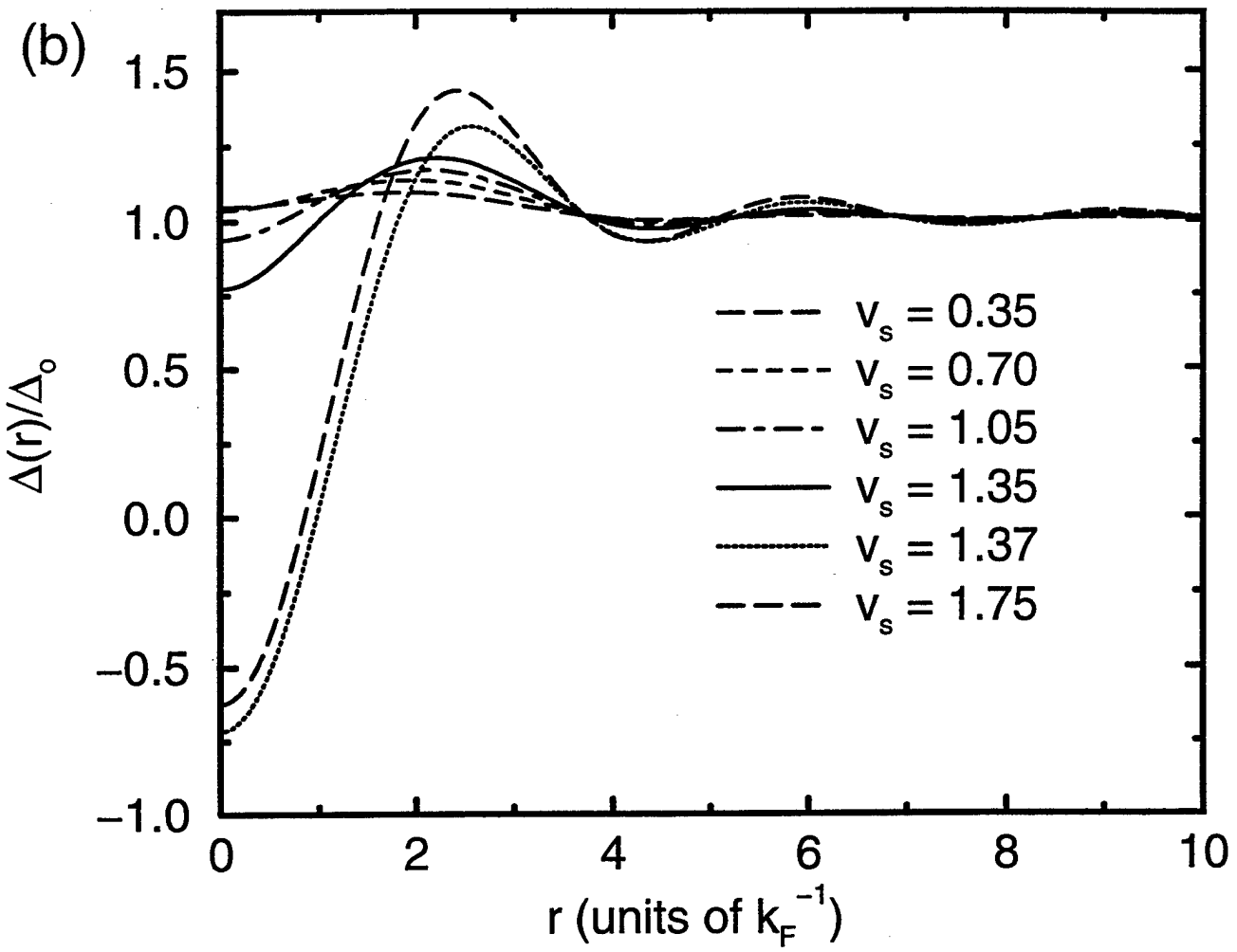

Figure 19(b), Flatte and Byers, "Local Electronic Structure of Defects in Superconductors", Solid State Physics Volume 52.

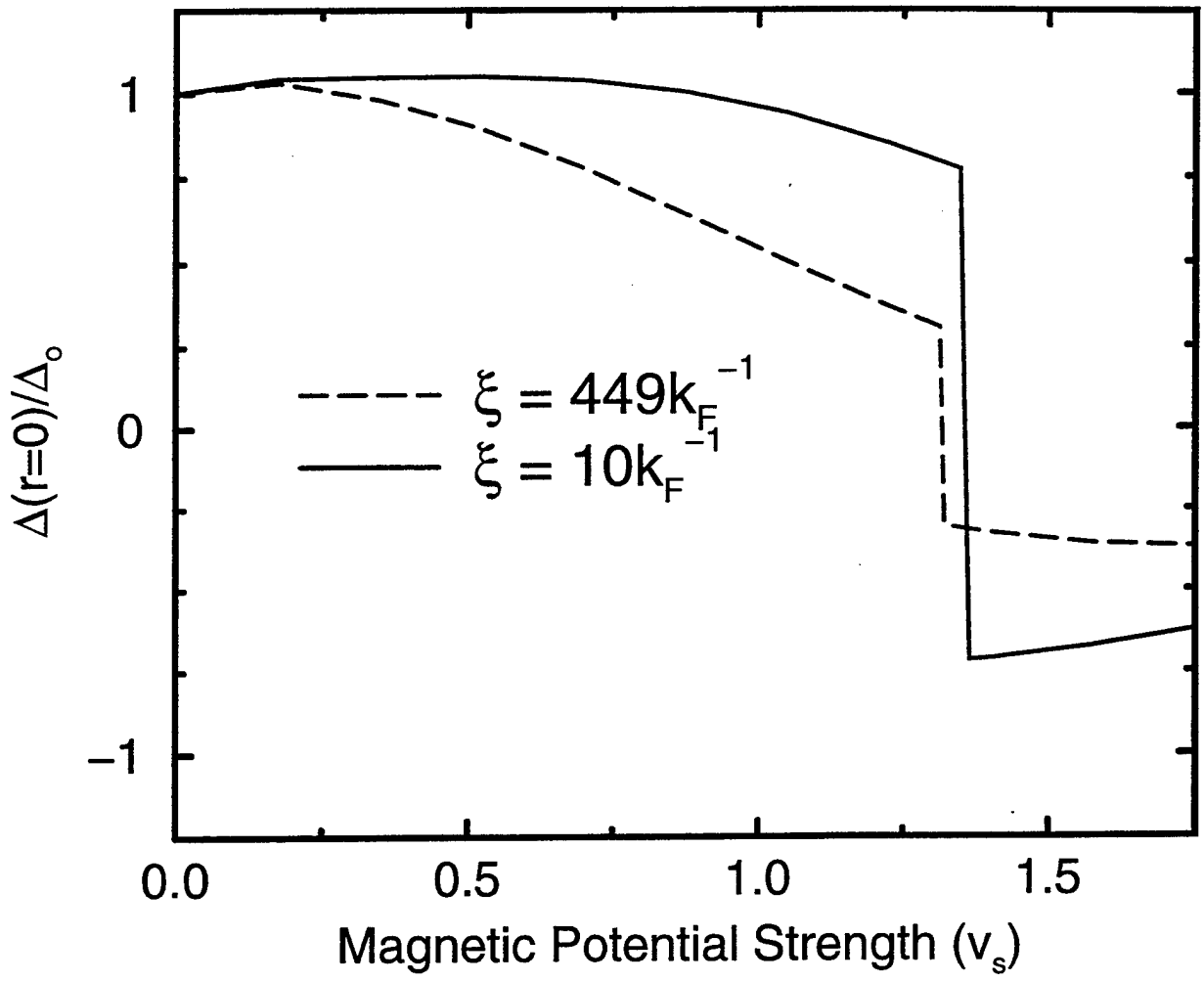

Figure 20, Flatte and Byers, "Local Electronic Structure of Defects in Superconductors", Solid State Physics Volume 52.

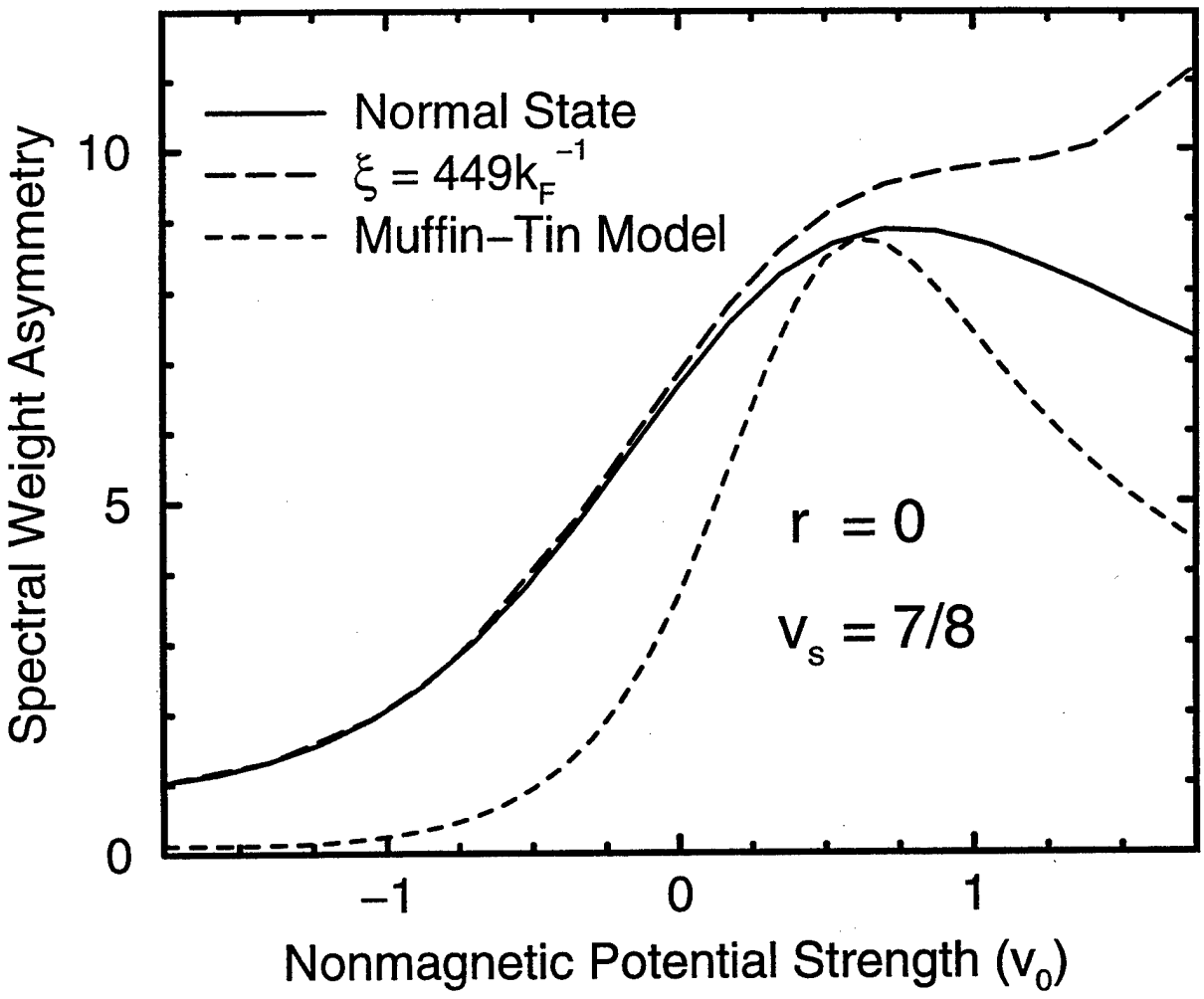

Figure 21, Flatte and Byers, "Local Electronic Structure of Defects in Superconductors", Solid State Physics Volume 52.

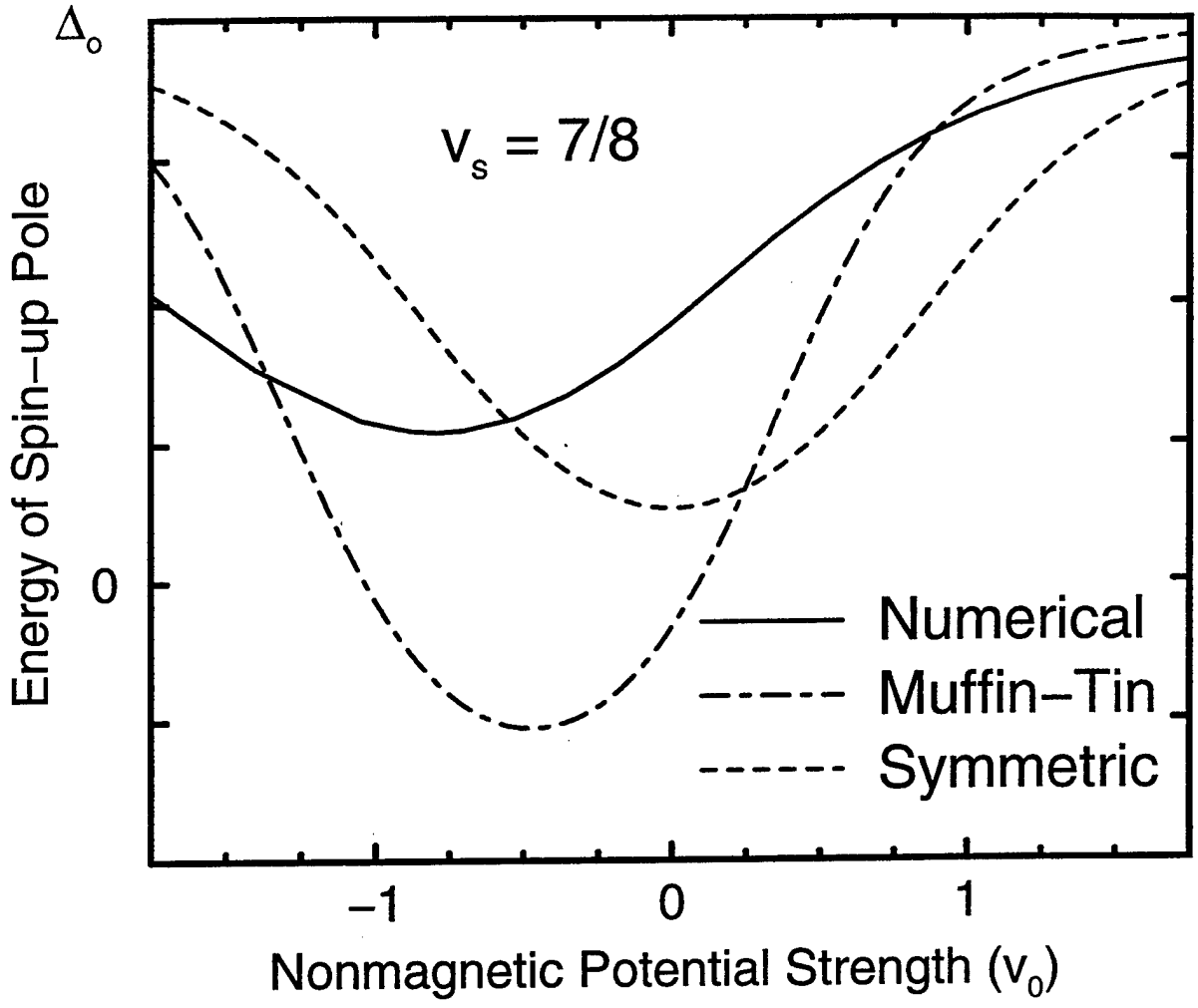

Figure 22, Flatte and Byers, "Local Electronic Structure of Defects in Superconductors", Solid State Physics Volume 52.

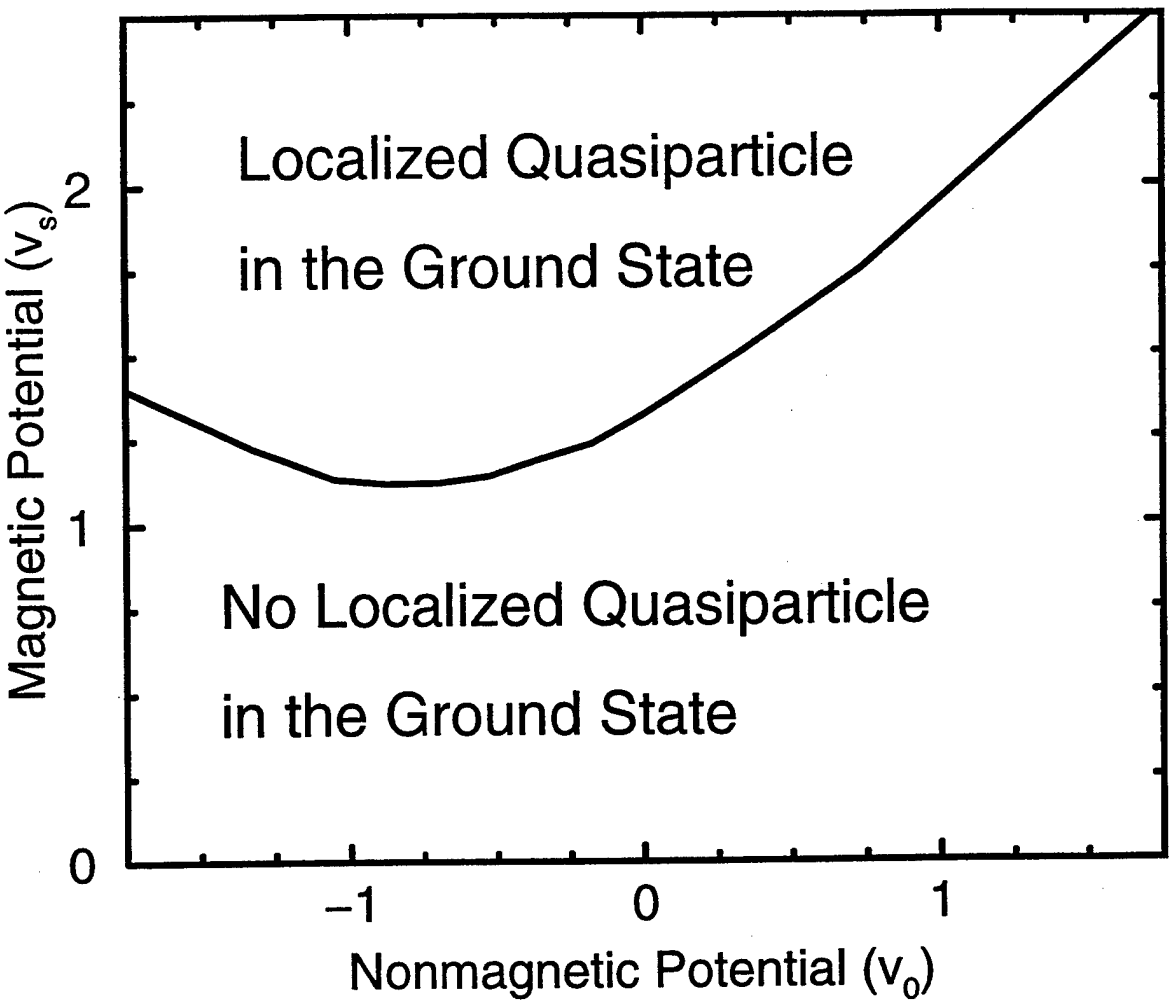

Figure 23, Flatte and Byers, "Local Electronic Structure of Defects in Superconductors", Solid State Physics Volume 52.

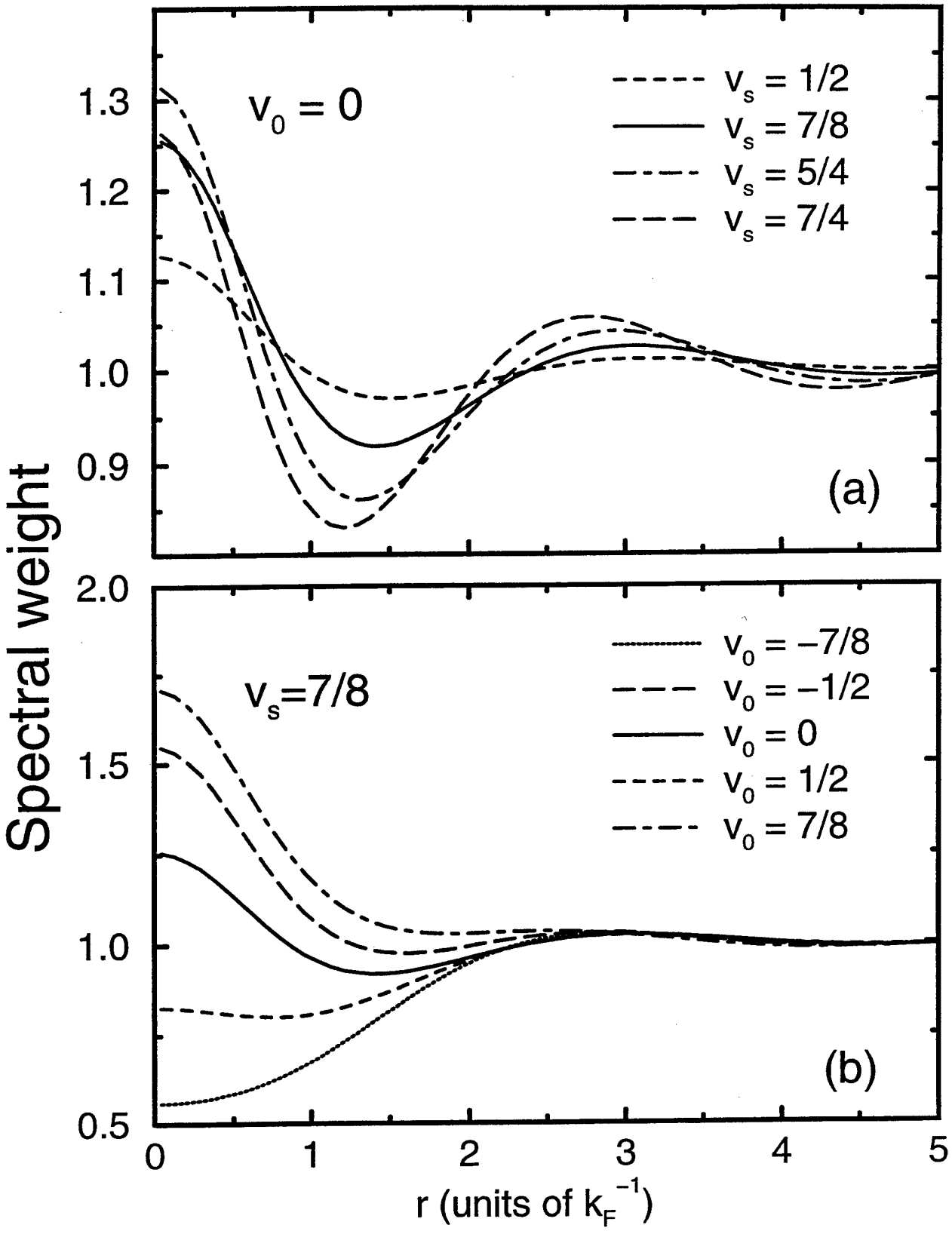

Figure 24, Flatte and Byers, "Local Electronic Structure of Defects in Superconductors", Solid State Physics Volume 52.

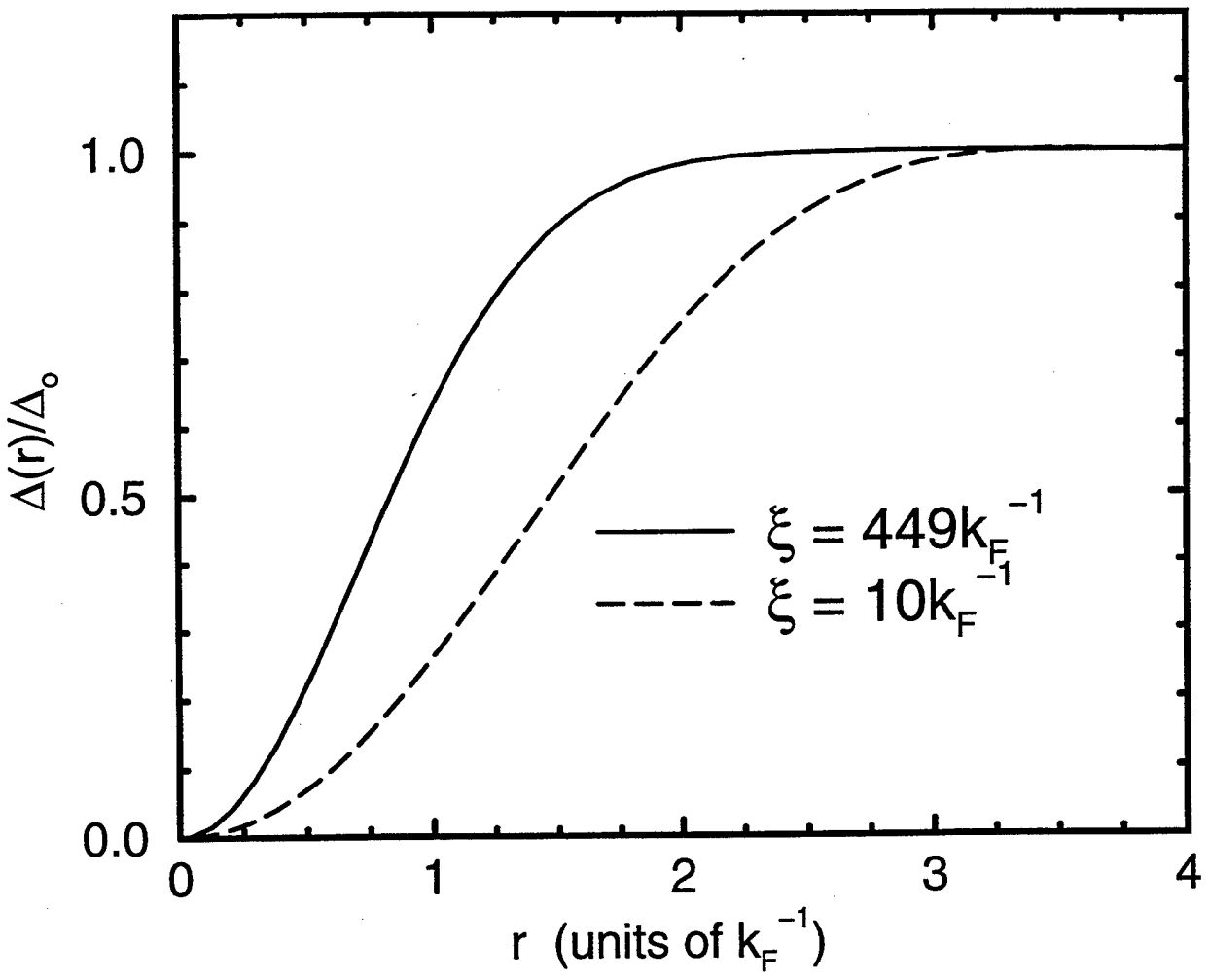

Figure 25, Flatte and Byers, "Local Electronic Structure of Defects in Superconductors", Solid State Physics Volume 52.

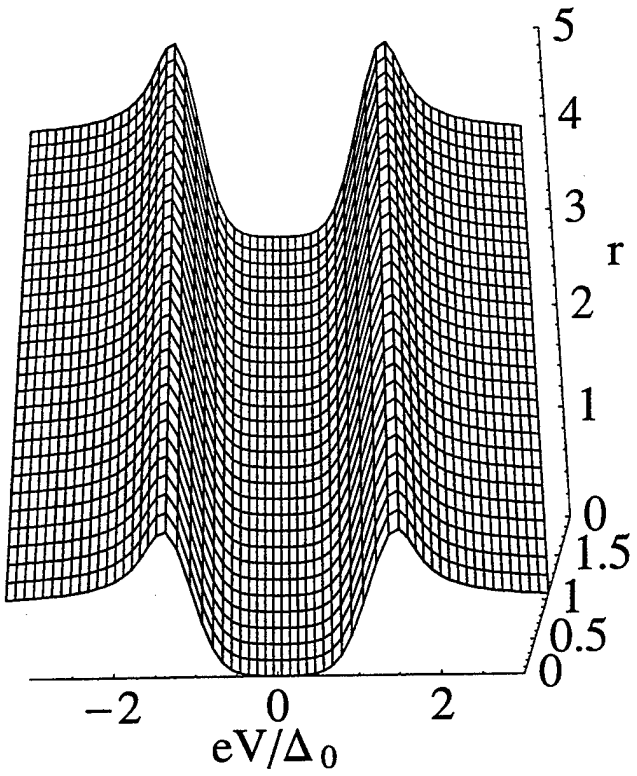

Figure 26(a), Flatté and Byers, "Local Electronic Structure of Defects in Superconductors", Solid State Physics Volume 52.

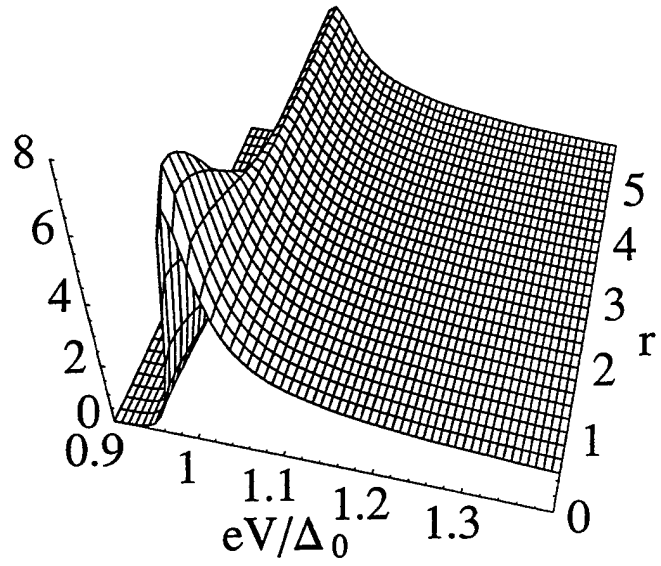

Figure 26(b), Flatté and Byers, "Local Electronic Structure of Defects in Superconductors", Solid State Physics Volume 52.

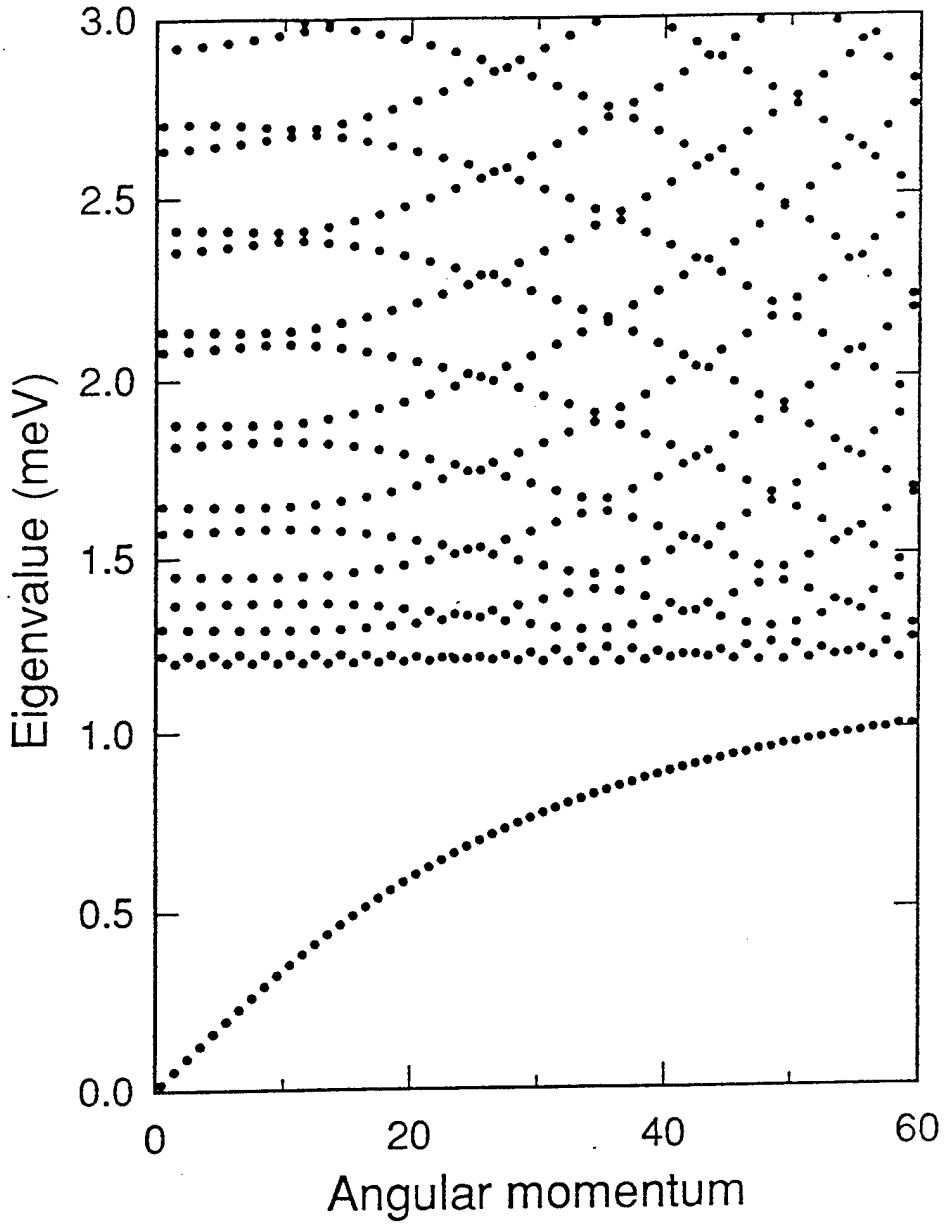

Figure 27, Flatté and Byers, "Local Electronic Structure of Defects in Superconductors", Solid State Physics Volume 52.

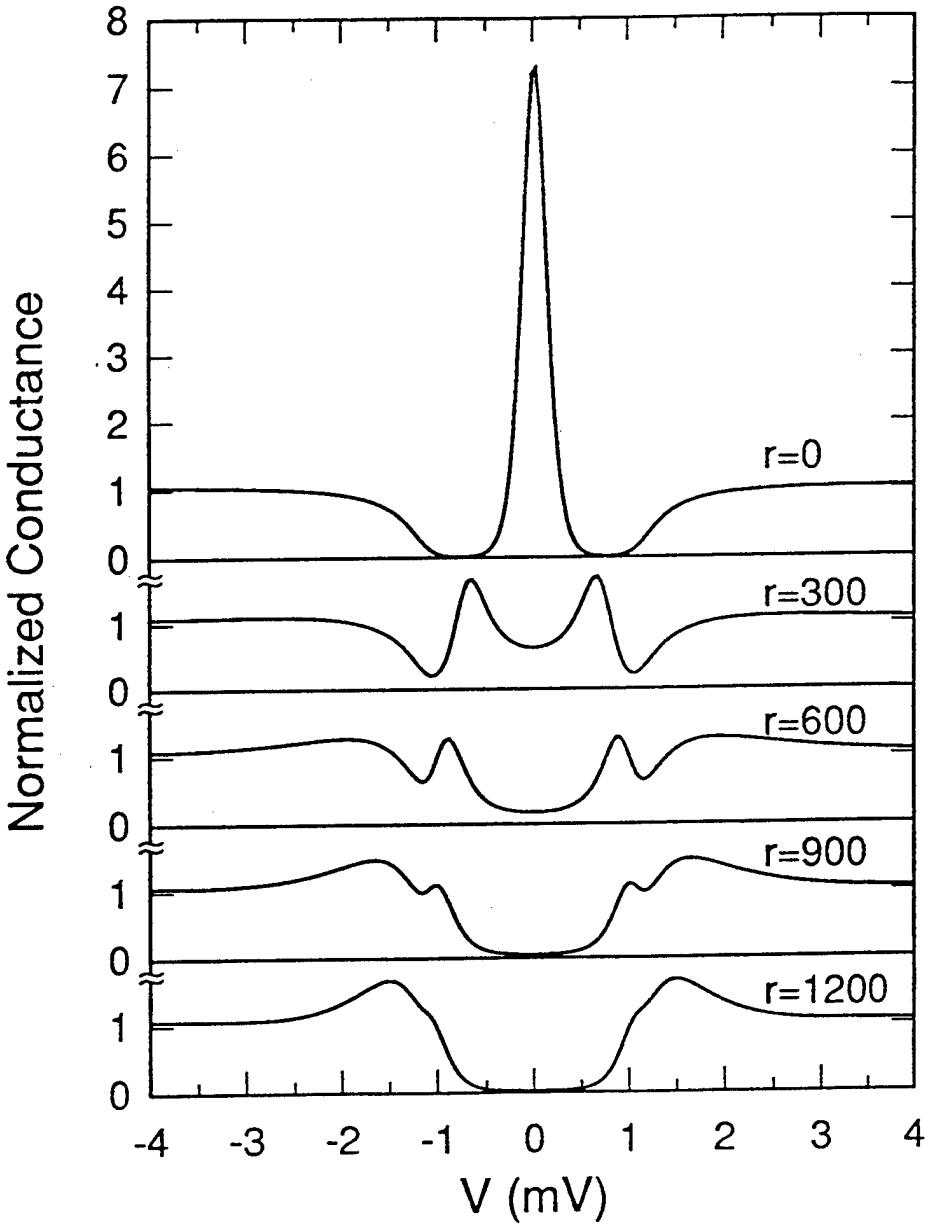

Figure 28, Flatté and Byers, "Local Electronic Structure of Defects in Superconductors", Solid State Physics Volume 52.

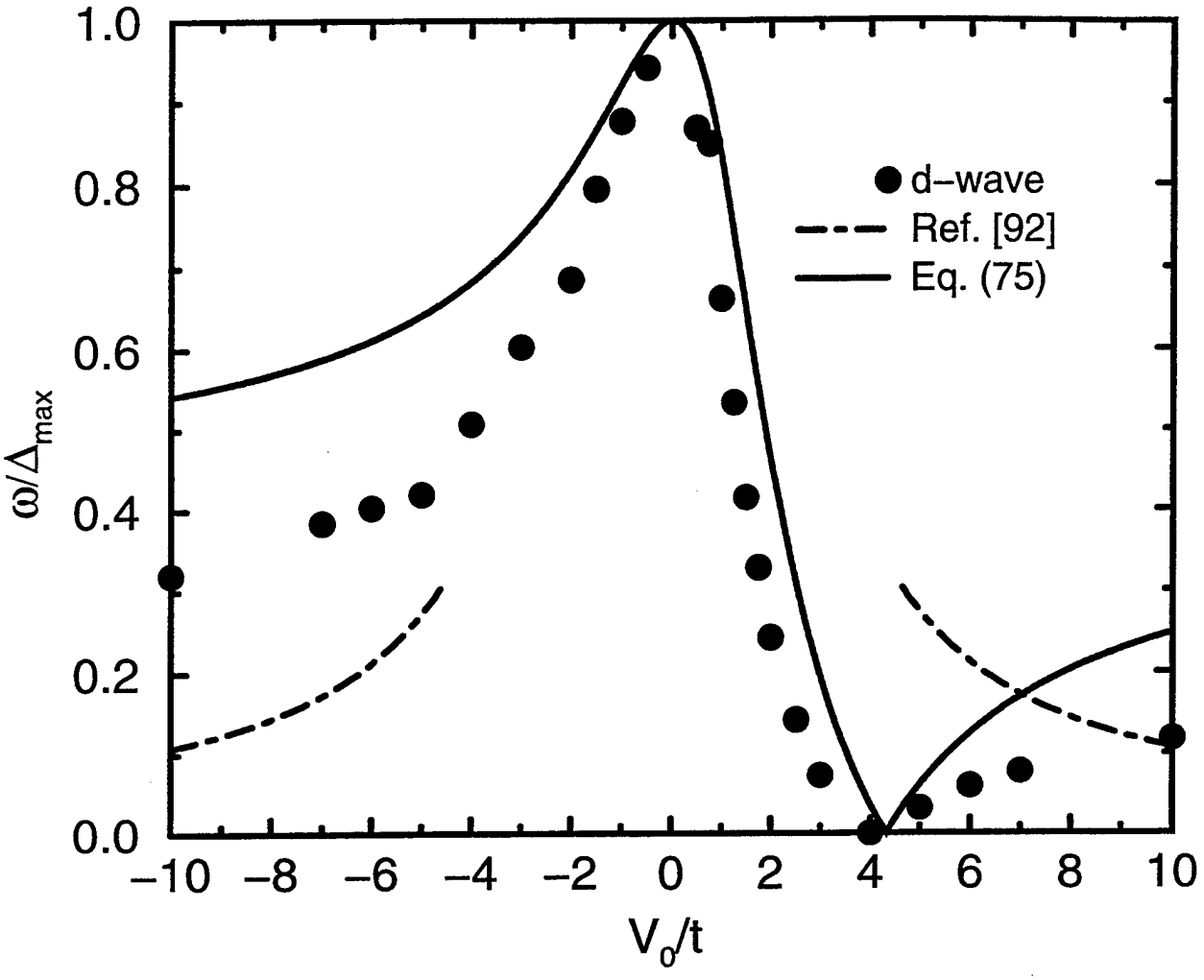

Figure 29, Flatte and Byers, "Local Electronic Structure of Defects in Superconductors", Solid State Physics Volume 52.

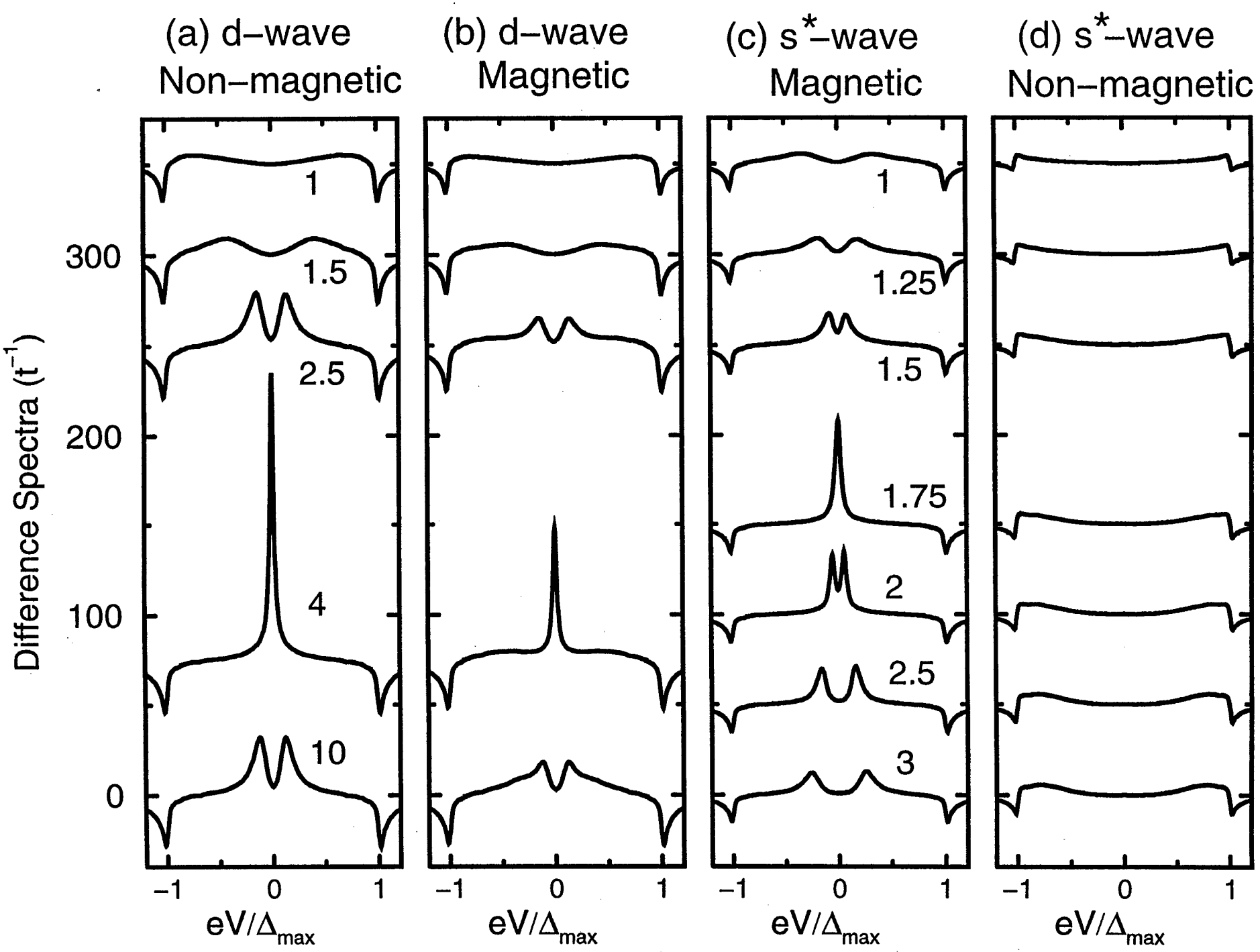

Figure 30, Flatte and Byers, "Local Electronic...", SSP Volume 52

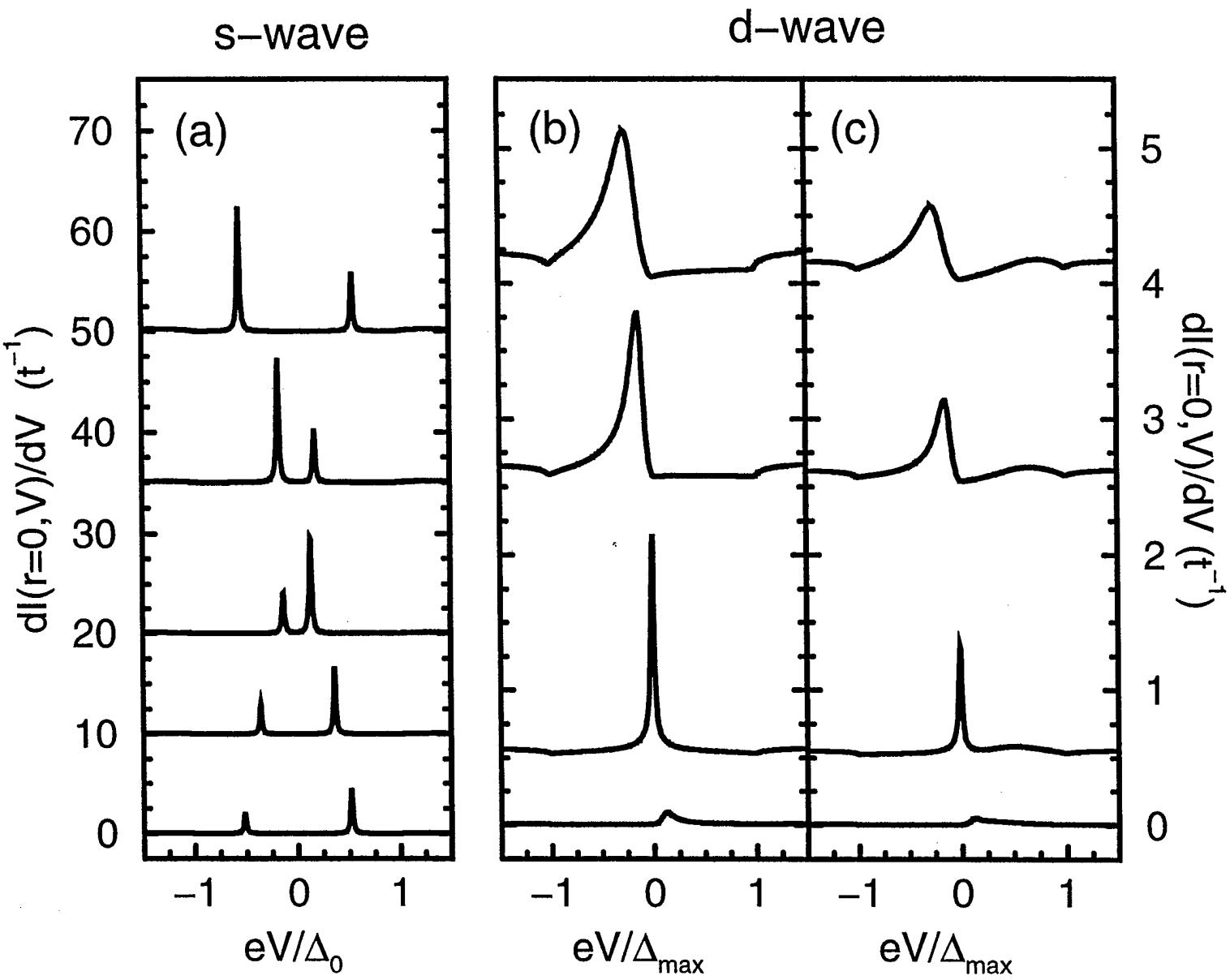

Figure 31, Flatte and Byers, "Local Electronic...", Solid State Physics Vol. 52

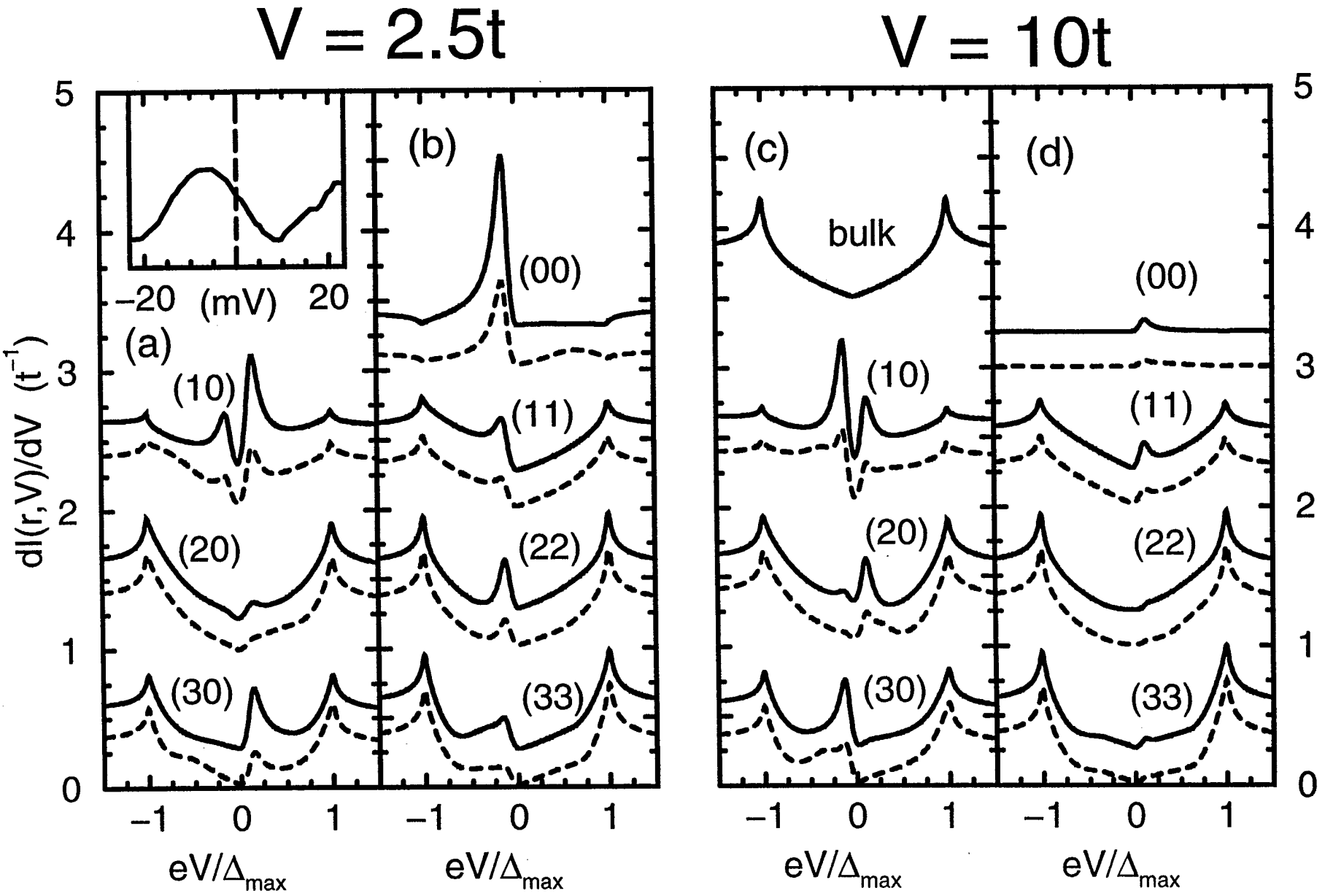

Figure 32, Flatte and Byers, "Local Electronic...", Solid State Physics Volume 52.

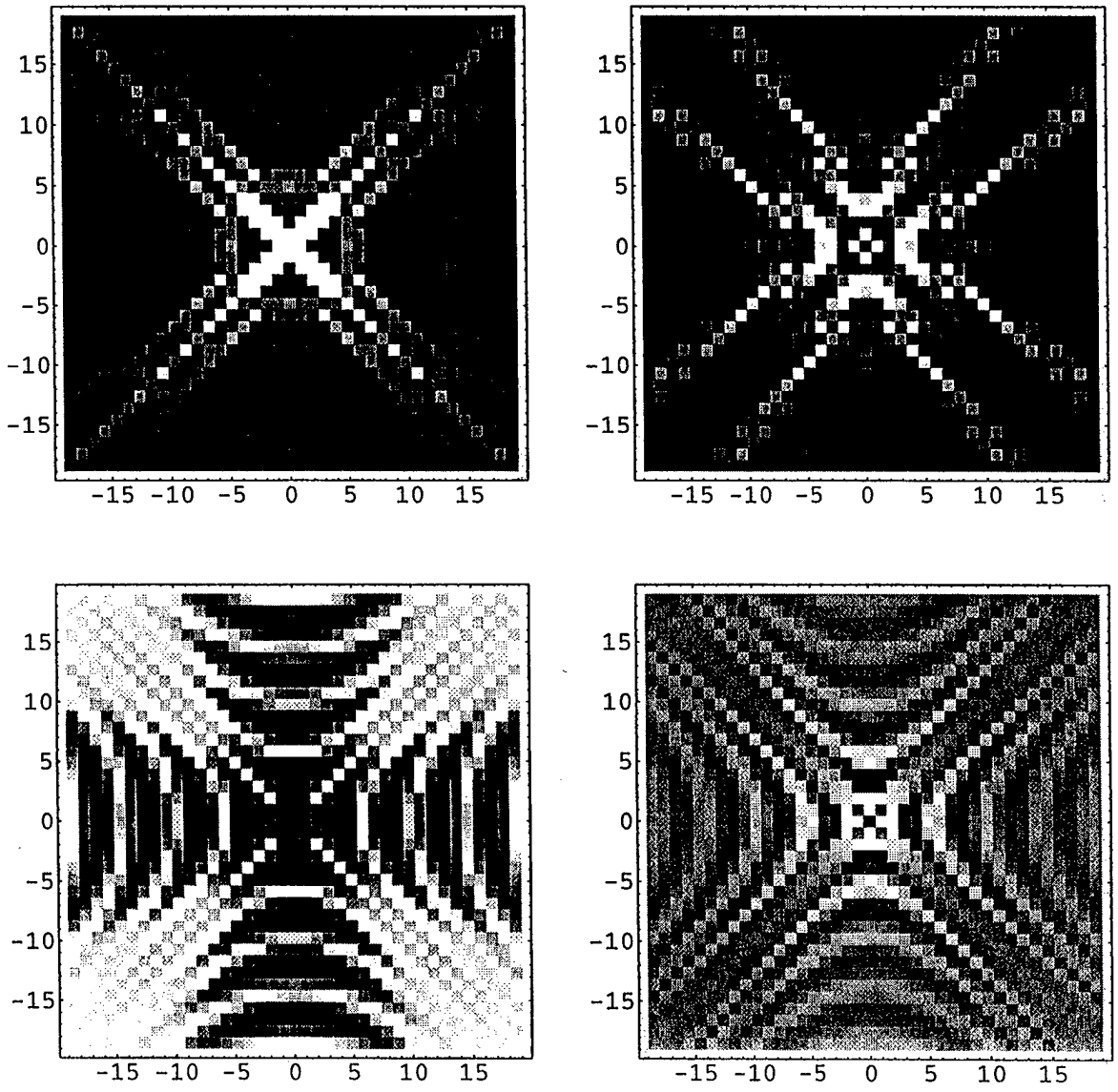

Figure 33,
Flatté and Byers,
"Local Electronic
Structure of Defects
in Superconductors",
Solid State Physics
Volume 52.

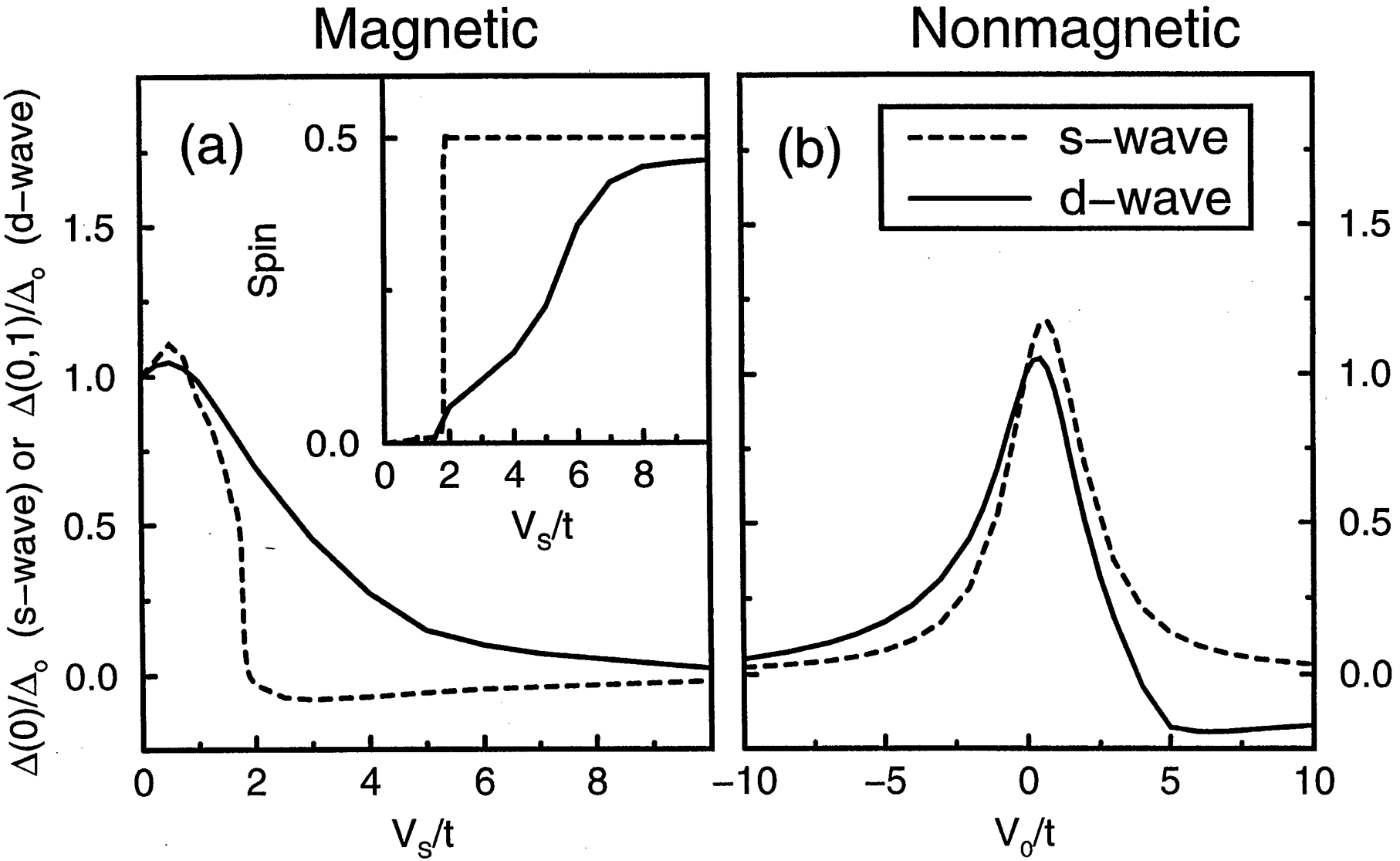

Figure 34, Flatte and Byers, "Local Electronic Structure of Defects in Superconductors", Solid State Physics Volume 52.

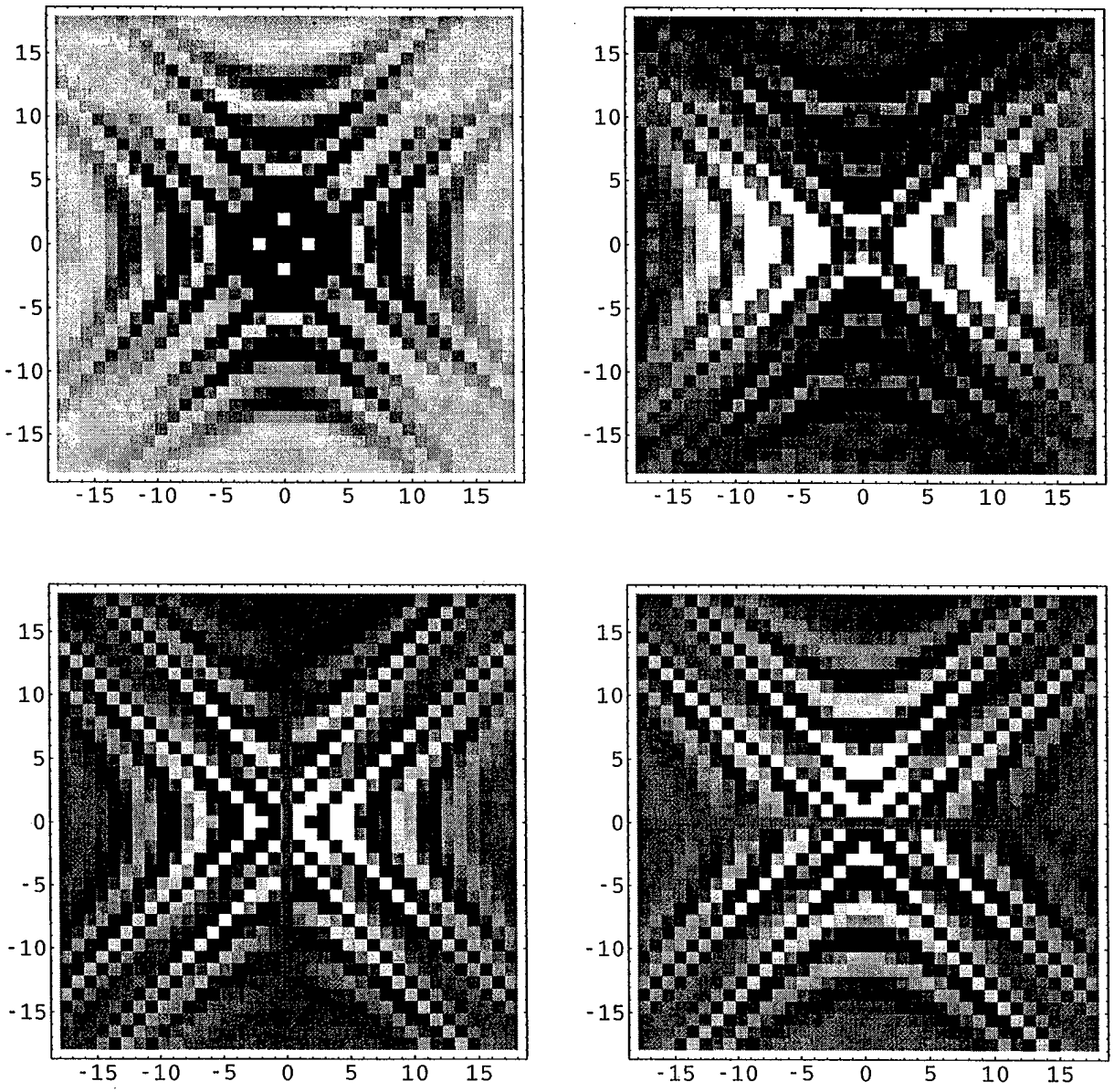

Figure 35

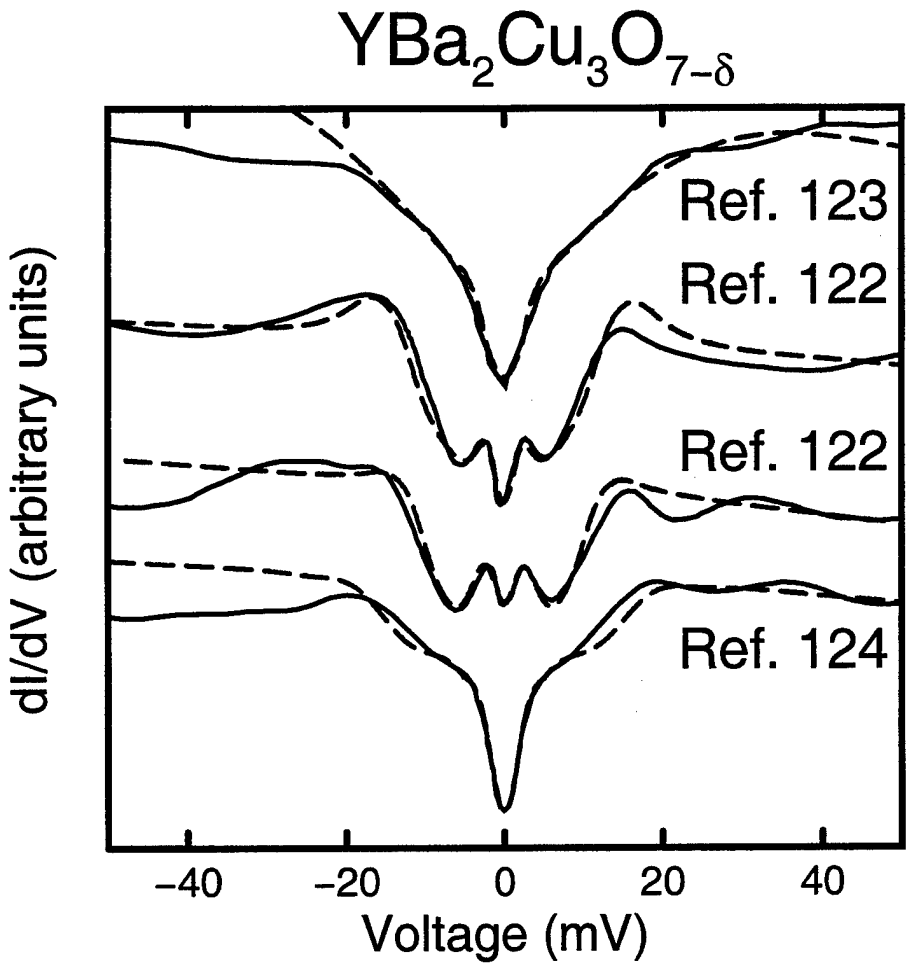

Figure 36, Flatte and Byers, "Local Electronic Structure of Defects in Superconductors", Solid State Physics Volume 52.

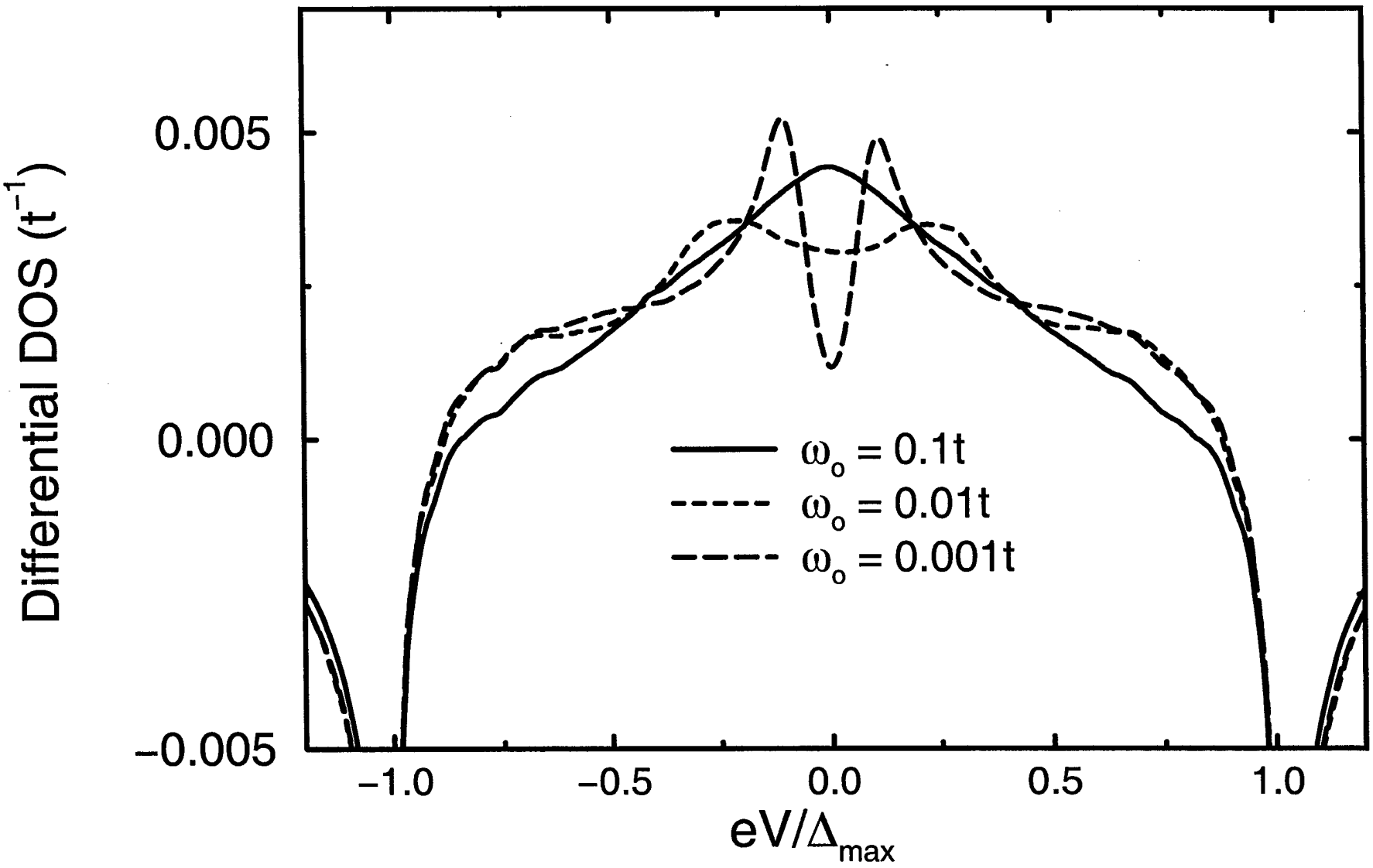

Figure 37, Flatte and Byers, "Local Electronic...", Solid State Physics Vol. 52.

REPORT DOCUMENTATION PAGE

Form Approved
OMB No. 0704-0188

1. AGENCY USE ONLY *(Leave blank)*	2. REPORT DATE	3. REPORT TYPE AND DATES COVERED
	October 30, 1998	Final (1 July 96 - 30 Sept 98)

4. TITLE AND SUBTITLE
Electronic Structure of Impurities and Vortices in Short Coherence Length Superconductors

5. FUNDING NUMBERS
N00014-96-1-1012

6. AUTHOR(S)
Michael E. Flatté

7. PERFORMING ORGANIZATION NAMES(S) AND ADDRESS(ES)
University of Iowa
Iowa City, IA 52242

8. PERFORMING ORGANIZATION REPORT NUMBER

9. SPONSORING / MONITORING AGENCY NAMES(S) AND ADDRESS(ES)
Office of Naval Research
Ballston Centre Tower One
800 North Quincy Street
Arlington, VA 22217-5660

10. SPONSORING / MONITORING AGENCY REPORT NUMBER

11. SUPPLEMENTARY NOTES

a. DISTRIBUTION / AVAILABILITY STATEMENT
APPROVED FOR PUBLIC RELEASE

12. DISTRIBUTION CODE

13. ABSTRACT ***(Maximum 200 words)***

This is a final report on theoretical calculation of scanning tunneling microscopy spectra near impurities in superconductors. Calculations have been performed for superconductors with isotropic and anisotropic gaps using a newly developed Green's function technique. This technique provides essentially arbitrary energy resolution and is applicable to strong or weak-coupling superconductors with long or short coherence lengths and arbitrary energy gaps. An analytic model has been developed for impurities in superconductors with either anisotropic or isotropic gaps. Calculation of planar tunneling spectra can reproduce the (quite different) results from several different groups with a d-wave gap and a small amount (1%) of impurities. These impurities are believed to be oxygen vacancies. A systematic investigation of the properties of impurity-associated resonance states in the gap has also been done.

14. SUBJECT TERMS
Superconductivity, magnetic impurities, scanning tunneling microscopy, planar tunneling, YBCO

15. NUMBER OF PAGES
95

16. PRICE CODE

17. SECURITY CLASSIFICATION OF REPORT	18. SECURITY CLASSIFICATION OF THIS PAGE	19. SECURITY CLASSIFICATION OF ABSTRACT	20. LIMITATION OF ABSTRACT